HEAT TRANSFER STUDIES FROM SINGLE CYLINDER AND TUBE BUNDLE IN FLUIDIZED BED

A THESIS

Presented to

the Faculty of the Division of Graduate Studies

by

Ravinder K. Bansal

In Partial Fulfillment

of the Requirements for the Degree

Doctor of Philosophy in Mechanical Engineering

Georgia Institute of Technology

March, 1978

HEAT TRANSFER STUDIES FROM SINGLE CYLINDER

AND TUBE BUNDLE IN FLUIDIZED BED

Approved by:

Prasanna V. Kadaba, Co-Chairman

P. V. Desai, Co-Chairman

T. W. Jackson

C. W. Gorton

H. M. McMahon

Date approved by Co-chairmans March 6, 1978

ACKNOWLEDGMENTS

I would like to take this opportunity to thank Dr. Prasanna V. Kadaba and Dr. P. V. Desai who suggested the thesis topic and were co-advisers during the development of this work. Their guidance, encouragement, patience throughout the entire course of this investigation, and especially the countless number of hours they spent working with me have led to the successful completion of this work. The constructive comments and time given by those who have served on my thesis committee, Dr. T. W. Jackson, Dr. C. W. Gorton, Dr. S. P. Kezios, and Dr. H. M. McMahon are gratefully acknowledged.

The assistance in fabrication and instrumentation of the experimental set up by Mr. L. A. Cavalli and Mr. T. E. Clopton is very much appreciated. Special thanks are extended to my friends Dr. Ravi Deo for his help in signal analysis of pressure fluctuations, and Mr. Vineet for taking the photographs and the willingness to help in anyway he could. The careful job of typing done by Ms. Annette Plunkett is greatly appreciated.

The financial support provided by the School of Mechanical Engineering, Georgia Institute of Technology is gratefully acknowledged. Finally, I would like to express my deepest gratitute to my parents, Dr. and Mrs. C. M. Bansal

for their continuous assistance, encouragement and love throughout my educational career.

TABLE OF CONTENTS

LIST OF TABLES

Table Page

LIST OF ILLUSTRATIONS

Figure Page

NOMENCLATURE

Latin Letters

Symbol	Definition	Units
A_1	constant in equation 1	dimensionless
A_2	constant in equation 2	dimensionless
A_n	Fourier coefficient of n^{th} term	dimensionless
a	effective heat transfer area per unit volume of the bed	ft^2/ft^3
a_n	real part of the Fourier coefficient of n^{th} harmonic term	dimensionless
B_1	constant in equation 1-a	dimensionless
B_2	constant in equation 2-a	dimensionless
b_n	imaginary part of the Fourier coefficient of n^{th} harmonic term	dimensionless
C	velocity of sound	ft/sec
C_g	specific heat of fluidizing medium at constant pressure	Btu/lbm °F
C_r	ratio of heat transfer at any radial location to that at the axis	dimensionless
C_R	correction factor	dimensionless
C_r	ratio of heat transfer at any radial location to that at the axis	dimensionless
C_s	specific heat of the solid particles	Btu/lbm °F
D_p	particle diameter	ft
D_r	distance between successive horizontal layers of particles	ft
D_t	tube diameter	inch
F_{max}	maximum frequency	Cps

Symbol	Definition	Units
G	mass flow rate	lbm/ft^2 hr
G_{mf}	mass flow rate at minumum fluidization	lbm/ft^2 hr
$G_p(f)$	power spectral density function defined for non-negative frequencies only	———
g	acceleration due to gravity	ft/hr^2
h	damping ratio defined by equation (B-3)	dimensionless
h_{avg}	average heat transfer coefficient over the circumference of the cylinder	Btu/hr ft^2 °F
h_r	local radiative heat transfer coefficient	Btu/hr ft^2 °F
h_t	local heat transfer coefficient due to both the convection and the radiation	Btu/hr ft^2 °F
h_θ	local convective heat transfer coefficient at an angular position θ measured from forward stagnation point	Btu/hr ft^2 °F
i	current	amperes
j	imaginary number	
j_h	Colburn's j factor for heat transfer $\dfrac{N_{Nu,p}}{N_{Re,p}\, N_{Pr}^{1/3}}$	dimensionless
k_e	effective thermal conductivity of "packets"	Btu/hr ft °F
k_g	thermal conductivity of fluidizing fluidizing medium	Btu/hr ft °F
k_N	thermal conductivity of Nichrome V	Btu/hr ft °F
k_p	thermal conductivity of solid particles	Btu/hr ft °F
L	height of the fins	inch
L_f	height of the fluidized bed under operating conditions	ft

Symbol	Definition	Units
L_s	settled bed height	ft
$N_{Ar,p}$	Archimedes Number, $\frac{\rho_g}{\rho_p} \cdot \frac{D_p^3 \rho_p^2 g}{\mu^2}$	dimensionless
$N_{Nu,p}$	particle Nusselt number, $\frac{h_{avg} D_p}{k_g}$	dimensionless
$N_{Nu,t}$	tube Nusselt number, $\frac{h_{avg} D_t}{k_g}$	dimensionless
N_{Pr}	Prandtle number, $\frac{\mu C_g}{k_g}$	dimensionless
$N_{Re,p}$	particle Reynolds number, $\frac{D_p G}{\mu}$	dimensionless
$N_{Re,t}$	tube Reynolds number, $\frac{D_t G}{\mu}$	dimensionless
P	center to center distance between tubes in a bundle	inch
$P_{(p)}$	probability density function	
p(t)	time dependent pressure	psid
Q	rate of heat transfer	Btu/hr
q_{rad}	radiative rate of heat transfer	Btu/hr
q_{conv}	convective rate of heat transfer	Btu/hr
q_{cond}	conductive rate of heat transfer	Btu/hr
q_{gen}	rate of heat generation	Btu/hr
R'	electrical resistance per foot of Nichrome V ribbon, a function of temperature	ohms/ft
r	radius of the pressure tap	inch
S	distance between fin tips	inch
S_L	stirring factor in equation (3)	dimensionless
T	absolute temperature	°R

Symbol	Definition	Units
T	thickness of Nichrome V ribbon	ft
T_a	absolute temperature of the air	°R
t	temperature of Nichrome V ribbon	°F
t	time in pressure fluctuation analysis	hr
t_b	temperature of the fluidized bed	°F
U	fluidization velocity	ft/hr
U_{mf}	minimum fluidization velocity	ft/hr
V	volume of the pressure transmitting cavity	$inch^3$
V_t	volume of the tubes in the tube bundle	ft^3
W	width of Nichrome V ribbon	ft
w_n	component of particle velocity normal to heat transfer surface	ft/hr
x	weight fraction of the sieved particles	dimensionless

Greek Letters

α_o	temperature coefficient of electrical resistivity	$°F^{-1}$
α_p	thermal diffusivity of particles	ft^2/hr
δ_w	mean distance from wall to surface of particles in the layer nearest to it	ft
ε	fluidized bed void fraction	dimensionless
ε_{bed}	settled bed void fraction	dimensionless
ε_N	emissivity of Nichrome V ribbon	dimensionless
θ	angle measured from forward stagnation point	degree,radian
ρ_{bed}	settled bed density	lbm/ft^3

Symbol	Definition	Units
ρ_e	effective density of the "packets"	lbm/ft^3
ρ_g	density of fluidizing medium	lbm/ft^3
ρ_p	density of the bed particles	lbm/ft^3
μ	dynamic viscosity of fluidizing medium	lbm/ft hr
μ_p	mean value of the pressure signal defined by Equation C-2	———
σ_p^2	variance of the pressure signal defined by Equation C-3	———
ψ_p^2	mean square value of the pressure signal defined by Equation C-1	———
ω	frequency of the pressure signal	cps

SUMMARY

This work presents an experimental investigation of the fluid flow and heat transfer mechanisms associated with the performance of an equilaterally pitched horizontal tube bundle in a gas fluidized bed. The effects of fluidization velocity and particle size/type on the flow patterns of the particles is examined. Also studied is the influence of the flow pattern on local heat transfer coefficient around the tube. A spirally wound Nichrome ribbon and flush mounted thermocouples under the ribbon on the test surface are utilized for the heat transfer studies. Another test cylinder with an embedded straingage type pressure transducer is used to measure local pressure fluctuations which are analyzed via Fast Fourier Transform techniques.

It has been observed that at flow rates in the range of incipient fluidization, the onset of fluidization occurs at the tube sides, with a corresponding increase in local heat transfer coefficient in that region. As the fluidization velocity increases the activity near the defluidized cap at the top of the cylinder becomes more intense, with a consequent large increase in the local heat transfer coefficient in this region when compared to that in other regions.

The average heat transfer coefficient based on the local values around the circumference has been observed to

increase with fluidization velocity for the range of particle sizes and types used in the investigation. Such an increase becomes more pronounced with increasing pitch-to-diameter ratios, levelling off at a value of the ratio of about 1.7. An empirical correlation patterned after earlier works on the subject, together with an additional correction factor for the influence of the pitch-to-diameter ratio, has been proposed.

CHAPTER I

INTRODUCTION

I.1 The Problem of Dense-Phase Fluidization

When gravitational force on a compact group of particles is countered by a fluid stream momentum to bring the particles in a floating state, the resulting flow field with solids in suspension is said to be in dense-phase fluidization. Such systems exhibit enhanced heat transfer rates and uniform fluidized bed temperature via particle mixing as well as due to favorable gas to solid contact that yields large surface area to volume ratios. Convenience in handling solid particles in transport with increased flow rates is an additional advantage of fluidized systems, all of which make fluidized bed reactors particularly attractive in chemical and petroleum process industries, as well as making fluidized bed technology generally adaptable in such varied applications as coal gasification/desulfurization and metal processing/extraction.

Basic mechanisms of the fluidization phenomenon, notwithstanding the extent of its application, are less than adequately understood; rather, engineering design of fluidized bed systems is based on prior experience and on a trial-error approach. This is not too surprising, considering the analytical complexities of turbulent gas-solid interactions,

the influence of physical properties on chemical rate processes and the cumbersome geometrical configuration factors associated with such units. Furthermore, a fluidized bed may operate in a uniform fluidization mode, or in a mode involving vigorous bubbling and mixing of solids, or even in a dilute phase conveyance mode. It is, therefore, not beneficial to examine fluidized systems only in the conventional unit operation mode. Rather, each flow field configuration must be investigated together with its peculiar characteristics in order to yield useful models that permit limited applicability.

The problem of dense-phase fluidized bed heat transfer primarily concerns an examination of the fluid dynamic and thermal characteristics of the flow field in the close vicinity of the heat exchange surfaces in a gas fluidized bed. This regime is characterized by the largest temperature gradients in the immediate neighborhood of the surface and the bulk particles. It is also possible to predict the surface to bed heat transfer from a knowledge of the residence time of a cloud of particles near the surface. It may be noted that the residence time is a direct consequence of the fluid dynamics of the bed, which is influenced by the overall bed geometry, the mean particle size and size distribution, and the flow field near the distributor plate of the bed. The influence of an immersed array of tubes on the gross fluidization patterns, such as particle movement near the

transfer surface and the residence time of particles in somewhat defluidized zones, further complicates the problem of heat transfer rate prediction via analytical means. It is seen that for higher heat exchange rates fresh particles from the central regions of the bed should be brought in contact with the heat transfer surface as rapidly as possible, and, conversely, a totally defluidized region near the exchange surface should correspond to reduced heat transfer rates. A detailed model of the dynamic interaction between the carrier gas flow, the heat exchange surface, and the particulates in the bed must be established before the problem of dense-phase fluidized bed heat transfer may be resolved.

I.2. Motivation for the Present Research

Controlled combustion reaction in a coal gasification process utilizes a liquid cooled tube bundle buried in a pulverized coal fluidized combustor. Early failures of such devices were traced to locally defluidized zones of burning particles, resulting in burnouts and hot spots. These could be avoided by periodic replacement of the hot particles by cooler ones from within the bed via appropriate choices of tube arrangement, fluidization velocity, particle size and distribution, and pitch to diameter ratio of the tube bundle. One proposed scheme of desulfurization of flue gases in coal burning power plants utilizes a fluidized bed of alkalized alumina to scrub the gases from the power plant to the stack.

A compact economizer in the form of a tube bundle immersed within the fluidized bed will not only force the bed to favor uniform fluidization at higher flow velocities with only a small percentage increase in pressure drop, but it will also form an attractive waste heat recovery system. Such tube bundles may also be utilized in petrochemical industrial applications to dissipate heat from the surface to the gas promoting dense-phase fluidization. Analysis and design of such fluidized bed heat transfer schemes requires a basic understanding of the mechanisms associated with the process.

In one of the earlier investigations of the fluid dynamic and thermal field in the vicinity of a horizontal tube with a gas fluidized bed, Glass and Harrison (1964)* obtained detailed flow patterns around the tube using photographic techniques in a two dimensional test section with sand and air. Their sequence of flow pictures showed an apparently defluidized region on the top of the tube, with irregular chains of rising bubbles causing significant particle activity near the tube sides. The resulting variation of the local Nusselt number around the circumference at incipient fluidization, as reported in the works of Gel'perin, et al. (1966), Keairns (1968), Noack (1970), and Baskakov, et al. (1973), showed that the heat transfer coefficient on the sides of the tube exceeded that at either the forward or the rear stagnation points by as much as

---

*See Bibliography at the end of the thesis.

seventy five percent. A detailed explanation of the mechanisms leading to such variation still remains to be established.

Staggered arrays of horizontal tubes with proper spacings for favorable flow patterns is likely to improve the heat transfer characteristics of the tube bundle. Neither the flow patterns of particles around the tubes in their vicinity, nor their influence on the bed-to-tube heat transfer rate, is available for such a tube bundle in a gas fluidized medium. In this connection, the work by Glass, et al. (1964) was confined to a two dimensional field.

Local gas pressure fluctuations in fluidized beds, observed by Fiacco (1964), Sutherland (1964), Kang, et al. (1967), Hilby (1967), Winter (1968), and Lirag (1971), have been generally attributed to the passage of particles and bubbles. A substantive correction of the local pressure fluctuations near the tube with the corresponding particle flow pattern which affects the heat transfer phenomena is not available in open literature.

The motivation for the present work arises out of a need to understand the interplay between the flow field variations and the resulting heat transfer augumentation in gas fluidized beds containing horizontal tube bundles. Heat exchangers of such a configuration have recently received wide attention in industry.

I.3. Statement of the Research Problem and the Plan of Attack

It is proposed to establish the potential of using local pressure fluctuations as a means of interpreting particle flow patterns near a horizontal tube within a tube bundle in gas fluidized beds. It is further proposed to determine the influence of such parameters as the tube arrangement and spacing, fluidizing velocity, bed particles size, and bed material on the variation of local Nusselt number around such a tube.

An experimental approach is taken. An apparatus consisting of a bank of horizontal tubes placed in a rectangular cross-section fluidized bed column, with 1 inch outer diameter tubes placed in staggered equilateral triangles or pitch, is fabricated for this purpose. Two of these tubes are used as test cylinders; one of these, a Teflon cylinder electrically heated by Nichrome V ribbon wound helically around the middle 2/3 of its length, with thermocouples placed underneath the central helix, is utilized for the heat transfer studies. The other tube, made out of steel, is used to measure local surface pressure fluctuations by incorporating strain gage pressure transducers within it.

The first series of experiments is confined to pressure fluctuation measurements. A Fast Fourier Analyzer is utilized to statistically analyze the measured fluctuations. The second group of experiments examines the influence parameters

with reference to the local Nusselt number variation using the circumferential temperature profile and accounting for variable ribbon resistivity and circumferential conduction.

CHAPTER II

LITERATURE SURVEY

II.1 Mechanisms of Heat Transfer Between Submerged Surfaces and Fluidized Bed

The augmented heat transfer in fluidized beds is a combined result of the thermal interaction between the particles, the fluidizing medium, and the submerged surfaces. This has led to three categories of investigations on heat transfer in fluidized beds during the past two decades. These refer to the heat exchange within the bed (particle to particle and fluid to particle), the interaction between the bed and its containing walls and the transfer between the bed and the submerged surfaces. The heat transfer aspects of the current investigation concern the exchange of heat between the fluid and a submerged surface in the presence of a dense phase fluidized bed, establishing the scope of this literature survey. Of a variety of mechanisms proposed by researchers for the rate of heat transfer between the bed and submerged surfaces, the three basic ones are turbulent convection, packet renewal transport, and unsteady conduction via individual particles.

Dow and Jakob (1951), Levenspiel and Walton (1954), and Wasan and Ahluwalia (1969) viewed solid particles as turbulence promoters which reduce the surface film resistance

to heat transfer. In adapting the boundary layer theory for flow of the fluidizing medium over vertical surfaces, Levenspiel and Walton (1954) conceptualized the fluidized bed to consist of uniform spherical particles arranged in horizontal layers, with the bed voidage determining the assumed constant distance between the layers and with the central part of the bed being isothermal. With the expansion of the bed, the distance between the layers was assumed to increase, although particles in each layer remained close to one another as well as to the wall. Assuming that a boundary layer formed anew over the distance between any two successive particles in contact with the surface, the authors proposed correlations between the void fraction, ε, of the bed, the Nusselt number based on interlayer distance, D_r, and the medium conductivity, k_g, and the Reynolds number based on mass flow rate per unit area, G, the layer spacing, D_r, and the medium viscosity, μ. The proposed equations, for laminar and turbulent flow, respectively, are:

$$\frac{h_{avg} D_r}{k_g} = \frac{0.417}{A_1} (1-\varepsilon)^{1/2} \left[\frac{D_r G}{\mu}\right]^{1/2}, \qquad (1)$$

and

$$\frac{h_{avg} D_r}{k_g} = \frac{8.02}{A_2} (1-\varepsilon)^{4/5} \left[\frac{D_r G}{\mu}\right]^{1/5}, \qquad (2)$$

where

$$A_1 = (1+B_1^{\,2})^{3/2} - B_1^{\,3} , \tag{1-a}$$

$$B_1 = .0294\ (1-\varepsilon)^{1/2} \left[\frac{D_r G}{\mu}\right]^{1/2} \tag{1-b}$$

$$A_2 = (1+B_2^{\,5/4})^{9/5} - B^{9/4} , \tag{2-a}$$

$$B_2 = .478\ (1-\varepsilon)^{4/5} \left[\frac{D_r G}{\mu}\right]^{1/5} . \tag{2-b}$$

Such a model presumes uniform fluidization. However, these equations do not agree with experimental observations by Van Heerden, et al. (1953), nor with those by Ziegler and Brazelton (1964). The latter authors attribute this lack of agreement to the neglect of heat absorption by the particles in the preceding equations. A further drawback to the model of a heat transfer mechanism which is based on turbulent convection is its disregard for the decreasing local temperature gradient with time near the surface owing to the continued contact of the particles.

The packet renewal transport mechanism is based on the hypothesis that packets of particulate material remove heat from the surface via transient conduction and that the packets are periodically renewed from the region near the wall into the bulk of the fluidized bed. This approach is forwarded in the works of Mickley and Fairbank (1955), Baskakov (1964), Patel (1967), and Yoshida, et al. (1969), who consider the effective thermal conductivity of the packets and their

renewal frequency as the main factors determining the heat transfer rate. The effective thermal conductivity in such an approach is taken as that corresponding to a fixed bed and the void fraction as that for a bed with minimum fluidizing velocity. In terms of a stirring factor, S_L, to allow for the replacement frequency of the particles at the heat exchange surface, together with the effective thermal conductivity, k_e, the effective density, ρ_e, and the specific heat, C_s, such an approach leads to an average heat transfer coefficient, such as

$$h_{avg} = \sqrt{k_e \rho_e C_s S_L} \qquad (3)$$

Equation (3) does not include any influence due to particle size. This is contrary to experimental observations. Furthermore, the theory also provides no upper bound on the heat transfer rate as the renewal frequency increases. Baskakov (1964) and Patel (1967) introduced a contact resistance between the surface and the bed to adjust for such a discrepancy. Although Yoshida, et al. (1969) envisioned a layer of particulates between the surface and the bed to account for the resistance to heat transfer, it must be noted that such a layer is nonhomogeneous and that the thermal responses of the gas and the particles are quite different, a fact which precludes the use of an effective thermal conductivity without further modifications. In fact, Harakas and Beatty (1963) reported that experimentally measured heat

transfer coefficients for moving packed beds, characterized by short particle residence times, were less than those predicted via the use of a single effective thermal conductivity for the bed.

Theories that attribute the heat transfer process primarily to unsteady conduction from the surface to a single or chain of particles have been proposed by Botterill, et al. (1962), Ziegler and Brazelton (1964), Couderc, et al. (1967), Brusenback (1963), and Gabor (1970). Such theories imply negligible internal thermal resistance of particle material as well as symmetrical heating due to particle rotation near the surface. Furthermore, it is assumed that between successive contacts with the wall, the particles assume the temperature of the bed core. In terms of the specific heat, C_s, and the density ρ_s, of the solids, the void fraction, ε, the gaseous medium thermal conductivity, k_g, the mean distance of particulates from the wall, δ_w, and the normal velocity component of particles in the first row, w_n, the preceding theory yields an expression for the average heat transfer coefficient as

$$h_{avg} = C_s w_n \rho_s (1-\varepsilon) \left[1-\exp\left(-\frac{1.2\, k_g}{\delta_w C_s \rho_s w_n (1-\varepsilon)^{1/3}}\right)\right]. \qquad (4)$$

It may be noted that an increase in the fluidizing velocity increases the solid circulation (and hence w_n) as well as the void fraction, the former tending to increase the heat

transfer coefficient and the later decreasing it. Furthermore, whereas in aggregative beds, due to the nonisotropicity, the vertical mixing of particles controls their renewal rate at the heat transfer surface, the theory leading to equation (4) utilizes the normal component of particle velocity as a measure of renewal rate. For rapid renewal rates, where internal temperature gradients within the particles are significant, equation (4) was modified by Botterill, et al. (1962) and Gabor (1970) who solved the unsteady conduction problem for varying thermophysical properties of the solid and the gaseous media to obtain isotherms for various contact times.

In order to apply any one of the three theories, it is essential to ascertain the particle movement near the surface by establishing whether the bed is under the conditions of channeling, or slugging, or uniform fluidization. Channeling refers to the tortuous flow through the bed via few open channels without disturbing the remaining solid particles. When slugging occurs, the particles agglomerate and get lifted by fluid bubbles with enough increase in size to fill most of the flow cross section containing the tube bundle. At the upper surface, the particulates fall off the bubbles and the slugs decompose eventually, resulting in intense mixing in the bed arising from random pulsating motion of the particles. The fluid velocity distribution during such a state of the bed is very uneven. Uniform fluidization corresponds to a

uniform rise of fluid through the bed and a somewhat even distribution of randomly circulating particles in the stream. A single fluidized bed may simulataneously exhibit one or more of the three basic flow states in varying degrees at various locations within it, rendering the task of assessing the exact particle motion almost untractable. On the basis of the numerous heat transfer research papers covering fluidized beds with embedded surfaces, it may be observed that increased particle activity coupled with an appropriate renewal rate of fresh particles from within the bed leads to augmented heat transfer. A detailed understanding of the mechanisms leading to heat transfer augmentation therefore requires a critical study of the particle flow patterns in the neighborhood of horizontal tubes in a fluidized bed.

II.2. Flow Visualization and Pressure Fluctuations Near Surfaces in Fluidized Beds

An air fluidized sand bed (mean diameter 100 μm) and a water fluidized glass ballotoni bed (mean diameter 500 μm) were examined via cine photography by Glass and Harrison (1964) to obtain the particle and fluid flow patterns near a horizontal tube. In a two dimensional bed (30 cm x 1 cm x 60 cm high), over a test cylinder (3 cm diameter x 1 cm long) placed symmetrically at one quarter of the way up the sand bed from the distributor, at air flow rates two to three times that needed for incipient fluidization, they observed three distinct flow regimes: an apparently defluidized region on

top of the horizontal cylinder, a thin film of air below the cylinder, and irregular chains of rising air bubbles on the sides of the tube. In an experiment to determine the amount of defluidized material resting on the top of the tube surface by weighing the cylinder while it was immersed in the air-fluidized bed, Glass (1967) noted that the apparent weight of the cylinder was less than that in the bed, while the Archimedean upthrust, i.e., the buoyant force, was less than that calculated from the volume of the tube and the bulk density of the bed. This difference in the upthrust, when used as a measure of the weight of the conical defluidized region, indicated a steady decrease in the weight for up to three times the minimum fluidization velocity. This loss of weight, in turn, implies an increase in the apex angle of the conical defluidized zone. The volume of the defluidized region increased with the cylinder diameter. Also, angular particles when compared to more spherically shaped particles, showed an increase in their stacking ability, resisting the influence of nearby fluid motion.

Morgan (1967) photographed the surface of a 20.3 cm square cross section air-fluidized sand bed with a 2.54 cm o.d. horizontal tube placed 20 cm above a porous plate distributor for specific bed heights at air flow rates ranging from four to twenty times the minimum fluidization rate. He observed the tube as continuing to have a marked influence on the bed behavior as the flow rate increased. The bubbling

of the bed was chiefly noted at the surface directly above the tube sides, the surface remaining unbroken by erupting bubbles between the two bubbling regions, although there remained some particle movement. A capacitance bridge technique to measure the time-averaged void fraction near a tube in an air fluidized bed, as used by Fakhimi (1969), also indicated fluidization initiating at the tube sides. Works by Glass (1967), Morgan (1967), and Fakhimi (1969) could only provide a qualitative picture of the unsteady flow patterns of gas and particles near a curved immersed surface in a fluidized bed. Pressure fluctuation measurements in the bed, it was argued, must be analyzed for a more quantitative description.

Shuster and Kisliak (1952) observed, in slugging beds, wide pressure fluctuations, with decreasing magnitude and increasing frequency, as the field approached a uniform fluidization state. They defined the quality index of the bed as the ratio of the average deviation of the pressure drop to the frequency of the pressure fluctuations. This index approaches a maximum from a value of zero for a uniformly fluidized bed as the bed approaches slugging. Similar observations were made by Fiacco and Sutherland (1964). Kang, et al. (1967) compared the pressure fluctuations in packed beds held with screens to those without packing. The decrease in magnitude of pressure fluctuations for packed beds was accounted for by the additional uniformity

of fluidization due to screen packing. Hilby (1967) hinted at the possibility of a correlation between pressure fluctuations in the bed on one hand and the particle motion as well as the passage of bubbles through the bed on the other. Lirag and Littman (1971) also linked passage of bubbles through the bed with pressure variations.

II.3. Heat Transfer to Tubes in Fluidized Beds

Vertical tubes in fluidized beds have been studied by a host of investigators, including Baerg, et al. (1950), Gamson (1951), Vreedenberg (1952, 1958, 1960), Toomey and Johnston (1955), Wender and Cooper (1958), and Ozkaynak and Chen (1975). The heat transfer and flow field around horizontal tubes in fluidized beds have been studied by Vreedenberg (1958), Gel'perin, et al. (1958, 1962), Zenz, et al. (1960), Glass and Harrison (1964), Botterill, et al. (1968), Petrie, et al (1967), Keairns (1968), Noack (1970), Lese and Kermode (1971), Genetti, et al. (1971), Andeen, et al. (1974), and Chen (1976). Major findings by these investigators may be summarized as follows: Horizontal tubes attract gas pockets at the bottom and stagnant caps of particles at the top. Gas channeling occurs between a vertical wall and a horizontal tube close to it. Bubbles generate from the tube sides, even in two dimensional beds. The local heat transfer coefficient around horizontal tubes is greatest on the sides, slightly less on the bottom and quite small at the top. When tubes are separated by at least 43 particle

diameters, any kind of barrier below the tube does not affect the heat transfer rates, although at least one investigation, namely that by Gel'perin, et al. (1962), found the barrier to adversely affect heat transfer rate. They found that when the barrier was another heat transfer tube, the exchange with the upper tube was adversely affected due to the particles having been partially heated by the lower tube. The heat transfer coefficient is minimum for tubes oriented at 45 degrees with the fluid stream. It may be pointed out that obstruction to a thorough fluidization due to extended surfaces rules them out as possible augmenters of heat transfer in fluidized beds. Moreover, even a ten fold increase in the heat transfer coefficient, attributed to a fluidized bed in the vicinity of a heated surface, renders rather low fin effectiveness. In fact, large variations in local heat transfer coefficients further complicate attempts to quantify the merits of finned surfaces in the presence of a fluidized bed. A literature review on finned surfaces in fluidized beds is, therefore, not pursued any further in this work.

II.4. Heat Transfer Correlations in Fluidized Beds

The multiplicity of parameters affecting the heat transfer phenomena in fluidized beds makes it unrealistic to attempt a generalized correlation scheme. Results by numerous investigators, therefore, must be examined with

reference to the limited scopes of the parameters they investigated.

Toomey and Johnston (1953) measured heat transfer from a vertical tube at the center of an air fluidized bed of variable-size glass beads as well as that from the bed to a water cooled outer wall. They proposed a correlation between Nusselt number based on particle diameter and gas medium conductivity, $\frac{h_{avg} D_p}{k_g}$, and Reynolds number based on particle diameter, mass velocity for minimum fluidization and gas viscosity, $\frac{D_p G_{mf}}{\mu}$ as

$$N_{Nu,p} = 3.75 \left[\left(\frac{D_p G_{mf}}{\mu} \right) \log \left(\frac{G}{G_{mf}} \right) \right]^{0.47} \qquad (5)$$

where G is the actual mass flow rate of air. Gamson (1951) correlated Mickley and Trilling's (1949) data for an air fluidized glass bead bed with a vertical heater at the center of the bed in terms of Colburn's j factors for heat transfer, such as

$$j_h = \frac{N_{Nu,p}}{N_{Re,p} (N_{Pr})^{1/3}} = 2.53 \left(\frac{6G}{a\mu} \right)^{-0.8} (1-\varepsilon)^{-0.3} . \qquad (6)$$

where a is the effective heat transfer area per unit volume of the bed. By varying the location of the vertical tube, Vreedenberg (1953) found that the maximum heat transfer coefficient occurred at $\frac{r}{R} = 0.4$. Based on an examination of earlier data, Wender and Cooper (1958) proposed the relation

$$\frac{N_{Nu,p}}{1-\varepsilon} = 0.01844\ C_r (N_{Re,p})^{0.23} \left(\frac{C_s}{C_g}\right)^{0.8} \left(\frac{\rho_p}{\rho_g}\right) \left(\frac{C_g \rho_g}{k_g}\right)^{0.43} \qquad (7)$$

where $\left(\frac{C_g \rho_g}{k_g}\right)$ is not dimensionless but has the units of sec/cm^2, and C_r represents the dimensionless correction factor for non axial tube location as given by Vreedenberg (1952). Here, the constant 0.01844 has compensating dimensions to render the right hand side of the above equation. Heat transfer from a tube within a tube bundle in a dense phase as well as in a dilute phase air fluidized bed was studied by Genetti and Knudsen (1968). For the dense phase fluidization they proposed the relation

$$N_{Nu,p} = \frac{5(1-\varepsilon)^{0.48}}{\left[1 + \frac{580}{N_{Re,p}} \left(\frac{\alpha_s}{D_p^{3/2} g^{1/2}}\right) \left(\frac{\rho_s}{\rho_g}\right)^{1.1} \left(\frac{G_{mf}}{G}\right)^{4/3}\right]^2}, \qquad (8)$$

and for the dilute phase they proposed the Colburn's j factor relation

$$j_h = \frac{N_{Nu,p}}{N_{Re,p} (N_{Pr})^{1/3}} = 0.14\ (N_{Re,p})^{-0.68} \qquad (9)$$

For a single tube at variable inclinations, as well as variable mass fluid rates and particle sizes, Genetti, et al. (1971) proposed the relation

$$N_{Nu,p} = \frac{11(1-\varepsilon)^{1/2}}{\left[\frac{0.44 - \frac{.20(\theta-45)^2}{(\theta-45)^2+120}}{(N_{Re,p})^{0.24}\left(\frac{D_p}{0.008}\right)^{1.23}} + 1\right]^2}, \qquad (10)$$

where θ is measured in degrees from the horizontal and D_p is in inches.

A correlation for a horizontal heated tube in a fine particle bed was proposed by Vreedenberg (1958) as

$$N_{Nu,t} = 0.66\ (N_{Pr})^{0.3}\left[N_{Re,t}\ \frac{(1-\varepsilon)\rho_p}{\varepsilon\rho_g}\right]^{0.44}, \qquad (11)$$

where the subscript t refers to the tube. For larger and heavier particles he proposed the relation

$$N_{Nu,t} = 420\ (N_{Pr})\left(N_{Re,t}/N_{Ar,p}\right)^{0.3} \qquad (12)$$

Average heat transfer coefficient for a horizontal tube bundle in a fluidized bed with a minimum tube separation of 43 particle diameters, and with mass velocities ranging from 60 to 300 $\frac{lb_m}{hr\text{-}ft^2}$, as reported by Petrie, et al. (1968), is given by

$$N_{Nu,t} = 14\left(\frac{G}{G_{mf}}\right)^{1/3}\left(N_{Pr}\right)^{1/3}\left(\frac{D_t}{D_p}\right)^{2/3}. \qquad (13)$$

However, the experimental scatter from this relation was as high as $\pm$43 percent.

For bare and serrated finned tubes in a horizontal bundle, with variable fin height, L, tube spacing, P, particle diameter, D_p, and fluidizing air velocity, Bartel and Genetti (1973) noted that heat transfer increased with increasing fin height before leveling off. They also noticed that tube spacing was an influence parameter only for short finned tubes. They proposed the relation

$$N_{Nu,p} = \frac{10(1-\varepsilon)^{0.5}\left[1 - \frac{0.027 + 4.3L^{1.5}}{P^{1.12} + 3.2L^{0.6}}\right]}{\left[1 + \frac{0.00102 + 0.047L^{0.8}}{(N_{Re,p})^{(0.33+0.4L^{9.33})}(D_p)^{(1.23-0.57L^{0.23})}}\right]^2}, \quad (14)$$

where L, D_p and P are expressed in inches.

Using horizontal tubes in shallow fluidized beds, Andeen and Glicksman (1976) contended that Vreedenberg's (1958) data correlated well only for low void fractions, but progressively worsened as the gas velocities were increased. This may be attributed to the fact that Vreedenberg's work was performed at low velocities. Andeen and Glicksman (1976) modified Vreedenberg's correlations to include the influence of void fraction, (with an RMS deviation of 13.8 percent), as

$$\frac{N_{Nu,t}}{(N_{Pr})^{0.3}} = 900(1-\varepsilon)\left(N_{Re,t}/N_{Ar,p}\right)^{0.326} \quad (15)$$

Ainshtein and Gel'perin's (1966) attempt to correlate the data for 0.2 mm diameter glass spheres in terms of

Nusselt number as a function of particle Reynolds number for room temperature air fluidized beds, together with Chen's (1976) further replotting of Ainshtein and Gel'perin's work as well as that of his own new data, indicated an uncertainty bound in the preceding correlations up to one hundred percent for either the vertical or the horizontal tubes. To quote Botterill (1975):

> Although workers were mostly only able to examine a limited range of experimental variables, they often presented their conclusions in the form of generalized correlations that may tend to obscure this. Although the power to which certain groups in the correlations occur give some indication of the importance of factors within the experimental range, it is rarely clear to what extent the results have been influenced by the scale of the equipment... through the effect that this had on the fluidization behavior.

It is imperative that further experimentation and analysis of fluidized bed heat transfer from and to tubes and tube bundles be conducted with at least as much emphasis on formulating physical mechanisms of exchange of momentum and energy as on the ensuing correlations.

CHAPTER III

EXPERIMENTAL PROGRAM

III.1. Design of Apparatus and Data Collection Procedure

The objective of the present investigation is to enhance the detailed understanding of the flow field in the immediate vicinity of horizontal tube bundles surrounded by a dense phase gas fluidized bed and the influence of flow field on the local heat transfer rates. The results of such an investigation are essential to the design of efficient and cost effective fluidized bed heat exchange equipment.

The test facility has a narrow rectangular test section housing the heat exchanger tube bundle. One of the tubes is instrumented to record pressure fluctuations, while another one is equipped to determine local heat transfer coefficients. Supporting instrumentation can be divided into that needed for flow visualization, data recording, and data analysis. The two cylinders can be located anywhere within the tube bundle in the test section, the remaining tubes in the bundle being dummy cylinders. The test section is designed to permit variations of the tube pitch, the material of the fluidized bed, the particle size and the fluidization velocity. The design and fabrication of the apparatus, as well as an outline of the data collection procedure, are

explained under the following categories:

The Fluidizing Column

The Flow System

Pressure Fluctuation Measurement

Heat Transfer Measurement

Supporting Instrumentation

Data Collection Procedure

III.1.1. The Fluidizing Column

The fluidizing column is made of 0.5-inch thick clear plexiglass sheets. The inside cross section is 11 inches x 6 inches and its height is 46 inches. Figure 1 shows two views and a cross section of the column. The plexiglass faces making the broad sides of the column are in several sections permitting location of tube bundles at any preselected height from the distributor plate. The two 12-inch high plexiglass pieces used to hold the tubes are identical except that 1 inch diameter holes have been drilled through one of these pieces, whereas in the other there are only 0.25 inch deep notches. Such a design permits introduction of tubes from the side. Three sets of such tube bundle holders accommodate three different pitch to diameter ratios.

In order to insure desirable uniform flow across the entire test section, a distributor plate and a flow straightening section upstream of it have been provided at the base of the column as shown in Figure 2. The distributor plate is a 0.25-inch thick porous sintered bronze plate with

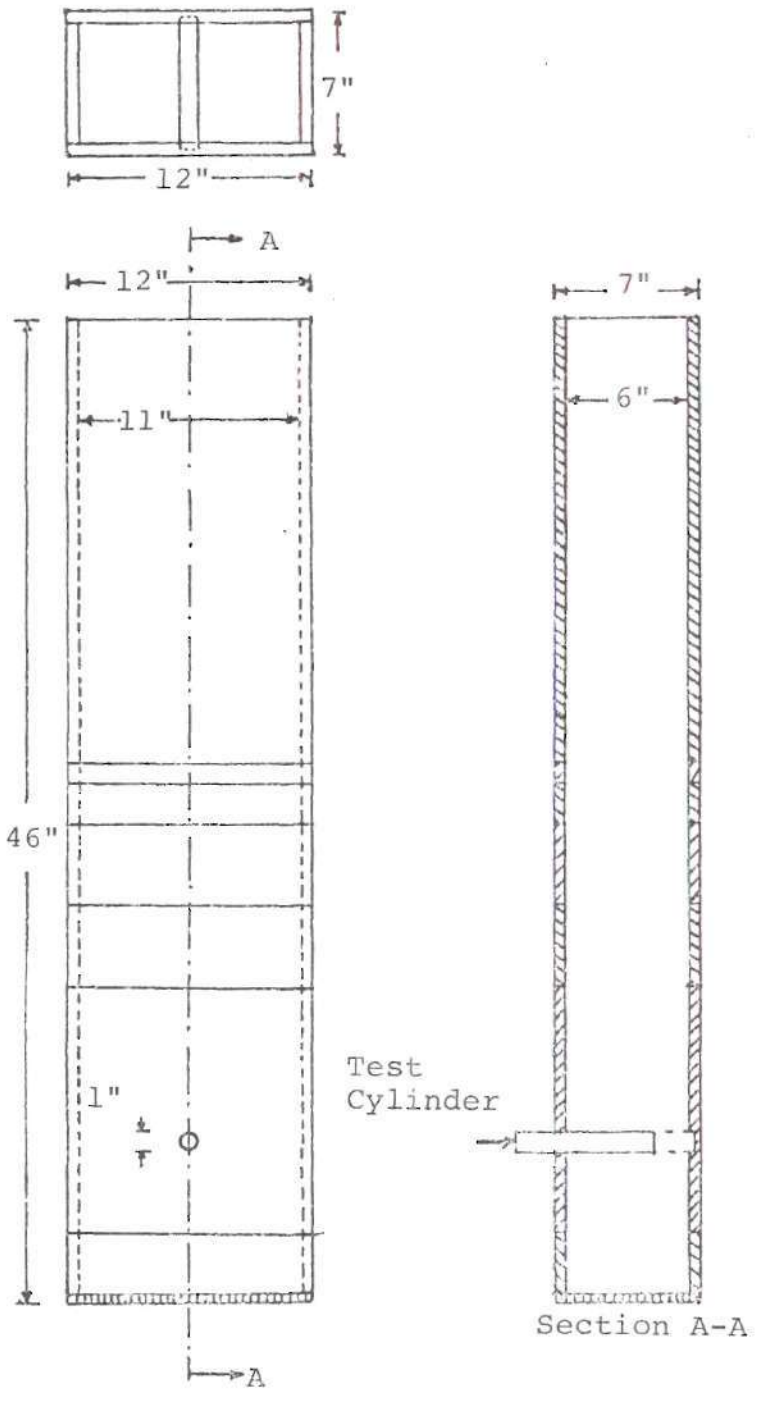

Figure 1. Details of the Fluidizing Column.

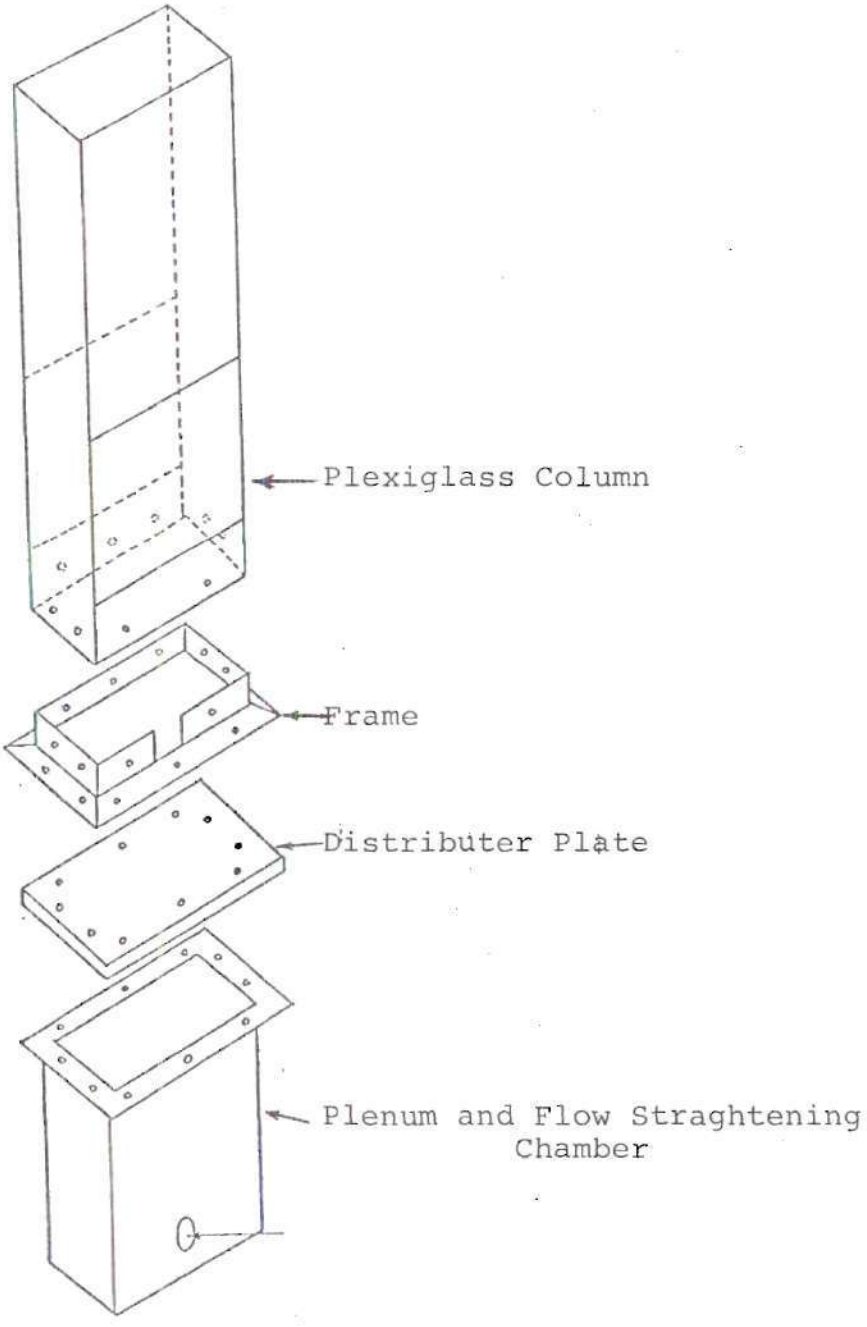

Figure 2. Exploded View of Fluidizing Column Assembly.

a mean pore size of 40 μm. The flow straightening section is a rectangular box with inside dimensions of 6-inch x 11-inch x 24-inch and open at the top. It is made out of 0.125-inch thick black iron sheets. Air enters through a two inch diameter hole at the lower part of this box. Bundles of screen mesh and a layer of honeycomb material have been placed in the upper part of flow straightening section in order to achieve a uniform flow through the entire face of the sintered plate. Air velocity surveys made with a vane type anemometer confirmed the existence of uniform inlet conditions to the fluidizing column. The fluidizing column, the distributor plate and the flow straightening section are held together with an angle iron frame (see Figure 2) and rubber gaskets (not shown).

III.1.2. The Flow System

Figure 3 shows the general layout of the air flow system. The air compressor is capable of supplying up to 400 cfm at 85 psi, allowing experimentation at very high values of face or superficial air velocity. The controlled air flow rate is admitted by using an air pressure regulator and it is measured by using a laminar flow element. Line pressure fluctuations at the upstream of the test section are dampened out by using a surge tank. A simple U-tube manometer measures the pressure drop in the bed while an inclined manometer measures the pressure drop across the flow meter.

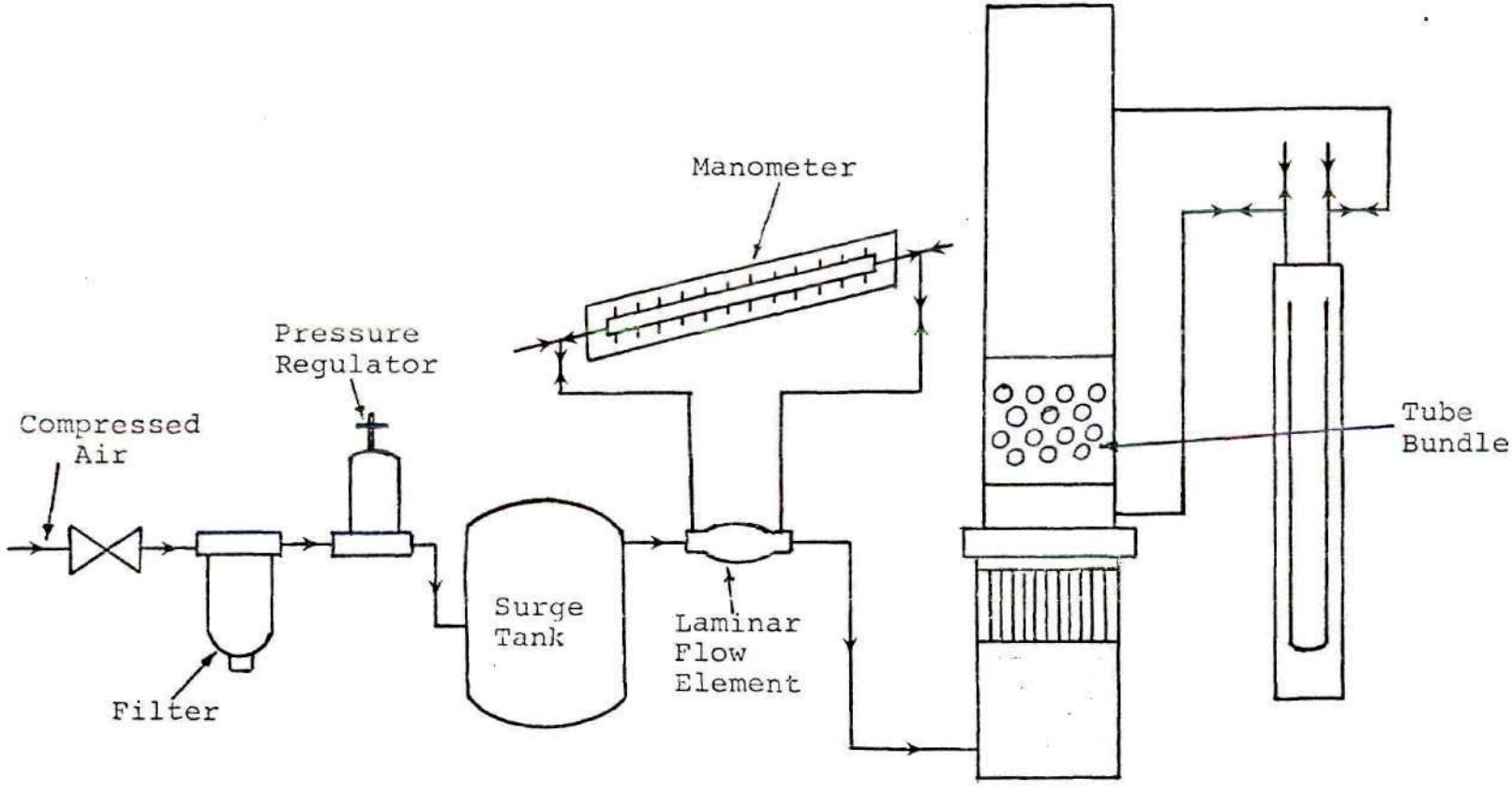

Figure 3. General Layout of the Test Apparatus.

III.1.3. Pressure Fluctuation Measurements

A careful review of literature containing the efforts by several investigators (Fiacco (1964), Sutherland (1964), Kang, et al. (1967), Hilby (1967), and Lirag and Littman (1971)) to study the pressure fluctuations in fluidized beds show that the fluctuations are below 20 Hz at amplitudes less than 30 percent of the total bed pressure drop. This pressure drop is approximately equal to the weight of the particulate material per unit area of the distributor plate. In the present investigation the total bed pressure drop is about 0.7 psi. It is expected that the amplitude of the pressure fluctuations would be below 0.2 psi at a frequency below 20 Hz. Thus, a strain gage type pressure transducer with a flat frequency response up to 500 Hz, and capable of measuring $\pm$ 2.5 psi should be quite suitable. Because of the danger of impacting particles on the sensing element flush mounting of the transducer is not desirable. Therefore, the pressure transducer has been mounted inside the test cylinder. Figure 4 shows the installation of the sensor inside the steel test cylinder. The pressure transmitting system consists of pressure tap and a pressure transmitting cavity. The pressure tap is 0.0135 inch in diameter and 0.20 inch long, and the cavity is 0.6 inch in diameter and 0.25 inch deep. The calculations shown in Appendix B show that the natural frequency of the trapped air column is approximately 9000 Hz, and that even for frequencies of up to 200 Hz no attenuation

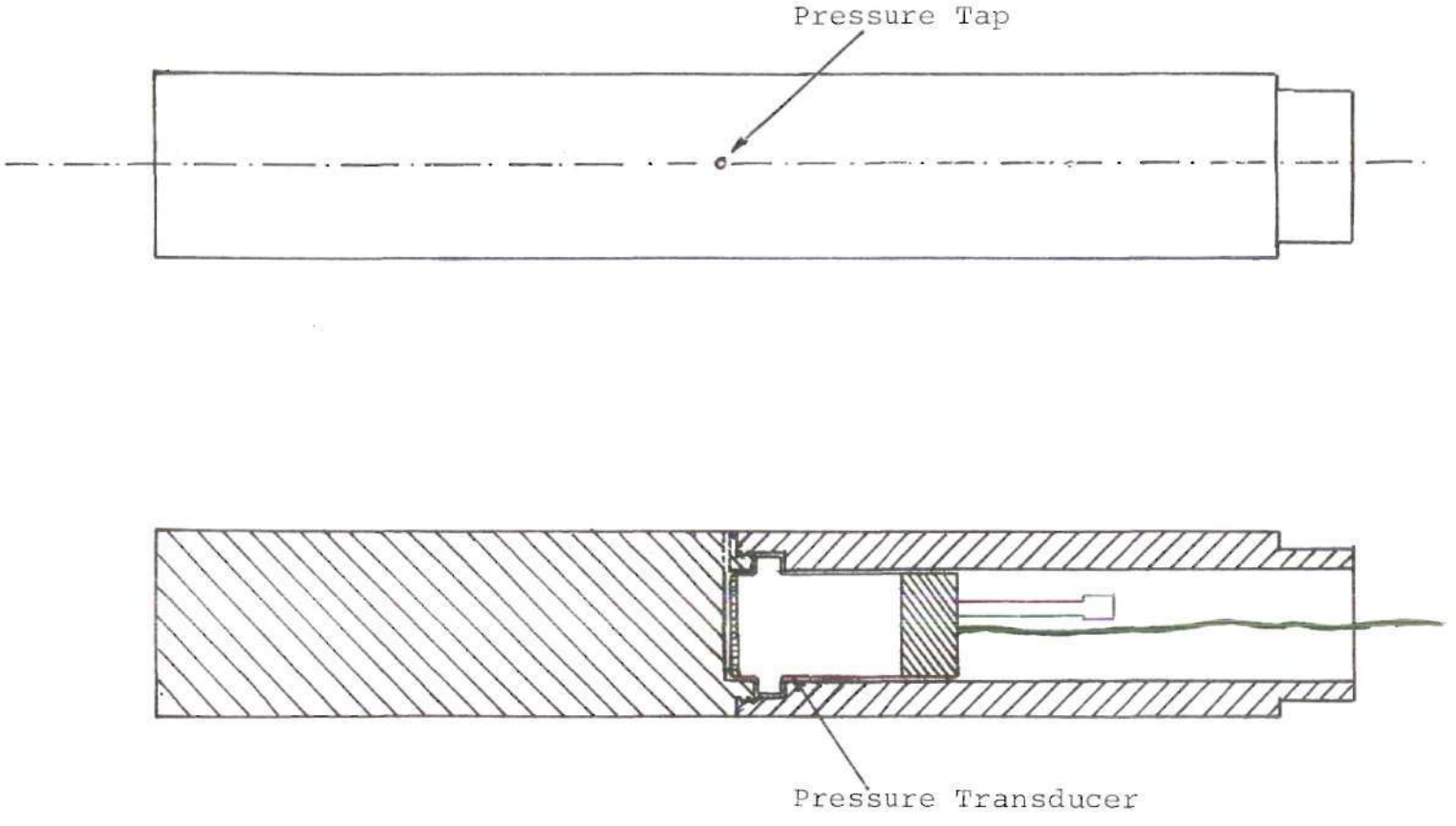

Figure 4. Installation Detail of Pressure Transducer.

Figure 5. Pressure Measurement Test Cylinder.

of the dynamic pressure occurs. The pressure tap has been made small to prevent the particles of the bed from getting into the pressure transmitting cavity.

The cylinder used for pressure fluctuation measurements has been made out of steel stock. Steel has been selected because of its strength and abrasive resistance. One end of the cylinder has been milled into a rectangular shape in order to rotate the cylinder inside the test section. A protractor is mounted on this rectangular end to measure the position of the pressure tap relative to the cylinder forward stagnation point located at the bottom of the cylinder. Figure 5 is a photograph of the exploded view of the test cylinder for pressure fluctuation measurements.

III.1.4. Heat Transfer Measurement

The test cylinder for heat transfer measurements is a hollow teflon cylinder electrically heated by a .010-inch thick and .125-inch wide Nichrom V resistance ribbon wound helically around the middle four inches of the outisde cylindrical surface (see Figure 6). Copper constantan thermocouples have been placed underneath the central turn of this ribbon in order to measure the temperature variation around the circumference of the cylinder. The measured temperature profile is used to evaluate the local heat transfer coefficient after making allowance for the circumferential conduction along the ribbon. The integrated value of this local heat transfer coefficient provides the average value.

Teflon has been selected as the material for the test cylinder because of its ability to withstand temperatures up to 350°F and its good machinability properties. Nichrome V has been used as the heating element because of its high electrical resistance and very small temperature coefficient of electrical resistivity. The cross section of the Nichrome ribbon, 0.125-inch x 0.010-inch thick, provides enough thermal inertia to damp out most of the rapid fluctuations in temperature caused by the flow fluctuations in the vicinity of the ribbon surface located inside of the fluidized bed. Ribbons thicker than .010-inch and wider than 0.125-inch have not been considered to keep the effect of circumferential conduction through the ribbon on the local heat transfer coefficient below ten percent. Evaluation of circumferential conduction requires an accurate knowledge of the second derivative of the temperature profile. It is difficult to make temperature measurements accurate enough to provide reliable values for this second derivative.

Figure 6 also shows the locations of the thermocouple junction and terminal posts for power lead wires. The test cylinder is constructed from 1-inch diameter teflon stock. A 0.375 inch hole throughout its length provides sufficient space for thermocouple wires and power leads. A helical thread (0.010 inch deep, 0.125 inch wide and 7 threads per inch) is cut on the exterior surface of the teflon cylinder. A spirally wound Nichrome V ribbon is placed in the groove

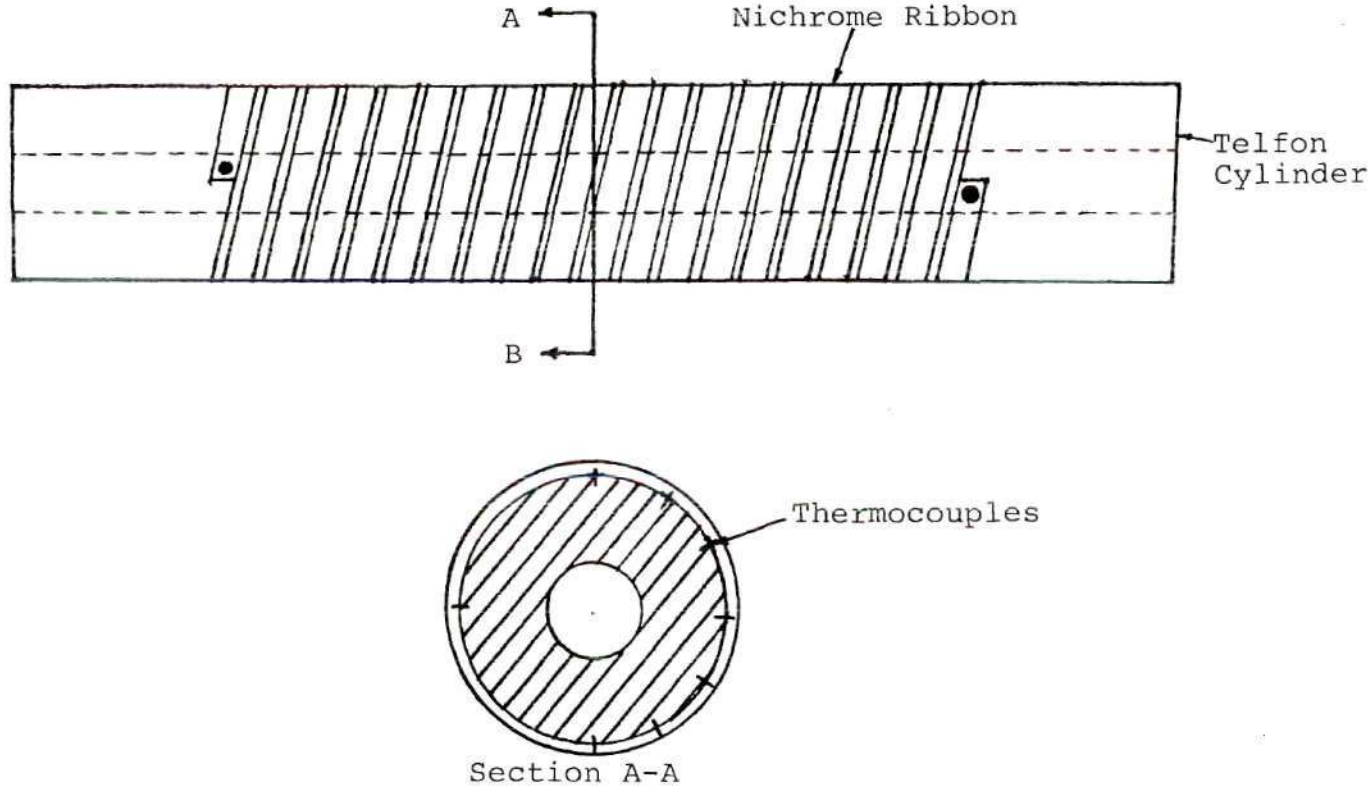

Figure 6. Construction Details of Heat Transfer Test Cylinder.

which is separated by 0.0156 inch ridges. The heated section covers a 4-inch span which occupies the central portion of the fluidized bed. Nichrome ribbon is placed in the groove by first holding the cylinder in a lathe chuck, and slowly rotating the chuck by hand. Care has been taken to apply uniform tension to entire length of the ribbon. The ends of the ribbon are secured in place using two 8 x 32 screws completely embedded in the cylinder wall. The screw posts also serve as power supply leads. The central two helices of the twenty eight turns are used for the determination of the local and the average heat transfer coefficient from the heated cylinder. The test cylinder has seven thermocouples placed at intervals of 30 degrees from each other covering one half of the circumference. Another thermocouple is placed at symmetrical location with respect to thermocouple number four (see Figure 6). Preliminary test runs showed that temperature data obtained using these eight thermocouples is sufficient to establish a good approximation to actual circumferential temperature profile. Other pertinent data needed for evaluation of local heat transfer coefficients are the voltage drop across the heating ribbon and the current flowing through it.

Each of the eight copper constantan thermocouples made out of 30 gage wire has been drawn through a 0.0625-inch diameter hole and placed at the angular locations along the centered two helices shown in Figure 6. The ninth thermocouple is located in the core of the cylinder. These thermo-

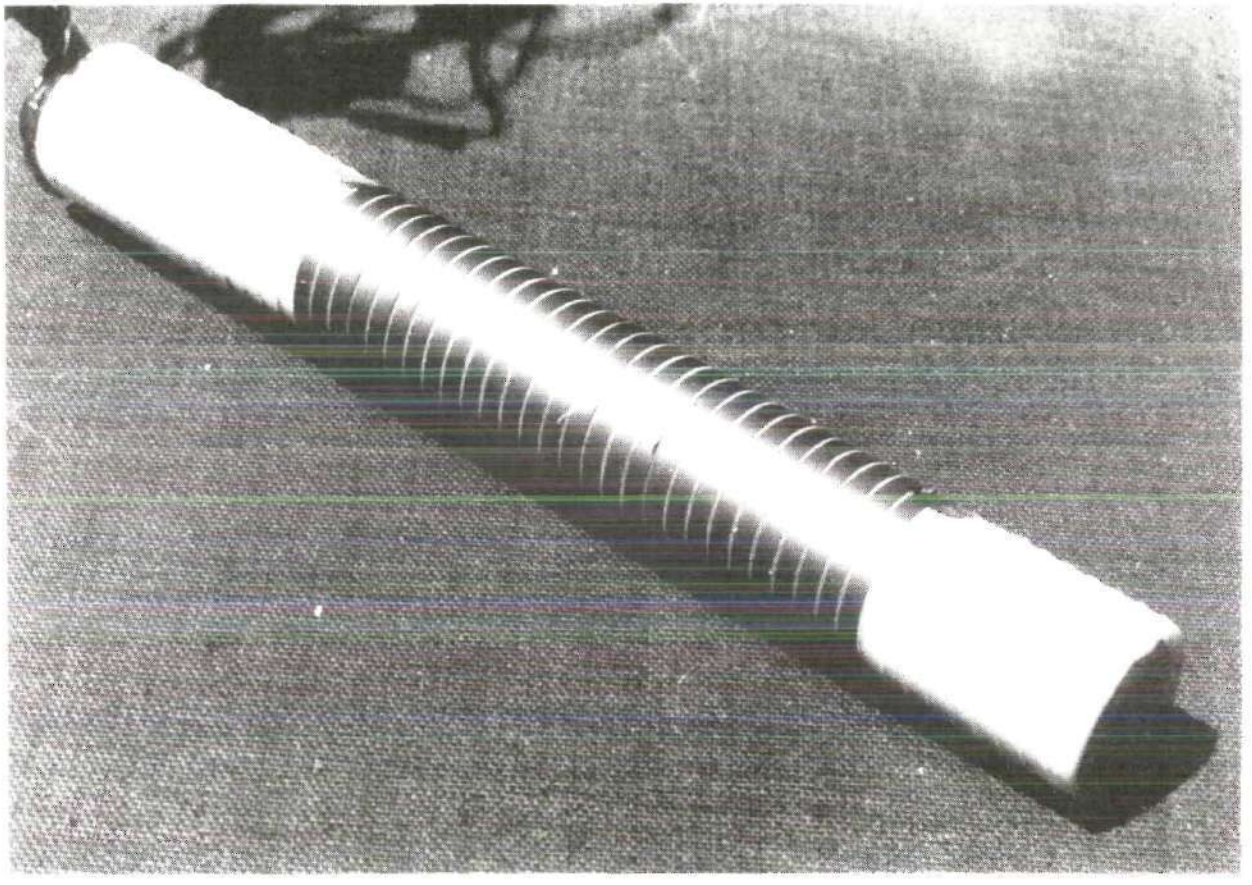

Figure 7. Finished Heat Transfer Test Cylinder.

couple wires coming out of the core are carefully tagged for future identification.

Electrical continuity between each thermocouple and the ribbon checked by using an ohmmeter insured good pressure contacts of thermocouples to the ribbon. The test cylinder has been examined for any short circuits or nonuniformities under a magnifying glass. Outside ribbon surface and the top of the ridges between them are in flush with each other, assuring smooth four inch span on the surface of the test cylinder. Figure 7 is a photograph of the finished cylinder prior to its installation in the test section. Since the central two turns are instrumented for temperature measurements thirteen turns on either sides of the test section act as guard heaters assuring no axial conduction from the central portion of the test cylinder.

III.1.5. Supporting Instrumentation

The test cylinders developed for measuring local pressure fluctuations and heat transfer have been adequately instrumented. A concise description of the set up is given here. A preamplifier with its own power source is used to supply the excitation voltage. A strain gage type transducer, with its sensitive resistance elements arranged electrically in the form of a wheatstone bridge, is connected to the carrier preamplifier. Excitation and signal circuits are carried in a single cable with individually shielded lead wires. A 2400 Hz-5 volts signal supplied by the preamplifier is used as

excitation signal for the strain gage pressure transducer, and the preamplifier reference circuit. The reference circuit of the preamplifier provides the voltage necessary to correct the transducer unbalance. It also furnishes an adjustable zero suppression voltage and it is used in the calibration of the preamplifier as well as setting the zero output position of the indicator.

Before recording the signal it is monitored on a dual beam oscilloscope. Stripchart records of the signals are obtained using a direct writing strip chart recorder. The signal is also recorded on tape with a F-M recorder. Figure 8 is a photographic view of the set up used for recording the pressure fluctuations. A schematic diagram of the equipment used is shown in Figure 9 and experimental procedure for recording of pressure fluctuations is presented in a later section of this report.

The recorded pressure fluction signal is analyzed for its basic statistical properties (i.e., root mean square value, power spectrum, autocorrelation function, and probability density function) with a Fast Fourier analyzer system. An x-y plotter is used to obtain these graphs. Figure 10 shows a general view of the arrangement used for pressure fluctuations analysis. Figure 11 shows in schematic form the equipment used in Fourier analysis of the recorded signals.

Figure 12 is a view of the experimental set up for heat transfer studies and Figure 13 shows the associated

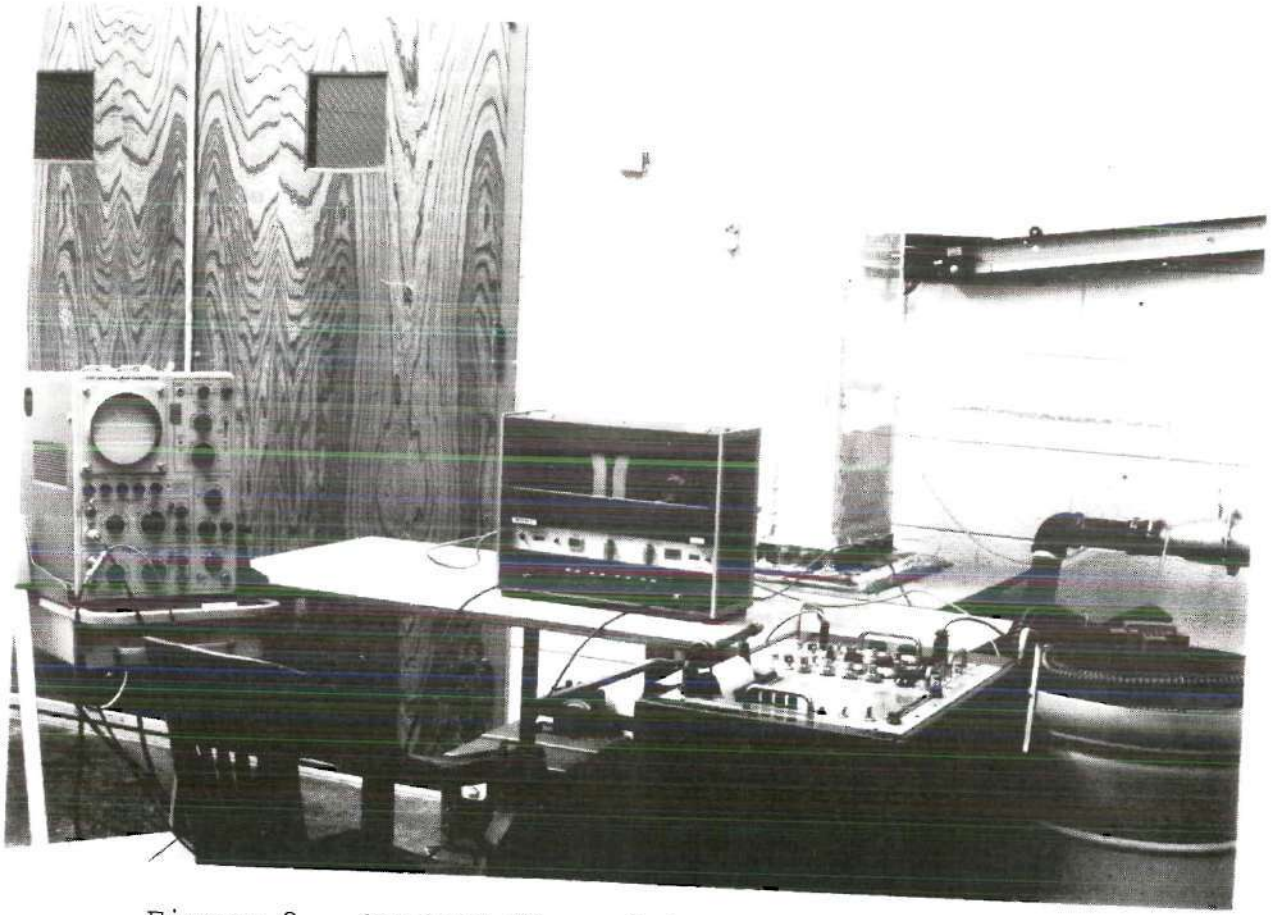

Figure 8. General View of Set-Up Used for Pressure Fluctuations Recording.

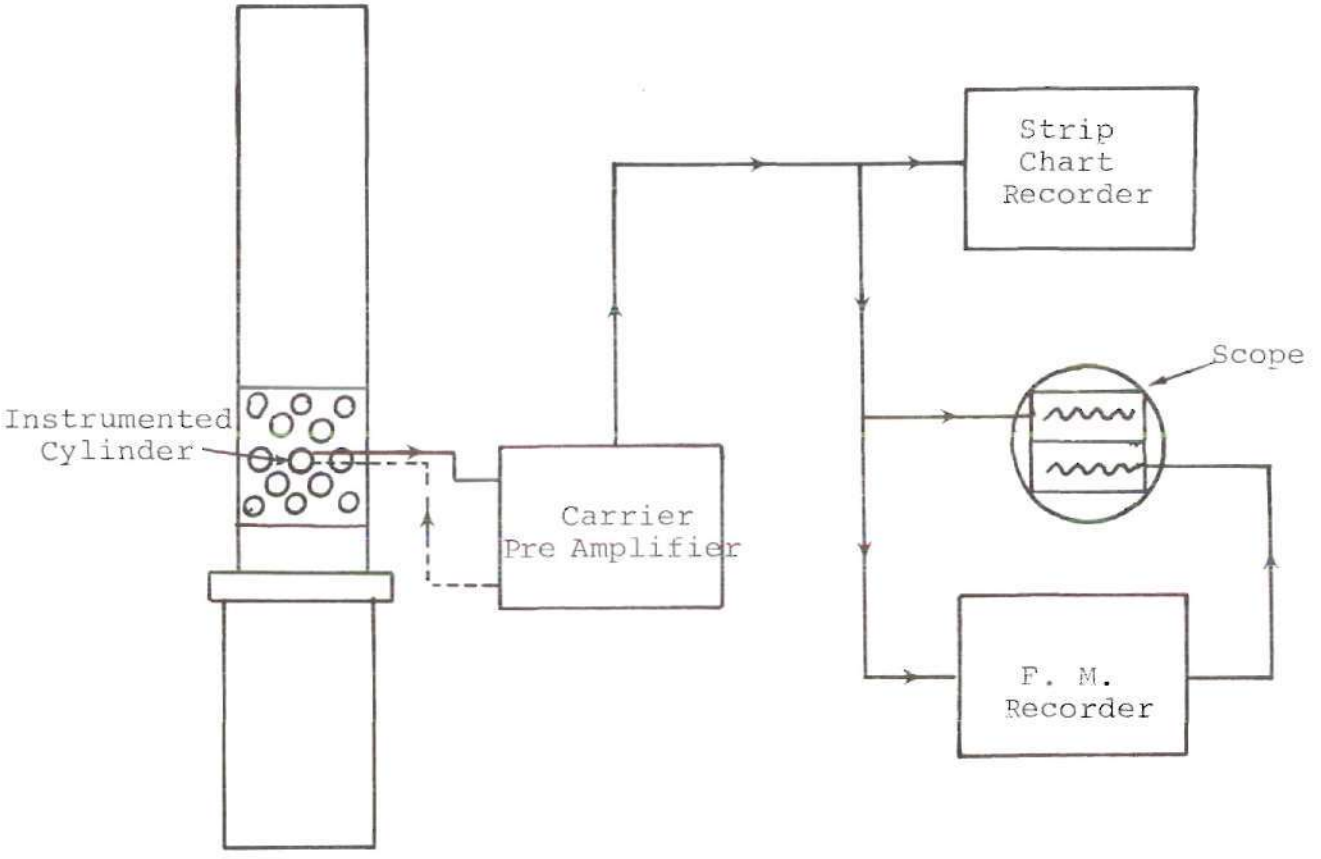

Figure 9. Schematic Diagram of Pressure Fluctuation Recording Circuit.

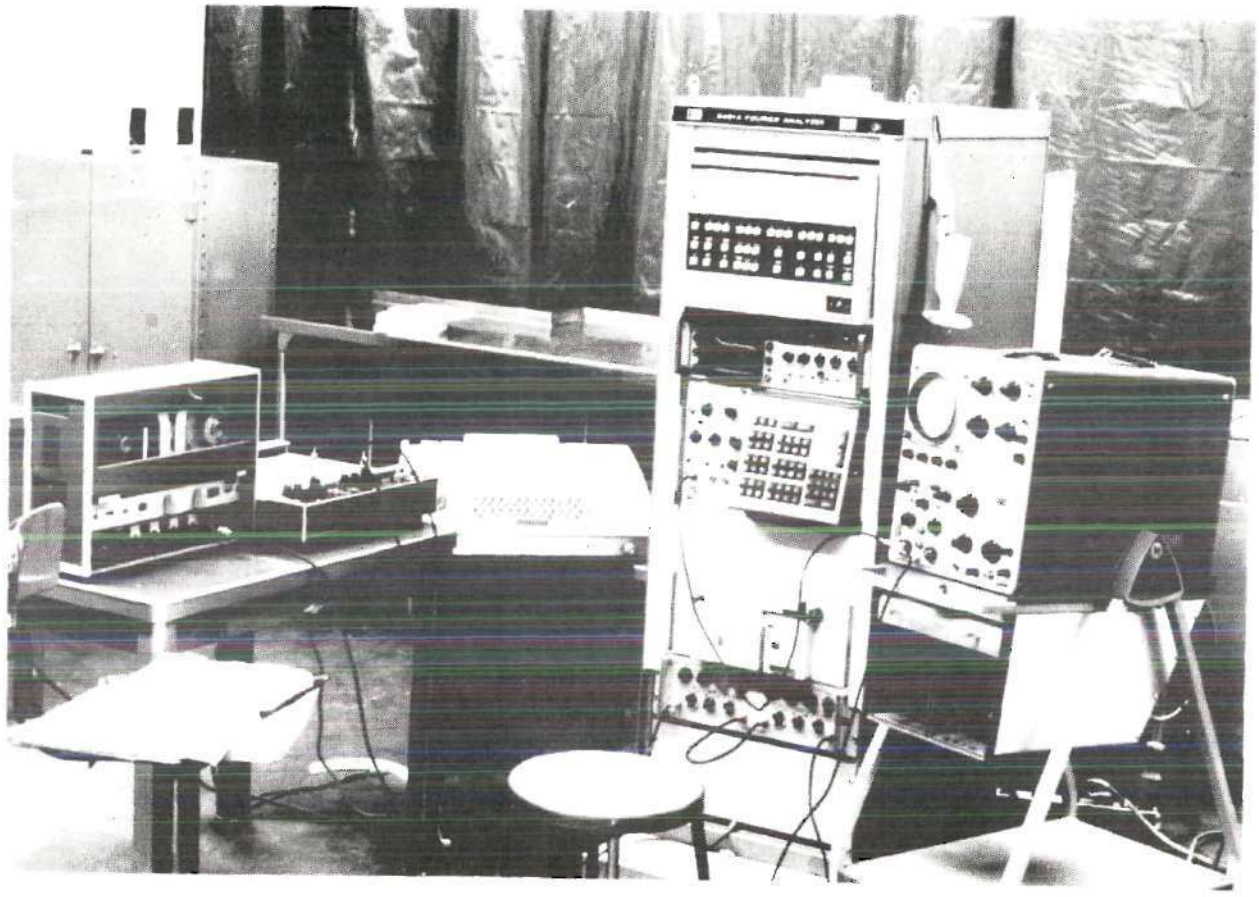

Figure 10. General View of the Instrumentation Used for Analysis of Pressure Fluctuations.

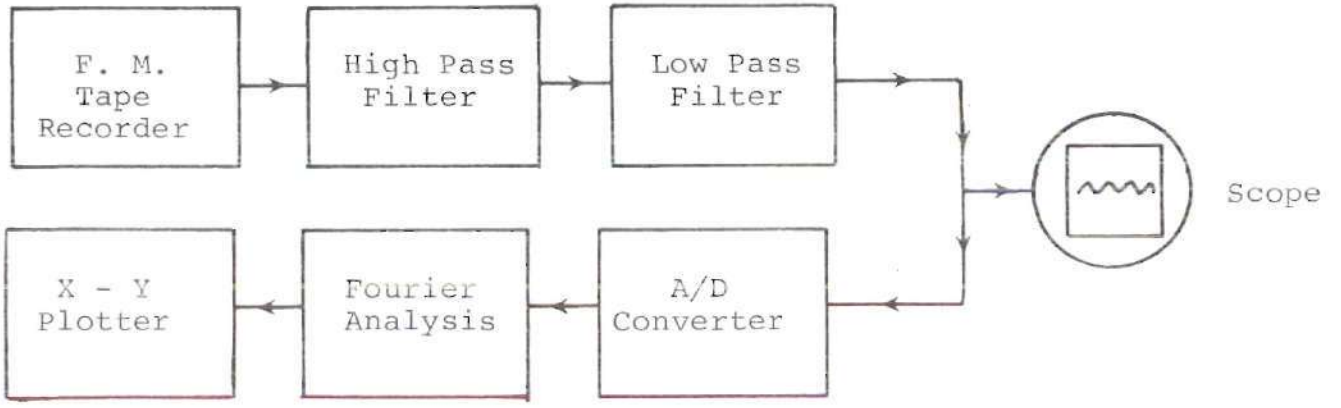

Figure 11. Block Diagram of the Processing Scheme Used for Pressure Fluctuation Analysis.

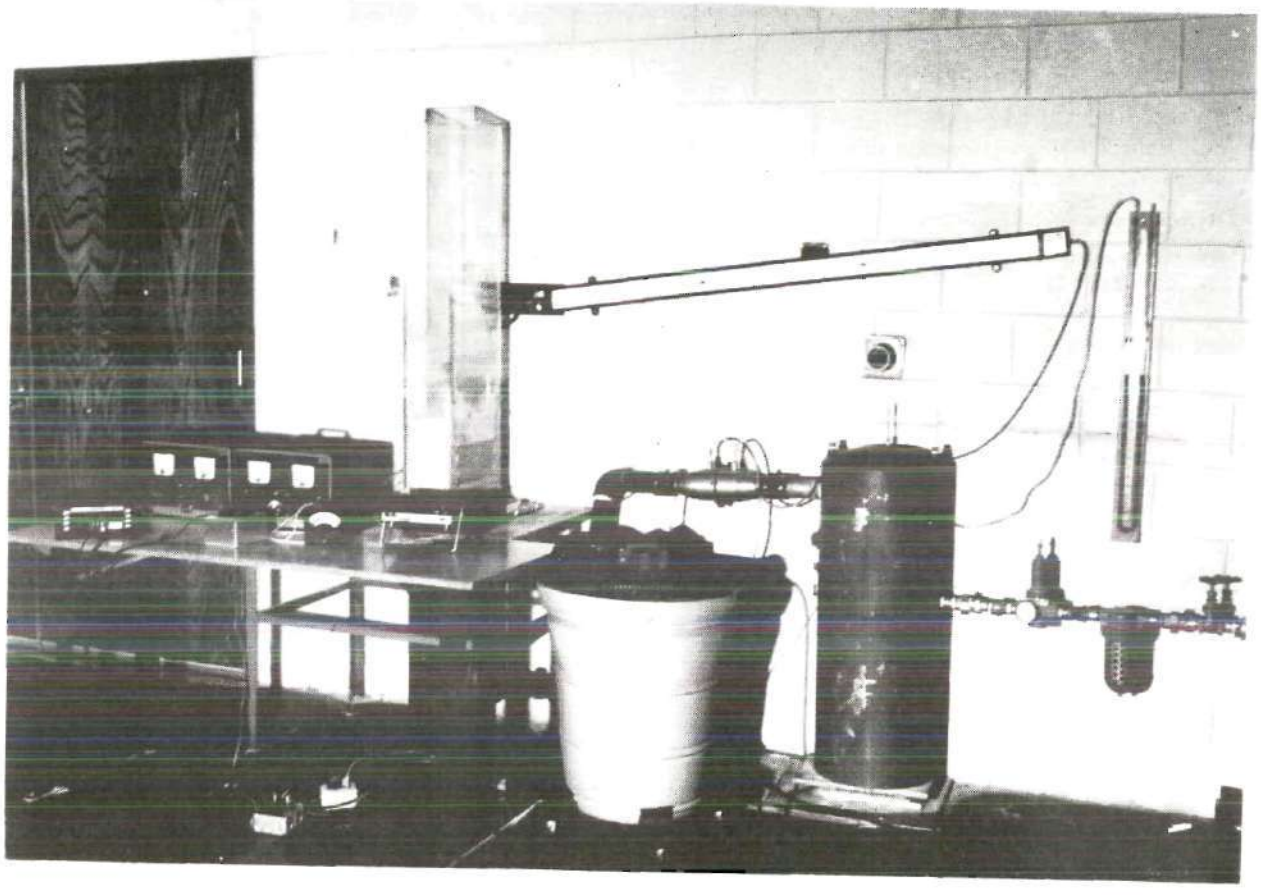

Figure 12. General View of the Experimental Arrangement for Heat Transfer Measurements.

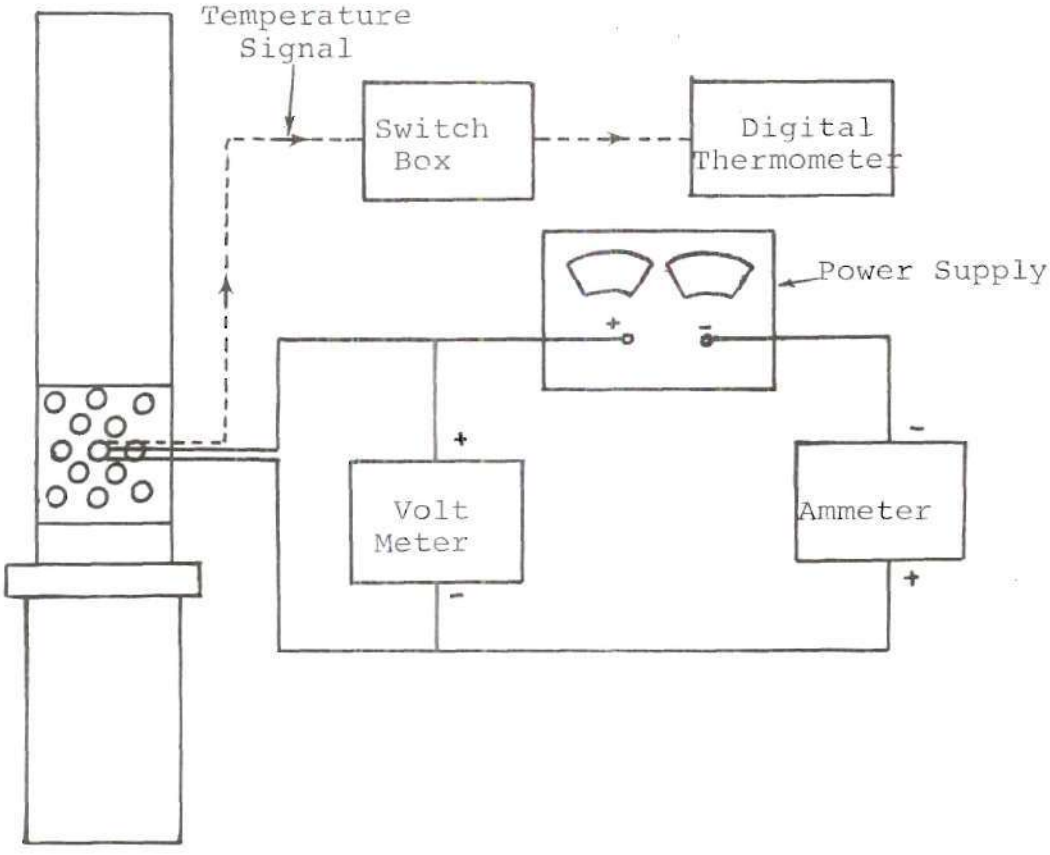

Figure 13. Schematic Diagram for Heat Transfer Measurements Circuit.

equipment in schematic form. During the heat transfer measurements power to the Nichrome ribbon is supplied from a 12 volt constant power supply. Thermocouple readings are taken manually with a digital thermometer. They are used in the calculation of the local heat transfer coefficients.

III.1.6. Data Collection Procedure

Pertinent data for any set of experimental variables are gathered in two phases because of the complex nature of the experimentation. During phase I, pressure fluctuations are recorded. At the conclusion of the experiments of phase I heat transfer measurements are made during phase II. During both of these phases every effort has been made to assure the same fluidized conditions.

A series of test runs is initiated by placing a known quantity of fluidizing material in the column. The material is then fluidized for several minutes with air. The bed is then allowed to settle down by slowly reducing the air flow, and the resulting settled bed height is measured and recorded. Next, an initial air flow rate sufficient to cause incipient fluidization of the bed is established. Each successive test run is then made by slowly increasing the air flow rate, in steps, until the desired highest flow rate for the particular series of runs is reached. Data collection procedure for both phases of test runs is discussed under the following categories.

Procedure for Recording of Pressure Fluctuations. The signal from the strain gage transducer is balanced and ampli-

fied. The adjustable zero suppression voltage is used to suppress the mean (or a steady component close to mean) of the fluctuating signal. The signal is monitored on a dual beam oscilloscope simultaneously, before and after recording on tape. A representative strip chart records of the signal are also obtained. The output signal level of the F-M recorder used in this investigation is $\pm$ 1 volt peak to peak. Hence, it is possible to have one to one correspondence between the input and the output signals from the tape recorder, provided that the input signal does not exceed $\pm$ 1 volt, peak to peak. In case the output signal from the preamplifier exceeds $\pm$ 1 volt, peak to peak, in any test run, the input signal to the recorder is attenuated by reducing the amplifier gain. This is accomplished by using the attenuator switch on the preamplifier panel which is a stepped gain control and attenuates the input signal by a predetermined factor.

Heat Transfer Data Collection Procedure. The evaluation of local heat transfer coefficient requires a prior knowledge of the temperature distribution around the circumference of the tubes. The temperature profile is utilized to estimate local circumferential conduction losses which aids in the determination of true local transfer coefficients. These are then integrated around the circumference in order to obtain the average heat transfer coefficient as a function of operating variables such as tube spacings, fluidizing

velocity and bed material.

Test runs during phase II of the experiments are conducted to measure the temperature distribution around the circumference of the horizontal tubes placed in fluidized beds of different materials, and under different conditions. After the test cylinder has been placed at the desired location in the tube bundle, the fluidizing material to be tested is poured in the fluidizing column and air flow rate is set at some initial value. Voltage and current through the ribbon is adjusted to the desired value. Two to three hours time has been allowed for the system to come to a steady state. It is important to mention here that because of the passage of bubbles in the fluidized beds the heat transfer coefficient at any location in the fluidized bed is expected to fluctuate with time. These fluctuations in heat transfer coefficient result in fluctuating temperatures at all locations on the cylinder in the fluidized bed. Though the heat capacity of the Nichrome ribbon is enough to damp out most of the rapid fluctuations of the temperature, still the temperature of the ribbon has been found to drift slowly. In most cases the drift at any particular thermocouple location did not exceed by more than $\pm$ 2°F from a mean temperature excess (over ambient) of 175°F. In some cases the drift reached a value of $\pm$ 3°F. In such instances the duration of the experiment has been extended long enough to minimize these temperature fluctuations.

The ribbon is assumed to be operating under steady state conditions if the arithmetic mean of the high and low value of fluctuating temperature at a location did not change more than 0.1°F in about three minutes. Once such a steady state criterion is reached, the arithmetic mean of high and low value of fluctuating temperature at each of the nine locations (eight around the circumference and one in the core), voltage drop across the ribbon, and flow of current through the ribbon are recorded. In most of these experiments the top of the fluidized bed has been found to be fluctuating. In such cases the arithmetic mean of the low and high value of the fluctuating height is taken to be the height of the fluidized bed.

III.2. Analysis of Experimental Data

The heat transfer coefficient in a fluidized bed is governed by the movement of particles in the vicinity of the heat exchange surface. Thus it is important to establish the extent of particles movement in order to explain the mechanism associated with the variation of the experimentally determined local heat transfer coefficient. The movement of particles and/or bubble passage is intimately related to the magnitude and frequency of pressure fluctuations in the vicinity of the heat transfer surface. For instance, defluidization corresponds to a level of pressure fluctuations lower by an order of magnitude below that of a highly

fluidized zone. Slugging and/or passage of bubbles on the other hand corresponds to intense and somewhat regular (narrow band) fluctuations. Small random fluctuations at relatively high frequencies suggest uniform fluidization. Since passage of bubbles in the vicinity of the surface is a major source of particle movement near the surface, a moderately bubbling bed exhibits higher local and average heat transfer coefficients when compared to those obtainable in a uniformly fluidized bed.

Pressure fluctuations in the present study have been characterized by their statistical properties. The records of the characteristics of pressure fluctuations have been used as a basis to assess the particle movement in the vicinity of the heat transfer surface. Measured values of temperature and power input have been utilized to calculate the local heat transfer coefficient around the circumference of the tubes placed in the fluidized bed. Average heat transfer coefficients for the tubes have been obtained by integrating the local heat transfer coefficients. The procedure used to analyze the pressure fluctuations records, and the heat transfer data is discussed under the following categories:

Analysis of Pressure Fluctuations

Evaluation of Local and Average Heat Transfer Coefficients

III.2.1. Analysis of Pressure Fluctuations

The pressure signals have been analyzed via digital methods to obtain such statistical properties as mean square values, probability density functions, power spectra, and autocorrelation functions. The mean (or steady) component of the fluctuating pressure signal is annuled at the time of the recording but to make it absolutely certain that mean component is zero, the recorded signal is passed through a high pass filter. This filter nullified any fluctuations below 0.2 Hz. The next step is to digitize the analog signal. A Hewlett Packard analog to digital converter has been used for this purpose. "Aliasing," which comes about from the fact that, when an analog signal is sampled, the spectrum replicates around multiples of the sample frequency, is avoided by using a low-pass filter. This filter blocks off fluctuations above a certain set frequency F_{max} (criteria for the selection of F_{max} are discussed in a later part of this discussion). For this filtered signal, the Nyquist frequency (or folding frequency) is F_{max}. Shannon's sampling theorem requires that, for such signals, the sampling time interval must be at least equal to $\frac{1}{2F_{max}}$. The analog signals in these tests have been sampled at intervals of $\frac{1}{2F_{max}}$. After the digitization process, the Fast Fourier Transform algorithm is used to calculate the coefficients of all the harmonics of the Fourier series representing the signal. Using these coefficients, the power spectra of 55 sampled

records have been averaged in order to obtain a final power spectra. Initially, power spectra for all the recorded signals were obtained by choosing a very high value for F_{max} (500 Hz), and it was found that power spectra in all cases become negligible after about 12 Hz. Hence, an F_{max} of 12.8 has been selected, and all the signal records have been re-analyzed on this basis. This is done for the sake of consistency. A spectral band width of .2 Hz has been used in all the cases. This band width is chosen as a compromise between the resolution and the length of a signal record required for accurate analysis. "Leakage" (which comes about from the fact that if the signal is non-periodic in the sample window, i.e., if the signal frequency falls between two (2) discreet spectral lines, then the signal's power "leaks" out to the adjacent lines) has been reduced by using a "Hanning" sample window in this analysis. Mean square values for the signals have been obtained by integrating the power spectral density function and then correcting it for the Hanning factor. Power spectra have been normalized by dividing them by the mean square value. Normalized power spectra have been plotted with an x-y plotter. Since the power spectral density function and the autocorrelation function furnish similar information in the time domain and frequency domain respectively, autocorrelation functions have been obtained for a few cases only. This provides a check on the two methods. Probability density functions have been obtained by first obtaining the

histograms for the signals and then normalizing the histograms to unit area. For the recorded pressure signals, the power spectra, autocorrelation function, mean square values, and probability density function have been obtained in this manner and are discussed in Chapter IV.

III.2.2 Evaluation of Local and Average Heat Transfer Coefficients

The local heat transfer coefficient is evaluated by using the experimental data and the heat balance model applied to a differential arc length of the Nichrome V ribbon. The method of analysis is as follows:

Consider the differential length of Nichrome V ribbon shown in Figure 14. Steady state conditions yield the following heat balance

Heat generated by current i + Heat conducted in left face = Heat conducted out of right face + Heat transferred to the fluidized bed

or in symbolic form

$$3.412\ i^2\ R'\ dx + \left(k_N \frac{dt}{dx}\ TW\right) = -k_N\ TW\ \left(\frac{dt}{dx} + \frac{d}{dx}\ \left(\frac{dt}{dx}\right)\ dx\right) + h_t\ W dx\ (t-t_b), \tag{16}$$

where k_N is the thermal conductivity of the Nichrome V ribbon. k_N is assumed to be constant. The theraml conductivity of Nichrome V is equal to 6.473 BTU/hr °F ft.

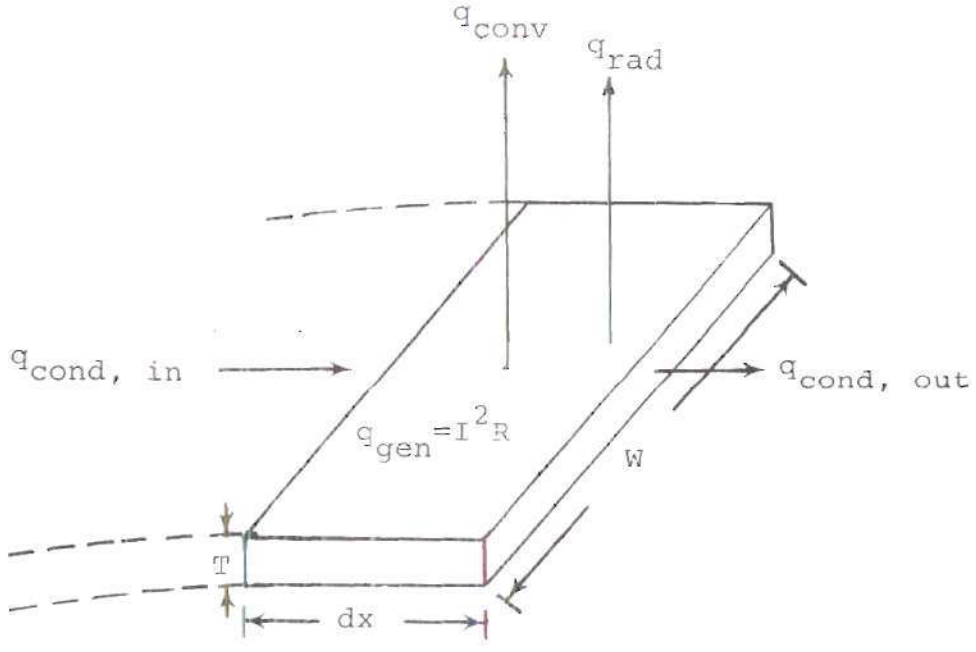

Figure 14. Heat Balance for a Differential Length of the Nichrome V Ribbon.

Expressing the arc length of the ribbon around the teflon cylinder in terms of θ, the angle subtended and solving for h_t gives

$$h_t = \frac{327.56\ R'\ i^2}{(t-t_b)} + \frac{10200\ \frac{d^2t}{dx^2}}{(t-t_b)} \quad . \tag{17}$$

The expression for h_t in Equation 17 contains two terms, the first term representing the contribution due to the heat generation in the ribbon, and the second term accounting for the effect of circumferential conduction along the ribbon.

Tests have been conducted with a single cylinder with air flowing normal to it without any fluidizing medium. The primary objective of these tests are to estimate the extent of augmentation in heat transfer due to fluidization as influenced by the various parameters considered in this investigation. The combined local heat transfer coefficient (h_t), as determined by using Equation 17 has been corrected for radiative heat transport. In other words,

$$h_r = \frac{\sigma\ \varepsilon_N\ (T^4-T_a^4)}{(T-T_a)} \quad , \tag{18}$$

where ε_N is the emissivity of the Nichrome V ribbon and T_a is the absolute temperature of the air when the fluidizing material is not present. Finally, the convective heat transfer coefficient is obtained from the gross value in a fluidized medium, h_t, from the equation

$$h_\theta = h_t - h_r \quad . \tag{19}$$

For those tests conducted in the presence of fluidization the local heat transfer coefficients as obtained from Equation 17 has not been corrected since the heat transfer surface is in intimate contact with the fluidizing medium which is exchanging heat through conduction from the surface as well as convection from the gas in its immediate vicinity. Moreover, the magnitude of convective heat transfer coefficient is many times greater than that for the case of an air enclosure while the magnitude of radiative heat transfer coefficient remains essentially unchanged.

In addition, it is assumed that no heat is lost by conduction through the teflon cylinder in the axial or radial direction. The facts that Nichrome V ribbon has been wound on a relatively poor heat conducting material (i.e., Teflon), and that the temperature inside the core of the hollow cylinder has been found to be less than 1% different from the average surface temperature of the ribbon have led to the assumption that the radial and circumferential conduction in teflon can be neglected.

The use of Equation 17 to calculate the local heat transfer coefficients require a prior knowledge of variation of unit resistance with temperature, R', and the second derivative of temperature of the ribbon, $\frac{d^2t}{dx^2}$, at each point

around the circumference of the cylinder. R' is calculated from equation

$$R' = R'_o \left[1 + \alpha_o (t-t_o)\right] . \qquad (20)$$

where t_o is any reference temperature at which R'_o and temperature coefficient of resistivity α_o is known. A Kelvin bridge and a D-C null detector have been used to measure the resistance of Nichrome ribbon at 74.1°F and also its temperature coefficient of resistivity. The resistance of 8 ft. length of ribbon is found to be 3.4736 ohms thus providing a value of 0.4342 ohms per foot for the resistance at the reference temperature of 74.1°F. The temperature coefficient of resistivity at 74.1°F has been calculated to be 1.100×10^{-4} per °F. The temperature at any location of the ribbon around the circumference of the cylinder has been obtained by interpolating the seven measured temperatures. A piecewise cubic spline interpolation technique has been adapted for this purpose. Cubic spline interpolation technique is preferred over the other available interpolation methods because it results in temperature functions which are twice continuously differentiable. The resulting temperature functions from spline interpolation have been differentiated twice to determine values for $\frac{d^2t}{d\theta^2}$ at all locations around the circumference of the cylinder. The computer program written for spline interpolation required prior knowledge of slopes of temperature distribution at two end points (i.e., at 0° and 180°

from the forward stagnation point) before interpolation could begin. In this investigation the temperature distribution around the test cylinder is assumed symmetric which provided the required condition of zero slope at the forward and backward stagnation points. This assumption in part is substantiated since the temperature at the 90° and 270° location varied within 1°F at all times.

The temperature distribution obtained by such a cubic spline interpolation is continuous permitting evaluation of local heat transfer coefficient at intervals other than 30 degree intervals. The local heat transfer coefficients evaluated at 5 degree intervals over the entire circumference have been averaged to obtain the average heat transfer coefficients, i.e.,

$$h_{avg} = \frac{1}{2\pi} \int_0^{2\pi} h_\theta \, d\theta \tag{21}$$

The integration is performed numerically using the trapezoidal rule. Using these local and average values of heat transfer coefficient, the corresponding Nusselt numbers have been evaluated using the following equations, i.e.,

$$N_{Nu,\theta} = \frac{h_\theta D_t}{k_a} \tag{22}$$

and

$$N_{Nu,avg} = \frac{h_{avg} D_t}{k_a} \tag{23}$$

where k_a is the thermal conductivity of air evaluated at the film temperature, and D_t is the outside diameter of the test cylinder.

III.3. Range of Experimental Conditions

The experimental program in this investigation has been done in two phases. In the first phase, tests have been conducted to record pressure fluctuations around the circumference of the test cylinder. The second phase, under similar flow conditions, consisted of test runs for making heat transfer measurements. The fluidization material consisted of, Ottawa sand, silica sand, and glass beads. These materials have been selected to cover a wide range of particle diameters. They also cover a spectrum of particle shapes, ranging from the almost spherical shape of glass beads to the angular shape of silica sand particles. The physical properties of the various particles are listed in Table 1.

On the basis of preliminary observations it was decided to exclude any further experiments for the case of a tube arrangement with a pitch to diameter ratio of 1.1, in large particle bed, since this resulted in a tendency to form bridges between adjacent tubes. Such bridging causes fluidization behavior of the bed which is deterimental to satisfactory operation of such heat exchangers.

A tube bundle with a pitch to diameter ratio of 1.3, has been used to conduct the test runs during phase I of the

Table 1. Physical Properties of the Solid Particles*.

Material	Approximate Shape	Mean Size Microns	Particle Density lbm/cu-ft	Packed Bed Density lbm/cu-ft	Packed Bed Void Fraction	Minimum Fluidization Velocity ft/sec
Glass Beads	Spherical	230	138	91.75	.335	.16
Ottawa Sand	Spherical	514	159	103.65	.355	.74
Silica Sand	Angular	715	160.7	94.53	.406	1.34

*The procedures for estimating the physical properties of particles are described in Appendix B.

program. This compromise avoids bridging between adjacent tubes and the spacing is not wide as to avoid the influence of neighboring tubes of the tube bundle. In these experiments, the tube bundle has five rows, with the test cylinder located in the central location of the bundle. A range of superficial air velocities has been selected from a minimum value at which the pressure fluctuations at the narrowest spacings of the tubes are barely noticeable up to a maximum velocity at which the pressure fluctuations at all locations appeared to be uniformly intense.

At the lower range of the superficial velocity of the air, the pressure signal at different locations around the tube circumference vary significantly. Hence these signals have been recorded at a large number of circumferential locations. But as the superficial air velocity is increased, the signal around the periphery of the cylinder progressively become uniform. Hence, the number of locations at which the signals are recorded has been reduced. The recording time for the signal at each location is five minutes. This time interval is based on the experience gained during the preliminary test runs. In those tests, signals were recorded for up to twenty minutes at each location. On comparison of the power spectra corresponding to the signal recorded for twenty minutes with that recorded for five minutes, it was decided that the latter was of acceptable duration. Test condition for phase I of the experiments are summarized in

Table 2.

In phase II of this study, tests have been conducted to measure local heat transfer coefficients around the circumference of tubes of horizontal tube bundle placed in fluidized beds. Several initial runs were made with single cylinder and no fluidized bed to systematize the test procedure. These runs also helped in checking the accuracy of measurements. Three different tube bundles with pitch to diameter ratios of 1.1, 1.3, and 1.5 have been chosen for these tests. The pitch to diameter ratios of the three tube bundles cover the range from a minimum tube spacing below which good fluidization cannot be obtained, because of the bridging of solid particles and channeling of fluidizing air, to a maximum spacing above which each tube in the tube bundle acts as an independent tube and thus makes the heat transfer from individual tubes unaffected by the presence of other tubes. Almost all of the tests have been conducted with tube bundles having five rows. In these tests, the instrumented cylinder is located in the middle of the tube bundle. In a few tests tube bundles having three rows have been used, in which case the instrumented cylinder provides a basis to describe the effect of position of the tube in a tube bundle on the heat transfer. The superficial air velocities tested for each material, range from velocities at which the bed stayed packed, to highest velocities at which measured average heat transfer coefficient start to drop off or

Table 2. Summary of Test Conditions (Phase I).

Run No.	Material	Superficial Air Velocity ft-sec	U/U_{mf}	Number of Location for Recording Signals
1	Ottawa Sand	.72	.97	7
2	Ottawa Sand	.89	1.2	7
3	Ottawa Sand	1.14	1.54	3
4	Ottawa Sand	1.56	2.11	3
5	Glass Beads	.21	1.3	7
6	Glass Beads	.29	1.8	7
7	Glass Beads	.35	2.19	5
8	Glass Beads	.50	3.13	5

Table 3. Summary of Test Conditions (Phase II).

Bed Material	P/D_t	Number of Rows in the Tube Bundle	Total Number of Runs	Superficial Air Velocity Range ft/sec
None	-	Single Cylinder	6	0.205 - 3.866
Glass Beads	-	Single Cylinder	6	0.190 - 1.032
Ottawa Sand	-	Single Cylinder	6	0.481 - 1.958
Silica Sand	-	Single Cylinder	6	0.942 - 3.259
Glass Beads	1.5	5	6	0.185 - 1.629
Ottawa Sand	1.5	3	6	0.506 - 1.844
Ottawa Sand	1.5	5	6	0.536 - 2.097
Silica Sand	1.5	5	6	0.747 - 3.407
Glass Beads	1.3	5	6	0.150 - 1.153
Ottawa Sand	1.5	5	6	0.511 - 2.288
Silica Sand	1.3	5	6	1.057 - 3.823
Glass Beads	1.1	5	4	0.151 - 0.303

essentially become constant. Table 3 summarizes the test conditions for the experiments done under phase II of this study.

CHAPTER IV

RESULTS AND DISCUSSION

VI.1. Introduction

The rate of heat transfer from tube bundles to the gas streams in the presence of a fluidized bed is strongly influenced by the particle movement. Such a movement of particles is intimately associated with the formation, growth and separation of bubbles, as well as on their passage through the fluidized bed. The entire bubble history gets somewhat altered by the presence of a tube bundle of a constant or a varying pitch to diameter ratio. The central problem of energy transport mechanisms in such systems focuses on an examination of the fluidization phenomena in the immediate vicinity of the tube surface not only at the bottom portion leading into the region of maximum local gas velocities but also in the wake regions where there are tendencies for formation of a defluidized cap.

Visual observations in this investigation are generally restricted to the region of contact of tubes with the transparent vertical end walls of the flow test section. In order to ascertain an extension of these observations across the width of the bed in the direction of the tube axis, additional schemes chosen from such techniques as particle tagging,

capacitance probes and radioactive tracer techniques can be adopted. However, in similarity to the case of flowing fluids over submerged bodies, the local heat transfer rates in the presence of fluidized particles are also dominated by the activity within a film in the immediate vicinity of the surface. In the present investigation an embedded sensitive pressure transducer has been used to record the pressure fluctuations at 30 degree intervals around the tube periphery.

As the general fluidization activity increases, the bubble passage imposes dominant pressure pulses in the vicinity of tube surface. These have been recorded by utilizing an imbedded pressure transducer with a pressure tap and analyzed via Fast Fourier Transform techniques. An associated teflon cylinder, equipped with spirally wound nichrome ribbon heating element and embedded thermocouples placed at 30 degree intervals has been used to determine the local heat transfer coefficients in the dense phase fluidized bed. As the general fluidization activity increases, the influence of bubble passage in the vicinity of the heat transfer surface on the heat transfer coefficient has been recorded. The experimental variables are; bed material, particle size, fluidization velocity, tube spacings and the location of heat transfer cylinder in the tube bundle. The results of visual observations in a plane of intersection of the tube with the vertical end wall, the pressure fluctuations in a vertical plane in the central region of the test section

and the calculated local and average heat transfer coefficients from the heated cylinder have been discussed in this chapter.

VI.2. Visual Observations

The bed was fluidized both with and without tube bundles a number of times for visual observations of particle flow patterns. It was observed that for all materials of the bed the particle flow patterns changed significantly with the presence of tube bundle and also to a greater extent with the changes in air velocity. For column having no internal tubes and at minimum fluidization velocity no visible particle circulation patterns were observed. The movement of particles observed at low fluidizing velocity was a random pulsing motion in a generally vertical direction. Transition from smooth fluidization to bubbling was observed to take place at approximately twice the minimum fluidization velocity. For flow rates more than twice the minimum fluidization velocity, particles seemed to acquire a general overall circulation pattern, rising towards the free surface in the central portion of the bed and then moving downwards towards the bottom distributor plate along the walls as shown schematically in Figure 15.

Particle activity in the bed containing a single tube or tube bundles was a function of the fluidizing velocity of the air, the tube spacing, and the shape and size of the particles. For a bed containing a single tube, the initial

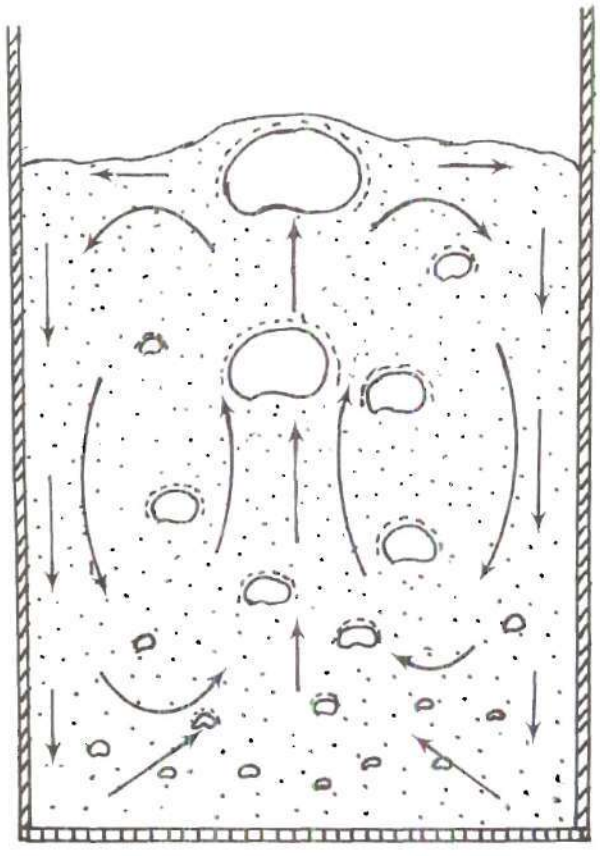

(Arrows show the general patterns of particles movement away from the bubbles)

Figure 15. Particles Flow Patterns in the Bed Without Any Tube Bundle.

activity of particles was noticed at the 90 degree location of the tube. When the particles were fluidized at flow rates about one and a half times that required for minimum fluidization, three distinct flow patterns were observed near the tube. They are illustrated in Figure 16(a). Visual observations indicated that at the bottom of the tube there was a thin film of air of nonuniform thickness. On the top of the tube there was a visible defluidized region. At either side of the tube, air from the thin air film adjoining the bottom of the tube escaped in a sequential chain of bubbles, rather in an alternate manner. Details of such bubble motions were not obtained in this work. Nonetheless, this observation is consistent with the observation of Glass and Harrison (1964) in their experiments with a two-dimensional bed. At increased flow rates the size and frequency of the bubbles originating from either sides of the tube were observed to increase. As the flow rates were further increased to about U/U_{mf} equal to 1.8 (for Ottawa sand) a condition was reached where the defluidized region over the top of the tube was frequently broken up due to the particle circulation pattern caused by the rising chain of bubbles from either side of the tube. Figure 16(b) illustrates such a flow pattern. A similar flow pattern has been observed for the tube bundles. The condition at which the defluidized region at the top of the single tube can be disrupted will have a special significance in the design of fluidized bed heat exchangers containing

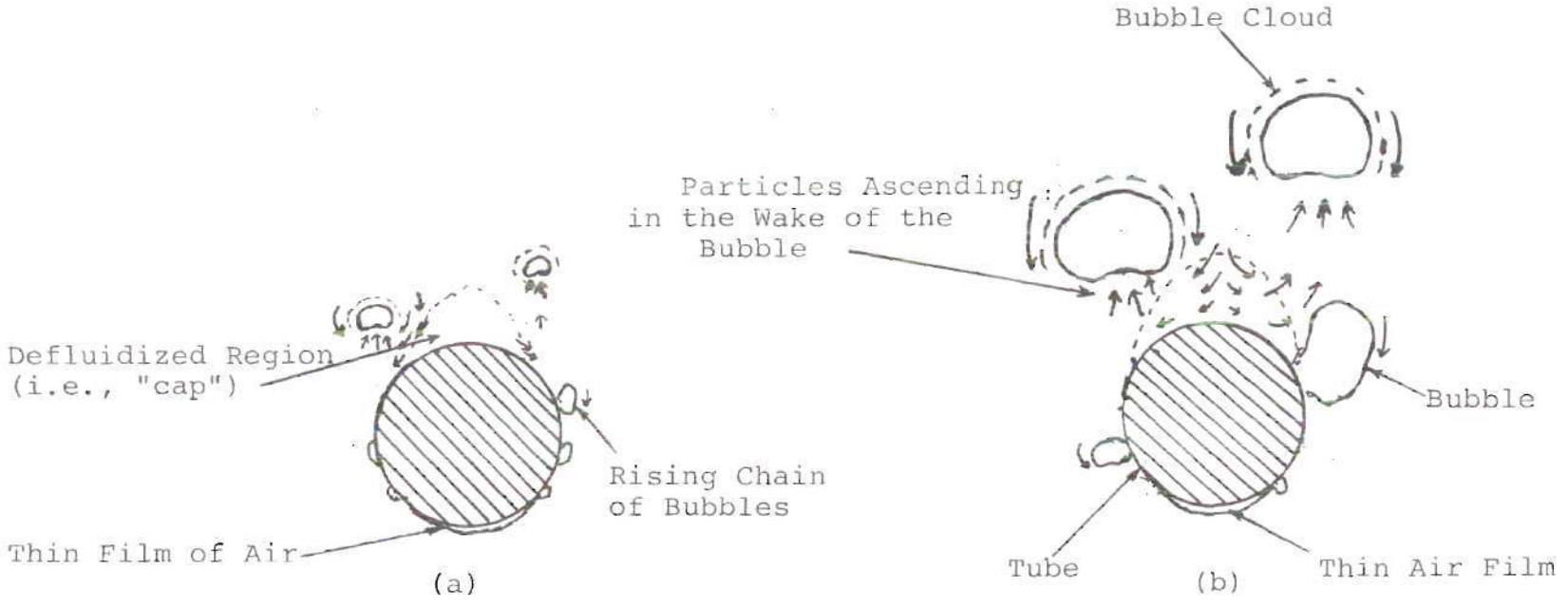

Figure 16. Fluidized Bed Containing a Single Cylinder Operating.
(a) With Fluidization Velocity ≈ 1.0 U_{mf}

(b) With Fluidization Velocity ≈ 1.8 U_{mf}

horizontal tubes. Under these circumstances it is expected that the intensity of the activity of particles on the top of the tubes will increase in comparison with the single tube. As discussed later the local heat transfer coefficient at the top of the cylinder was found to be about one half its value when compared to the bottom at velocities barely under the minimum fluidization velocity.

At fluidization velocities close to minimum fluidization, the bed containing a tube bundle behaved in a manner similar to the bed having a single tube. The initial particle activity was noticed at the region of minimum tube spacing in the horizontal plane. The activity in this region increased with increasing flow rate. The particles between the lower row of tubes and the distributor plate were inactive until the bed was uniformly fluidized. But the activity of the bubbles in the vicinity of the narrow spacing of the tubes was noticed at flow rates even smaller than that required for minimum fluidization. However, there being no visual evidence of the bubbles reaching the top surface of the bed, it is only a conjuncture to state that these bubbles leaked into interstitial particle space. The activity of particles at the top row of tubes was visibly less than that at the lower rows of tubes. For tube bundles with smaller P/D_t ratios (i.e., P/D_t equal to 1.1), particle bridging between adjacent tubes was noticed. This is illustrated in Figure 17. The tubes nearest in the walls inhibited particle

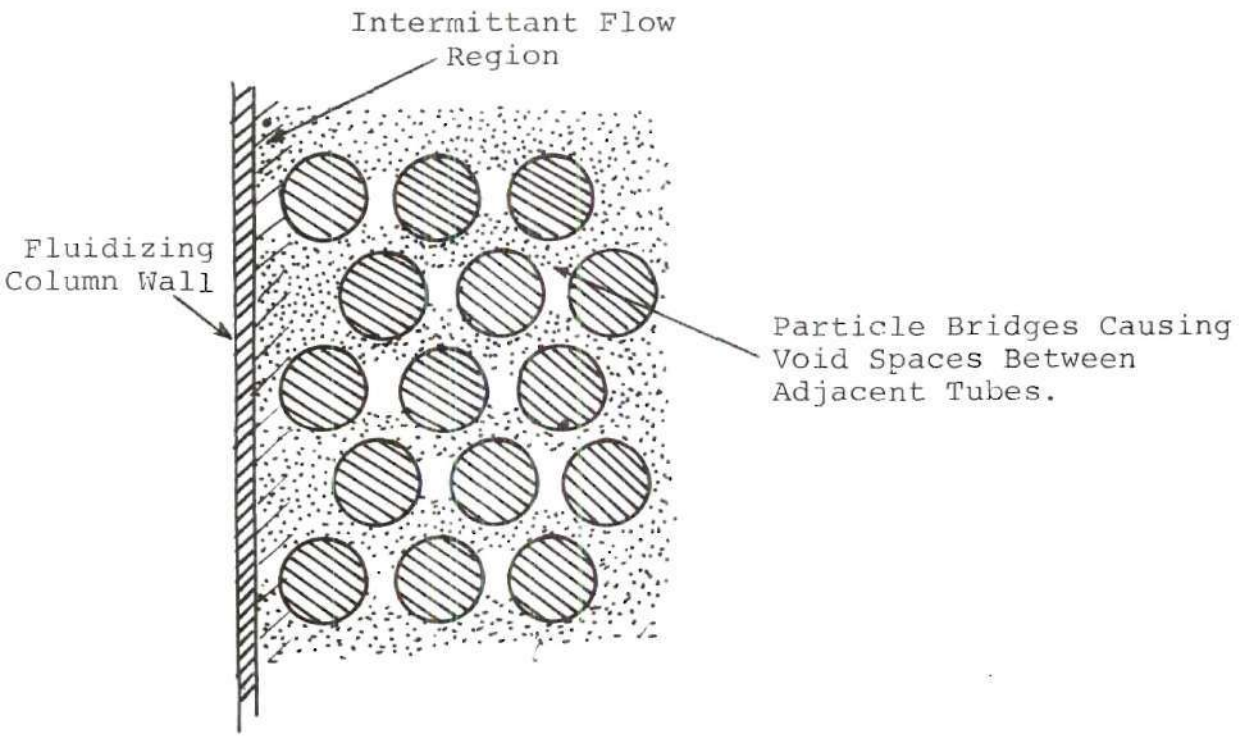

Figure 17. Representation of Particle Bridging and Tube-Wall Effects.

flow and produced intermittant flow in the bed at all P/D_t ratios. In similarity to the observation for the case of a single tube, at higher flow velocities the defluidized caps on the top of the tubes were disrupted and broken up by rising chains of bubbles originating from both sides of the tubes. Depending upon P/D_t ratio of the tube bundle this disruption of the caps was observed to take place at flow rates 1.3 to 1.5 times the minimum fluidization velocity which is considerably lower than the 1.8 value reported for the single cylinder. Based on visual observations the plausible reason for this reduction in the minimum fluidization velocity is that the bubbles originating from the sides of adjacent tubes have a tendency to coalesce to form bigger bubbles which are than broken up because of the zig-zag passage through the staggered arrangement of tubes. Figures 18 and 19 are stop action photographs of the bed during operation. The bed material in both cases was Ottawa sand (514 μm) and the tube bundle in the bed consisted of 5 rows of tubes in a staggered arrangement with P/D_t ratio of 1.5. The bed shown in Figure 18 was operating at room temperature and at an air velocity corresponding to a U/U_{mf} of 1.4. It shows the type of bubbles that are forming and going through the tube bundle. Thin film of gas is apparent under all the tubes and at this instant seem to be a bit more pronounced under the third tube from the right at the top row. Bubbles originating from the sides of the tubes are visible in the

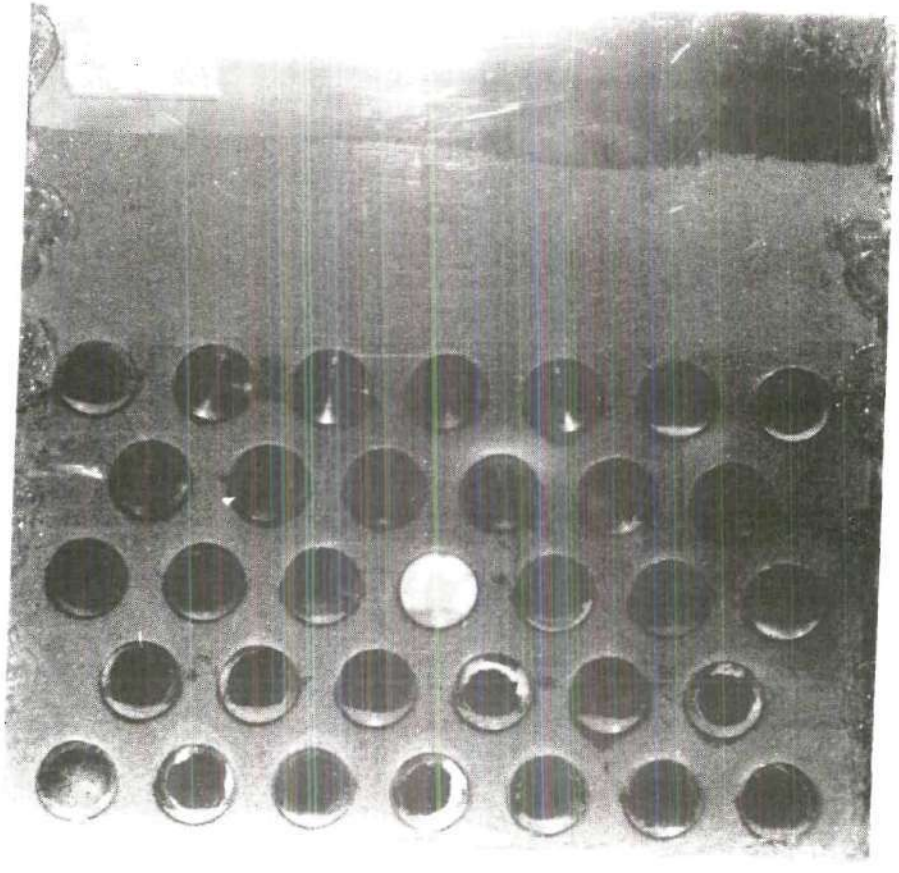

Figure 18. Fluidized Bed Operating at 1.04 ft/sec. (Ottawa sand (514 μm), P/D_t = 1.5, U/U_{mf} = 1.4)

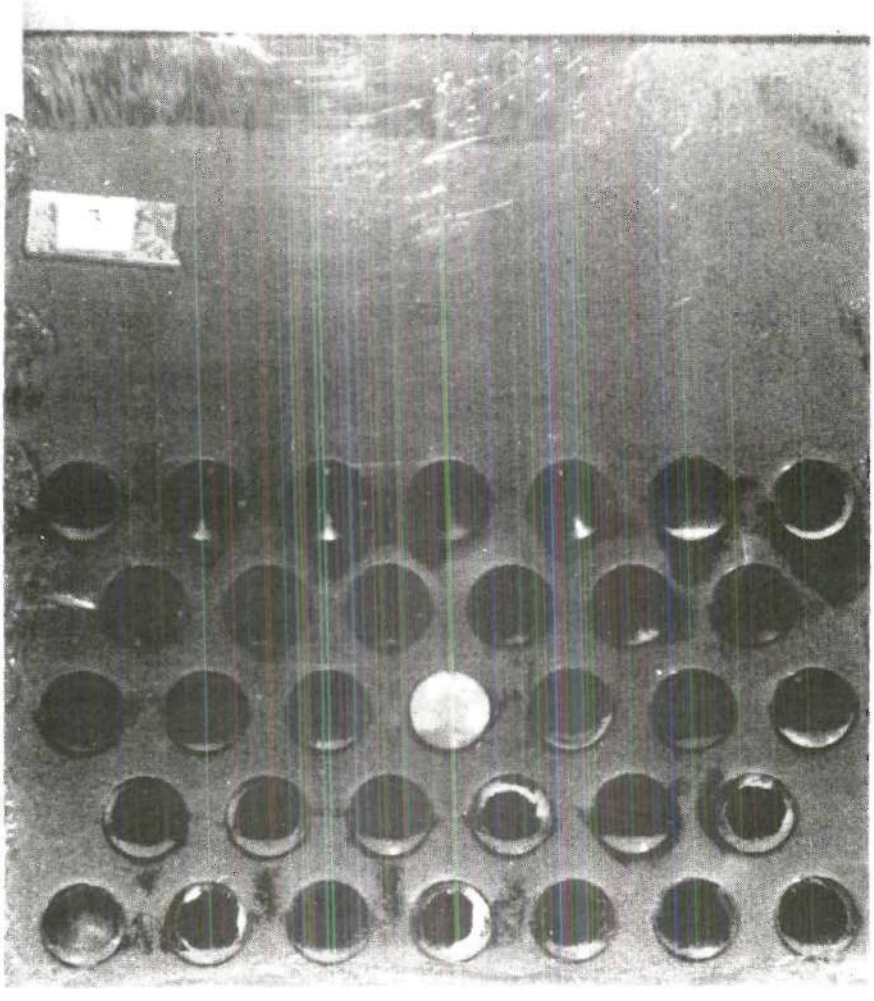

Figure 19. Fluidized Bed Operating at 2.1 ft/sec. (Ottawa sand (514 μm), P/D_t = 1.5, U/U_{mf} = 2.86).

second row in the space between first and second tube from left. Figure 19 shows the same bed operating at air velocity corresponding to U/U_{mf} of 2.86. The bed in this case is bubbling freely and single isolated bubbles are not visible in the photograph. What is apparent from the shadowy patches between the tube spacing is that, in general, particle activity around the tubes has increased significantly.

The visual observations described above have been made through the transparent walls and near the junction of the vertical face with the tube bundle. Hence, they provide definitie information regarding the particle movement patterns only near the containment walls. It is not entirely clear whether similar particle movement patterns apply to the interior of the bed, suggesting the need for pressure fluctuation measurements as were conducted in this investigation.

IV.3. Results of Pressure Fluctuation Measurements

In order for the bubbles to exist inside the fluidized bed its pressure should be sufficient to generate additional upward force to support its roof where the particles are relatively dense when compared to other regions near the vicinity of the bubble. It is natural to expect that the surrounding particles will force the bubbles to the top and their relative movement will cause fluctuations in pressure. These fluctuations in pressure are further superimposed by relatively smaller magnitude fluctuations caused by particle

movement, they (particles) being in a fluidized state. Hence, the pressure fluctuations in fluidized bed are indicative of particle movement both caused by the bubbles and also due to particles being in fluidized state.

A detailed experimental investigation of the local pressure fluctuations around the tube circumference has been undertaken to assess the particle movement in the vicinity of the tube in the interior of the fluidized bed. Besides recording these pressure fluctuations due to bubbles which hit the probe directly, the pressure probe can also pick up signals caused by the particle oscillations. In addition it can sense the bubble passage in the immediate vicinity of the test cylinder. If the distance of the bubble from the probe location increases then the signals will be damped to a larger extent. Figure 20 shows a representative pressure signal record at different locations around the tube circumference. At the time of recording the test section contained Ottawa sand the bed was operating at a fluidizing velocity slightly less than the minimum fluidizing velocity for Ottawa sand (i.e., $U/U_{mf} = .95$). It is apparent from the record that at the 90 degree position,i.e., at the sides of the tubes, the activity of the particles is initiated. No significant fluctuations are observed at the 180 degree location which suggests nonexistence of particle oscillations at the top of the tube thus substantiative, the idea of a defluidized cap existence on the top of the horizontal tubes.

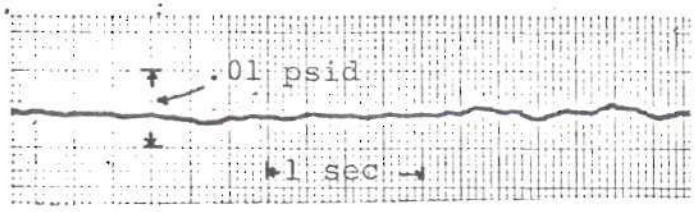

θ = 0°

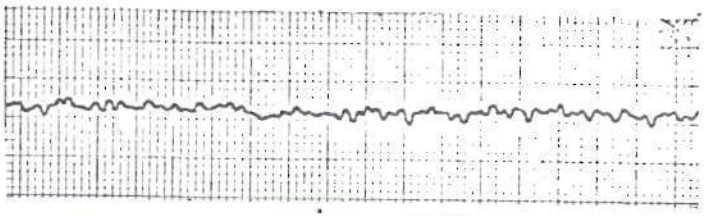

θ = 90°

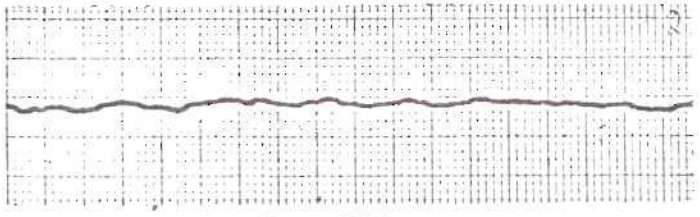

θ = 30°

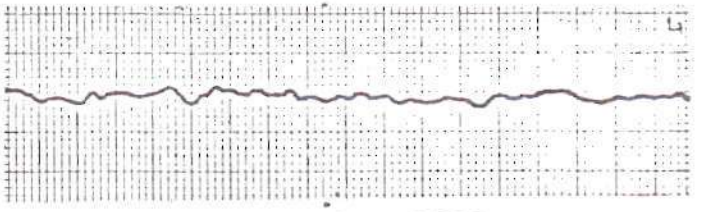

θ = 120°

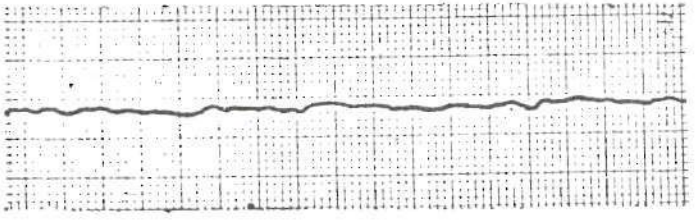

θ = 60°

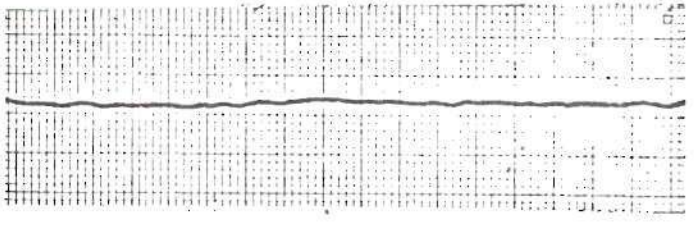

θ = 180°

Figure 20. Representation Pressure at Different Locations. (Ottawa sand (514 m), P/D_t = 1.3 and U = .7 ft/sec)

Also apparent from the record at the 120 degree location is the fact that activity originated at the 90 degree location prefer to propagate downstream of the flow.

Figure 21 displays another set of representative signals recorded in the same bed at a fluidization velocity 1.2 times that required for minimum fluidization of the bed. Pressure fluctuations at all locations can be noticed in this case. It appears that a 20% increase in velocity from the minimum fluidization velocity is sufficient to mobilize the particles in the defluidized cap at the top of the cylinder. It should be expected that the increase in velocity necssary to affect the cap in such a way is a strong function of tube spacing and arrangement. The smaller the P/D_t ratio of the tube, the smaller will be the flow rate required to disrupt the defluidized region. In order to identify the presence of any periodic component, the records shown in Figure 21 have been analyzed for their variance, probability density, and the autocorrelation function, for three locations of the probe (i.e., θ equal to 0 degree, 90 degree, and 180 degree). The shape of the power spectrums shown in Figure 22 demonstrates the characteristics of a spectra typically obtained from random signal. The corresponding autocorrelation function shown in Figure 23 also exhibits the same character. The probability density function shows a normal distribution for the fluctuations. Since the magnitude (the rms value) of the fluctuations is small (generally less than 0.005 psid),

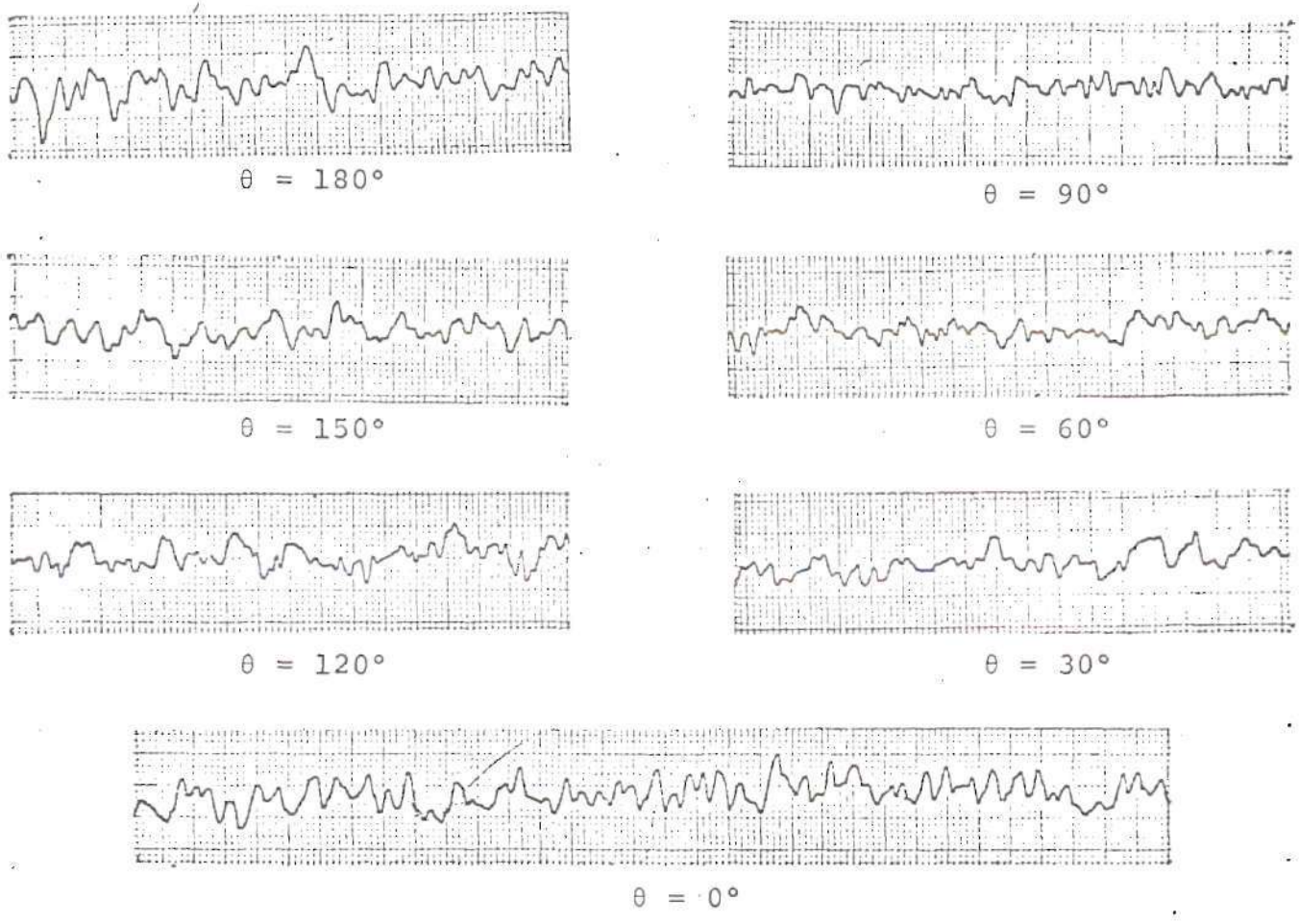

Figure 21. Representative Pressure Signal at Different Locations. (Ottawa sand (514 μm), P/D_t = 1.3 and U = .89 ft/sec)

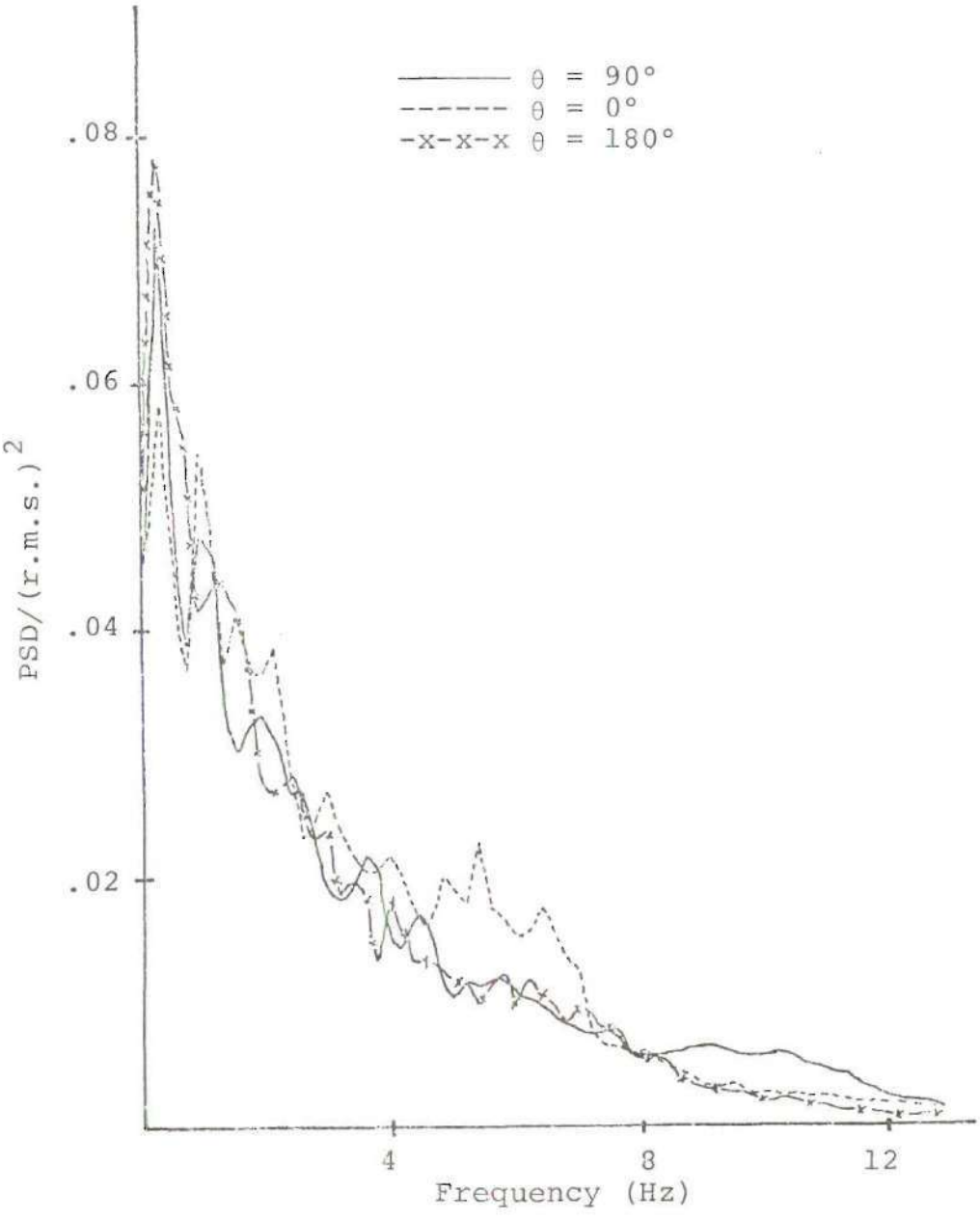

Figure 22. Normalized Power Spectral Density Function. (Ottawa sand (514 μm), P/D_t = 1.3 and U = .89 ft/sec)

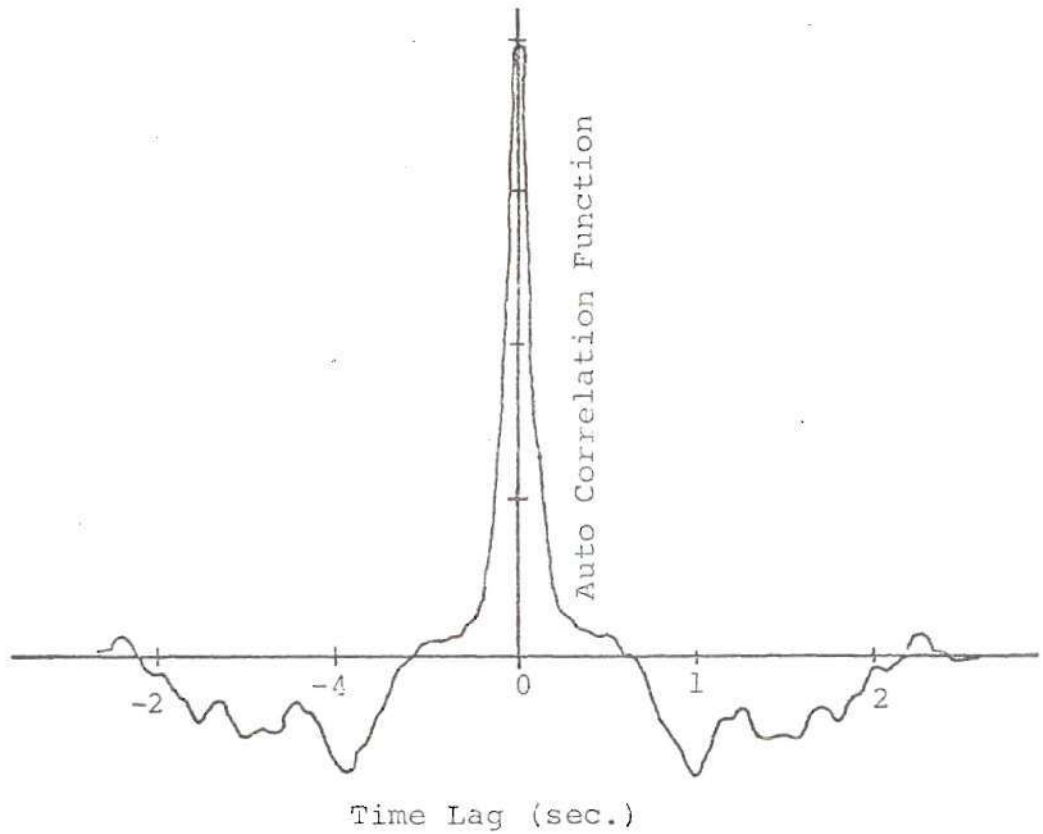

Figure 23. Auto Correlation Function.
(Ottawa Sand (514 μm), P/D_t = 1.3, and U = .89 ft/sec)

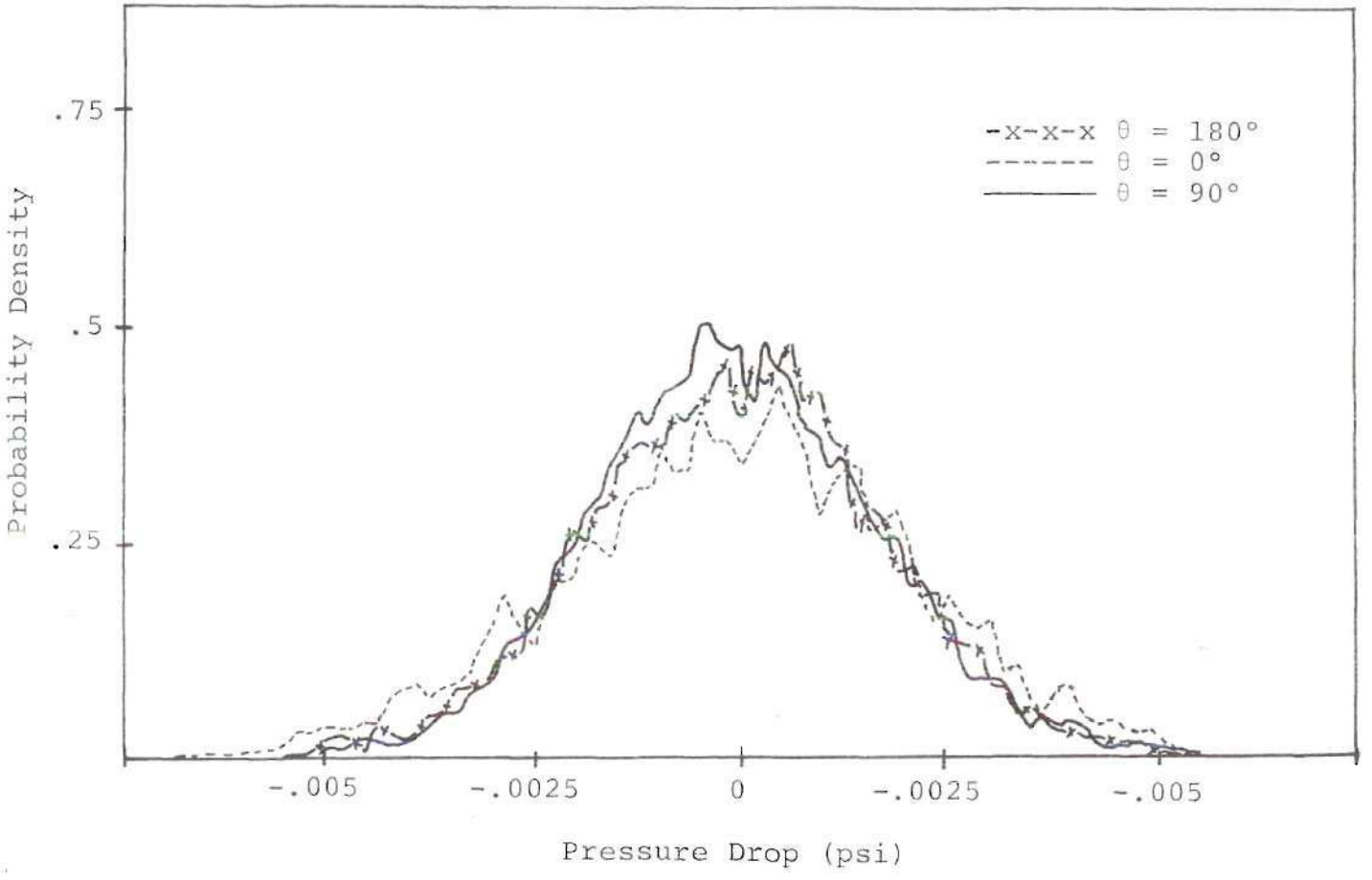

Figure 24. Probability Density Function
(Ottawa sand (514 μm), P/D_t = 1.3 and U = .89 ft/sec)

these fluctuations may be due to random particle movement caused by initiation and breaking up of small bubbles. It appears that the small amount of bubbling that occurs is highly irregular. The presence of the tubes promotes the initiation of bubbles at low fluidization velocities but these bubbles leak away into general interstitial space between the tubes as they rise through the bed. This phenomena causes some particle mixing but this mixing is restricted to the local region of the bed containing the tube bundle. For the data shown in Figure 21-24, no escaping of the bubbles was noticed on the surface of the bed. For this case viewing from the end faces of the test section no visible activity of particles was noticed above or below the tube bundle. Power spectra and probability density functions for all three locations around the tube circumference are very similar in shape and magnitude, suggesting a similar quality of fluidization around the tube circumference.

Figure 25 is similar to Figure 22, and shows the power spectra at the same three locations with the same bed operating at a fluidization velocity corresponding to U/U_{mf} equal to 1.54. At all these locations the power spectra in this case show the presence of a sharp peak, suggesting that the frequency of bubble passage has become more regular at higher fluidizing velocities. Figure 26 shows the autocorrelation functions for θ = 90 degree and it exhibits the characteristics trend typical of both random and periodic

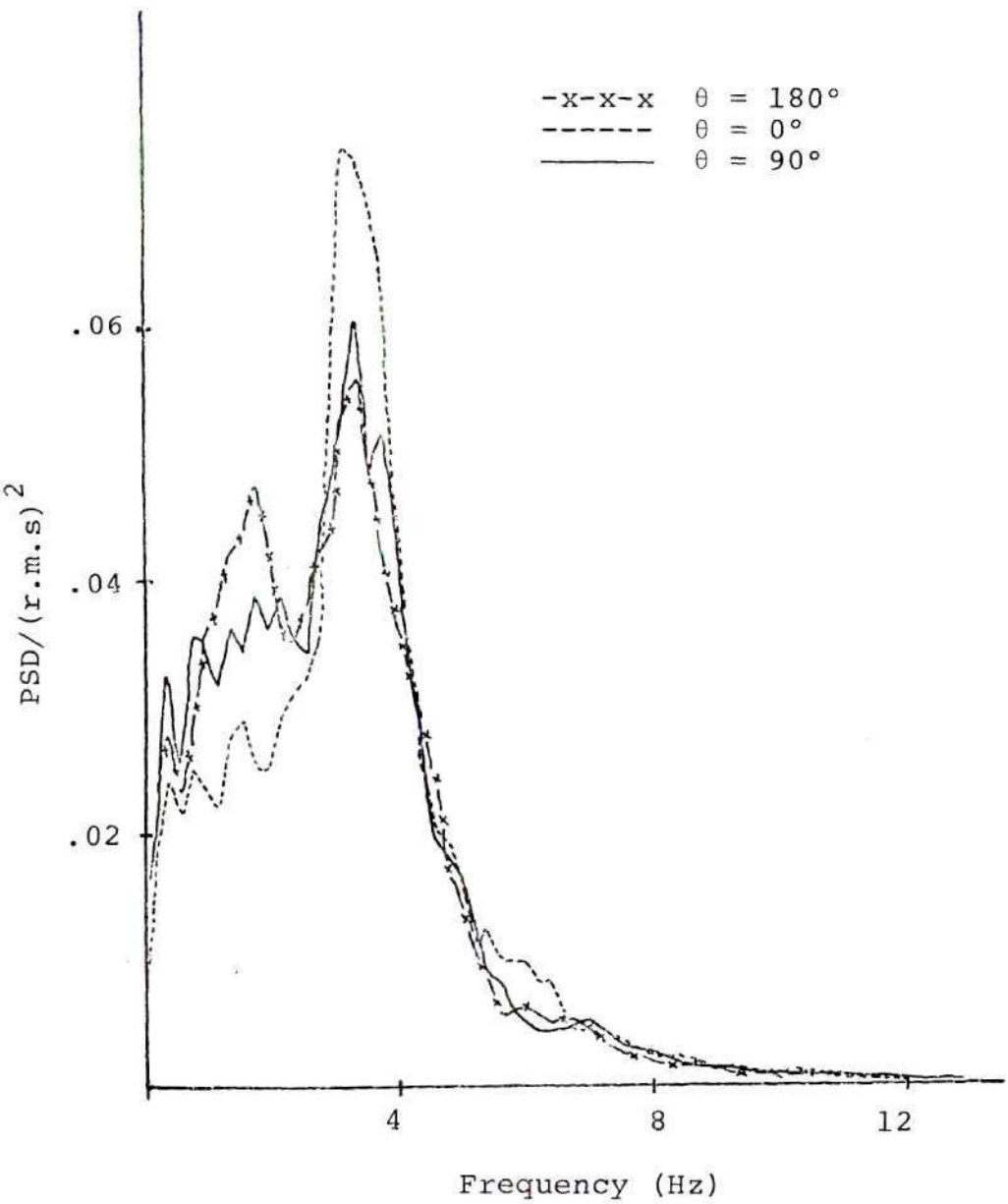

Figure 25. Normalized Power Spectral Density Function (Ottawa sand (514 μm), $P.D_t$ = 1.3, and U = 1.14 ft/sec)

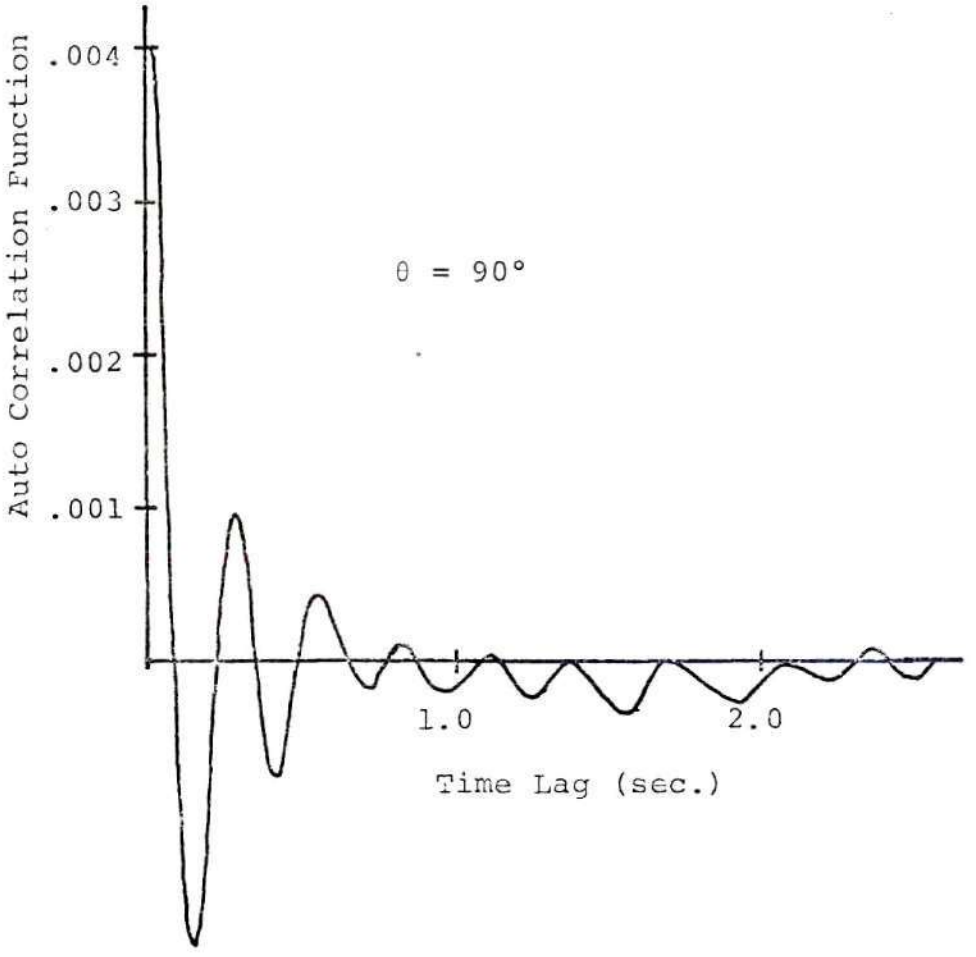

Figure 26. Auto Correlation Function.
(Ottawa sand (514 μm), P/D_t = 1.3, and U = 1.14 ft/sec)

signals. The autocorrelation function is maximum at zero time lag and this function becomes sinusoidal with a fairly constant period as the time lag is increased. This observation is consistent with the results shown in the power spectra in Figure 25. The magnitude of the fluctuations increased by an order of magnitude (see Table 9 for rms values), which suggests that smaller bubbles coalescence near the surface of the tubes (at $\theta \approx 60$ degree) resulting in bigger bubbles which in turn periodically escape from the bed by breaking the bed surface. The particle mixing in this case is intense and, in contrast to the previous case is not restricted to the local region of the bed containing the tube bundle. A rather large increase in heat transfer coefficient is expected with such a level of activity in the bed, since the tube surface is subjected to periodic replacement of particles from the bulk regions of the bed due to particle entrainment associated with the passage of bubbles.

Similar general behavior has been noticed for smaller size particles (i.e., glass beads (230 μm)). The only difference in this case, when compared to Ottawa sand (514 μm) is that the frequency of fluctuations has increased significantly. Figure 27 shows the power spectra for the same tube bundle placed in bed of glass beads (230 μm) operating at a fluidization velocity corresponding to, U/U_{mf} equal to 1.81. The spectra have the characteristics of the one which is typical of random signals. The energies of the spectra in

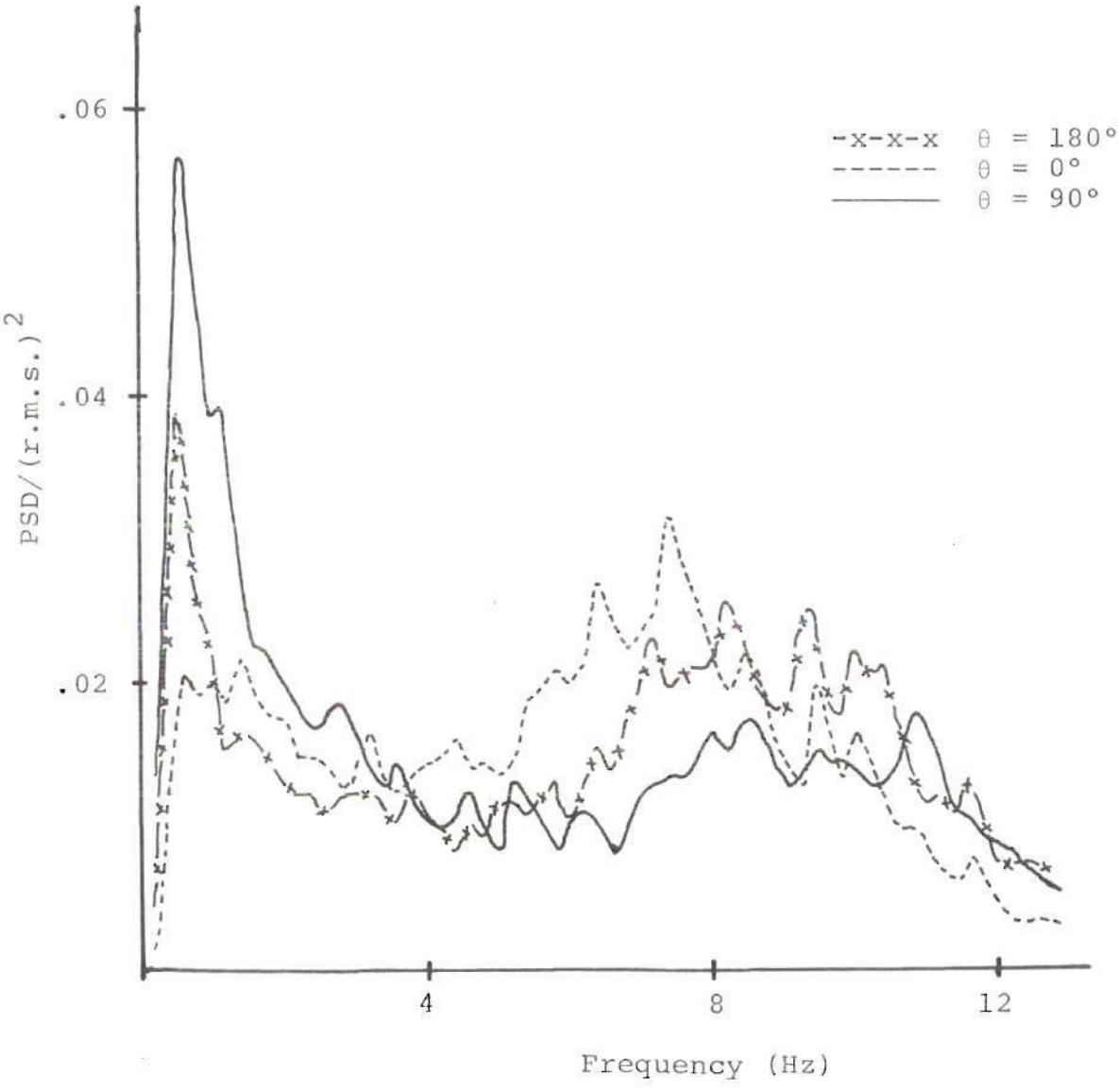

Figure 27. Normalized Power Spectral Density Function. (Glass beads (230 μm), P/D_t = 1.3, and U = .29 ft/sec)

Figure 27 are concentrated at higher frequencies compared to those in Figure 22. This increased frequency of fluctuations favors good heat transfer characteristics which is typical of rapid movement of particles. Similar to the case of larger particles, the pressure fluctuations in the case of smaller particles also become regular in nature at high flow rates.

The strip-chart record samples, the power spectra, the autocorrelation functions, and the probability density functions for all the test runs are included in Appendix D for completeness and further clarification of the remarks made above.

The particle activity in the proximity of a heat transfer surface in fluidized bed has a significant bearing on the heat transfer rates. Review of literature contained in Chapter II present pertinent detailed discussion of the views of several investigators. In order to achieve desirable heat transfer characteristics the transfer surface needs to be brought into rapid contact with fresh particles from regions of the bed away from the surface. In the light of this comment the defluidized cap is detrimental to the desired favorable heat transfer characteristics. Hence, several qualitative conclusions regarding the local heat transfer coefficient from horizontal tubes of a staggered tube bundle in a gas fluidized bed can be drawn from the visual observations and pressure fluctuations study described in the above

paragraphs. In general, based on the above comments related to pressure fluctuation analysis describing the particle movement and bubble formation and their escape, it can be expected that the local heat transfer coefficient around a single horizontal tube placed in a fluidized bed operating at fluidization velocities close to incipient fluidization will be highest near the sides, small at the bottom, and negligible at the top of the tube. This pattern of local heat transfer coefficient is expected to change significantly with increasing fluidization velocity.

Since it was observed that the defluidized region at the top of a single tube can be broken up at fluidization velocities approximately 1.75-1.85 times the minimum fluidization velocity, the local heat transfer coefficient at the top of the tube is expected to increase rapidly with increasing fluidization velocity. Similar behavior is expected for the tubes in tube bundles. Recall that the disruption and break-up of the defluidized region at the top of these tubes occurred at significantly lower fluidization velocities than in the case of a single tube. Hence, it can be concluded that heat transfer coefficients on the top of the tubes will increase more rapidly with increases in fluidization velocities than that for the case of single tube. It is also concluded that, in general, with increased fluidization velocity the increase in the average heat transfer coefficient for staggered horizontal tubes placed in gas fluidized beds

is primarily due to the increased local heat transfer coefficient at the top and at the bottom of the tubes with only a slight increase in the local heat transfer coefficient at the sides of the tube.

IV.4 Results of Heat Transfer Measurements

Experimental tests for heat transfer measurements have been organized with increasing degree of complexity. A series of test runs involving the measurement of local and average heat transfer coefficient from a single cylinder placed in fluidizing column without any fluidizing material has been carried out at the conclusion of pressure fluctuation experiments of phase I. The purpose of these tests is to establish a standard for comparison with the measurements involving the fluidized bed. The average heat transfer coefficients based on these tests have been used in later analysis to evaluate the extent of augmentation of heat transfer coefficient due to fluidization. The rest of the heat transfer measurements were taken with either single tube or a horizontal tube bundle placed in fluidized beds of different materials. The experimental variables are: bed material and particle size, fluidization velocity, and tube spacing. A series of measurements to evaluate the effect of test cylinder location in the tube bundle, and the number of rows in a tube bundle, have also been carried out.

IV.4.1. Local and Average Heat Transfer Coefficients (No Fluidization)

The test cylinder for these measurements was located at a distance of 6.6 inches above the distributor plate. The range of Reynolds numbers covered is from 100 to 2000. The variation of average Nusselt number with Reynolds number is shown in Figure 28. Comparison of the present work is made with Hilpert's (1933) work on average heat transfer coefficients for a single cylinder in cross flow. The results of the present work are approximately 30% higher than those obtained by Hilpert. This deviation of present work results from that of Hilpert whose experiments were carried out at very low turbulence air streams may be attributed to the free shear vortices of the air jets issuing from sintered porous distributor plate which is essential to the operation of the fluidized bed and having a mean pore size of 45 μm. These vortices may be characterized as large scale low intensity turbulence which did not have enough time to attenuate during its short passage towards the cylinder. It is natural to expect the boundary layer phenomena and the associated wake to be influenced by this type of air stream causing the improvement in heat transfer coefficients of approximately 30 percent as shown in Figure 28. This figure also shows the least squared curve of the experimental data which corresponds to

$$N_{Nu,t} = 1.447 \ (N_{Re,t})^{.379} \qquad (24)$$

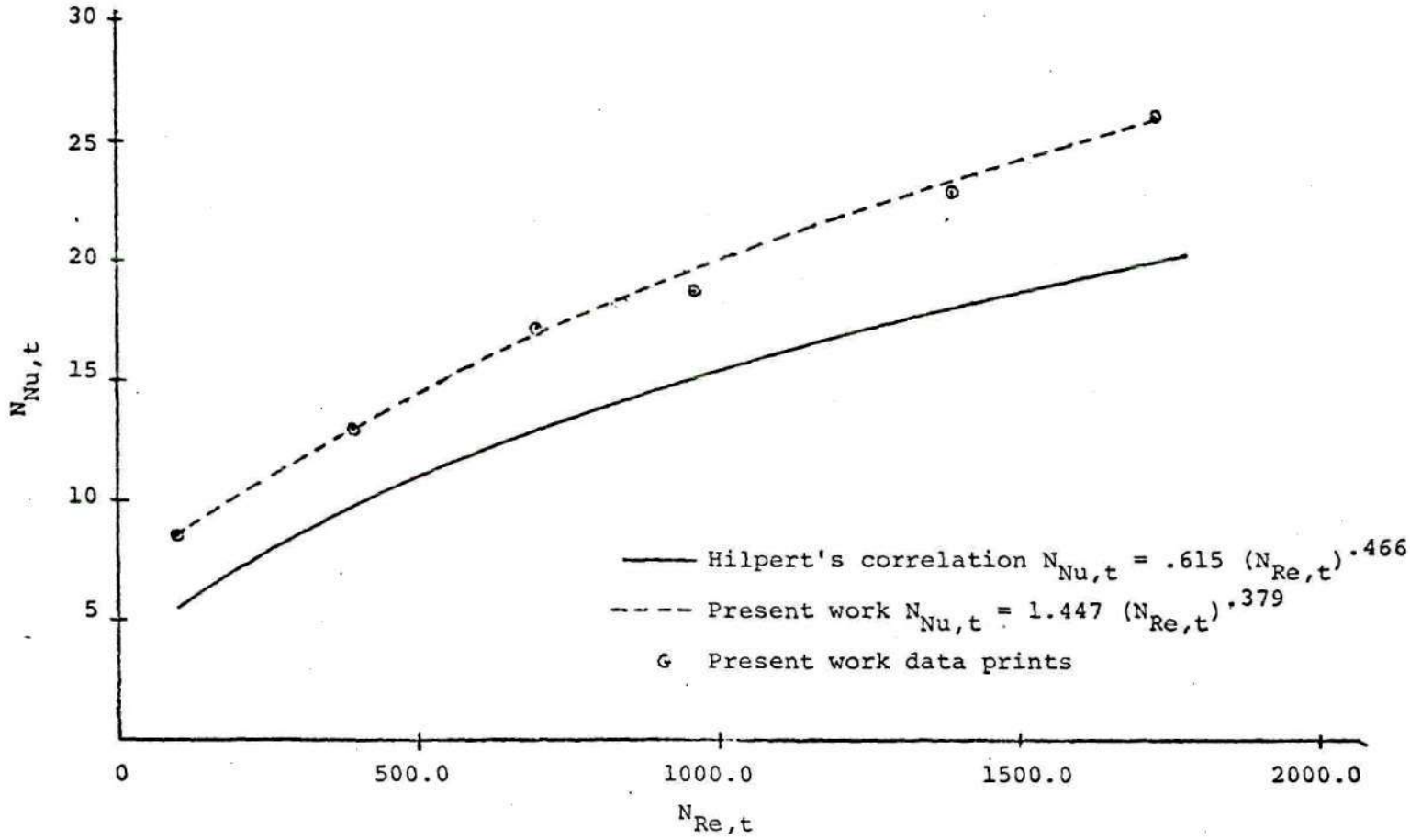

Figure 28. Comparison of Heat Transfer Coefficients (No Fluidization) With that of Hilpert's (1933).

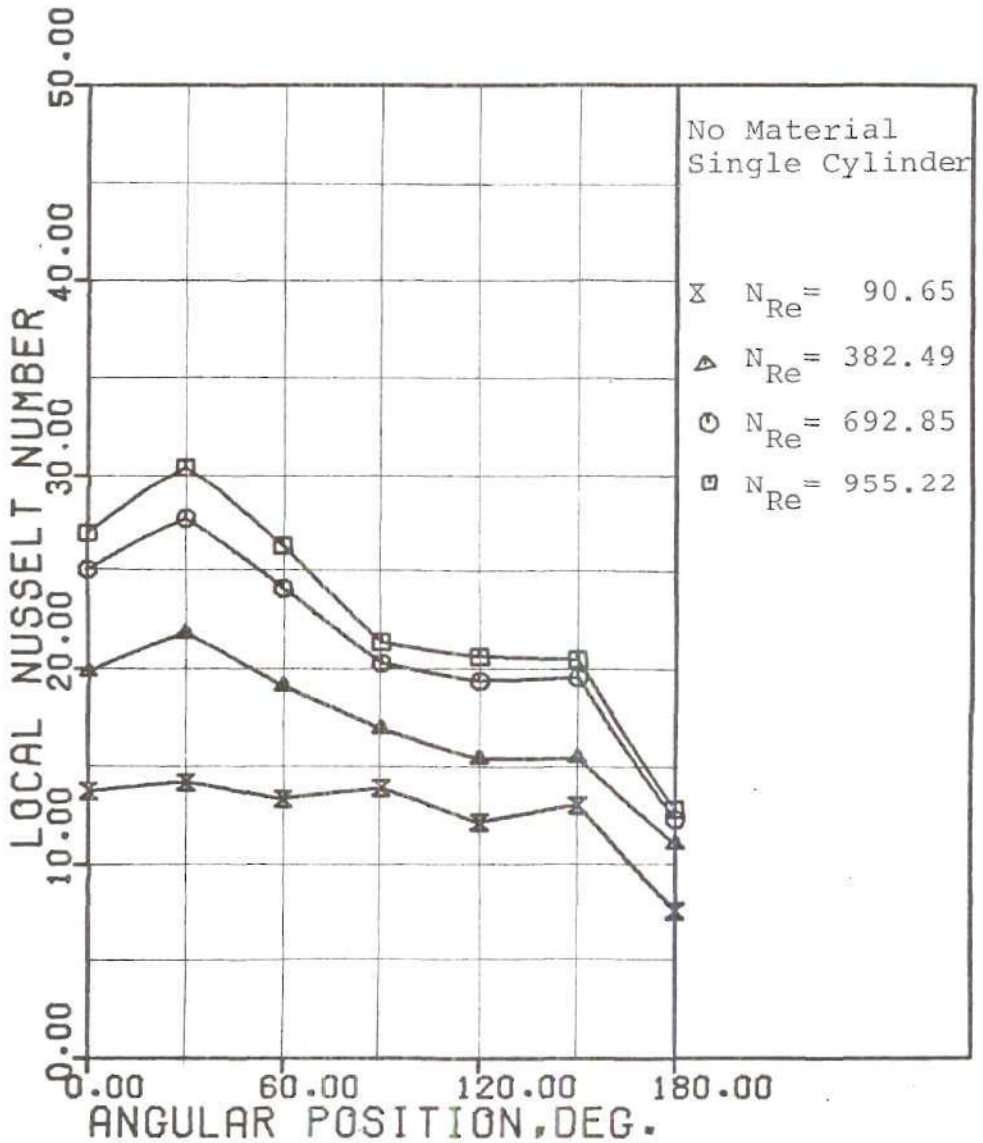

Figure 29. Effect of Air Velocity on Local Heat Transfer. (Single Cylinder, No Fluidization)

Figure 29 shows the variation of the local Nusselt numbers, with the angular position around the cylinder circumference, for various Reynolds numbers. In the present work, the measurements with single cylinder for the case of no fluidization have been confined to low Reynolds numbers only, because of the range of flow velocities encountered in the dense phase gas fluidized beds is generally very small and correspond to low Reynolds numbers only.

IV.4.2. Local Heat Transfer Coefficients (Fluidization)

Visual observations and analysis of pressure fluctuations in the vicinity of tube surface reveal that the flow pattern of the fluidizing medium is considerably different than that for the case of a cylinder in cross flow without any fluidizing medium. The local heat transfer coefficient variation around tube circumference should reflect such a difference in the flow field. Comparison of experimental results have been made with a single tube as well as with tube bundles placed in fluidized bed of different materials operating at various flow rates.

The results obtained from the heat transfer experiments for a single cylinder are presented in Figures 30, 32, and 33. Figure 31 is taken from Noack (1970) for comparative purposes. In Figures 30 through 33 local heat transfer coefficients have been plotted as a function of angular position with reduced velocity (i.e., U/U_{mf}) as a parameter. It may be noted that the heat transfer coefficient in fluidized beds

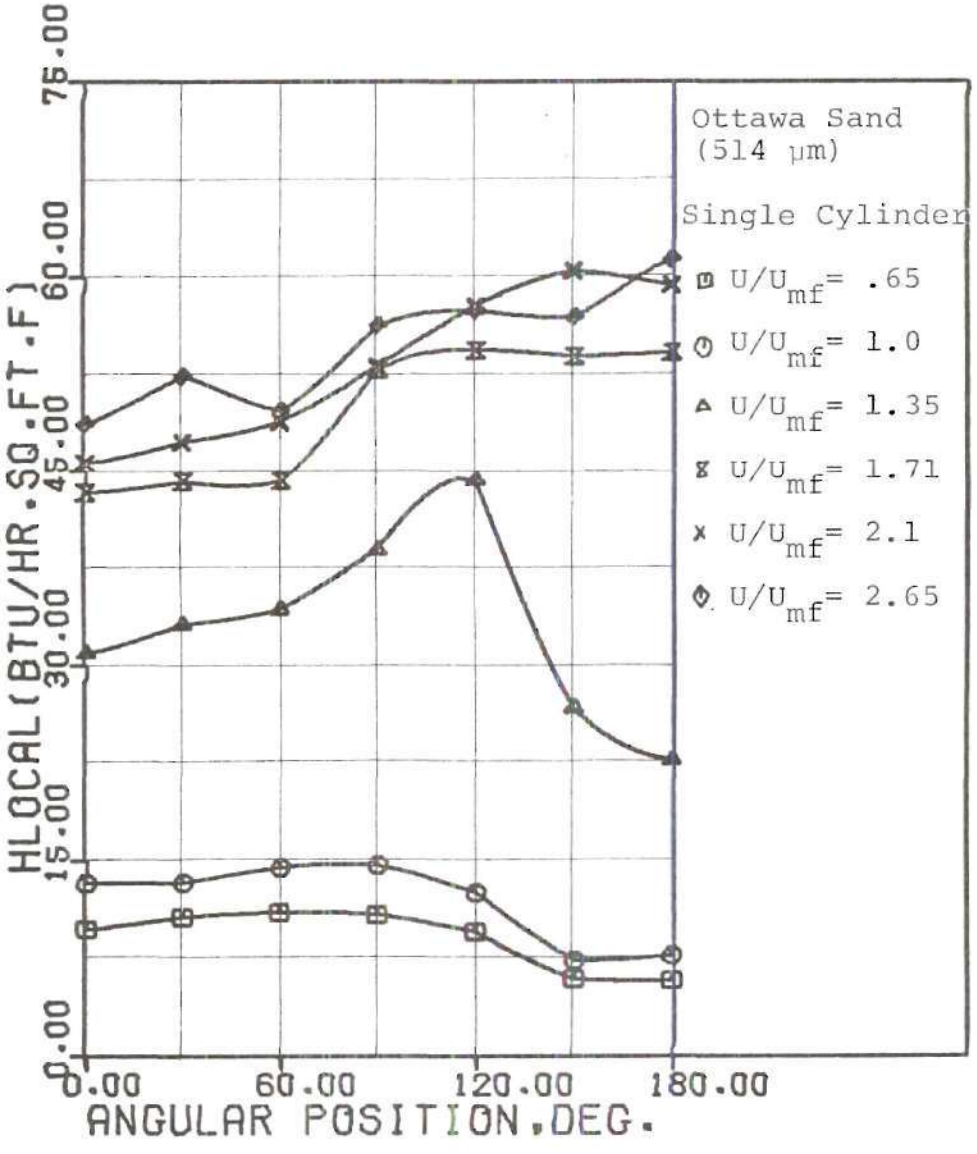

Figure 30. Effect of Fluidization Velocity on Local Heat Transfer. (Single Cylinder, Ottawa Sand (514 μm))

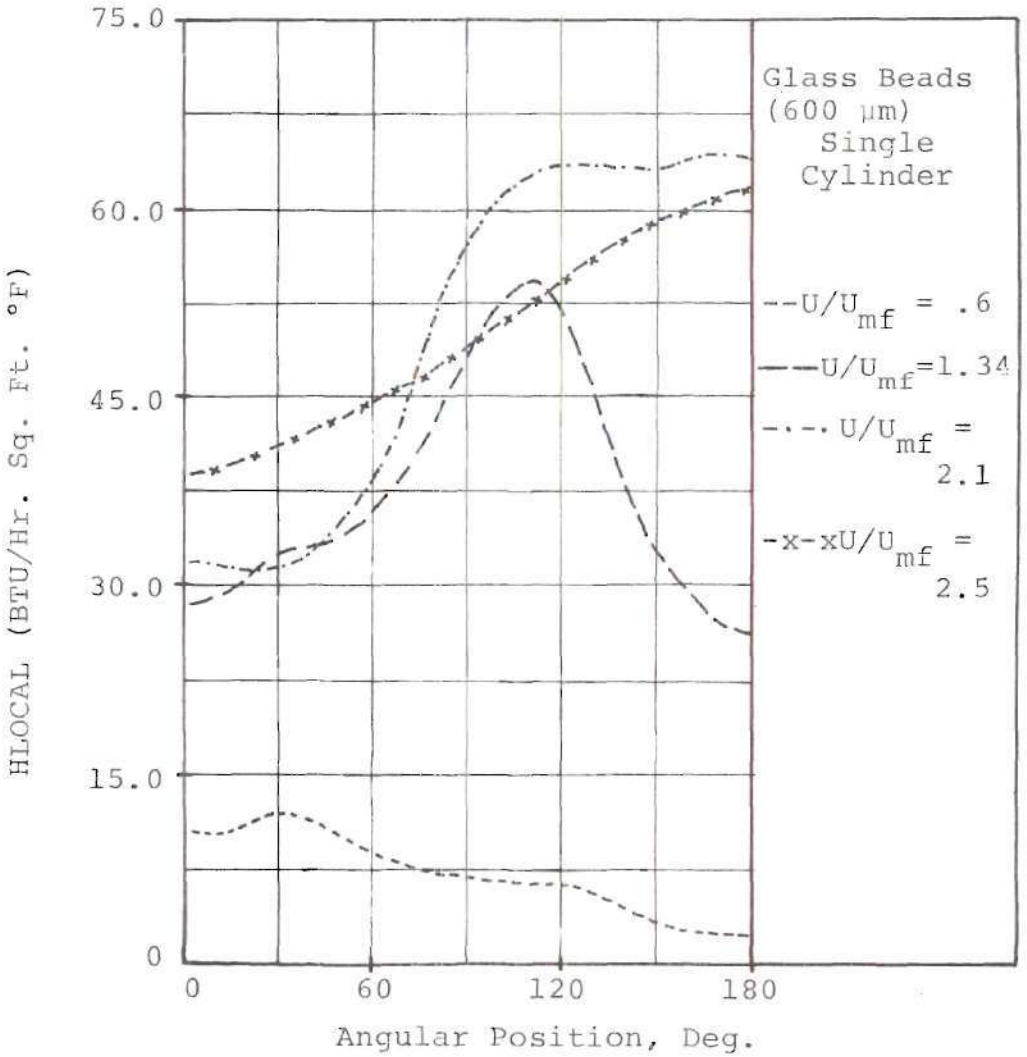

Figure 31. Local Heat Transfer Coefficients vs. Angular Position for Single 1" Diameter Horizontal Cylinder in Air Fluidized Bed. [Noack (1970)].

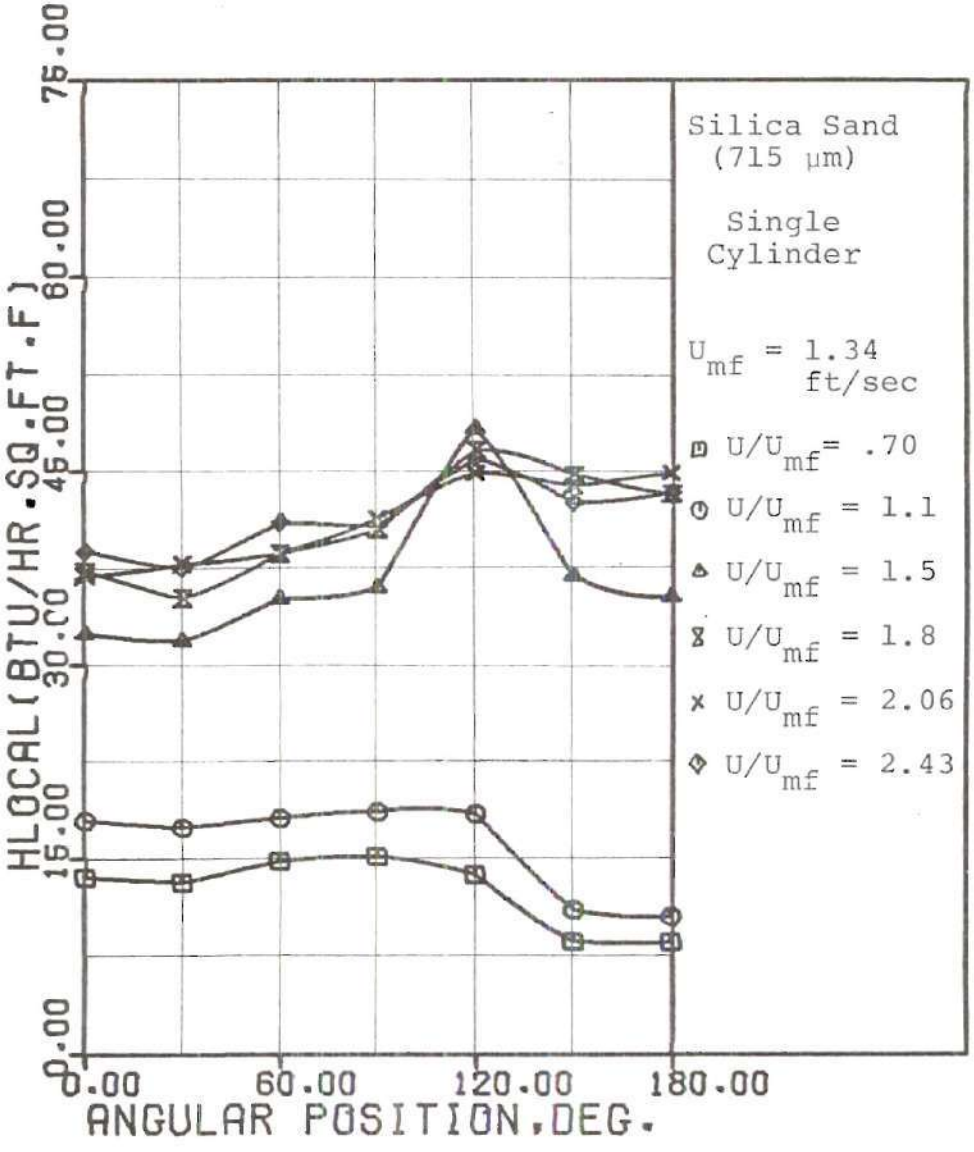

Figure 32. Effect of Fluidization Velocity on Local Heat Transfer. (Single Cylinder, Silica Sand (715 μm))

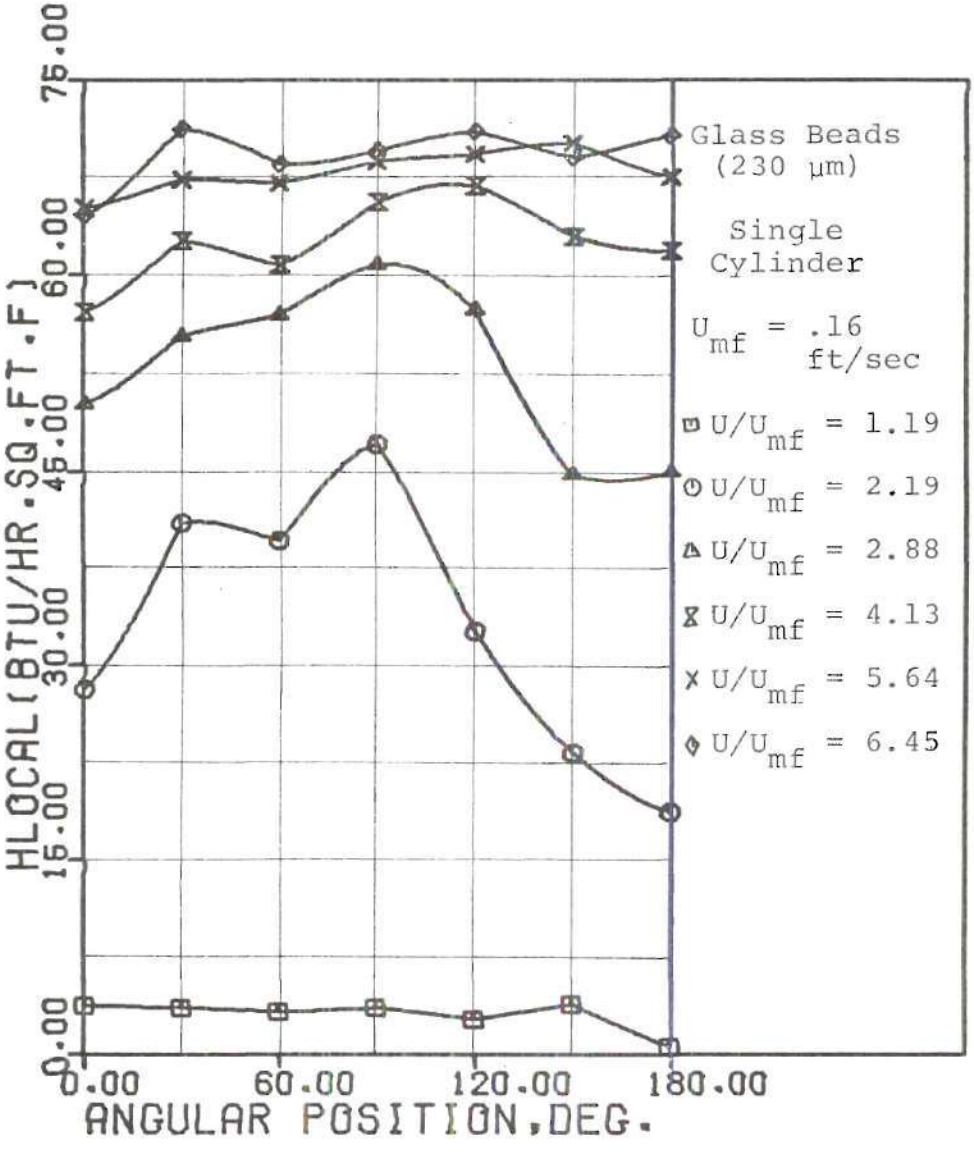

Figure 33. Effect of Fluidization Velocity on Local Heat Transfer. (Single Cylinder, Glass Beads (230 μm)

at any location fluctuates due to the passage of bubbles through the bed. This is particularly true at relatively high fluidizing velocities. Figures 30, 32, and 33 show results of the measurements as obtained. It may be further noted that measurements obtained at same velocities at different locations have been simply joined by straight lines on a calcomp plotter. Figure 31 shows the data of Noack (1970) using glass beads (600 μm) which are slightly different in shape and size than any of the materials used in the present work. A direct, one to one comparison, therefore may not be possible. The Ottawa sand used in the present work closely resembles in shape and size to the glass beads used by Noack in his work. Thus Figures 30 and 31 can be compared qualitatively. It is apparent that the two figures depicting angular variation of the local heat transfer coefficient, show a similarity in shapes. The magnitude of heat transfer coefficient for similar cases are of the same order in the two figures.

The results of Figures 30, 32, and 33 show that, at velocities close to minimum fluidization velocity, the heat transfer coefficient is maximum at the sides of the tube and minimum at the top of the tube. The pressure fluctuations study describing the particle activity suggests this type of variations in the local heat transfer coefficients. The maximum heat transfer coefficient at incipient fluidization velocities occurred at 120 degree location in the case of

larger particles (i.e., Ottawa sand and silica sand), whereas it occurred at 90 degree location in the case of smaller particles (i.e., glass beads). This may be directly attributed to the better stacking ability of the smaller particles.

Figure 34 is a representative plot of the local heat transfer coefficients as a function of the ratio of the superficial air velocity to the minimum fluidization velocity, i.e., h_θ vs U/U_{mf}, for the case of Ottawa sand and single cylinder. Table 4 is based on the data contained in Figure 34. The entries in the table refer to relative improvement in the local heat transfer coefficient when compared to the experimentally measured value of the heat transfer coefficient, $h_{avg,o}$ obtained from the same cylinder in the absence of a fluidized bed. The choice of this latter value for normalization allows a direct measure of the heat transfer augmentation in a fluidized bed heat exchanger over the one without a fluidized bed. The value of superficial velocity, U, and the corresponding base value of $h_{avg,o}$ along with U/U_{mf} appear as column headings. Table 4 also contains similar experimental results obtained for silica sand (715 μm) and glass beads (230 μm).

It can be seen from Figure 34 that for Ottawa sand and superficial air velocities less than 1.5 times the minimum fluidization velocity, the local heat transfer coefficients are highest at 90 degree location (i.e., at the sides) and lowest at 180 degree location (i.e., top of the

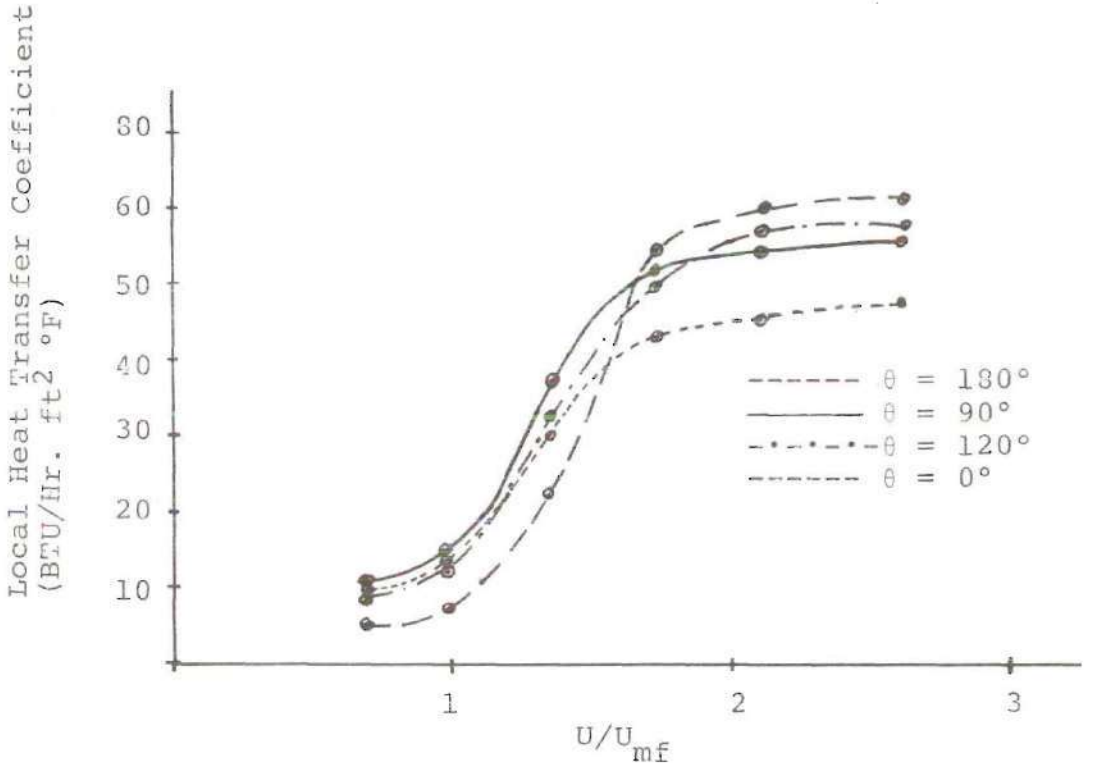

Figure 34. Variation of Local Heat Transfer Coefficient with Increase in Superficial to Minimum Fluidization Velocity Ratio. (Single Cylinder, Ottawa Sand (514 μm))

Table 4. Relative Improvement in Local Heat Transfer Coefficient (i.e., $h_\theta/h_{avg,o}$) for Single Cylinder in Fluidized Bed.

Ottawa Sand O. S. 514	Angular Position Deg.	U/U_{mf}	1.0	1.25	1.5	1.75	2.0	2.5
		U ft/sec	0.74	0.93	1.11	1.3	1.48	1.85
		$h_{avg,o}$ (B/hr ft^2F)	2.3	2.5	2.7	2.9	3.1	3.4
	0		5.7	9.4	13.7	14.8	14.6	14.2
	90		6.0	11.3	16.5	17.8	17.4	16.2
	120		6.1	10.1	14.8	17.3	17.4	17.5
	180		3.1	6.4	12.3	19.0	19.1	18.2
Silica Sand S. S. 715	Angular Position (Deg.)	U/U_{mf}	1.0	1.25	1.50	1.75	2.0	2.5
		U (ft/sec)	1.34	1.68	2.0	2.35	2.68	3.35
		$h_{avg,o}$ (B/hr ft^2F)	2.93	3.25	3.5	3.85	4.1	4.6
	0		4.8	8.0	10.2	9.9	9.3	8.5
	90		6.1	8.0	10.7	10.6	10.0	8.9
	120		5.5	9.8	13.9	12.0	11.2	10.0
	180		3.5	6.2	10.7	11.5	11.0	9.3
Glass Beads G. B. 230	Angular Position (Deg.)	U/U_{mf}	1.0	2.0	3.0	4.0	5.0	
		U (ft/sec)	0.16	0.32	0.48	0.64	0.80	
		$h_{avg,o}$ (B/hr ft^2F)	1.5	1.75	2.0	2.2	2.4	
	0		2.6	1.31	25.5	26.9	25.9	
	90		3.2	22.9	34.0	30.0	28.4	
	120		1.6	15.5	29.0	30.0	29.2	
	180		.8	8.6	22.5	27.7	27.1	

cylinder). Based on the earlier discussions relating to visual observations and pressure fluctuations as well as that reported in the literature survey, such a maximum and a minimum in the value of the local heat transfer coefficient can be attributed to the initial local fluidization at the sides and diffusion dominated heat transfer at the defluidized cap on the top of the cylinder. According to Figure 34, with an increase in superficial air velocity beyond 1.7 times the minimum fluidization velocity, the local heat transfer coefficients at the top of the cylinder increases rather rapidly and assumes largest values when compared to corresponding values at other locations. This rapid change can be attributed to rapid replacement of the bed material contained in the defluidized cap, promoting heat capacity transport into the main body of the bed. In Figure 34, beyond this value of U/U_{mf}, the local heat transfer coefficients at all locations demonstrate tendency to level off at respective maximum values.

The designer of heat exchangers, who considers tube bundles in a fluidized bed as a preferred arrangement, would like to select such values of U/U_{mf} that provide the highest local heat transfer coefficient assuring a high average value. According to Figure 34, he would select the lowest possible value for U/U_{mf} which in the case of Ottawa sand is 1.7. Moreover he is not faced with detrimental effects due to the defluidized cap. Since the circumferential variations of the

local heat transfer coefficients, when compared to the average value, is minimum, the corresponding circumferential temperature gradient for the nonconducting surfaces is also minimum.

Table 4 also contains results of relative improvement in local heat transfer coefficients for silica sand and glass beads. Their trend is similar to Ottawa sand shown in Figure 34. The minimum fluidization velocity for silica sand (715 μm) is almost twice that for Ottawa sand (514 μm) and the minimum leveling off value for the local heat transfer coefficient occurs at $U/U_{mf} = 1.7$ for this case. However, this maximum relative improvement is about 16 times for spherical Ottawa sand but it is only about 12 times for angular silica sand. Similarly, the minimum fluidization velocity for glass beads (230 μm) is about one fifth of the value for Ottawa sand, and the minimum leveling off value occurs at about $U/U_{mf} = 4.0$. The maximum relative improvement for small spherical glass beads is about 28 when compared to the value of 16 for large spherical Ottawa sand.

The local heat transfer coefficient as a function of angular positions obtained from heat transfer tests with tube bundles using three different types of particles are presented Figures 35 through 41 and Tables 5 and 6. The results of Figure 37 were obtained by placing the heat transfer cylinder in the middle of the bottom row. The results of Figures 35, 36, 38, 39, 40, and 41 were obtained with the test cylinder placed in the center of the bundle. These tables are organized

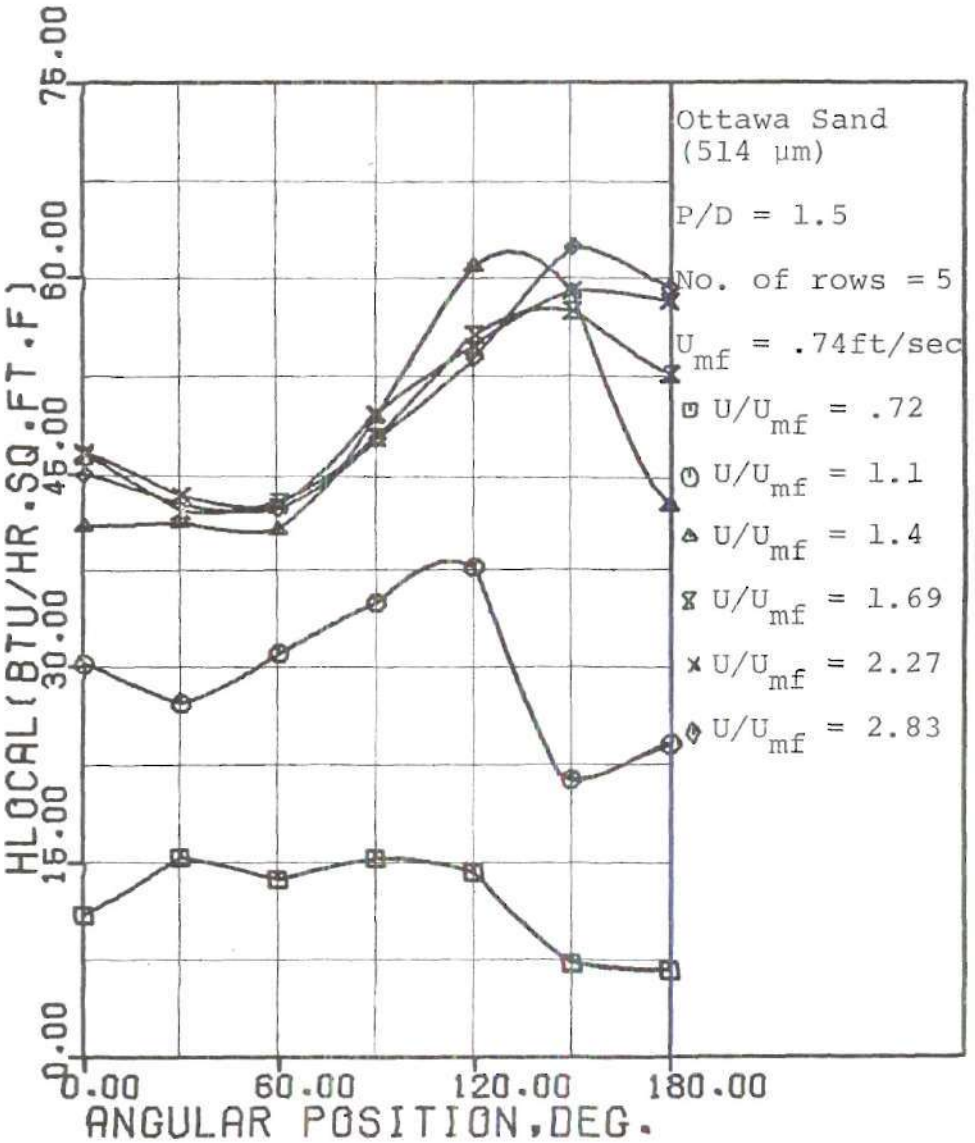

Figure 35. Effect of Fluidization Velocity on Local Heat Transfer. (P/D_t = 1.5, Ottawa Sand (514 μm))

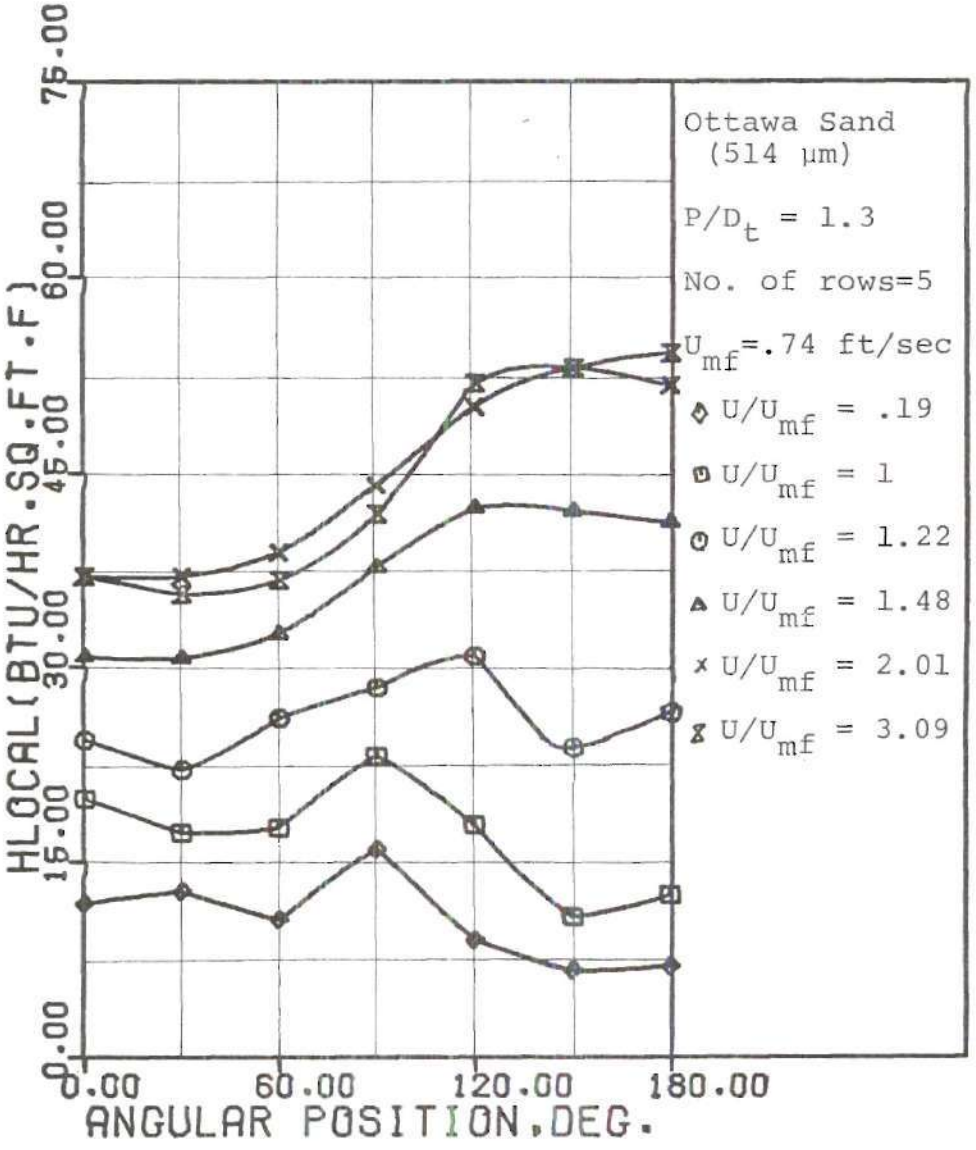

Figure 36. Effect of Fluidization Velocity on Local Heat Transfer. (P/D$_t$ = 1.3, Ottawa Sand (514 μm))

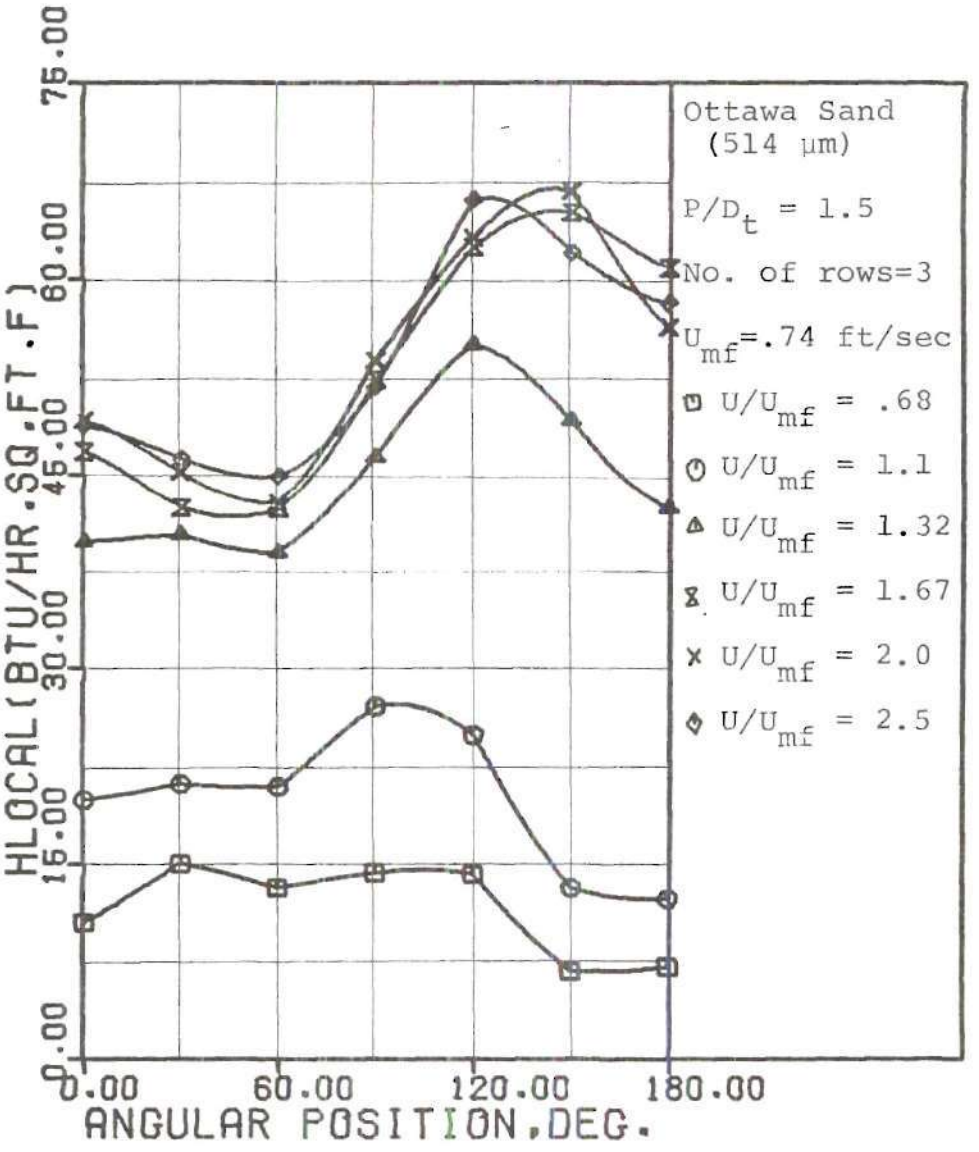

Figure 37. Effect of Fluidization Velocity on Local Heat Transfer. (P/D$_t$ = 1.5, Ottawa Sand (514 µm), 3 Rows)

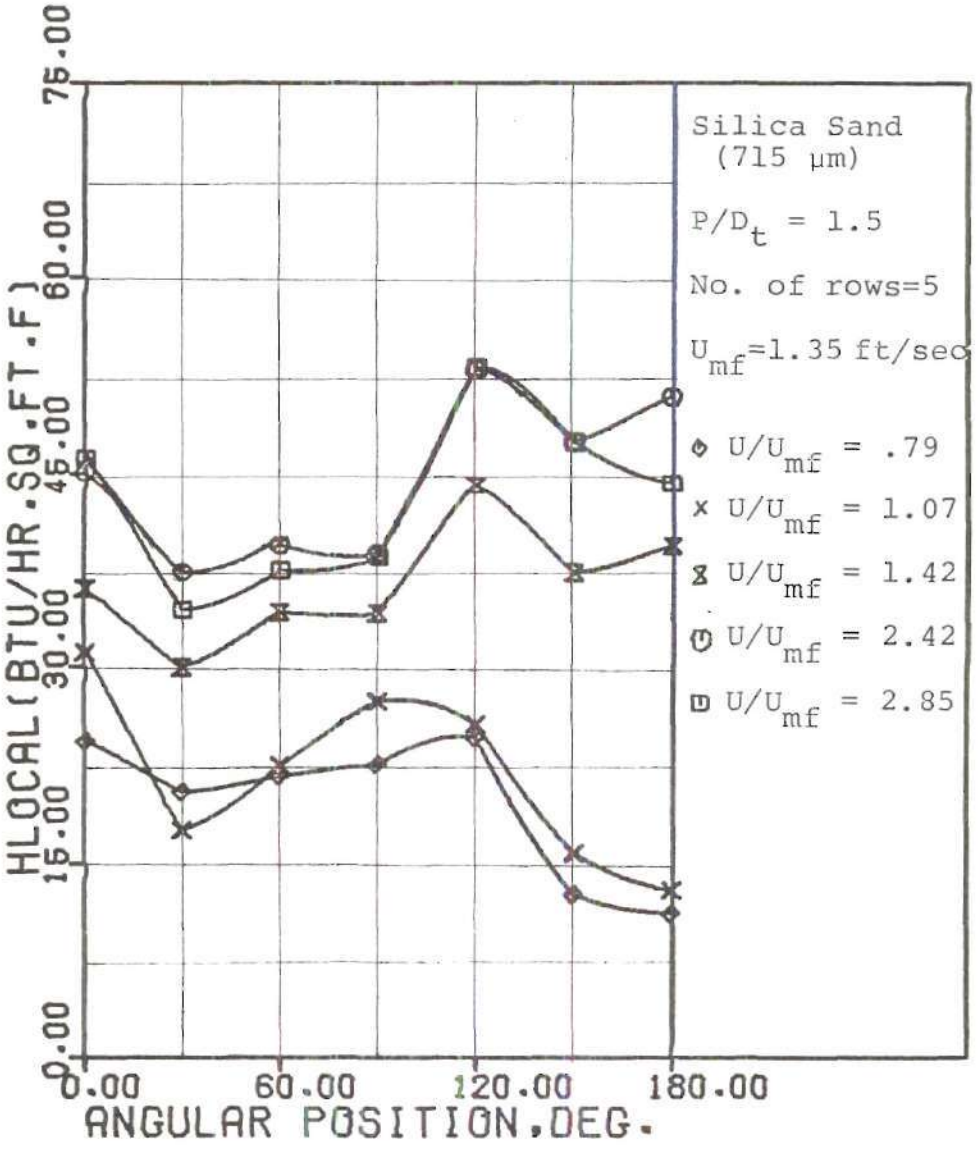

Figure 38. Effect of Fluidization Velocity on Local Heat Transfer. (P/D$_t$ = 1.5, Silica Sand (715 μm))

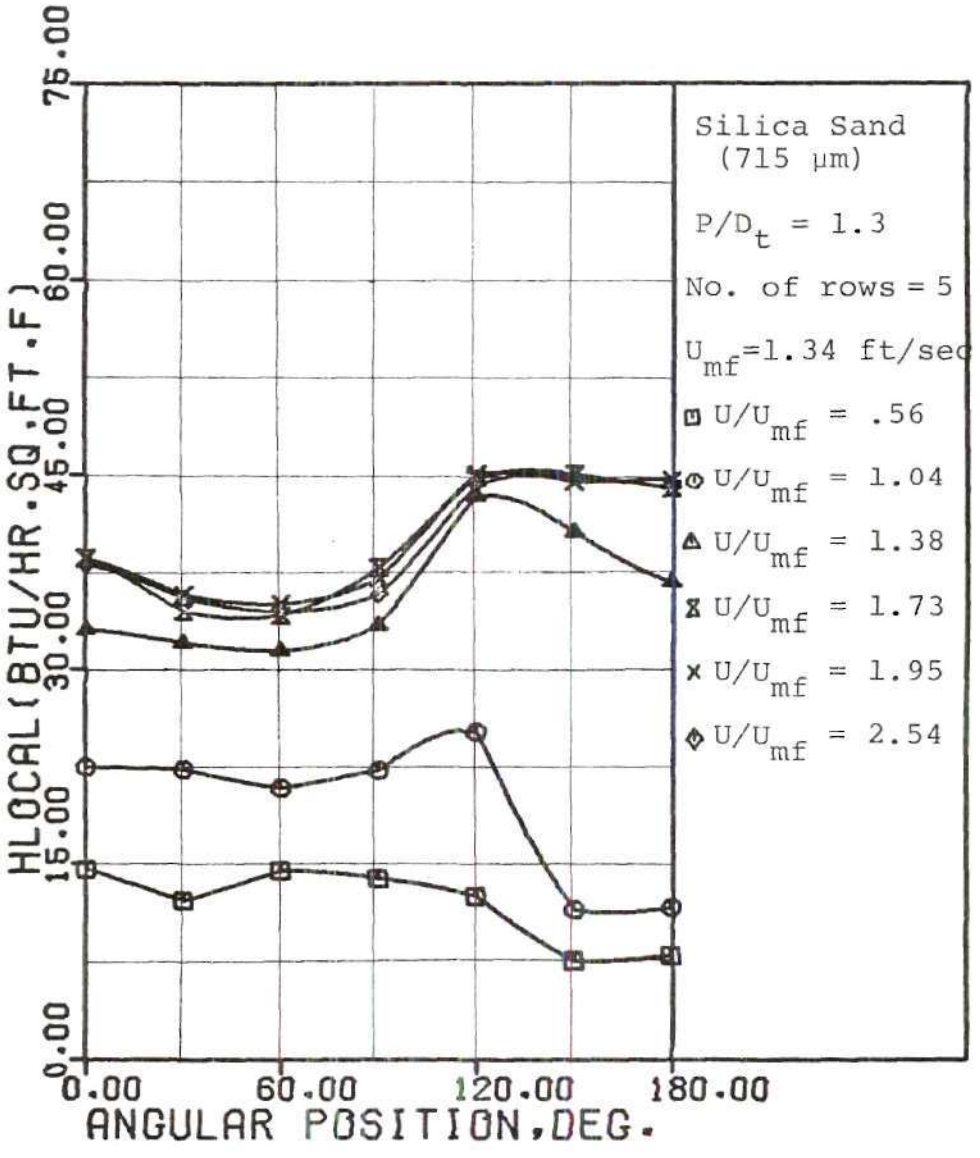

Figure 39. Effect of Fluidization Velocity on Local Heat Transfer. (P/D$_t$ = 1.3, Silica Sand (751 μm))

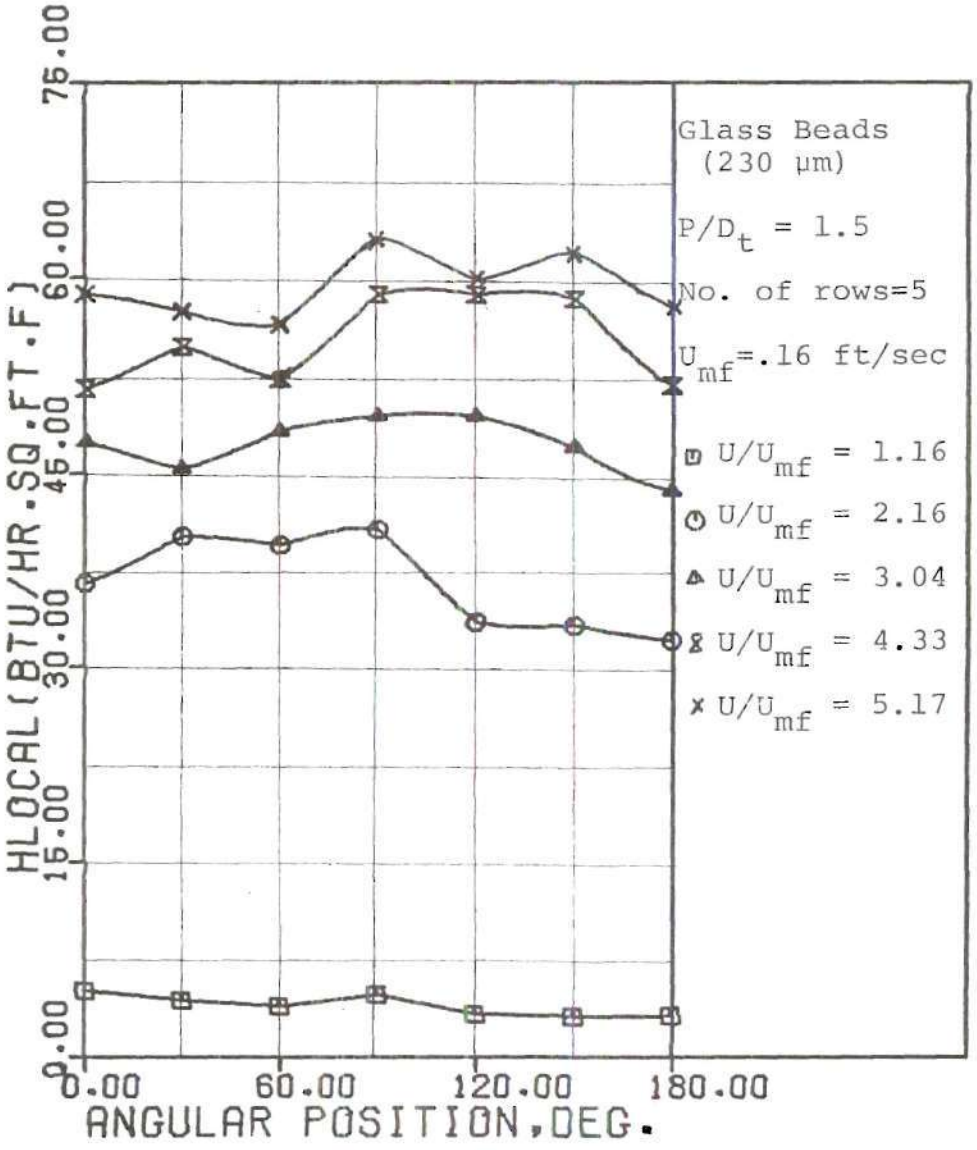

Figure 40. Effect of Fluidization Velocity on Local Heat Transfer. (P/D$_t$ = 1.5, Glass Beads (230 μm))

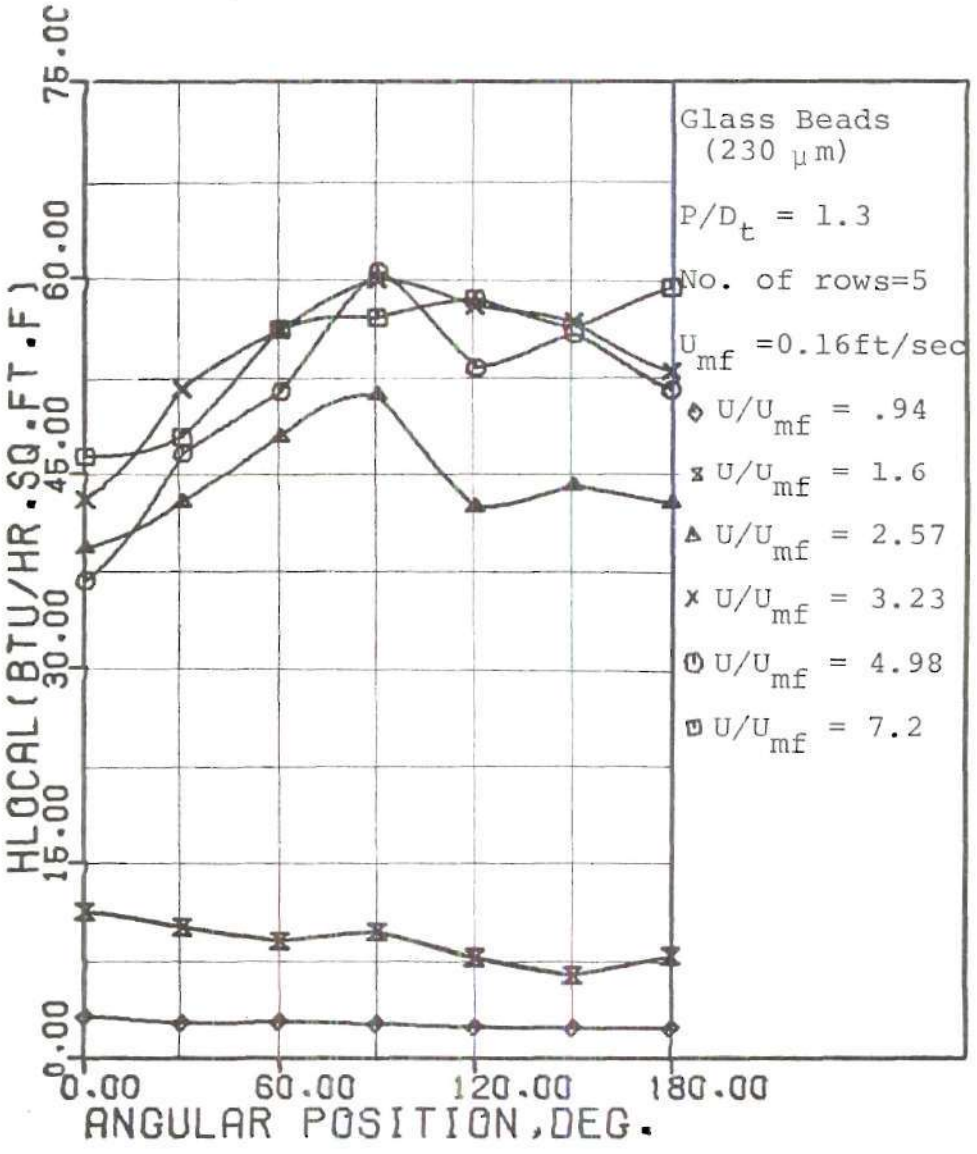

Figure 41. Effect of Fluidization Velocity on Local Heat Transfer. (P/D$_t$ = 1.3, Glass Beads (230 μm))

similar to Table 4 for ease of comparison. Figures 35 through 37 are for Ottawa sand, Figures 38 and 39 are for silica sand, and Figures 40 and 41 are for glass beads. The caption of these figures contain P/D_t ratio, number of rows in the bundle, and minimum fluidization velocity. Preliminary tests conducted at $P/D_t = 1.1$ exhibited bridging of particles, preventing good fluidization. This bridging effect results in voids near 90 degree location, with consequent local hot spots. Hence, the data for $P/D_t = 1.1$ were not considered as a part of this investigation.

The general shape of the local heat transfer coefficient curves for heated tubes in tube bundles are similar to the shapes of the single cylinder local heat transfer coefficient curves shown in Figures 31, 32, and 33. In beds containing larger particles (i.e., Ottawa sand and silica sand) and at velocities slightly below incipient fluidization velocities, the local heat transfer coefficient are maximum at about 90 degree location as can be seen in Figure 36. This slight improvement in local heat transfer coefficient can be attributed to local fluidization that occurs between minimum tube spacings before the general fluidization of the bed, represented by U_{mf} in this study. Figures 35 through 39 show a steady increase in local heat transfer coefficients at all angular locations, with the maximum value shifting towards the downstream location. It should be noted that the zone of the defluidized cap is minimized due

Table 5. Relative Improvement in Local Heat Transfer Coefficient (i.e., h_θ/havg,o) for Tube Bundle (P/D = 1.5) in Fluidized Bed.

Ottawa Sand O. S. 514	Angular Position (Deg.)	U/U_{mf}	1.0	1.25	1.5	1.75	2.0	2.5
		U ft/sec	0.74	0.93	1.11	1.3	1.48	1.8
		havg,o (B/hr ft^2F)	2.3	2.5	2.7	2.9	3.1	3.4
	0		9.2	14.0	15.9	16.2	15.5	13.8
	90		12.7	16.9	18.5	16.9	15.9	14.4
	120		13.1	20.0	22.3	19.0	17.4	16.2
	180		7.8	12.4	16.7	18.2	18.5	17.7
Silica Sand S. S. 715	Angular Position (Deg.)	U/U_{mf}	1.0	1.25	1.5	1.75	2.0	2.5
		U (ft/sec)	1.34	1.68	2.00	2.35	2.68	3.3
		havg,o (B/hr ft^2F)	2.93	3.25	3.5	3.85	4.1	4.6
	0		9.6	10.5	11.3	11.5	11.2	10.0
	90		8.5	9.2	10.2	9.6	9.3	9.1
	120		8.5	9.2	12.0	12.7	12.2	11.8
	180		4.1	6.2	11.6	14.3	13.0	10.6
Glass Beads G. B. 230	Angular Position (Deg.)	U/U_{mf}	1.0	2.0	3.0	4.0	5.0	
		U (ft/sec)	0.16	0.32	0.48	0.64	0.80	
		havg,o (B/hr ft^2F)	1.5	1.75	2.0	2.2	2.4	
	0		3.4	18.3	23.9	24.5	23.3	
	90		2.7	19.5	25.1	26.3	25.5	
	120		2.7	16.0	24.5	26.3	25.5	
	180		2.1	14.3	22.0	23.6	23.3	

Table 6. Relative Improvement in Local Heat Transfer Coefficient (i.e., h_θ/havg,o) for Tube Bundle (P/D = 1.3) in Fluidized Bed.

Ottawa Sand O. S. 514	Angular Position (Deg.)	U/U_{mf}	1.0	1.25	1.5	1.75	2.0	2.5
		U ft/sec	0.74	0.93	1.11	1.3	1.48	1.8
		havg,o (B/hr ft^2F)	2.3	2.5	2.7	2.9	3.1	3.4
	0		8.2	10.3	11.7	12.0	12.0	11.1
	90		10.4	12.0	14.1	14.5	14.2	13.3
	120		7.8	14.0	16.3	16.2	16.1	15.1
	180		5.3	13.2	15.9	15.9	16.5	16.2
Silica Sand S. S. 715	Angular Position (Deg.)	U/U_{mf}	1.0	1.25	1.5	1.75	2.0	2.5
		U (ft/sec)	1.34	1.68	2.00	2.35	2.68	3.3
			2.93	3.25	3.5	3.85	4.1	4.6
	0		7.5	8.0	10.2	10.1	9.3	8.3
	90		7.5	8.0	10.2	9.9	9.3	8.1
	120		8.5	12.3	12.7	11.7	10.8	9.6
	180		5.3	7.4	11.6	11.7	10.8	9.6
Glass Beads G. B. 230	Angular Position (Deg.)	U/U_{mf}	1.0	2.0	3.0	4.0	5.0	
		U (ft/sec)	0.16	0.32	0.48	0.64	0.80	
		havg,o (B/hr ft^2F)	1.5	1.75	2.0	2.2	2.4	
	0		2.7	11.4	22.0	20.0	16.3	
	90		1.9	14.3	29.0	28.2	25.1	
	120		1.3	10.3	26.5	26.9	22.9	
	180		.8	10.3	25.1	24.5	22.1	

to the proximity of the tubes and zigzag flow pattern of the air stream, and it is subjected to rapid changes at higher fluidization velocities.

A comparative study of Tables 5 and 6 for P/D_t = 1.5 and 1.3 shows a pattern of improvement similar to the single tube results discussed earlier with the aid of Figure 34 and Table 4. Even for the case of tube bundles there is rapid improvement in the local heat transfer coefficient at the 180 degree location over a narrow range of fluidization velocities, besides the general increases at all locations with increasing air flow rates. The leveling off values of the local maximum heat transfer coefficients occur at U/U_{mf} = 1.5 for tube bundles when compared to the value of 1.7 for the single cylinder for the case of Ottawa and silica sand. The magnitude of improvement ratio for P/D_t = 1.5 is about the same, i.e., 16 times for spherical Ottawa sand and 12 times for angular silica sand. In the case of glass beads for P/D_t = 1.5, the U/U_{mf} is about 3.0 instead of 4.0 and the magnitude of the maximum improvement is about 23.0 instead of 28.0 for the case of single cylinder. When the P/D_t ratio is reduced to 1.3, the magnitude of the maximum improvement reduced to about 14.0 for Ottawa sand and 10.5 for silica sand but increased to about 25.0 for glass beads.

A detailed comparison of Figure 30 for the single cylinder and Figuer 35 for the tube bundle further reveals the effect of the P/D_t ratio of tube bundle on the local

heat transfer coefficients. It is observed that at less than 1.5 times the minimum fluidization velocity, the shape of the local heat transfer coefficient curves are essentially similar in these two cases. At higher flow velocities whereas the local heat transfer coefficient curves for single cylinder show little difference in magnitude around the cylinder circumference, the shape of the local heat transfer coefficient curves for tubes in tube bundles is such that there exists a considerable difference in the magnitude for the local heat transfer coefficients around the tube circumference. The magnitude of local heat transfer coefficient is considerably higher at the top of the tubes in tube bundle than that at 60 degree location as depicted in Figure 35. This phenomena is to be expected at higher velocities because of the presence of adjacent tubes, and the tubes of the next rows which help in creating mobility of particles in the cap region. On the other hand the proximity of adjacent tubes tend to destroy the particles flow near the sides of the tubes (i.e., in the neighborhood of 60 degree to 90 degree location). The net effect is that the overall heat transfer coefficients for tubes in tube bundle is less than that for a single tube. A comparison of Figure 35 and Figure 36 further reveals that the local heat transfer coefficients for tube bundle with P/D_t equal to 1.3 are generally lower at all locations when compared to those for tube bundle with P/D_t equal to 1.5. In the design of heat exchangers this decrement in heat transfer

per tube is more than compensated since the number of tubes per unit volume can be increased.

The effect of the location of the test cylinder in the tube bundle is seen by comparing Figure 35 with Figure 37. Figure 35 shows the local heat transfer coefficients for the test cylinder placed centrally in a five row tube bundle, and Figure 37 shows the local heat transfer coefficients for the test cylinder placed in the middle of the bottom row of a three row tube bundle. At velocities close to incipient fluidization velocities, the magnitude of the local heat transfer coefficients for the cylinder placed in the middle of the tube bundle is greater than those for the cylinder placed in the bottom row. This is also evident from the visual observations described earlier. It is observed that the particles between the lower rows of tubes and the distributor plate stay relatively inactive until uniform fluidization on the bed surface is observed. Hence, the heat transfer coefficients for a cylinder placed in the bottom row are lower than those for the cylinder placed in the middle of the tube bundle which is experiencing the effects of local fluidization. At higher velocities (i.e., greater than 1.3 times the minimum fluidization velocity) the trend is reversed, i.e., the magnitudes of the local heat transfer coefficients for the heated cylinder placed in the bottom row are higher than those for the cylinder placed in middle of the tube bundle. Here, the reasoning is that even though the particle

activity is more intense, in the region of the tube bundle, the void fraction is also considerably higher in this region when compared to that in the region below the tube bundle. The particle activity and the void fraction affect the magnitude of heat transfer coefficient in opposing ways. The intense activity of particles promotes better heat transfer whereas the high void fraction is detrimental to good heat transfer. The net effect is that at higher flow rates the heat transfer coefficients are higher for the cylinder placed in the bottom row than those for the cylinder placed in the middle row of the tube bundle.

IV.4.3. Average Heat Transfer Coefficients (Fluidization)

Average heat transfer coefficients have been obtained by integrating the local heat transfer coefficients over the entire circumference of the cylinder, i.e.,

$$h_{avg} = \frac{1}{2\pi} \int_0^{2\pi} h_\theta \, d\theta. \qquad (25)$$

The parameters considered are: pitch to diameter ratio of the tube bundle, particle size, type of material, location of the test cylinder in the tube bundle, and superficial air velocity.

Figure 42 and Table 7 show the variation of average heat transfer coefficient for a single cylinder as a function of fluidization velocity with the particle size and type as parameters. The results obtained for the case of no material

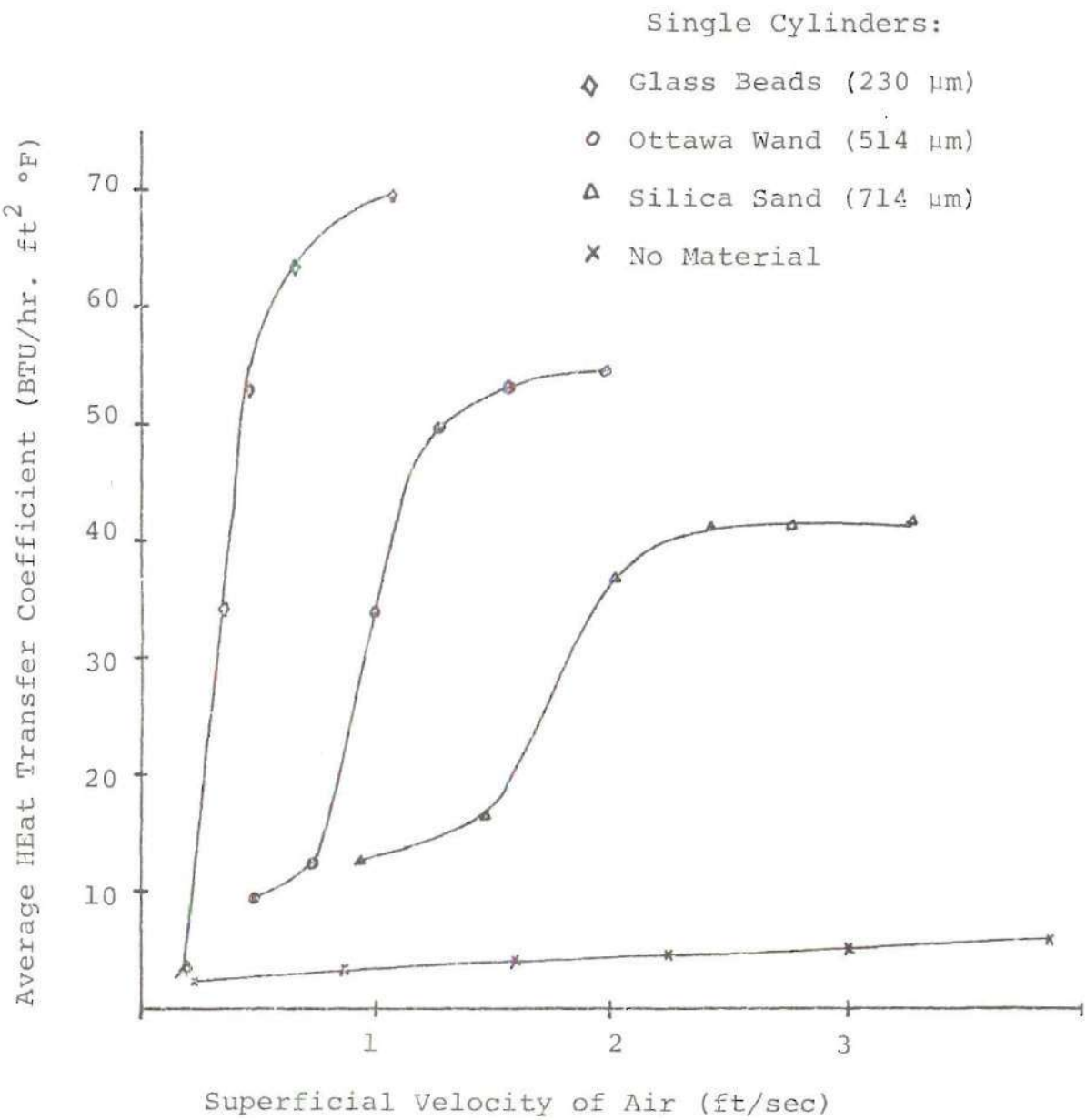

Figure 42. Effect of Fluidization Velocity and Bed Material on Average Heat Transfer. (Single Cylinder)

Table 7. Average Heat Transfer Coefficient and Comparison of Relative Improvement with Single Cylinder (No Material).

		Ottawa Sand (514 μm)						Silica Sand (715 μm)						Glass Beads (230 μm)				
	U/U_{mf}	1.0	1.25	1.5	1.75	2.0	2.5	1.0	1.25	1.5	1.75	2.0	2.5	1.0	2.0	3.0	4.0	5.0
	U (ft/sec)	.74	.93	1.1	1.3	1.48	1.85	1.34	1.68	2.0	2.35	2.68	3.35	0.16	0.32	0.48	0.64	0.80
SINGLE CYLINDER	h_{avg} (B/hr-ft^2-°F)	14.1	26.5	42.8	50.2	52.4	55.0	15.6	23.9	37.4	40.9	41.7	41.3	2.4	28.1	54.9	63.0	66.9
	$h_{avg}/h_{avg,o}$	6.13	10.6	15.8	17.3	16.9	16.18	5.32	7.35	10.7	11.1	10.2	9.0	1.6	16.1	27.5	28.6	27.9
TUBE BUNDLE (P/D_e = 1.5)	h_{avg} (B/hr-ft^2-°F)	23.0	40.1	49.0	49.4	50.0	49.9	21.45	28.14	38.3	42.8	44.1	42.4	2.4	28.1	49.0	56.1	60.2
	$h_{avg}/h_{avg,o}$	10.0	16.0	18.1	17.0	16.1	14.7	7.32	8.66	10.9	10.6	10.8	9.2	1.6	16.1	24.5	25.5	25.1
TUBE BUNDLE (P/D_e = 1.3)	h_{avg} (B/hr-ft^2-°F)	17.6	26.9	37.1	41.8	44.0	45.2	19.5	27.3	37.4	40.0	40.2	39.8	2.4	28.1	52.1	56.1	55.0
	$h_{avg}/h_{avg,o}$	7.7	10.8	13.7	14.4	14.2	13.3	6.66	8.4	10.7	10.4	9.8	8.7	1.6	16.1	26.1	25.0	22.9

are included for comparison. The average heat transfer coefficient is very low at first, and increases slowly for velocities below minimum fluidization velocity. After the minimum fluidization velocity is reached, the heat transfer coefficient increases rapidly over a comparatively narrow velocity range for $U > U_{mf}$. A review of Table 7 shows that for, the case of single cylinder when compared to the case with no fluidization the magnitude of these improvements are about 11, 16, and 28 times, respectively for silica sand, Ottawa sand and glass beads. The variation in heat transfer coefficient with increase in velocity is the result of rapid particle movement and the associated bed voidage. The increase in particle movement causes the heat transfer coefficient to increase, but the increase in bed voidage is somewhat detrimental to good heat transfer. Initially, when the voidage is small, and the particle movement is insufficient, a small increase in particle movement has a strong effect, i.e., the average heat transfer coefficient increases rapidly. At higher fluidization velocities the particle movement becomes too rapid for the temperature of the particle to increase appreciably during the short residence time it is in contact with the heat transfer surface. A further increase in superficial fluid velocity beyond this point has practically no effect, whereas the negative effect of bed voidage comes to prominence. This voidage increases with increase in velocity, which explains

the flat plateau and subsequent decrease in the average heat transfer rates. The velocity at which the transition to fluidization takes place is obvious from the curves, and is in agreement with the minimum fluidization velocities calculated using Leva's (1959) correlation. Figure 42 also shows that about an order of magnitude increase in heat transfer rates can be easily attained by using any of the materials used in the present investigation. These curves show that smaller particles give better heat transfer coefficients than the larger particles considered in this investigation. Maximum heat transfer coefficient obtained with glass beads is about 70 percent higher than that obtained with silica sand. Similarly, the increase in the maximum value of average heat transfer coefficient for Ottawa sand is about 30 percent over that for silica sand.

Figure 43 and Table 7 show the results obtained with the tube bundle of pitch to diameter ratio of 1.5. Figures 44 and 45 are for the pitch to diameter ratios of 1.3 and 1.1 respectively. The shape of the curves is similar to the ones obtained with a single cylinder. A comparison of Figure 42 with Figure 43 shows the effect of the presence of other tubes of the bundle on the heat transfer rate from the test cylinder to the bed. The highest values of the average heat transfer coefficient obtained with the tube bundle and glass beads is about 20 percent lower than that obtained with a single cylinder. The highest values of the average heat

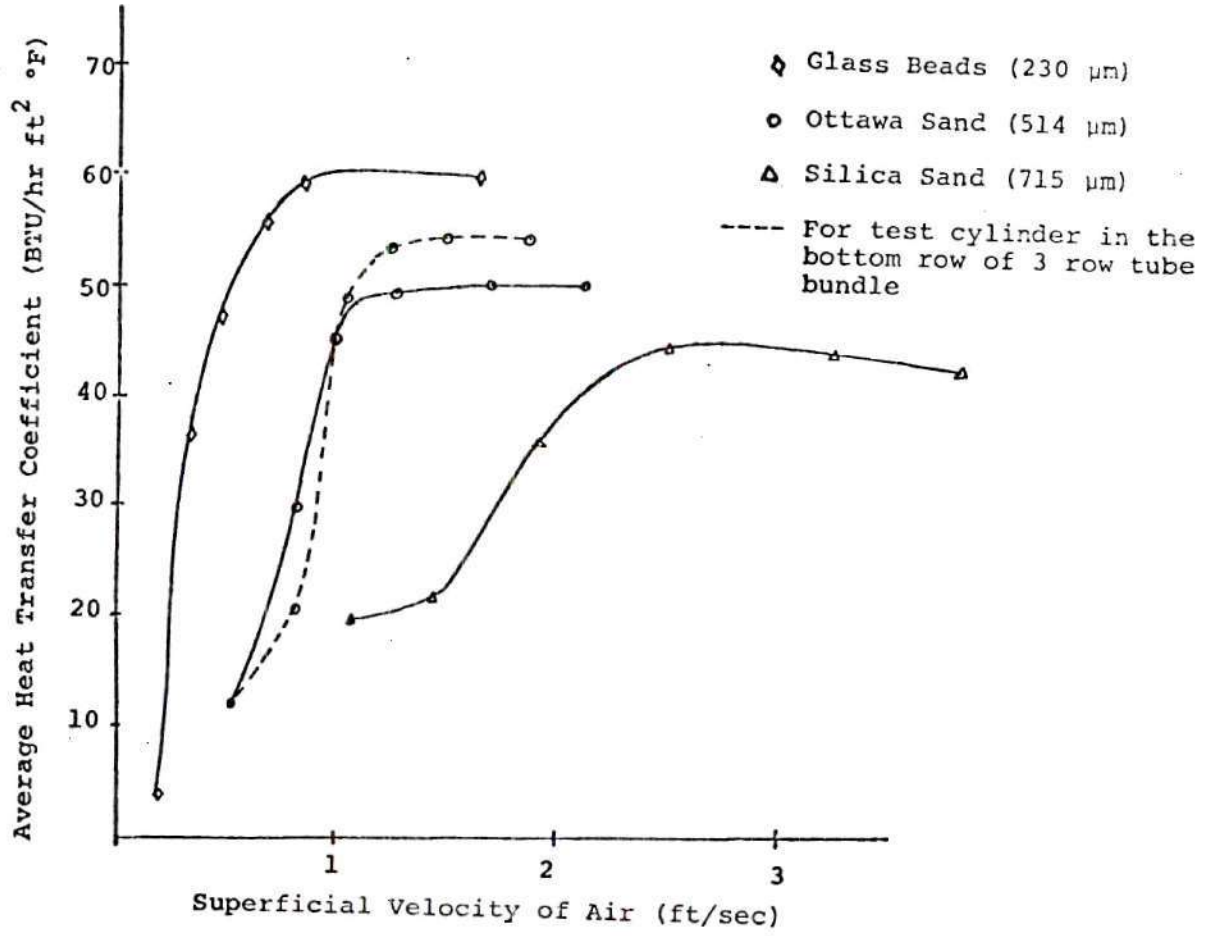

Figure 43. Effect of Fluidization Velocity and Bed Material on Average Heat Transfer. (Tube Bundle, $P/D_t = 1.5$)

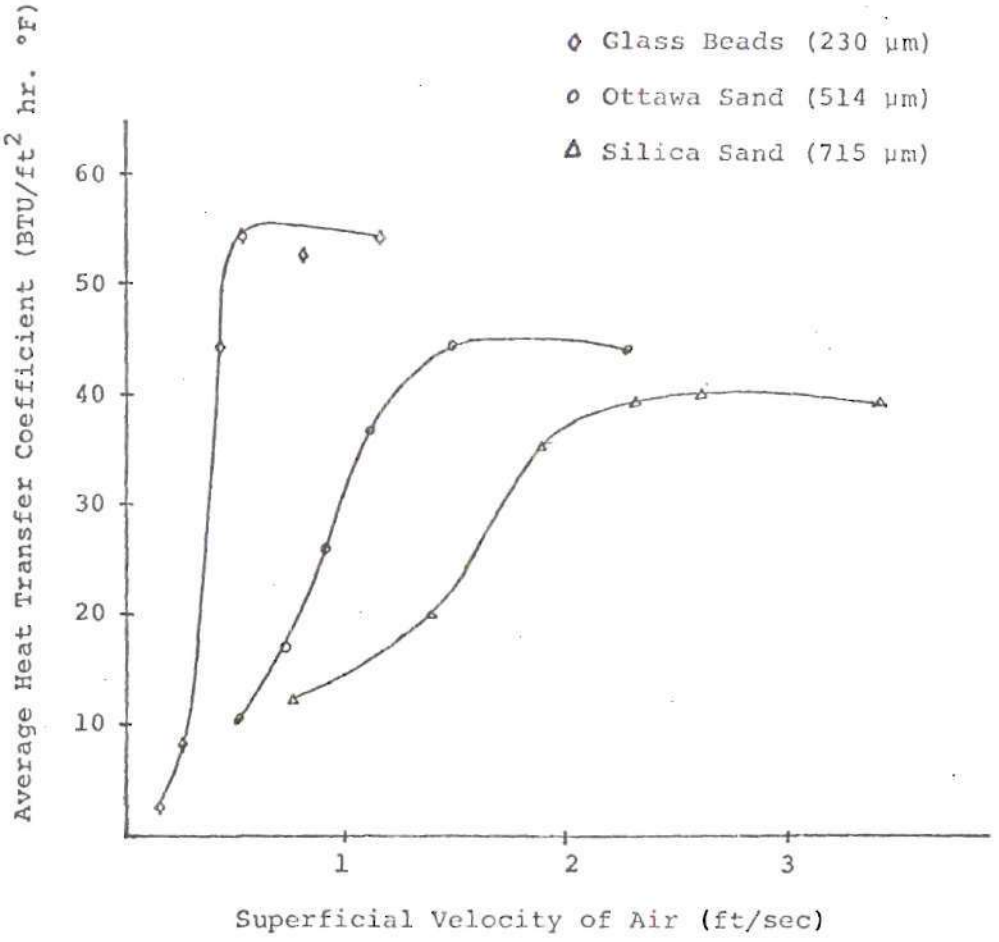

Figure 44. Effect of Fluidization Velocity and Bed Material on Average Heat Transfer. (Tube Bundle, $P/D_t = 1.3$)

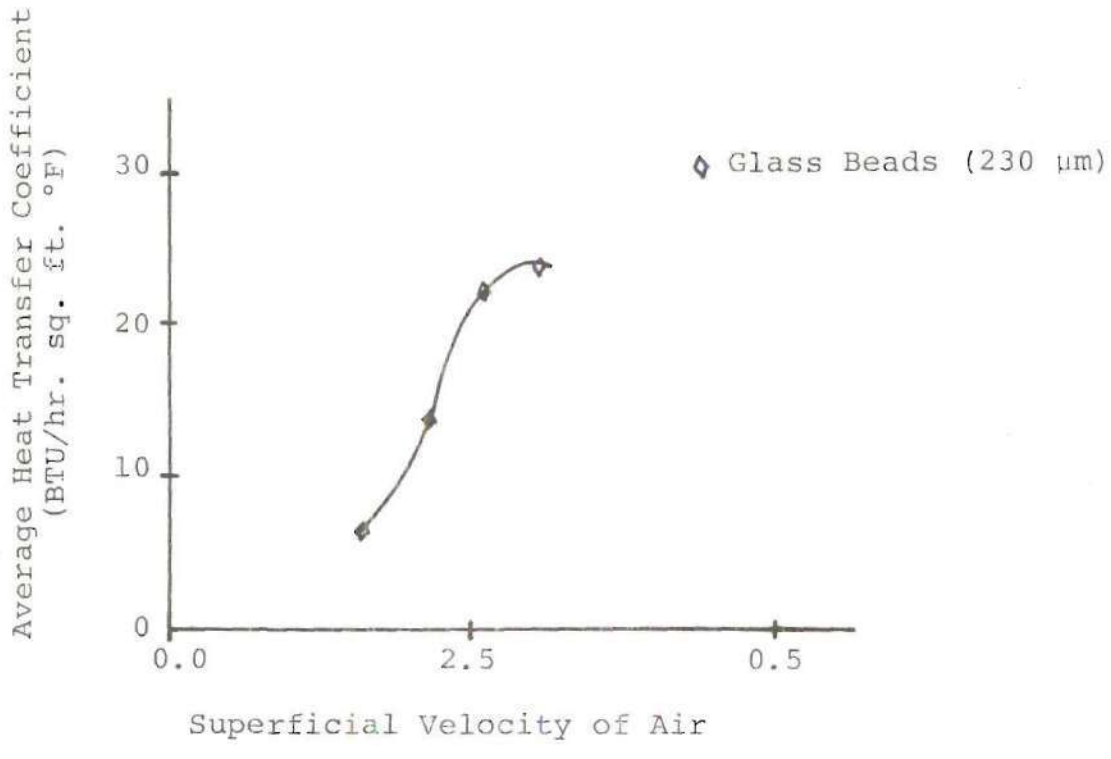

Figure 45. Effect of Fluidization Velocity and Bed Material on Average Heat Transfer. (Tube Bundle, $P/D_t = 1.1$)

coefficients are about the same for the silica sand and Ottawa sand. Based on the results of local heat transfer coefficients with tube bundles, it can be concluded that the presence of adjacent tubes in a tube bundle increases the heat transfer coefficient on the top of the tubes but at the same time their presence inhibits the activity of the particles in the horizontal spacing between the tubes. The net effect is to decrease the average heat transfer coefficient. This reduction is evident from a comparison of Figure 42 with Figure 43. A comparison of Figures 42 and 45 shows that a rather large decrease in heat transfer coefficient takes place for very closely spaced tube bundles utilizing glass beads.

The effect of locating the test cylinder in the bottom row is seen in Figure 43 by a comparison of the dotted curve with the solid line for Ottawa sand. The solid line curve is for the cylinder placed in the middle row of the tube bundle. The average heat transfer coefficient at low velocities in the region of transition for a cylinder in the bottom row is less than that for the cylinder in the middle row. The reasons discussed earlier in the section on local heat transfer coefficients also apply for the trend in the average heat transfer coefficients shown in Figure 43.

Several tests have been repeated to check the reproducibility of the average heat transfer coefficients. These tests have been conducted with different power levels applied to Nichrome V ribbon. A comparison has been made between the

values for the average heat transfer coefficients from the original and duplicate tests. The difference between results are less than three percent in all cases.

IV.4.4. Proposed Mechanism of Heat Transport

A critical review of the observations and experimental results related to the visual observations, the local pressure fluctuations and the variation of heat transfer coefficients around the cylinder suggest the following mechanisms for heat transfer.

At the sides of the cylinder, near minimum fluidization velocities, the particle activity causes increases in the local heat transfer coefficient. Such increases are the result of grazing particles with a region of relatively high local porosity. The movement of particles and associated local flow may be viewed as a thinning of the boundary layer or tripping of the existing boundary layer or transient conduction due to the residence time of these particles causing improvements in the local heat transfer coefficient. It should be noted that, in the case of a cylinder surrounded by a bed of particles there is no separation point which exists for the case of cylinder in cross flow without any fluidized bed. As the flow velocities are increased, this region of relatively high local heat transfer coefficient near the sides of the cylinder spreads from its initial 90 degree position, towards the bottom and the top of the cylinder showing more or less steady improvement in the local heat transfer coefficient.

The tube bundles, when compared to the single cylinder, experience a venturi effect at the 90 degree position because of the minimum area the adjoining tube presents, causing increase in the local air velocity. Such an increase in the local air velocity increases particle activity around 90 degree location at velocities even slightly less than the minimum fluidization velocity. The increased particle activity in turn causes initial improvement in the local heat transfer coefficient at the 90 degree location.

At the low fluidization velocities where initial activity of the particles in the 90 degree position is observed, the tendency for the air to move away from the solid surface to the central regions of the bed causes the existence of a defluidized cap at the top of the cylinder. The size of this cap is somewhat smaller for the tube bundle with an equilateral pitch than for the case of the single cylinder because of the zig-zag nature of the general air flow passage. In both cases, the local heat transfer coefficient near the top of the cylinder (180 degree position) is considerably less than in the other regions since the heat dissipation is governed by a diffusion mechanism instead of the desired convective mechansim with considerable particle activity.

Visual observation has demonstrated the presence of a thin air film relatively void of solid particles at the bottom of the cylinder over its entire length. The existence

of such film was clearly visible at or above $U/U_{mf} \approx 1.5$. Such a cavity can be sustained if the bed, in the presence of a single cylinder or tube bundles, exhibits a tendency to draw air from the adjoining regions of the bed towards the bottom curved surface of the cylinder. These cavities at the bottom of each cylinder are the source for the bubbles which tend to graze around the cylinder. The inflow of cool air into the cavity, its local interaction with the hot cylindrical surface, and the outflow from the cavity are the reasons for the improvement in heat transfer near the zero degree position. Figure 34, for the case of single cylinder, shows a nearly ten fold increase in the local heat transfer coefficient at this zero degree position over a narrow increment in the flow velocity through the bed. The reason for this rapid improvement is due to the pulsating nature of this cavity resulting from bubble formation at the tip of the air film and their subsequent breakaway which occurs at increasing frequencies. Such a flow pattern not only affects the inflow of air into the cavity but also the bubble flow pattern around the entire cylinder, which in turn affects to a smaller extent the defluidized cap.

In the case of tube bubbles, the size of the cavity and the volume of the air passing through it is somewhat diminished because of the proximity of the tubes and the zig-zag passage for the air instead of the straight channelling that occurs in the case of single cylinder. Hence, the improvement in the local heat transfer coefficient over

the range of the fluidization velocities is lower than in the case of single cylinder. But the tube bundle, like the single cylinder, also experiences a rapid rise in the local heat transfer coefficient over a narrow range of increases in the fluidization velocities. This sudden increases in the magnitude of the improvement diminishes, and the location of fluidization velocity at which this occurs decreases with P/D_t ratio.

The visual observations and the pressure fluctuation data at the top of the cylinder for lower range of U/U_{mf} has demonstrated the persistence of the defluidized cap with a consequent low value for the local heat transfer coefficient. As the bubble size and its frequency at the sides of the cylinder increases, the bubbles tend to entrain the material contained in the defluidized cap which is, in turn, replaced by a fresh batch of the particles. Finally, as the fluidization velocity increases the rapid bubbling activity completely replaces the material in the defluidized cap with increasing frequency.

The heat transfer characteristics at the top of the cylinder are influenced greatly by the movement of the particles. In general, the particles are better conductors than stagnant air and they have a very large heat capacity when compared to air. The particles resting on the hot surface absorb heat by conduction similar to the cell of a regenerator matrix used for example in stirling engine. At

low fluidization velocity, the residence time of the particle is too long because of the lack of particle movement and these particles reach the temperature of the surface. Thus the heat is transferred by pure conduction. In a regenerator this ratio of the actual time of exposure to the time required for saturation is termed as exhaustion coefficient. Here, a too long a residence time is an indication that the maximum heat has been stored (or depleted) and residence time longer than that required for the exhaustion coefficient to reach a value say 0.9 will not contribute to the overall heat transfer characteristics. The rate of heat absorption from the surface, and consequent storage in these particles, is rapid at first but is greatly diminished as the surface temperature gradient becomes unfavorable due to the storage of heat. As the residence time decreases because of the increased fluidization velocity and the consequent replacement of the heat-saturated particles by a fresh charge of cold particles the local heat transfer coefficient increases. Before the displaced hot particle finds its way back to the vicinity of the heated cylinder, it will have dissipated all its heat to the flowing air in the interstitial space between the cylinders. Figure 34, drawn for a single cylinder in the presence of Ottawa sand particles, shows the lowest value of heat transfer coefficient at the top of the cylinder and at the minimum fluidization velocity. The heat transfer coefficient increases to a maximum value at about $U/U_{mf} = 1.8$.

This velocity ratio represents the optimum time for replacement of the material in the defluidized cap. Beyond this point the improvement is very slight, indicating a frequency of replacement of the particles is too fast to take full advantage of the largest temperature gradient between the surface and the particles of the bed. Here principle mechanism of heat transfer is assumed to be heat absorption and storage by the particles and their subsequent removal. If particles are removed too quickly the full storage potential of particles is not utilized. This concept is similar to a regenerator cell having a low utilization coefficient.

In the case of tube bundles, the proximity of the tubes reduces the size of the defluidized cap. Except for the bridging experienced with glass beads at a $P/D_t = 1.1$, the lower P/D_t is a preferable arrangement. The zig-zag passage of air tends to reduce the size of the bubbles, increase their frequency, and also the passage of the bubbles close to the defluidized cap influences the rapidity with which the material in the defluidized cap can be replaced. The experimental data on the maximum local heat transfer at the top of the cylinder for the tube bundles with Ottawa sand shows a leveling off at $U/U_{mf} = 1.5$ instead of 1.8 for the single cylinder.

Fluidized beds used in a thermal system are a high pressure drop device. Yet they are used in the chemical and petroleum industries because of the uniform temperature

characteristics and high surface to volume ratio they present to the processing streams. Introduction of a tube bundle into the bed to promote heat exchange adds insignificantly to the total bed pressure drop. In fluidized beds which exhibit large bubbling and channelling activity, introduction of such a tube bundle favors formation and passage of small bubbles and/or uniform fluidization, which is the desirable effect. The current investigations using visual observations and pressure fluctuation techniques have confirmed this trend towards the desirable behavior of the bed.

In recent engineering applications such as coal gassification and the desulfurization of flue gases, the fluidized bed also plays a prominent role. The temperature of the bed in a coal gassification plant needs to be controlled at the desired temperature for optimum output of the plant; this is accomplished by immersing tube bundles to remove the heat at a controlled rate. This source of heat can be utilized to generate power and sustain the electrical needs of the plant and the nearby community. Unfortunately, the burning coal particles in the defluidized cap creates hot spots and failure of the equipment. The pressure drop for the passage of flue gases in a power plant utilizing a fluidized bed for desulfurization is objectionable. However, if the economizer used in the power plant for heating feed water can be located in this section it can take advantage of the superior heat transfer characteristics, thus reducing its physical size. Moreover,

the trend towards uniform fluidization enhances the effectiveness of desulfurization. It is obvious that if the same thermal system is used for more than one function such as in this case of fluidized bed economizer, then the combined effectiveness will reduce the draw backs of separate units for each function. Furthermore, it will promote the cost effectiveness of arrangement and operation of the entire plant.

The designers of heat transfer equipment would like to realize an essentially uniform heat transfer coefficient around the circumference of a tube and also the highest possible value of this coefficient with minimum expenditure of power. Recognizing the fact that the defluidized cap is detrimental to this desired goal, Figure 34 suggests that the value of U/U_{mf} for a particular P/D_t ratio and particle size should be such that there is rapid replacement of material in the defluidized cap region, thus permitting the attainment of maximum local heat transfer coefficient. Increased air flow beyond this point will only increase the fan power without increasing the heat transfer rates. As explained earlier, the disruption of the defluidized cap is caused by vigorous bubble circulation on the sides and the pulsating air cavity at the bottom. Figure 34 indicates that at the minimum fluidization velocity corresponding to disruption of the defluidized cap at optimum frequency, the local heat transfer coefficients at other parts of the circumference are also

past their rapid rise, thus favoring a more or less uniform local heat transfer coefficient all around the circumference. For the case of tube bundles, the data is similar to Figure 34 except the magnitude of this favorable velocity is less than that for the single cylinder, thus reducing frictional power requirements. The lowest permissible P/D_t ratio should be somewhat larger than the value which exhibits bridging between tubes. Under the condition of bridging there will be drastic reduction in local heat transfer coefficient, a situation analogous to the change between nucleate and film boiling, though its effects on the average value is not so catastrophic. A selection of optimum tube spacing and fluidization velocity for a given particle size and type accommodates largest amount of tube surface per unit volume of the bed permitting not only the amount of the heat transfer surface to be maximum but also the velocity of fluidization to be set at a minimum. A good designer would exhibit a margin of safety to assure that the minimum velocity of air under variable conditions of load will not fall below the -shaped plateau suggested in this investigation.

IV.4.5. Correlation of Experimental Data

The data obtained from the experiments conducted in the present investigation are very limited. Therefore, a generalized correlation of the present data has not been attempted. In the absence of extensive data, generalized heat transfer correlations of previous investigators are used

to compare the results of this investigation. The most frequently quoted correlations are: Vreedenberg (1958), Petrie (1967), Lese (1972), and Andeen, et al., (1976). Vreedenberg's (1958) original correlation, or a modification of it, has been used for the comparison of the present heat transfer data obtained with horizontal tubes. Andeen (1976) found that Vreedenberg's (1958) original empirical relation correlates low void data very well. But, as no account for the void fraction has been made in Vreedenberg's (1958) original correlation, it does not satisfactorily represent the heat transfer data obtained for high velocities of fluidization (i.e., high voidage). Andeen, et al., (1976) modified Vreedenberg's correlation to account for high voidage. The modified correlation is found to represent Andeen, et al., data as well as the data obtained by other investigators (i.e., Petrie, et al., (1967), Vreedenberg (1958), Wender and Cooper (1958), and Ainshtein (1959) very well. This modified correlation of Andeen, et al., is

$$\frac{N_{Nu,t}}{(N_{Pr})^{0.3}} = 900\ (1-\varepsilon)\,[N_{Re,t}/N_{Ar,p}]^{.326} \qquad (26)$$

The experimental conditions for this correlation are very similar to the conditions of the experiments in the present study. The major difference is that Andeen's (1976) experiments were conducted in shallow fluidized beds, with only the

average heat transfer coefficients being reported.

The overall average heat transfer coefficients obtained with a single cylinder for all the three materials used in the present investigation have been correlated using the Vreedenberg's modified correlation as proposed by Andeen (1976). The constants of the correlation proposed by Andeen (1976) have been further modified to fit the data obtained in the present investigation. A least-square fit technique has been used to calculate the new constants. The correlation obtained is

$$\frac{N_{Nu,t}}{(N_{Pr})^{0.3}} = 898.2\ (1-\varepsilon)\,[N_{Re,t}/N_{Ar,p}]^{.3287} \qquad (27)$$

This correlation is further modified to account for the effect of the P/D_t ratio of the tube bundles. The final correlation obtained is

$$\frac{N_{Nu,t}}{(N_{Pr})^{0.3}} = 898.2\ (1-\varepsilon)\,[N_{Re,t}/N_{Ar,p}]^{.3287}\ C_R \qquad (28)$$

where C_R is the correction factor to correct for the effect of the P/D_t ratio of the tube bundles.

The form of equation selected for the correction factor C_R is such that its value is unity for P/D_t tending to ∞ and approaches zero as the P/D_t assumes the minimum value of unit. When using large particles, bridging effects

at P/D_t = 1.1 prevented any further experimentation. Hence, for the case of glass beads only the data for P/D_t = 1.1, 1.3, and 1.5 as well as single cylinder (assumed P/D_t = 6) have been used to develop the correction factor C_R. Again a least-square technique has been used to obtain the expression for C_R, which is

$$C_R = [1 - 0.40\ (P/D_t)^{-2.5}] \tag{29}$$

The properties of air used to obtain the correlation have been evaluated at a film temperature which is defined as

$$T_{film} = \frac{T_{cyl} + T_{bed}}{2} \tag{30}$$

Here T_{cyl} is the average temperature of the cylinder surface, and has been evaluated by integrating the measured local temperatures.

In order to demonstrate the degree of proposed correlation for C_R represented by Equation 29, and graphically shown in Figure 46, all the experimental data (single cylinder and all the tube bundles data for all the three materials tested) have been plotted in Figure 47. For Figure 47, the coordinates chosen are

$$\frac{N_{Nu,t}}{N_{Pr}^{\cdot 3}\ (1-\varepsilon)C_R} \quad \text{and} \quad \frac{N_{Re,t}}{N_{Ar,p}},$$

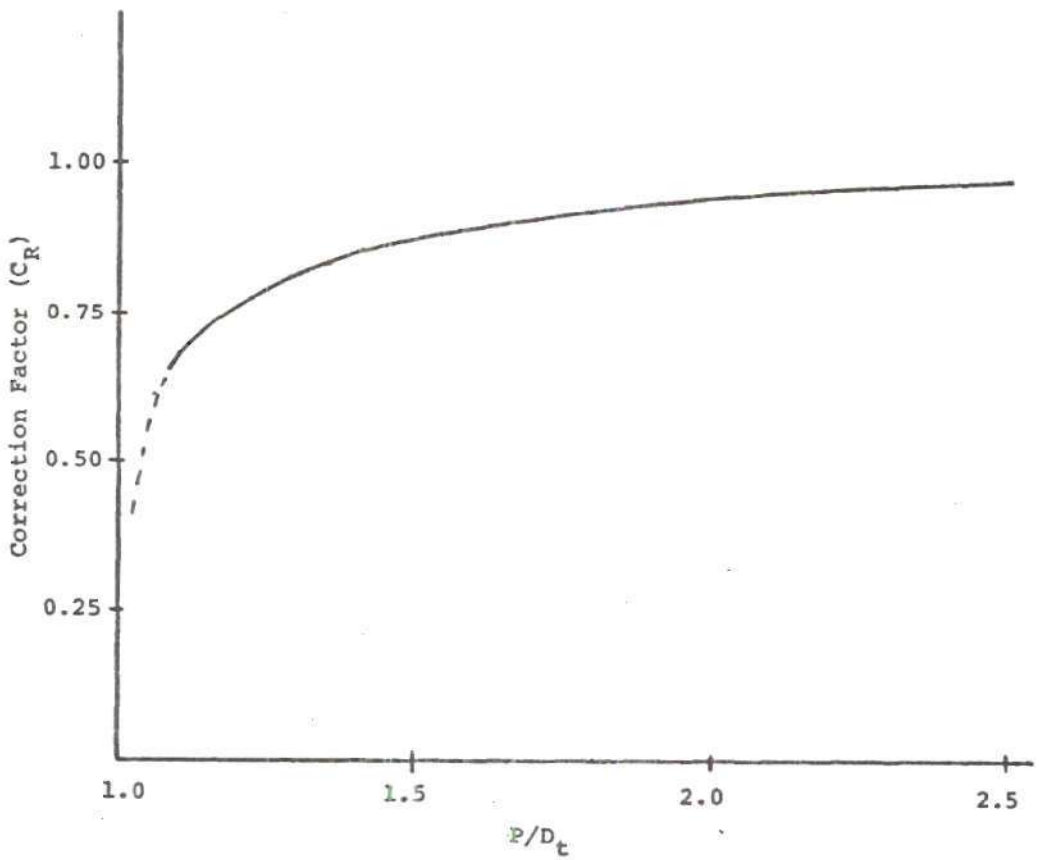

Figure 46. Plot of Correction Factor vs. P/D_t.

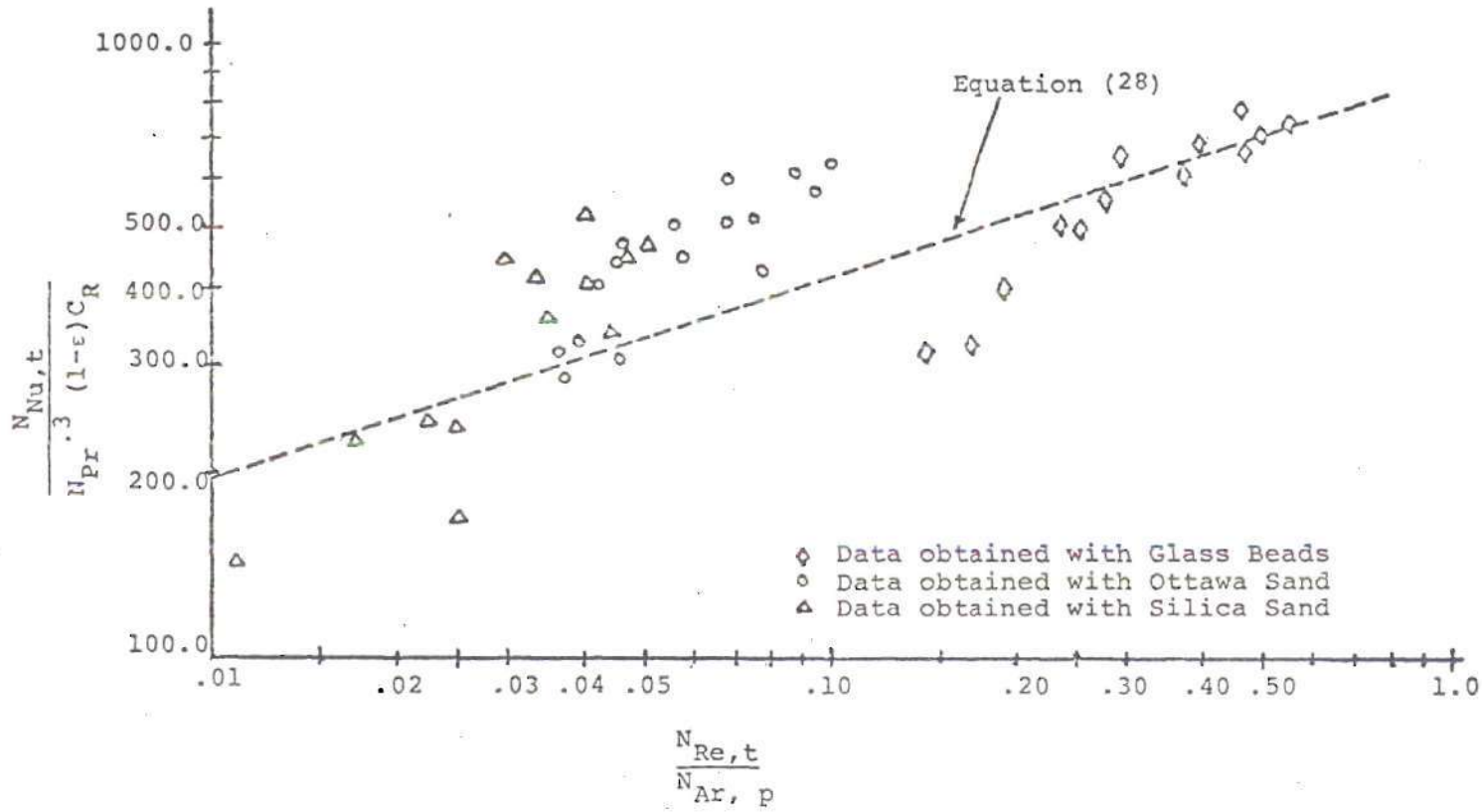

Figure 47. Correlation of Heat Transfer Results.

where the respective values of the parameters are determined by using the experimentally determined values, the properties of the gas/solid media and the arrangement for the particular test. The dashed line shown in Figure 47 represents the solution to Equation 28. The maximum deviation of the proposed correlation from any of the data points is 49%. The scatter in experimental data is in part due to the fact that most of the data has been obtained in fluidized beds operating in bubbling regime. Under bubbling conditions the surface of the fluidized bed fluctuates violently and it has been difficult to make accurate measurements of the expanded bed height. The void fraction (i.e., ε) of the fluidized bed have been calculated, by using a mass balance of particles for the settled bed and for the bed under operating conditions (see Appendix B). This method provides an average void fraction of the fluidized bed. But in real case the local void fraction in the bed under operating conditions, vary with the location in the bed and it exhibits random distribution. More extensive data and a better way of estimating the operating bed void fraction in the vicinity of the heat transfer surface is needed to refine the proposed heat transfer design correlation.

CHAPTER V

CONCLUSIONS AND RECOMMENDATIONS

V.1. An Afterword on This Research Investigation

It is essential to study the particle and gas flow patterns in the vicinity of heat transfer surfaces in order to understand the governing exchange mechanisms. Visual observations from the transparent end faces of a narrow bed in the presence of tube bundles provides an excellent insight into the gross behavior of the bed. Fluidized beds used in industry, generally, possess low aspect ratios and have metallic containers. This, in addition to the opacity of the bed material, render flow visualization techniques useless for tracking the internal behavior of the beds.

The pressure fluctuations recorded by an embedded transducer, and the associated Fourier analysis demonstrated in this study, prove to be useful tools in describing the mechanisms in the interior of the bed. Interpretation of these results provides information about the bubble formation and growth, bubble passage, the defluidized cap at the top of horizontal tubes, and the interaction of the bubble passage with the defluidized regions. In addition the interpretation of results also provide information about the possible existence of uniform fluidization regions. Such a thorough understanding of the flow phenomena forms a basis for

explaining the heat transfer results obtained in this experimental investigation.

In this experimental study horizontal tube bundles of 1-inch diameter tubes, with pitch to diameter ratios of 1.5, 1.3, and 1.1 in a fluidized bed made of either spherically shaped Ottawa sand (514 μm) and glass beads (230 μm) or angular silica sand (715 μm) have been considered. A spirally wound Nichrome ribbon on a slotted teflon cylinder has been used to study the local and average heat transfer coefficients at air velocities from slightly below minimum fluidization to several times above this value. The test cylinder has been located at the bottom row and third row from the bottom in order to study the effect of equilateral pitch and particle flow pattern in the interstitial space on the heat transfer characteristics. Additional data obtained by using only the instrumented heat transfer cylinder with and without defluidized bed have provided a basis for comparison with the previous work and for normalizing the data. Limited tests conducted with an associated cylinder equipped with a pressure transducer has provided a basis to explain the principle mechanism in the fluidized bed used in this experimental study.

V.2. Conclusions

(i) On the basis of the present investigation it is concluded that the onset of local fluidization occurs at 90 degrees from the forward stagnation point of the horizontal cylinder much before general fluidization is observed or

recorded. The latter is recognized when the weight of the bed is balanced by the bed pressure drop. The onset of fluidization has been observed visibly at the intersection of the horizontal tube and the boundary of the fluidized bed and it extends into the interior of the bed as demonstrated by the pressure fluctuations. In the case of horizontal tube bundles with varying pitch to diameter ratios the onset of fluidization occurs at velocities lower than those required for minimum fluidization for the case of a single cylinder. This exhibits the effects of minimum area offered for the through flow by the tube bundles.

(ii) At low fluidization velocities a defluidized cap on the top of the cylinder is evident over the entire length of the tube. In the case of tube bundles, the size of such caps are somewhat reduced due to the zigzag flow pattern of the mean flow. For tubes with a pitch to diameter ratio of 1.1 in beds of small particles (glass beads 230 μm) bridging between tubes was observed, inhibiting a good circulation of the solids. Since these conditions are deterimental to the satisfactory operation of the heat exchanger equipment no additional tests were conducted under such conditions.

(iii) Near the forward stagnation point of the cylinder there is a tendency for a thin air gap to form at minimum fluidization. This air gap provides the source for bubbles which form and then pass around the sides of the cylinder,

resulting in local fluidization. The size of this air gap, fed by the mainstream, grows as the fluidization velocity is increased, and the measured pressure fluctuations are attributed to the formation and detachment of larger size bubbles from this air gap. Eventually, at higher velocities the bubbles form the source for a disruption of the defluidized cap.

(iv) The flow visualization and the pressure fluctuation analysis has helped define three distinct regions of flow patterns around the cylinder at definite velocities of fluidization. For beds using large particles (Ottawa sand or silica sand) the velocity was fifty percent in excess of the minimum fluidization, whereas for beds using small particles (glass beads) it was three hundred percent. These regimes are: (a) the pulsating air gap at the bottom third of the cylinder which bring in cold air to the vicinity of the heat transfer surface. These pulsations are caused by the bubble separation at the edges of the air gap, (b) the bubble passage on both sides of the cylinder, with relatively fewer particles grazing the heat transfer surface, and (c) the interaction of bubbles with the defluidized cap at the top third of the cylinder causing frequent replacement of its contents from the bulk region, thus favoring superior heat transfer characteristics.

(v) The average heat transfer coefficient for the case of a single cylinder with no fluidization is about 30

percent higher than that obtained from Hilpert's (1933) correlation. This has been attributed to the vortices of the free shear layers caused by the jetting fluid from the ragged surface of the distributor plate used in this study. It should be noted that Hilpert's data are for relatively turbulent free air streams. The experimentally determined average heat transfer coefficients have been used in determining the magnitude of improvement in the presence of a fluidized bed both in the case of a single cylinder and tube bundles.

(vi) In general, the average heat transfer coefficient from the horizontal cylinder in the presence of the fluidized bed is several times larger than that for the case of no fluidization.

(vii) The local heat transfer coefficient attains its highest value at the 90 degree location when the gas velocity corresponds to that for incipient fluidization. This may be attributed to the onset of local fluidization. A decrease in the pitch to diameter ratio shifts this peak to lower velocities provided that there is no bridging effect.

(viii) The local heat transfer coefficients at all locations (and also average values of these) exhibit a typical $\int$-shaped curve with increasing fluidization velocity. Over a narrow range of velocities the local value increases rather rapidly. The increase first occurs at the 90 degree location and spreads onto other angular locations.

The propagation of the rapid increase in local heat transfer coefficients is faster towards the forward stagnation point, with 180 degree location being the last one to experience such a rapid rise.

(ix) At minimum fluidization velocity near the defluidized region located at the top of the cylinder, the local heat transfer coefficient is the lowest, suggesting a diffusion dominated heat transfer. At the highest position of the ∫-shaped curve the local heat transfer coefficient at the top of the cylinder reaches a maximum when compared with other locations. At the highest plateau of the ∫-shaped curve it is suggested that the defluidized cap is being periodically replaced due to the passage of the neighboring bubbles. The particles conduct heat better and have larger heat capacity than air. These favorable properties, in addition to periodic particle replenishment, enhance the heat transfer rates near the defluidized region in a fashion somewhat similar to that in a regenerator. It needs to be emphasized that in present design practice, in contrast to the preceding observation, the designer considers the defluidized region dangerous from the viewpoint of industrial equipment design.

(x) At the highest plateau of the ∫-shaped curve the relative improvement due to fluidization when compared with the single cylinder with no fluidization is by a factor of about seventeen for a bed of large spherically-shaped

Ottawa sand, ten for a bed of angularly shaped silica sand and twenty-eight for a bed of small spherical glass beads bed.

(xi) The effect of the proximity of tubes, i.e., decreasing pitch to diameter ratios from 1.5 to 1.3, only slightly reduces the factors by which heat transfer is augmented (over the case without a fluidized bed) for larger particles but reduces to a somewhat larger extent that for glass beads.

(xii) The experimentally determined minimum fluidization velocity is 1.34 ft/sec. for silica sand (715 μm), 0.74 ft/sec. for Ottawa sand (514 μm), and only 0.16 ft/sec. for glass beads (230 μm). The absolute value of maximum average heat transfer coefficient for silica sand (715 μm) is about 44 B/hr-ft^2-f at a fluidization velocity of 2.3 ft/sec. The corresponding values for Ottawa sand (514 μm) is 49 B/hr-ft^2-F at 1.2 ft/sec and for glass beads (230 μm) it is 54 B/hr-ft^2-F at 0.5 ft/sec.

(xiii) The average heat transfer coefficients have been found to agree with modified Vreedenberg's correlation as proposed by Andeen (1976), provided that their correlation is multiplied by a correction factor to account for the effect of P/D_t ratio. This correction factor is given by

$$C_R = [1 - 0.4\ (P/D_t)^{-2.50}].$$

V.3. Recommendations

(i) The pressure probe located inside the test cylinder records all the bubbles that impact on the hole (i.e., on the heat transfer surface) leading to the cavity as well as those passing in its immediate vicinity. It has not been possible to isolate signals originating from these two sources. However, the two have distinctly different influences on the heat transfer mechanism. In particular, the frequency of the bubble contact and the bubble size at the heat transfer surface will have a strong influence on the mechanism.

It is possible to obtain information on the history of the bubbles in motion, originating from the air gap present at the bottom of the cylinder by using at least two pressure probes. One fixed at the 90 degree location and the other moved around the tube circumference as well as within the bed. Comparative study of these two signals, recorded simultaneously and analyzed using Fast Fourier Transform analyzer, will provide joint properties (i.e., joint probability density function, cross correlation function and cross spectral density function). These data will provide the needed information to calculate particle residence times. The time delay measurements via the cross correlation function can be useful in determining the bubble rise velocity as well as its path, the latter by studying the decay of the amplitude around the cylinder at the dominant frequency. The cross-spectral density function

and the coherence functions can also be used to determine the bubble contact frequency. Careful experiments and their analyses based on the signals obtained from two probes is likely to lead to a better description of the flow pattern around the tube in a tube bundle.

(ii) Use of two pressure probes and their interpretation of the signals as proposed here can be successfully used to survey over the entire length of the cylinder to evaluate the two dimensionality of the fluidization flow phenomena. Such an experimentation should include several circumferential locations at a fixed position of the test cylinder, the effect of location of the test cylinder in a tube bundle and the pitch to diameter ratio for various particle sizes and types.

(iii) The proposed replacement theory for the defluidized cap can be confirmed by recording dynamic pressure fluctuations at the top of the cylinder. They should show relatively flat response with a periodic change in pressure signal, this period decreasing with increasing flow velocity.

(iv) It is recommended that a large number of tests be planned to more precisely determine the functional form of rapid rise in the local heat transfer coefficient and the adjoining plateau for such experimental variables as the fluidization velocity, the pitch to diameter ratio and the particle size and type.

(v) The experimental data have been processed using the film temperature for the thermophysical property of the air. This value is the arithmetic mean of the cylinder temperature which is widely varying and the constant free stream temperature. Considering the large heat capacity of the bed material and the ability for the fluidized bed to provide uniform temperature it is recommended that the free stream temperature be tried for future empirical correlations in order to compare the scatter with that of the existing correlation. The basis for this recommendation stems from the experimental observation of Prasanna (1964) about the Mallock-Benard-von Karman vortex shedding behind a single cylinder in cross flow in the presence of heat transfer. Even in the presence of heat transfer the Vortex shedding frequency correlated better when free stream temperature was used instead of the customary film temperature. It should be noted that for the case of a single cylinder with gas flow normal to it, the heat capacity of the fluid contained in vortices is negligibly small when compared to that of the fluidized bed in this investigation, yet it is many times greater than the fluid passing through the boundary layer in the forward half of the cylinder prior to separation.

APPENDIX A

PHYSICAL PROPERTIES OF THE SOLID PARTICLES

The procedure used to estimate the physical properties of the bed material is discussed in this appendix. The physical properties required to describe any particular bed material are, the mean particle size, D_p, the particle density, ρ_p, the packed bed density, ρ_{bed}, the packed bed void fraction ε_{bed}, and the minimum fluidization velocity, U_{mf}.

The mean particle size has been determined by using the method described by Kunii (1968). The size distribution of the particles is first determined by taking a weighted quantity of the material and then passing it through Tyler Standard Screens. The mean diameter, D_p, of the particles is then calculated by using the equation

$$D_p = \frac{1}{\Sigma(x/D_{p,i})} \qquad \text{(A-1)}$$

where

x = weight fraction between consecutive sieving screens

$D_{p,i}$ = geometric mean opening between consecutive screens/ft.

Packed bed density, ρ_{bed}, of a material has been determined by filling the particular material in a container of known volume, and weight. Container filled with the

material is weighted and the packed bed density, ρ_{bed}, has been calculated by taking the ratio of its mass to the volume of the container. Water is then poured into the container filled with material until no more water can be poured with out causing it to overflow. The differential mass has been used to find the volume of the water, that filled void spaces. Packed bed void fraction, ε_{bed}, and the particle density, ρ_p, is calculated from the equations

$$\varepsilon_{bed} = \frac{\text{volume of the water poured}}{\text{volume of the container}} \qquad \text{(A-2)}$$

and

$$\rho_p = \frac{\text{weight of the material in the container}}{\text{volume of container } (1 - \varepsilon_{bed})} \qquad \text{(A-3)}$$

Minimum fluidization velocity, U_{mf}, for the particles has been calculated using Leva's (1959) correlation

$$U_{mf} \cdot \rho_g = \frac{D_p^{1.85}[\rho_g(\rho_p - \rho_g)]}{\mu.88} \qquad \text{(A-4)}$$

where

ρ_p = density of the particles, lb/ft^3

ρ_g = density of the fluidizing air, lb/ft^3

μ = viscosity of the fluidizing air, lb/ft-hr

D_p = mean particle size, ft

U_{mf} = minimum fluidization velocity, ft/hr

The void fraction (ε) of the bed under operating conditions has been estimated by using known mass of the solid

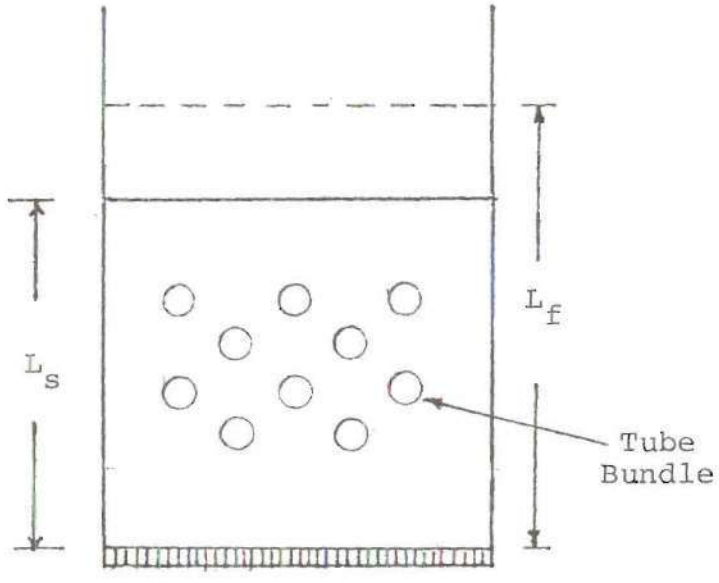

Volume of the tubes = V_T

Area of Cross-section of the Bed = A

Figure A-1. Cross-Sectional View of the Bed Under Operating and Non-Operating Conditions.

for the settled bed and the operating bed volume. Figure A-1 shows the section of a bed containing a tube bundle. The volume occupied by the tubes of the bundle is, V_t. The settled height of the bed is, L_s. Let the height of the bed under operating conditions be, L_f. Under steady state conditions the mass balance for the particles in the bed can be written as

$$\rho_p(L_sA - V_t)\ (1 - \varepsilon_{bed}) = \rho_p\ (L_fA - V_t)\ (1 - \varepsilon) \qquad \text{(A-5)}$$

where

A is the area of crossection of the bed.

ρ_p is the density of the solid particles

Equation A-6 provides an expression for estimating in terms of known quantities, i.e.,

$$\varepsilon = 1 - \frac{(1 - \varepsilon_{bed})\ (L_sA - V_t)}{(L_fA - V_t)} \qquad \text{(A-6)}$$

APPENDIX B

DYNAMIC RESPONSE CONSIDERATIONS OF THE PRESSURE TRANSMITTING SYSTEM

The transient response of pressure measuring instruments is dependent on, the response of the transducer element that senses the pressure, and the response of the pressure-transmitting fluid and the connecting tubing, etc. This latter factor is frequently the one which determines the overall frequency response of a pressure-measurement system. An estimate of the behavior is obtained with the following analysis.

Figure B-1 shows the enlarged view of the cylinder used for pressure fluctuations measurements in the present investigation. The fluctuating pressure has a frequency of, ω, and an amplitude of p_o. The fluctuating pressure is impressed on the tube of length, L, and radius, r. At the end of the tube is a chamber of volume, V, where the connection to the pressure transducer is made. The mass of the fluid contained in this volume vibrates due to pressure fluctuations on the outside of the hole. Because of the influence of fluid friction in the volume space it tends to dampen these pressure fluctuations. Using the conventional formula for laminar friction resistance in tube flow the resulting expression for the pressure amplitude ratio is (Holman (1971)).

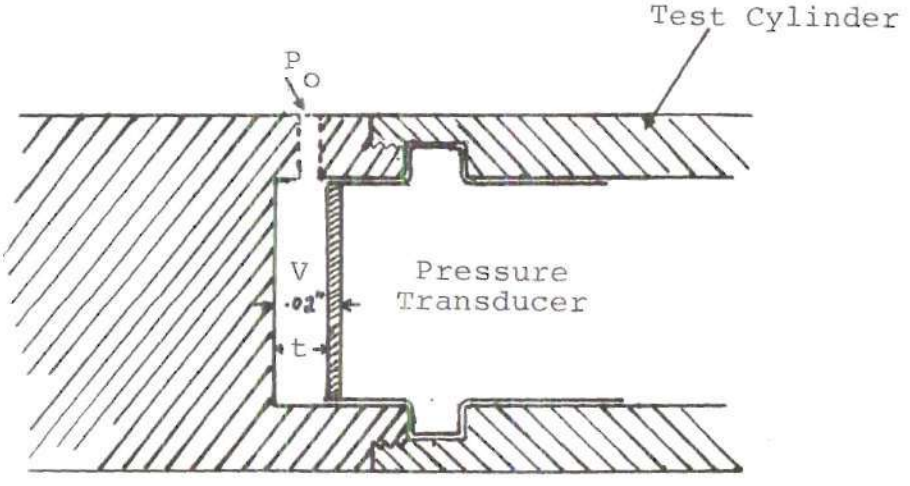

Figure B-1. Pressure Transmitting System.

$$\left|\frac{p}{p_o}\right| = \frac{1}{\{[1 - (\frac{\omega}{\omega_n})^2]^2 + 4h^2 (\frac{\omega}{\omega_n})^2\}^{1/2}} \qquad \text{(B-1)}$$

where p is the amplitude of the pressure signal impressed on the transducer. The natural frequency ω_n is given by

$$\omega_n = \frac{3\pi r^2 c^2}{4LV} \qquad \text{(B-2)}$$

The damping ratio h is given by

$$h = \frac{2\mu}{\rho C r^3} \quad \frac{3LV}{\pi} \qquad \text{(B-3)}$$

where C is the velocity of sound in the fluid, μ is the dynamic viscosity of the fluid, and ρ is the fluid density. The velocity of sound is calculated from

$$C = 49.1\ T^{1/2}\ \text{ft/sec} \qquad \text{(B-4)}$$

where T is the absolute temperature in °R.

In the case of present investigation

L = .2 = inch

r = .0067 inch

V = .0057-cubic inches

For a fluctuating pressure signal of 200 Hz frequency equation B-1, B-2, and B-3 give

$$p/p_o = 1$$

and ω_n is approximately equal to 9 kHz.

The operating variables for pressure fluctuations experienced in this investigation is well below these values.

APPENDIX C

STATISTICAL PROPERTIES OF THE PRESSURE FLUCTUATIONS

In general four types of statistical functions are needed to describe the basic properties of pressure fluctuations signals that have been observed and recorded. Mean square value of the signal furnishes a description of the intensity of pressure fluctuations. The probability density function provides information concerning the properties of the signal in amplitude domain. The autocorrelation function and the power spectral density function contains similar information in the time domain and the frequency domain respectively.

The mean square value is simply the average of the squared value of the time history of the signal or

$$\psi_p^2 = \lim_{T\to\infty} \frac{1}{T} \int_0^T p^2(t)\,dt \qquad \text{(C-1)}$$

where ψ_p^2 is the mean square value of the pressure signal and p(t) is the pressure at any time t.

Furthermore, it is desirable to view the signal as a combination of a static (or steady) and a dynamic (or fluctuating) component. The static component may be described by a mean value which is the average of all values. It is defined by

$$\mu_p = \lim_{T\to\infty} \frac{1}{T} \int_0^T p\ (t)dt \qquad (C\text{-}2)$$

The dynamic component may be described as a variance which is exactly the mean square value of the fluctuations about its mean which is given by

$$\sigma_p^{\ 2} = \lim_{T\to\infty} \frac{1}{T} \int_0^T [p(t)-\mu_p]^2 dt \qquad (C\text{-}3)$$

For the cases where the static component is zero and has been filtered out,

$$\sigma_p^{\ 2} = \psi_p^{\ 2} \qquad (C\text{-}4)$$

The probability density function describes the probability that the signal will assume a value with in some defined range at any instant of time. A probability density function may be defined as

$$\begin{aligned} P(p) &= \lim_{\Delta p\to 0} \text{Prob}\frac{[p < p(t) < p+\Delta p]}{\Delta p} \\ &= \lim_{\Delta p\to} \frac{1}{\Delta p} \left[\lim_{T\to\infty} \frac{T_p}{T}\right] \end{aligned} \qquad (C\text{-}5)$$

where T_p is the total amount of time that p(t) falls inside the range (p, p+Δp) during an observation time T (see Figure C-1a). The probability density function P(p) is always a real-valued non-negative function.

In order to understand the practical significance of probability density functions and their use in analyzing local pressure signals, four examples of idealized sample time

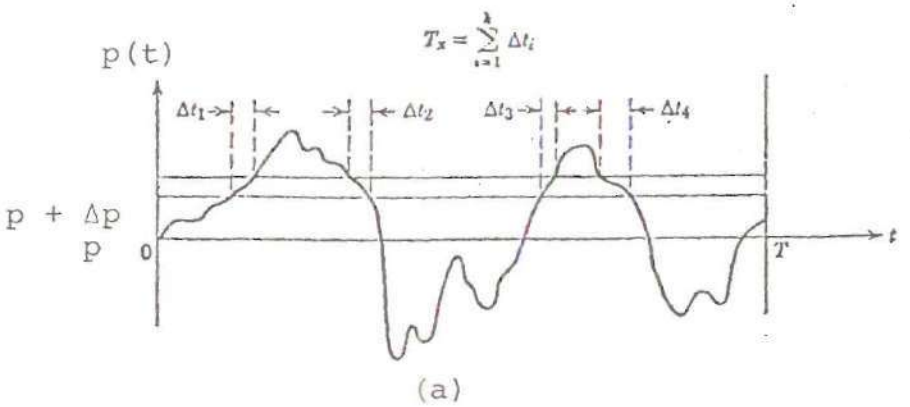

(a)

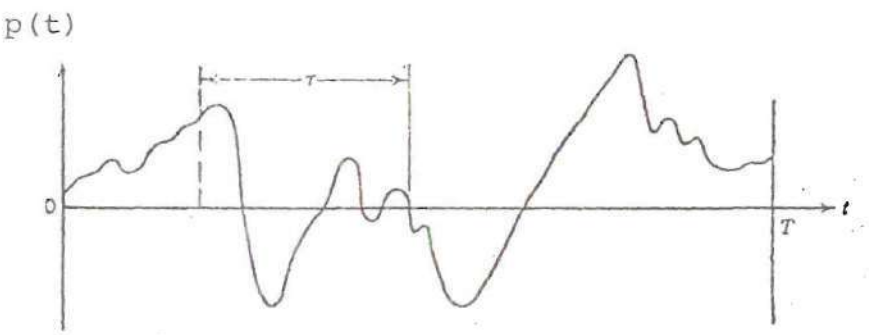

(b)

Figure C-1. Time History Measurements.
(a) Probability Measurement
(b) Auto Correlation Measurement

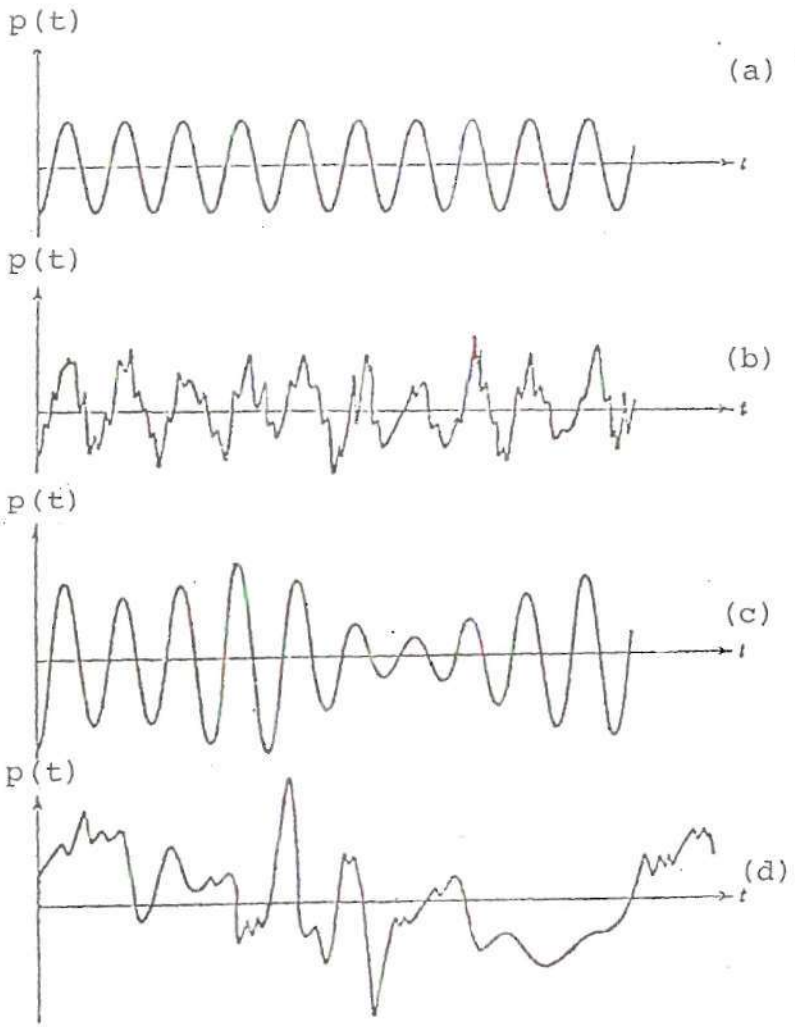

Figure C-2. Four Special Time Histories.
(a) Sine Wave
(b) Sine Wave plus Random Noise
(c) Narrow-Band Random Noise
(c) Wide-Band Random Noise

history records are considered. These are: (a) sine wave, (b) sine wave plus random noise, (c) narrow-band random noise, and (d) wide-band random noise. Typical time history records for each of these examples are presented in Figure C-2. In all cases the mean value is assumed to be equal to zero ($\mu_p = 0$) for convenience. A typical plot of the probability density function, P(p), versus the instantaneous value, p, for each of the four examples is presented in Figure C-3. The four examples in this figure illustrate distinct features of the probability density function covering the range from the sine wave case to the wide-band random noise case.

The autocorrelation function describes the general dependence of the value of the signal at one time to that at another time. Considering the signal time history record p(t) as shown in Figure C-1b, an estimate for the autocorrelation between the values of p(t) at times t and $t+\tau$ can be obtained by taking the produce of the two values and averaging over the observation time T. The resulting average produce will approach an exact autocorrelation function as T approaches infinity, i.e.,

$$R_p(\tau) = \lim_{T\to\infty} \frac{1}{T} \int_0^T p(t)p(t+\tau)dt \qquad (C\text{-}6)$$

where $R_p(\tau)$ is the autocorrelation function or autocorrelogram. The quantity $R_p(\tau)$ is always a real-valued even function having a maximum at $\tau = 0$. It can be either positive or negative.

A typical plot of autocorrellograms, $R_p(\tau)$ as a function of time displacement, τ, for each of the four time histories shown in Figure C-2 is presented in Figure C-4. The important feature of the autocorrelogram is that it persists periodically over all time displacements with the same period as the underlying sine wave. The sharply peaked autocorrelogram which diminishes rapidly to zero as shown in Figure C-4d is typical of wide-band random data with zero mean value. The autocorrelogram for sine wave plus random noise is simply the sum of the autocorrelograms for sine wave and random noise separately, as shown in Figure C-4b. The principle application for an autocorrelation function of measured physical data is to establish the influence of values at any time over values at a future time. Autocorrelation measurements can also be used for detecting deterministic data which might be masked in a random background.

The power spectral density function describes the general frequency composition of the data in terms of the spectral density of its mean square value. The mean square value of a sample time history record in a frequency range between f and $f+\Delta f$ can be obtained by filtering the sample record with a band-pass filter having sharp cutoff characteristics, and computing the average of the squared output from the filter. This average squared value approaches an exact mean square value as the observation time T approaches infinity, i.e.,

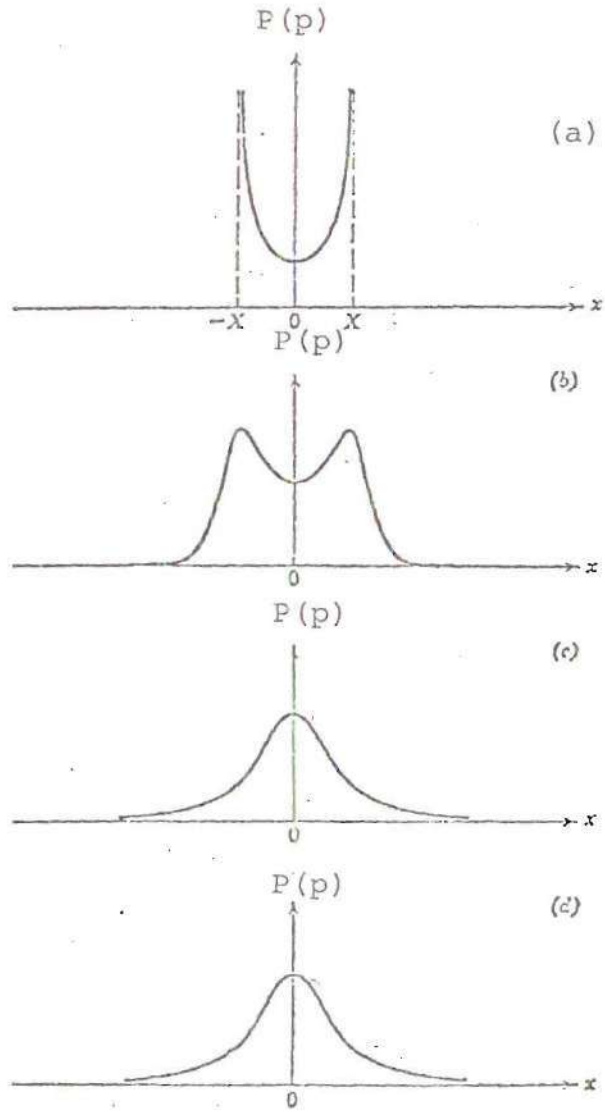

Figure C-3. Probability Density Function Plots.
(a) Sine Wave
(b) Sine Wave Plus Random Noise
(c) Narrow-Band Random Noise
(d) Wide-Band Random Noise

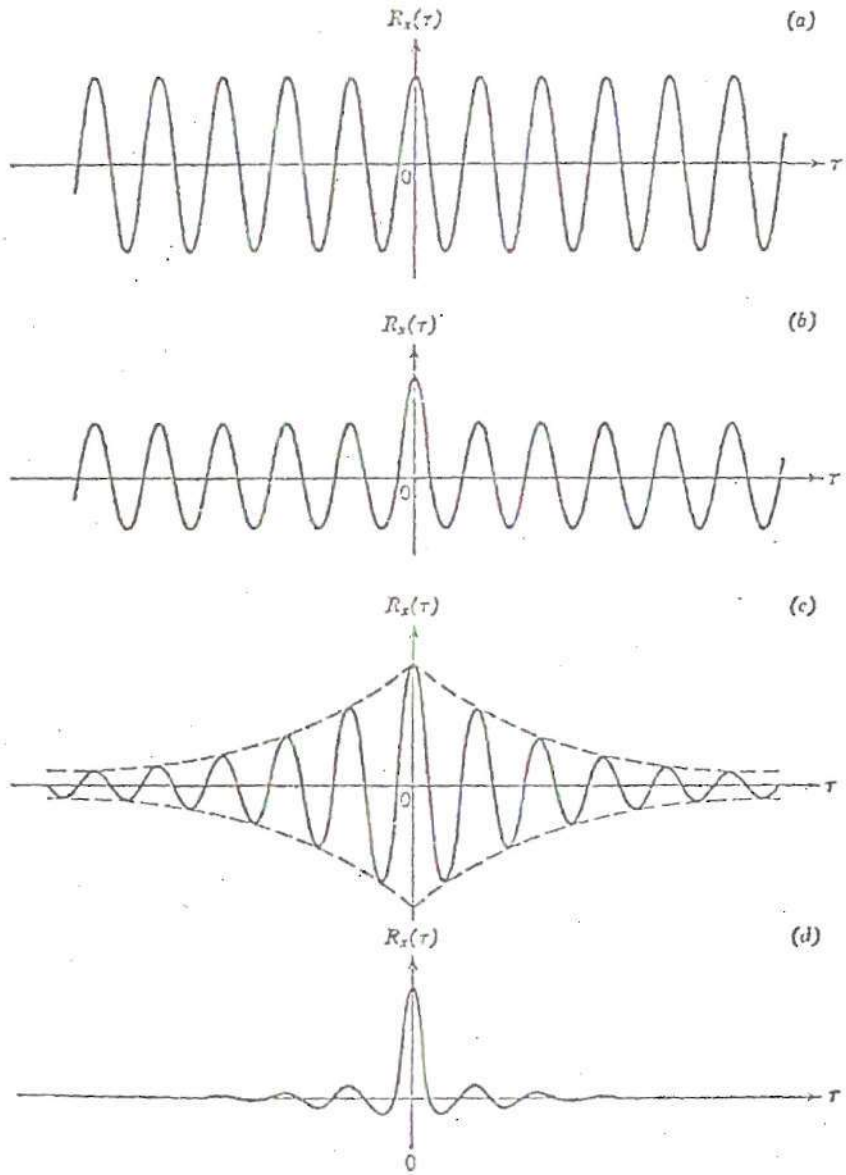

Figure C-4. Auto Correlation Function Plots.
(a) Sine Wave
(b) Sine Wave Plus Random Noise
(c) Narrow-Band Random Noise
(d) Wide-Band Random Noise

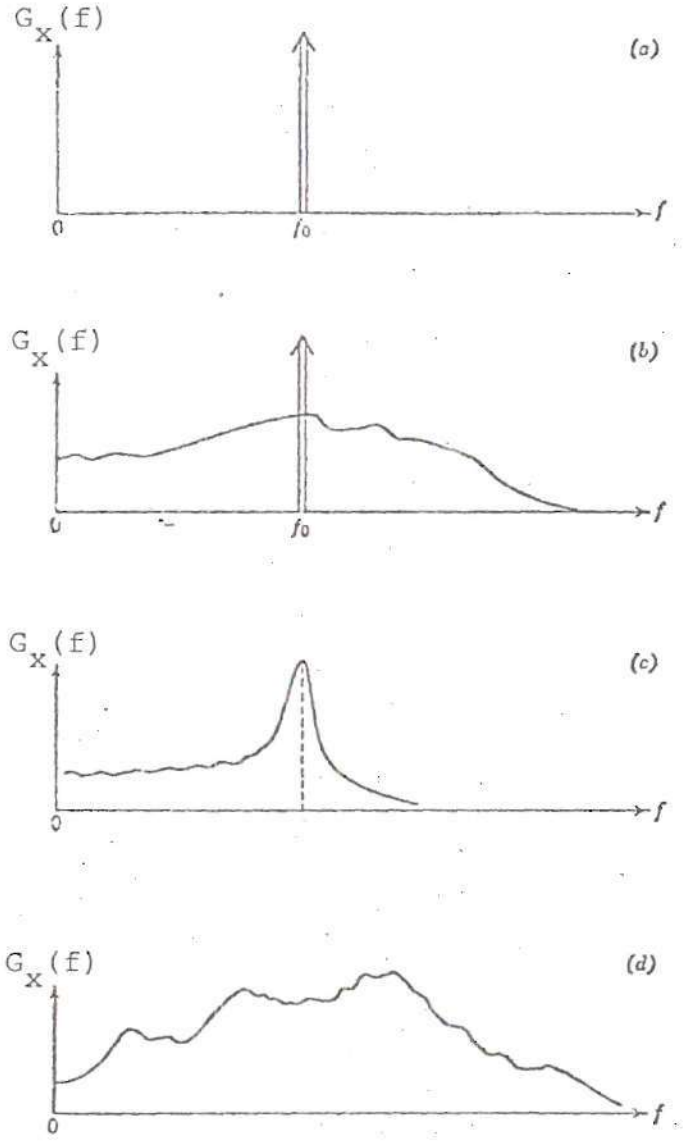

Figure C-5. Power Spectral Density Plots.
(a) Sine Wave
(b) Sine Wave Plus Random Noise
(c) Narrow-Band Random Noise
(d) Wide-Band Random Noise

$$\psi_p^2(f,\Delta f) = \lim_{T\to\infty} \int_0^T p^2(t,f,\Delta f)\,dt \qquad \text{(C-7)}$$

where $p(t,f,\Delta f)$ is that portion of $p(t)$ in the frequency range from f to $f+\Delta f$. For small Δf, a power spectral density function $G_p(f)$ is defined such that

$$\psi_p^2(f,\Delta f) \approx G_p(f)\Delta f \qquad \text{(C-8)}$$

More precisely

$$\begin{aligned} G_p(f) &= \lim_{\Delta f\to 0} \frac{\psi_p^2(f,\Delta f)}{\Delta f} \\ &= \lim_{\Delta f\to 0} \frac{1}{(\Delta f)} \left[\lim_{T\to\infty} \frac{1}{T} \int_0^T p^2(t,f,\Delta f)\,dt \right. \end{aligned} \qquad \text{(C-9)}$$

The quantity, $G_p(f)$, is always a real-valued non-negative function.

A typical plot of power spectral density, $G_p(f)$, versus frequency, f, for each of the four time histories considered in Figure C-2 is presented in Figure C-5. In the present investigation, the purpose in making power spectral density function measurements is to establish the frequency composition of the signal, which in turn provides a qualitative measure of fluidization behavior of the bed.

The method used in the present investigation to obtain the statistical properties of the signal is based on the work of Joseph Fourier (1807) who showed that any well-behaved function can be expanded into an infinite sum of properly

weighted sine and cosine functions of proper frequency, i.e.,

$$p(t) = \sum_{n=0}^{\infty} A_n e^{j(2\pi nt/T)} \qquad \text{(C-10)}$$

where A_n is the fourier coefficient of the n^{th} harmonic term in the series and

$$e^{\pm j(2\pi nt/T)} = \cos(2\pi nt/T) \pm j \sin(2\pi nt/T) \qquad \text{(C-11)}$$

A_n may be found by the fourier transform

$$A_n = \frac{2}{T} \int_{-T/2}^{T/2} p(t) e^{-j(2\pi nt/T)} dt = a_n + jb_n \qquad \text{(C-12)}$$

The power spectral density function can then be constructed from known values of a_n and b_n. The magnitude of the power spectral density function at each frequency is equal to $(a_n^2 - b_n^2)$. A fast Fourier analyzer system was used to simulate such an approach. The analyzer system incorporates the fast Fourier transform algorithm of Cooley and Tuckey (1965) to calculate the discreet fourier transform of the time functions.

APPENDIX D

ERROR ANALYSIS

As in any experimental investigation, the results of this study are subject to an uncertainty interval resulting from specified errors in the individual measurements which are used in the determination of the desired parameters. For example, the temperature measurements are subject to uncertainties in the calibration of the thermocouples, uncertainty in the reading of the potentiometer and the basic inaccuracies in the instruments themselves. The determination of quantities such as heat transfer coefficients involve a larger number of operating variables besides the measurement of temperature. Hence, they have a larger uncertainty interval.

The method of Kline and McClintock (1953) was employed to assess the uncertainty interval for the resutls of this investigation. Basic uncertainties for each variable were estimated to guarantee a 95% confidence level for each of the evaluated variables. Summarized in the following tabulation are the significant measured variables and their associated uncertainty intervals to assure a 95% confidence level in the quoted values of the variables.

Resistivity (R')	1%
Current (i)	.5%
Temperature (t)	.1°F
Temperature ($t-t_b$)	1%

The local heat transfer coefficient for cylinder in the presence of a fluidized bed is given by Equation 17 which is

$$h_t = \frac{327.56\ R'i^2}{(t-t_b)} + \frac{10200\ \frac{d^2t}{dx^2}}{(t-t_b)} \qquad \text{(D-1)}$$

where the first term on the right hand side represents the contribution due to heat generation in the ribbon element and the second term accounts for the effect of circumferential conduction to or from the same ribbon element. The selection of the cross-section of Nichrome V ribbon was based on the premise that the contribution of circumferential conduction to the heat transfer coefficient in all cases is well below 10%. Hence, a maximum estimated uncertanty of 10% in calculating the contribution of circumferential conduction adds only 1% to the uncertainty interval of the local heat transfer coefficient.

Uncertainty interval for a 95% confidence level in the first term on the right hand side of Equation D-1 was calculated by using Kline and McClintock (1953) procedure which is as follows:

$$\text{Let, } A = \frac{327.56\ R'i^2}{(t-t_b)}$$

Therefore, the root mean square uncertainty in the determinants of quantity A is

$$\frac{\Delta A}{A} = \left[\left(\frac{\Delta R'}{R'}\right)^2 + \left(2\frac{\Delta i}{i}\right)^2 + \left(\frac{\Delta (t-t_b)}{t-t_b}\right)^2 \right]^{1/2} \qquad \text{(D-2)}$$

Substituting the values from the above tabulation into Equation D-2, the uncertainty in the calculated value of the heat generation contribution to the local heat transfer coefficient is found to be ±1.73%. Therefore, the uncertainty interval for 95% confidence level in the reported values of local heat transfer coefficients (as shown in Equation D-1) is ±2.73% which also includes 1% error contributed by the circumferential conduction term.

APPENDIX E

COMPUTER PROGRAM

The computer program used to analyze the experimental data is included in this appendix. Figure E-1 is flowchart of the data analysis procedure. The program itself consists of a main program and two subprograms. One of the subprograms utilizes a piecewire cubic spline curve fitting algorithm to calculate the coefficients of the cubic polynomials representing the temperature profile and the second subprogram is a combination of an interpolation subroutine and a curve fit for air-properties table which is used to calculate the properties of air at the local film temperature. The main program utilizes these two subprograms to calculate local and average heat transfer coefficients as well as other parameters of interest (e.g., N_{Nu}, N_{pr}, N_{Re}, etc.) after correcting for the local circumferential heat conduction in the nichrome ribbon.

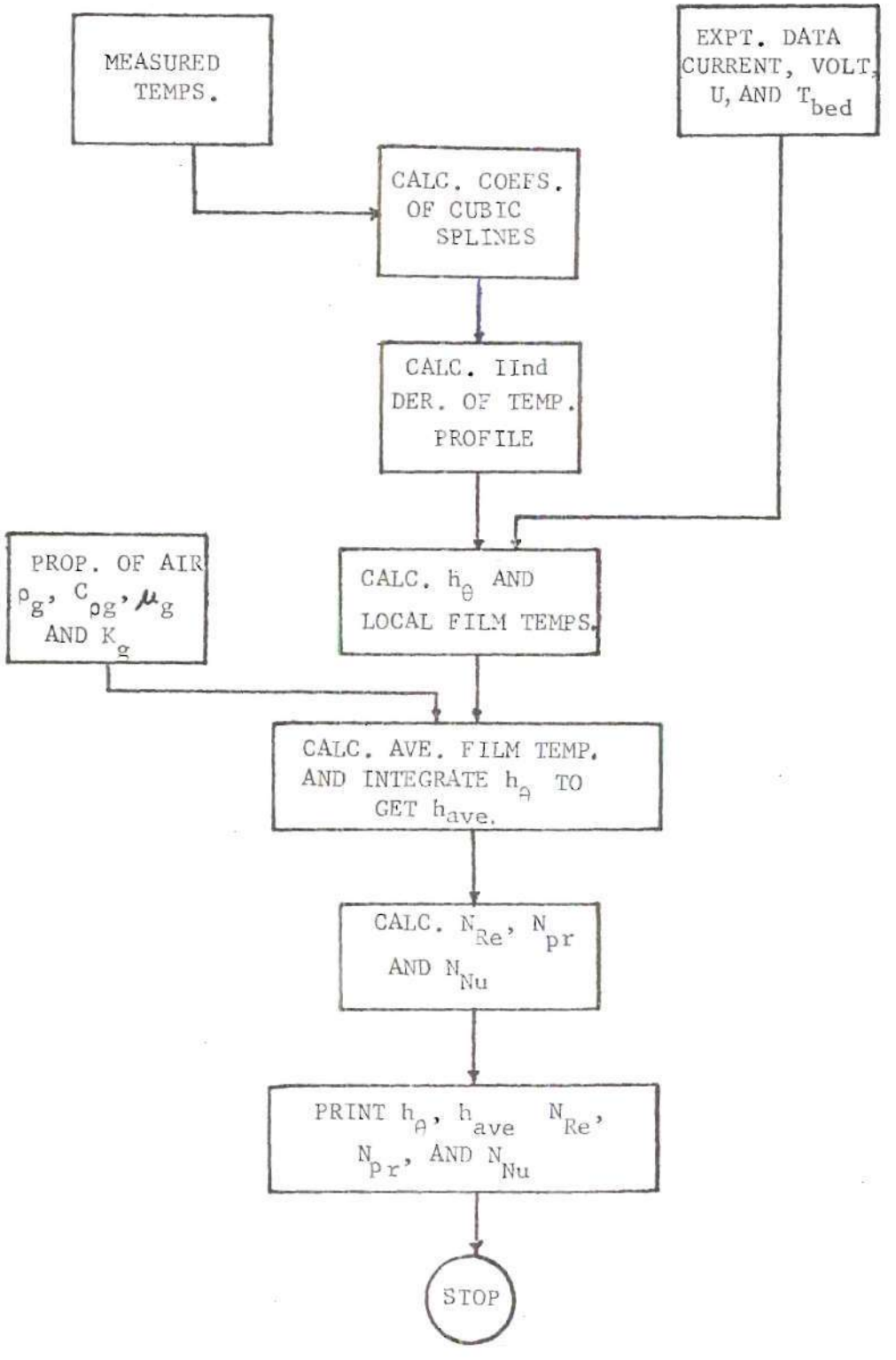

Figure E-1. Schematic of the Data Analysis Procedure.

```
      PROGRAM MAIN(INPUT,OUTPUT,TAPE5=INPUT,TAPE6=OUTPUT)
      INTEGER PR
      DIMENSION PR(7),CTEMP(7),CUR(7),TBED(7),HAVE(7),P(2)
      DIMENSION CRO(4,25),CMU(4,25),CCP(4,25),CK(4,25),XT(20)
      DIMENSION Q(2),T(2),S(2),FNUAV(2)
      DIMENSION FNUS(6,40),PRNAV(2),REYN(2)
      DIMENSION TAVE(6),F1(7),VEL(7),VOLT(7),CRCND(6,40)
      DIMENSION IP(125),NAME(4),F2(7),CCRT(7),EXHT(7)
      DIMENSION HLOC(6,40),DER(6,40),TEMP(6,40),XI(10),C(4,10)
      DATA PR(1),PR(2),PR(3),PR(4)/1H.,1H*,1H+,1H
      DATA PR(5),PR(6),PR(7)/1HX,1HO,1H /
      CALL PROP(XT,CRO,CMU,CCP,CK,N)
      N1=7
      C(2,1)=0.
      C(2,7)=0
      SUM=-30.0
      DO 10 I=1,7
      SUM=SUM+30.
10    XI(I)=SUM
      READ(5,12)(NAME(I),I=1,4)
12    FORMAT(4A2)
      READ(5,*)RATIO,ROWS,STHT
      DO 30 KI=1,6
      READ(5,*)(CTEMP(I),I=1,7),CUR(KI),TBED(KI),F1(KI),VOLT(KI),F2(KI),
     1CCRT(KI),EXHT(KI)
      DO 106 IM=1,7
      IRK=8-IM
106   C(1,IRK)=CTEMP(IM)
      N=N1-1
      CALL SPLINE(N,XI,C)
      CALL CALCCF(N,XI,C)
      X=0
      DO 20 K=1,37
      CALL PCUBIC(X,N,XI,C,P)
      TEMP(KI,K)=P(1)
      DER(KI,K)=P(2)
20    X=X+5.
30    CONTINUE
      DO 40 I=1,6
      DO 40 IJ=1,37
      R=.4342*(1.0+.0001195*(TEMP(I,IJ)-74.1))
      HLO1=142.16*CUR(I)*CUR(I)*R/(.434*(TEMP(I,IJ)-TBED(I)))
      CRCND(I,IJ)=10200*DER(I,IJ)/(TEMP(I,IJ)-TBED(I))
      HLOC(I,IJ)=HLO1+CRCND(I,IJ)
      TFLM=(TEMP(I,IJ)+TBED(I))/2.
      CALL PCUBIC(TFLM,19,XT,CK,P)
      FNUS(I,IJ)=HLOC(I,IJ)/12./P(1)
40    CONTINUE
      DO 60 KL=1,6
      SUM=0
      SUM2=0
      DO 50 IL=1,37
      HTEMP=HLOC(KL,IL)
      TTEMP=TEMP(KL,IL)
      IF(IL.EQ.1.OR.IL.EQ.37)TTEMP=TEMP(KL,IL)/2.
      SUM2=SUM2+TTEMP
      IF(IL.EQ.1.OR.IL.EQ.37)HTEMP=HLOC(KL,IL)/2.
      SUM=SUM+HTEMP
50    CONTINUE
      TAVE(KL)=SUM2/36.
60    HAVE(KL)=SUM/36
      DO 80 IC=1,6
      IR=-2
      FTEMP=F1(IC)*1.04
```

```
      F2(IC)=F2(IC)*1.75*.03611
      VEL(IC)=FTEMP*.48182
      IF(FTEMP.GT.4.)VEL(IC)=((FTEMP-4.)*12.6471+53.)*.036364
      NROWS=ROWS
      IF(ABS(RATIO-99.).LE.0.5)GO TO 181
      WRITE(6,258)(NAME(I),I=1,4),RATIO,NROWS
258   FORMAT(////////10X,"MATERIAL OF THE BED=",4A2/10X,"P/D=",F7.2
     1,5X,"NUMBER OF ROWS=",I2)
      GO TO 183
181   WRITE(6,182)(NAME(I),I=1,4)
182   FORMAT(////////10X,"MATERIAL OF THE BED=",4A2/10X,
     1"SINGLE CYLINDER")
C
183   WRITE(6,259)VOLT(IC),CUR(IC),VEL(IC)
      IF(ABS(F2(IC)-0.).LE.0.005)GO TO 171
      WRITE(6,260)STHT,EXHT(IC),F2(IC)
      GO TO 172
171   WRITE(6,173)STHT,EXHT(IC)
173   FORMAT(10X,"ST.HT.=",F5.1," INCHES",3X,"EX.HT.="
     1,F5.1," INCHES"/10X,"PRESSURE DROP IN THE BED NOT MEASURED")
260   FORMAT(10X,"ST.HT.=",F5.1," INCHES",3X,"EX.HT.="
     1,F5.1," INCHES"/10X,"PRESSURE DROP IN THE BED=",F6.3," PSI")
C
259   FORMAT(10X,"VOLTS=",F8.3,5X,"CURRENT(AMPS.)=",F6.2/
     110X,"SUPERFICIAL VELOCITY OF AIR=",F6.3," FT./SEC.")
172   WRITE(6,401)
401   FORMAT(/12X,"THETA",3X,"TEMP.",3X,"CRCOND",4X,"HLOCAL",3X,
     1"NULOCAL"/)
      THETA=-15
      DO 70 I=1,13
      THETA=THETA+15
      IR=IR+3
70    WRITE(6,204)THETA,TEMP(IC,IR),CRCND(IC,IR),HLOC(IC,IR),FNUS(IC,IR)
204   FORMAT(10X,F6.1,3X,F7.3,2X,F6.3,2(3X,F7.3))
      WRITE(6,257)TAVE(IC)
      WRITE(6,261)CORT(IC)
261   FORMAT(10X,"TEMPERATURE IN THE CORE OF THE CYL.=",F8.3)
257   FORMAT(/10X,"AVERAGE TEMPERATURE OF THE CYLINDER=",F7.3)
      WRITE(6,206)TBED(IC)
206   FORMAT(10X,"TEMPERATURE OF THE AIR STREAM=",F6.2)
      WRITE(6,203)HAVE(IC)
      TFLM=(TAVE(IC)+TBED(IC))/2.
      DO 33 LAC=1,2
      IF(LAC.EQ.2)TFLM=TBED(IC)
      CALL PCUBIC(TFLM,19,XT,CRO,P)
      CALL PCUBIC(TFLM,19,XT,CMU,Q)
      CALL PCUBIC(TFLM,19,XT,CCP,T)
      CALL PCUBIC(TFLM,19,XT,CK,S)
      FNUAV(LAC)=HAVE(IC)/12./S(1)
      PRNAV(LAC)=Q(1)*T(1)/S(1)
      REYN(LAC)=P(1)*VEL(IC)*3600./12./Q(1)
33    CONTINUE
      WRITE(6,333)FNUAV,PRNAV,REYN
333   FORMAT(10X,"NUS.NO.(F.T.)=",F6.2,"   NUS.NO.(A.T.)=",F6.2,/
     18X,"  PR.NO.(F.T.)=",F6.4,"    PR.NO.(A.T.)=",F6.4,/
     18X,"  REY.NO.(F.T.)=",F7.2,"  REY.NO.(A.T.)=",F7.2)
80    CONTINUE
203   FORMAT(10X,"AVERAGE HEAT TRANSFER COEFICIENT=",F7.3)
      WRITE(6,1)
1     FORMAT(//////30X,"HLOCAL(BTU/HR. SQ.-FT. F)"//9X,"0",18X,"25"
     1,18X,"50",18X,"75",/
     29X,"-"3("----------*"))
      DO 300 I=1,37
      DO 301 J=1,120
```

```
301   IP(J)=PR(7)
      KR=I
      IC1=HLOC(1,KR)*.8+.5
      IC2=HLOC(2,KR)*.8+.5
      IC3=HLOC(3,KR)*.8+.5
      IC4=HLOC(4,KR)*.8+.5
      IC5=HLOC(5,KR)*.8+.5
      IC6=HLOC(6,KR)*.8+.5
      IP(IC1)=PR(1)
      IP(IC2)=PR(2)
      IP(IC3)=PR(3)
      IP(IC4)=PR(5)
      IP(IC5)=PR(4)
      IP(IC6)=PR(6)
      WRITE(6,55)(IP(K),K=1,60)
300   CONTINUE
55    FORMAT(9X,"*",120A1)
      WRITE(6,11)
11    FORMAT(9X,"-"3("--------------------*")/9X,"0",18X,"25",18
     1X,"50",18X,"75",//////////)
      STOP
      END
      SUBROUTINE SPLINE(N,XI,C)
      DIMENSION XI(50),C(4,50),D(50),DIAG(50)
      DATA DIAG(1),D(1)/1.,0. /
      NP1=N+1
      DO 10 M=2,NP1
      D(M)=XI(M)-XI(M-1)
10    DIAG(M)=(C(1,M)-C(1,M-1))/D(M)
      DO 20 M=2,N
      C(2,M)=3.*(D(M)*DIAG(M+1)+D(M+1)*DIAG(M))
20    DIAG(M)=2*(D(M)+D(M+1))
      DO 30 M=2,N
      G=-D(M+1)/DIAG(M-1)
      DIAG(M)=DIAG(M)+G*D(M-1)
30    C(2,M)=C(2,M)+G*C(2,M-1)
      NJ=NP1
      DO 40 M=2,N
      NJ=NJ-1
40    C(2,NJ)=(C(2,NJ)-D(NJ)*C(2,NJ+1))/DIAG(NJ)
      RETURN
      END
      SUBROUTINE CALCCF(N,XI,C)
      DIMENSION XI(50),C(4,50)
      DO 10 I=1,N
      DX=XI(I+1)-XI(I)
      DIVDF1=(C(1,I+1)-C(1,I))/DX
      DIVDF3=C(2,I)+C(2,I+1)-2.*DIVDF1
      C(3,I)=(DIVDF1-C(2,I)-DIVDF3)/DX
10    C(4,I)=DIVDF3/DX/DX
      RETURN
      END
      SUBROUTINE PCUBIC(XBAR,N,XI,C,P)
      DIMENSION XI(50),P(2),C(4,50)
      DATA I/1/
      DX=XBAR-XI(I)
      IF(DX)10,30,20
10    IF(I.EQ.1)GO TO 30
      I=I-1
      DX=XBAR-XI(I)
      IF(DX)10,30,30
19    I=I+1
      DX=DDX
20    IF(I.EQ.N)GO TO 30
```

```
      DDX=XBAR-XI(I+1)
      IF(DDX)30,19,19
30    P(1)=C(1,I)+DX*(C(2,I)+DX*(C(3,I)+DX*C(4,I)))
      P(2)=2*C(3,I)+DX*6*C(4,I)
      RETURN
      END
      SUBROUTINE PROP(XT,CRO,CMU,CCF,CK,N)
      DIMENSION RO(20),AMU(20),CP(20),AK(20),XT(20)
      DIMENSION CRO(4,25),CMU(4,25),CCF(4,25),CK(4,25)
      DATA RO/.0829,.0795,.0764,.0736,.0710,.0685,.0662,.0641,.0621,
     1.0602,.0584,.0568,.0552,.0537,.0523,.0509,.0497,.0485,
     2.0474,.0463/
      DATA AMU/.0408,.0421,.0434,.0447,.0460,.0473,.0485,.0497,.0508,
     1.0520,.0532,.0543,.0554,.0565,.0576,.0588,.0599,.0610,.0620,
     2.0631/
      DATA CP/.2398,.2399,.2400,.2402,.2403,.2405,.2406,.2408,.2411,
     1.2413,.2416,.2419,.2422,.2425,.2429,.2432,.2436,.2441,
     2.2446,.2450/
      DATA AK/.0137,.0141,.0146,.0151,.0155,.0160,.0165,.0169,.0173,
     1.0178,.0182,.0186,.0191,.0195,.0199,.0203,.0207,
     2.0211,.0215,.0219/
      SUM=0
      DO 10 I=1,20
      SUM=SUM+20
      XT(I)=SUM
10    CONTINUE
      CRO(2,1)=-.0002
      CRO(2,20)=-.0001
      CMU(2,1)=.0001
      CMU(2,20)=.0001
      CCP(2,1)=.000005
      CCP(2,20)=.0000225
      CK(2,1)=.0000225
      CK(2,20)=.00002
      N=19
      DO 20 K=1,20
      CRO(1,K)=RO(K)
      CMU(1,K)=AMU(K)
      CCP(1,K)=CP(K)
20    CK(1,K)=AK(K)
      CALL SPLINE(N,XT,CRO)
      CALL SPLINE(N,XT,CMU)
      CALL SPLINE(N,XT,CCF)
      CALL SPLINE(N,XT,CK)
      CALL CALCCF(N,XT,CRO)
      CALL CALCCF(N,XT,CMU)
      CALL CALCCF(N,XT,CCF)
      CALL CALCCF(N,XT,CK)
      RETURN
      END
```

APPENDIX F

EXPERIMENTAL DATA AND RESULTS

The raw data obtained during the course of experimentation using pressure transducer imbedded in a cylinder and the spirally wound nichrome V ribbon on a teflon cylinder are included here. First part of this appendix contains data and results pertaining to heat transfer tests and the latter part contains graphical plots of data and results pertaining to pressure fluctuation tests.

Heat Transfer Tests

Table F-1 is a guide to review the heat transfer data and results contained in Tables F-2 through F-13. Some of the important parameters that were held constant during the experiments are contained in Table F-1. Static bed height in all these tests were kept essentially at a constant value of about 11 inches. The expanded height of the bed and the bed pressure drops were measured while the tests were under progress. The velocity range for tests with single cylinder in Table F-2 with no fluidizing material cover the entire spectrum of velocities considered in the fluidized column with various material. These tests and the results obtained from them aided in comparison of the various test results due to presence of fluidized bed. Tables F-3, F-4, and F-5 refer to single

cylinder with three different materials considered in this investigation. Tables F-6, F-7, and F-8 refer to corresponding tests for 5 row tube bundle placed in equilaterial pitch (P/D_t = 1.5) and the heated cylinder located centrally in the mid-row. Tables F-9, F-10, and F-11 refer to tests with P/D_t = 1.3. Results of additional tests conducted with glass beads (230 μm) and P/D_t = 1.1 is contained in Tables F-12. In order to study the effect of location of heat transfer cylinder tests were conducted in a three row tube bundle. Table F-13 refers to tests with Ottawa sand (514 μm), P/D_t = 1.5 and heat transfer cylinder located centrally at the bottom row of the three row tube bundle.

Test data and results contained in each of the tables F-3 through F-13 extend from superficial velocity slightly below that required for minimum fluidization to a value when the local heat transfer coefficient had leveled off essentially at the respective maximum values. Except for data in Table F-12 in all other cases six tests were conducted at various superficial velocities. When increasing velocity the expanded bed height increased. The bed pressure drop in at least four out of six tests remained essentially constant indicating fluidization of the entire bed. Table F-12 corresponds to tests with glass beads (230 μm) at P/D_t = 1.1. The combination of fine particles, narrow spaces between the tubes and the problems associated with bridging prevented extending the velocity range to higher values.

Tables F-2 through F-13 were generated on computers which necessitated some computer oriented nomenclature. They are included here. Included in these tables are temperature distribution around the cylinder at 15 degree intervals. They are based on the readings of thermocouples measured at 30 degree intervals. The need for smooth fitting of curves which assures continuous second derivatives and method of obtaining intermediate values of temperatures are described in the main body of the thesis. Included in these tables are the magnitude of circumferential conduction in the ribbon material which influences local heat transfer characteristics. Information contained at the top of each table are measured values. The numbers listed in columns are local variations obtained from computer-aided analysis. Average values based on these local values are listed at the bottom of each table. In addition, the applicable Reynolds number and Prandtle number based on the properties of air evaluated at the film temperature as well as at the ambient temperature are listed.

Nomenclature

Symbol	Quantity	Units
AMPS.	Current through the Nichrome V ribbon	Amperes
CRCOND	Contribution of conduction along the ribbon to the local heat transfer coefficient as calculated by the second term on the right hand side of equation 30.	BTU/hr ft^2°F

Symbol	Quantity	Units
Ex. Ht.	Expanded bed height or the height of the bed under operating conditions	inches
G. B. 230	Glass beads (230 μm)	--
HLOCAL	Local heat transfer coefficient	BTU/hr ft^2°F
NULOCAL	Local Nusselt number based on local film temperature	dimensionless
NUS. NO. (A.T.)	Average Nusselt number based on free stream temperature	dimensionless
NUS. NO. (F.T.)	Average Nusselt number based on average film temperature	dimensionless
O. S. 514	Ottawa sand (514 μm)	--
PR. NO. (A.T.)	Prandtle number based on properties evaluated at free stream temperature	dimensionless
PR. NO. (F.T.)	Prandtle number based on properties evaluated at average film temperature	dimensionless
REY. NO. (A.T.)	Reynolds number based on properties evaluated at free stream temperature	dimensionless
REY. NO. (F.T.)	Reynolds number based on properties evaluated at average film temperature	dimensionless
S. S. 715	Silica sand (715 μm)	--
ST. HT.	Static height of the bed	inches
TEMP.	Temperature	°F
THETA	Angular location	degrees

Table F-1. Arrangement of Heat Transfer Data and Results

Table No.	Cylinder Arrangement	Pitch/Dia. Ratio	Material of Bed	No. of Tests	Velocity Range ft/sec	Static Height inches	Expanded Height inches	Bed Pressure Drop psi
F-2.	Single	--	--	6	0.20-3.87	--	--	--
F-3.	Single	--	Ottawa sand (514 μm)	6	0.48-196	11.5	11.5-14.5	0.26-0.57
F-4.	Single	--	Silica sand (715 μm)	6	0.94-3.26	11.4	11.4-13.5	0.24-0.52
F-5.	Single	--	Glass beads (230 μm)	6	0.19-1.03	11.0	11.0-13.5	0.30-0.49
F-6.	5 Rows	1.5	Ottawa sand (514 μm)	6	0.54-2.10	11.3	11.3-14.0	0.35-0.54
F-7.	5 Rows	1.5	Silica sand (715 μm)	6	0.75-3.41	11.3	11.3-13.5	0.23-0.49
F-8.	5 Rows	1.5	Glass beads (230 μm)	6	0.18-1.63	11.2	11.2-15.5	0.32-0.47
F-9.	5 Rows	1.3	Ottawa sand (514 μm)	6	0.51-2.29	11.4	11.4-13.5	0.32-0.49
F-10.	5 Rows	1.3	Silica sand (715 μm)	6	1.06-3.82	11.5	11.5-15.3	0.35-0.47
F-11.	5 Rows	1.3	Glass beads (230 μm)	6	0.15-1.15	11.5	11.5-15.0	0.13-0.46
F-12.	5 Rows	1.1	Glass beads (230 μm)	4	0.15-0.30	11.5	11.5-12.0	0.30-0.42
F-13.	3 Rows	1.5	Ottawa sand (514 μm)	6	0.51-1.84	11.3	11.3-13.5	0.32-0.56

Table F-2. Local and Average Heat Transfer Results (Single Cylinder, No Bed Material).

MATERIAL OF THE BED=NOTHING
SINGLE CYLINDER
VOLTS= 4.520 CURRENT(AMPS.)= 1.20
SUPERFICIAL VELOCITY OF AIR= .205 FT./SEC.
ST.HT.= 0.0 INCHES EX.HT.= 0.0 INCHES
PRESSURE DROP IN THE BED NOT MEASURED

THETA	TEMP.	CROND	HLOCAL	NULOCAL
0.0	153.600	.051	1.764	9.290
15.0	153.660	.100	1.811	9.539
30.0	153.900	.149	1.852	9.753
45.0	154.374	.065	1.772	9.326
60.0	155.000	.021	1.687	8.877
75.0	155.708	.101	1.744	9.170
90.0	156.600	.178	1.793	9.424
105.0	157.757	.046	1.623	8.531
120.0	159.000	-.063	1.459	7.649
135.0	160.164	.037	1.545	8.093
150.0	161.400	.155	1.626	8.512
165.0	162.737	-.340	1.095	5.724
180.0	163.400	-.825	.591	3.088

AVERAGE TEMPERATURE OF THE CYLINDER=157.400
TEMPERATURE IN THE CORE OF THE CYL.= 156.400
TEMPERATURE OF THE AIR STREAM= 72.70
AVERAGE HEAT TRANSFER COEFICIENT= 1.599
NUS.NO.(F.T.)= 8.40 NUS.NO.(A.T.)= 8.92
PR.NO.(F.T.)= .7120 PR.NO.(A.T.)= .7114
REY.NO.(F.T.)= 90.65 REY.NO.(A,T.)= 103.93

MATERIAL OF THE BED=NOTHING
SINGLE CYLINDER
VOLTS= 5.125 CURRENT(AMPS.)= 1.38
SUPERFICIAL VELOCITY OF AIR= .667 FT./SEC.
ST.HT.= 0.0 INCHES EX.HT.= 0.0 INCHES
PRESSURE DROP IN THE BED NOT MEASURED

THETA	TEMP.	CROND	HLOCAL	NULOCAL
0.0	148.000	.103	2.920	15.447
15.0	148.143	.311	3.121	16.509
30.0	148.800	.515	3.292	17.404
45.0	150.213	.338	3.046	16.066
60.0	152.200	.166	2.782	14.665
75.0	154.495	.061	2.575	13.549
90.0	156.900	-.038	2.375	12.471
105.0	159.245	-.100	2.219	11.632
120.0	161.400	-.159	2.078	10.873
135.0	163.288	-.086	2.081	10.870
150.0	165.000	-.020	2.089	10.897
165.0	166.518	-.435	1.652	8.607
180.0	167.200	-.765	1.249	6.505

AVERAGE TEMPERATURE OF THE CYLINDER=156.983
TEMPERATURE IN THE CORE OF THE CYL.= 156.100
TEMPERATURE OF THE AIR STREAM= 73.10
AVERAGE HEAT TRANSFER COEFICIENT= 2.449
NUS.NO.(F.T.)= 12.86 NUS.NO.(A.T.)= 13.66
PR.NO.(F.T.)= .7120 PR.NO.(A.T.)= .7114
REY.NO.(F.T.)= 382.49 REY.NO.(A,T.)= 437.95

Table F-2. Cont'd. Local and Average Heat Transfer Results (Single Cylinder, No Bed Material).

MATERIAL OF THE BED=NOTHING
SINGLE CYLINDER
VOLTS= 5.880 CURRENT(AMPS.)= 1.60
SUPERFICIAL VELOCITY OF AIR= 1.583 FT./SEC.
ST.HT.= 0.0 INCHES EX.HT.= 0.0 INCHES
PRESSURE DROP IN THE BED NOT MEASURED

THETA	TEMP.	CRCOND	HLOCAL	NULOCAL
0.0	151.400	.097	3.911	20.645
15.0	151.567	.361	4.185	22.067
30.0	152.400	.658	4.412	23.272
45.0	154.251	.442	4.089	21.534
60.0	156.900	.233	3.735	19.624
75.0	159.979	.022	3.365	17.635
90.0	163.100	-.175	3.017	15.775
105.0	165.945	-.142	2.922	15.239
120.0	168.500	-.111	2.843	14.799
135.0	170.849	.001	2.859	14.851
150.0	173.200	.107	2.873	14.897
165.0	175.508	-.534	2.145	11.102
180.0	176.600	-1.161	1.479	7.646

AVERAGE TEMPERATURE OF THE CYLINDER=163.017
TEMPERATURE IN THE CORE OF THE CYL.= 161.500
TEMPERATURE OF THE AIR STREAM= 72.40
AVERAGE HEAT TRANSFER COEFICIENT= 3.262
NUS.NO.(F.T.)= 17.05 NUS.NO.(A.T.)= 18.21
PR.NO.(F.T.)= .7115 PR.NO.(A.T.)= .7114
REY.NO.(F.T.)= 692.85 REY.NO.(A.T.)= 801.80

MATERIAL OF THE BED=NOTHING
SINGLE CYLINDER
VOLTS= 6.720 CURRENT(AMPS.)= 1.82
SUPERFICIAL VELOCITY OF AIR= 2.240 FT./SEC.
ST.HT.= 0.0 INCHES EX.HT.= 0.0 INCHES
PRESSURE DROP IN THE BED NOT MEASURED

THETA	TEMP.	CRCOND	HLOCAL	NULOCAL
0.0	164.900	.048	4.301	22.459
15.0	165.074	.414	4.657	24.317
30.0	166.100	.772	4.958	25.884
45.0	166.528	.537	4.591	23.964
60.0	172.100	.310	4.182	21.709
75.0	176.327	.020	3.591	19.095
90.0	180.600	-.248	3.236	16.881
105.0	184.413	-.171	3.156	16.263
120.0	187.800	-.100	3.097	15.876
135.0	190.947	.002	3.084	15.769
150.0	194.100	.099	3.070	15.663
165.0	197.161	-.567	2.283	11.620
180.0	198.600	-1.255	1.568	7.973

AVERAGE TEMPERATURE OF THE CYLINDER=186.406
TEMPERATURE IN THE CORE OF THE CYL.= 179.000
TEMPERATURE OF THE AIR STREAM= 71.90
AVERAGE HEAT TRANSFER COEFICIENT= 3.576
NUS.NO.(F.T.)= 18.45 NUS.NO.(A.T.)= 20.00
PR.NO.(F.T.)= .7096 PR.NO.(A.T.)= .7115
REY.NO.(F.T.)= 955.22 REY.NO.(A.T.)=1136.13

Table F-2 Con'd. Local and Average Heat Transfer Results (Single Cylinder, No Bed Material).

MATERIAL OF THE BED=NOTHING
SINGLE CYLINDER
VOLTS= 5.526 CURRENT(AMPS.)= 1.50
SUPERFICIAL VELOCITY OF AIR= 3.015 FT./SEC.
ST.HT.= 0.0 INCHES EX.HT.= 0.0 INCHES
PRESSURE DROP IN THE BED NOT MEASURED

THETA	TEMP.	CRCOND	HLOCAL	NULOCAL
0.0	125.600	-.311	4.841	26.061
15.0	125.569	.469	5.624	30.302
30.0	126.100	1.237	6.334	34.113
45.0	127.678	.756	5.666	30.479
60.0	130.600	.300	4.944	26.546
75.0	133.731	-.044	4.322	23.154
90.0	136.600	-.356	3.763	20.115
105.0	139.449	-.265	3.659	19.516
120.0	141.700	-.182	3.567	19.100
135.0	143.684	-.043	3.597	19.123
150.0	145.600	.088	3.610	19.164
165.0	147.438	-.581	2.832	15.013
180.0	148.300	-1.235	2.130	11.281

AVERAGE TEMPERATURE OF THE CYLINDER=136.292
TEMPERATURE IN THE CORE OF THE CYL.= 136.000
TEMPERATURE OF THE AIR STREAM= 71.30
AVERAGE HEAT TRANSFER COEFICIENT= 4.285
NUS.NO.(F.T.)= 22.91 NUS.NO.(A.T.)= 23.97
PR.NO.(F.T.)= .7132 PR.NO.(A.T.)= .7116
REY.NO.(F.T.)=1378.98 REY.NO.(A,T.)=1532.16

MATERIAL OF THE BED=NOTHING
SINGLE CYLINDER
VOLTS= 6.625 CURRENT(AMPS.)= 1.79
SUPERFICIAL VELOCITY OF AIR= 3.566 FT./SEC.
ST.HT.= 0.0 INCHES EX.HT.= 0.0 INCHES
PRESSURE DROP IN THE BED NOT MEASURED

THETA	TEMP.	CRCOND	HLOCAL	NULOCAL
0.0	138.600	-.427	5.580	29.767
15.0	138.504	.466	6.483	34.610
30.0	139.100	1.348	7.305	38.975
45.0	141.381	.865	6.598	35.142
60.0	145.000	.414	5.811	30.862
75.0	149.273	-.027	5.033	26.637
90.0	153.500	-.413	4.337	22.876
105.0	157.114	-.332	4.177	21.967
120.0	160.100	-.259	4.065	21.324
135.0	162.632	-.031	4.144	21.696
150.0	165.100	.184	4.223	22.062
165.0	167.596	-.608	3.300	17.264
180.0	168.800	-1.377	2.469	12.860

AVERAGE TEMPERATURE OF THE CYLINDER=152.750
TEMPERATURE IN THE CORE OF THE CYL.= 152.900
TEMPERATURE OF THE AIR STREAM= 71.20
AVERAGE HEAT TRANSFER COEFICIENT= 4.958
NUS.NO.(F.T.)= 26.17 NUS.NO.(A.T.)= 27.74
PR.NO.(F.T.)= .7125 PR.NO.(A.T.)= .7116
REY.NO.(F.T.)=1722.53 REY.NO.(A,T.)=1965.48

Table F-3. Local and Average Heat Transfer Results (Single Cylinder, Ottawa Sand (514 μm)).

MATERIAL OF THE BED=O.S.514
SINGLE CYLINDER
VOLTS= 9.220 CURRENT(AMPS.)= 2.44
SUPERFICIAL VELOCITY OF AIR= .481 FT./SEC.
ST.HT.= 11.5 INCHES EX.HT.= 11.5 INCHES
PRESSURE DROP IN THE BED= .265 PSI

THETA	TEMP.	QRCOND	HLOCAL	NULOCAL
0.0	157.600	-.574	9.718	50.947
15.0	157.200	-.164	10.177	53.371
30.0	156.500	.250	10.679	56.035
45.0	156.189	.456	10.923	57.333
60.0	156.700	.656	11.059	58.021
75.0	158.405	.859	11.053	57.906
90.0	161.700	1.035	10.847	56.673
105.0	166.927	1.003	10.266	53.408
120.0	174.200	.955	9.550	49.387
135.0	183.086	-.322	7.578	38.911
150.0	191.200	-1.415	5.942	30.323
165.0	196.193	-1.261	5.799	29.480
180.0	197.800	-1.150	5.819	29.549

AVERAGE TEMPERATURE OF THE CYLINDER=169.667
TEMPERATURE IN THE CORE OF THE CYL.= 173.600
TEMPERATURE OF THE AIR STREAM= 74.50
AVERAGE HEAT TRANSFER COEFICIENT= 9.302
NUS.NO.(F.T.)= 48.28 NUS.NO.(A.T.)= 51.77
PR.NO.(F.T.)= .7105 PR.NO.(A.T.)= .7112
REY.NO.(F.T.)= 207.67 REY.NO.(A,T.)= 241.91

MATERIAL OF THE BED=O.S.514
SINGLE CYLINDER
VOLTS= 10.530 CURRENT(AMPS.)= 2.80
SUPERFICIAL VELOCITY OF AIR= .737 FT./SEC.
ST.HT.= 11.5 INCHES EX.HT.= 11.5 INCHES
PRESSURE DROP IN THE BED= .430 PSI

THETA	TEMP.	QRCOND	HLOCAL	NULOCAL
0.0	153.900	-.164	13.261	69.418
15.0	153.736	-.202	13.249	69.366
30.0	153.200	-.241	13.296	69.643
45.0	157.380	.242	13.913	72.921
60.0	157.000	.731	14.464	75.835
75.0	157.931	1.169	14.750	77.272
90.0	161.000	1.558	14.658	76.599
105.0	166.884	1.446	13.717	71.330
120.0	175.700	1.309	12.517	64.626
135.0	186.757	-.452	9.660	49.441
150.0	196.700	-1.914	7.383	37.507
165.0	202.361	-1.432	7.458	37.735
180.0	204.000	-1.021	7.757	39.205

AVERAGE TEMPERATURE OF THE CYLINDER=171.675
TEMPERATURE IN THE CORE OF THE CYL.= 176.300
TEMPERATURE OF THE AIR STREAM= 75.00
AVERAGE HEAT TRANSFER COEFICIENT= 12.129
NUS.NO.(F.T.)= 62.83 NUS.NO.(A.T.)= 67.45
PR.NO.(F.T.)= .7102 PR.NO.(A.T.)= .7112
REY.NO.(F.T.)= 316.78 REY.NO.(A,T.)= 369.82

Table F-3. Cont'd. Local and Average Heat Transfer Results (Single Cylinder, Ottawa Sand (514 μm)).

MATERIAL OF THE BED=O.S.514
SINGLE CYLINDER
VOLTS= 17.700 CURRENT(AMPS.)= 4.80
SUPERFICIAL VELOCITY OF AIR= 1.002 FT./SEC.
ST.HT.= 11.5 INCHES EX.HT.= 11.6 INCHES
PRESSURE DROP IN THE BED= .569 PSI

THETA	TEMP.	CRCOND	HLOCAL	NULOCAL
0.0	178.800	-1.118	30.940	159.307
15.0	177.749	-.530	31.853	164.145
30.0	175.500	.071	33.172	171.253
45.0	173.054	-.282	33.637	173.997
60.0	170.000	-.658	34.343	178.090
75.0	165.884	-.134	36.440	189.604
90.0	161.500	.442	38.855	202.906
105.0	158.661	3.359	43.067	225.433
120.0	162.000	6.021	44.214	230.799
135.0	174.533	1.340	34.760	179.590
150.0	190.000	-2.232	26.734	136.460
165.0	201.018	-2.537	23.924	121.139
180.0	205.000	-2.945	22.716	114.705

AVERAGE TEMPERATURE OF THE CYLINDER=175.150
TEMPERATURE IN THE CORE OF THE CYL.= 187.700
TEMPERATURE OF THE AIR STREAM= 75.30
AVERAGE HEAT TRANSFER COEFICIENT= 33.977
NUS.NO.(F.T.)=175.46 NUS.NO.(A.T.)=188.85
PR.NO.(F.T.)= .7098 PR.NO.(A.T.)= .7112
REY.NO.(F.T.)= 428.55 REY.NO.(A.T.)= 502.67

MATERIAL OF THE BED=O.S.514
SINGLE CYLINDER
VOLTS= 21.700 CURRENT(AMPS.)= 5.85
SUPERFICIAL VELOCITY OF AIR= 1.268 FT./SEC.
ST.HT.= 11.5 INCHES EX.HT.= 12.0 INCHES
PRESSURE DROP IN THE BED= .569 PSI

THETA	TEMP.	CRCOND	HLOCAL	NULOCAL
0.0	188.500	-.375	43.251	221.001
15.0	188.116	-.174	43.598	222.842
30.0	187.300	.029	44.116	225.628
45.0	186.157	-.742	43.794	224.179
60.0	183.200	-1.555	44.187	226.710
75.0	177.444	-.084	48.205	248.454
90.0	171.500	1.566	52.806	273.478
105.0	168.091	1.036	54.139	281.167
120.0	166.800	.455	54.300	282.299
135.0	166.531	.168	54.170	281.689
150.0	166.600	-.120	53.842	279.964
165.0	166.561	-.011	53.973	280.654
180.0	166.500	.097	54.117	281.420

AVERAGE TEMPERATURE OF THE CYLINDER=175.483
TEMPERATURE IN THE CORE OF THE CYL.= 184.700
TEMPERATURE OF THE AIR STREAM= 75.40
AVERAGE HEAT TRANSFER COEFICIENT= 49.650
NUS.NO.(F.T.)=256.31 NUS.NO.(A.T.)=275.92
PR.NO.(F.T.)= .7097 PR.NO.(A.T.)= .7112
REY.NO.(F.T.)= 541.77 REY.NO.(A.T.)= 635.66

Table F-3. Cont'd. Local and Average Heat Transfer Results (Single Cylinder, Ottawa Sand (514 μm)).

MATERIAL OF THE BED=O.S.514
SINGLE CYLINDER
VOLTS= 21.580 CURRENT(AMPS.)= 5.83
SUPERFICIAL VELOCITY OF AIR= 1.553 FT./SEC.
ST.HT.= 11.5 INCHES EX.HT.= 12.5 INCHES
PRESSURE DROP IN THE BED= .569 PSI

THETA	TEMP.	CRCOND	HLOCAL	NULOCAL
0.0	180.700	-.690	45.673	234.849
15.0	180.023	-.366	46.292	238.161
30.0	178.500	-.038	47.299	243.635
45.0	176.683	-.253	47.920	247.194
60.0	174.300	-.479	48.838	252.413
75.0	171.043	-.230	50.741	262.945
90.0	167.300	.037	53.053	275.773
105.0	163.607	.249	55.453	289.129
120.0	160.400	.477	57.735	301.825
135.0	158.054	.597	59.458	311.437
150.0	156.800	.714	60.469	317.067
165.0	156.639	.179	60.051	314.915
180.0	156.800	-.357	59.399	311.452

AVERAGE TEMPERATURE OF THE CYLINDER=167.675
TEMPERATURE IN THE CORE OF THE CYL.= 176.300
TEMPERATURE OF THE AIR STREAM= 75.10
AVERAGE HEAT TRANSFER COEFICIENT= 53.320
NUS.NO.(F.T.)=277.07 NUS.NO.(A.T.)=296.45
PR.NO.(F.T.)= .7107 PR.NO.(A.T.)= .7112
REY.NO.(F.T.)= 672.02 REY.NO.(A.T.)= 779.64

MATERIAL OF THE BED=O.S.514
SINGLE CYLINDER
VOLTS= 21.660 CURRENT(AMPS.)= 5.85
SUPERFICIAL VELOCITY OF AIR= 1.958 FT./SEC.
ST.HT.= 11.5 INCHES EX.HT.= 14.5 INCHES
PRESSURE DROP IN THE BED= .569 PSI

THETA	TEMP.	CRCOND	HLOCAL	NULOCAL
0.0	173.800	-1.336	48.669	251.604
15.0	172.787	-.127	50.391	260.720
30.0	171.500	1.110	52.296	270.860
45.0	171.640	-.273	50.840	263.285
60.0	171.200	-1.662	49.683	257.387
75.0	168.202	-.343	52.640	273.378
90.0	164.500	1.072	56.230	292.913
105.0	162.316	.713	57.240	298.715
120.0	161.500	.329	57.386	299.680
135.0	161.247	-.261	56.963	297.529
150.0	160.500	-.859	56.861	297.182
165.0	158.708	.372	59.319	310.492
180.0	157.600	1.643	61.376	321.554

AVERAGE TEMPERATURE OF THE CYLINDER=165.817
TEMPERATURE IN THE CORE OF THE CYL.= 175.400
TEMPERATURE OF THE AIR STREAM= 75.30
AVERAGE HEAT TRANSFER COEFICIENT= 54.572
NUS.NO.(F.T.)=283.96 NUS.NO.(A.T.)=303.31
PR.NO.(F.T.)= .7109 PR.NO.(A.T.)= .7112
REY.NO.(F.T.)= 849.14 REY.NO.(A.T.)= 981.99

Table F-4. Local and Average Heat Transfer Results (Single Cylinder, Silica Sand (714 μm)).

MATERIAL OF THE BED=S.S.715
SINGLE CYLINDER
VOLTS= 9.934 CURRENT(AMPS.)= 2.72
SUPERFICIAL VELOCITY OF AIR= .942 FT./SEC.
ST.HT.= 11.4 INCHES EX.HT.= 11.4 INCHES
PRESSURE DROP IN THE BED= .240 PSI

THETA	TEMP.	CRCOND	HLOCAL	NULOCAL
0.0	152.600	-.043	13.522	71.196
15.0	152.494	-.283	13.300	70.035
30.0	151.900	-.527	13.160	69.328
45.0	150.643	.068	13.978	73.713
60.0	149.500	.681	14.801	78.126
75.0	149.410	1.014	15.150	79.977
90.0	151.000	1.318	15.163	79.943
105.0	154.780	1.431	14.632	76.900
120.0	161.100	1.488	13.737	71.822
135.0	169.657	-.245	10.917	56.672
150.0	177.700	-1.700	8.602	44.368
165.0	182.516	-1.396	8.454	43.436
180.0	184.000	-1.151	8.567	43.966

AVERAGE TEMPERATURE OF THE CYLINDER=159.917
TEMPERATURE IN THE CORE OF THE CYL.= 161.200
TEMPERATURE OF THE AIR STREAM= 74.30
AVERAGE HEAT TRANSFER COEFICIENT= 12.743
NUS.NO.(F.T.)= 66.69 NUS.NO.(A.T.)= 70.94
PR.NO.(F.T.)= .7116 PR.NO.(A.T.)= .7113
REY.NO.(F.T.)= 412.97 REY.NO.(A,T.)= 474.05

MATERIAL OF THE BED=S.S.715
SINGLE CYLINDER
VOLTS= 11.100 CURRENT(AMPS.)= 3.03
SUPERFICIAL VELOCITY OF AIR= 1.468 FT./SEC.
ST.HT.= 11.4 INCHES EX.HT.= 11.5 INCHES
PRESSURE DROP IN THE BED= .392 PSI

THETA	TEMP.	CRCOND	HLOCAL	NULOCAL
0.0	148.700	.204	17.983	94.963
15.0	148.796	-.056	17.701	93.465
30.0	148.600	-.315	17.440	92.091
45.0	148.434	-.042	17.801	94.024
60.0	148.000	.235	18.182	96.070
75.0	147.969	.595	18.550	98.015
90.0	148.900	.943	18.674	98.599
105.0	151.541	1.837	18.965	99.917
120.0	157.300	2.571	18.517	97.095
135.0	166.729	.070	14.401	74.922
150.0	176.300	-1.963	11.033	56.956
165.0	182.282	-1.711	10.573	54.318
180.0	184.200	-1.540	10.531	54.024

AVERAGE TEMPERATURE OF THE CYLINDER=157.625
TEMPERATURE IN THE CORE OF THE CYL.= 159.400
TEMPERATURE OF THE AIR STREAM= 74.60
AVERAGE HEAT TRANSFER COEFICIENT= 16.339
NUS.NO.(F.T.)= 85.65 NUS.NO.(A.T.)= 90.91
PR.NO.(F.T.)= .7118 PR.NO.(A.T.)= .7112
REY.NO.(F.T.)= 645.63 REY.NO.(A,T.)= 738.09

Table F-4. Cont'd. Local and Average Heat Transfer Results (Single Cylinder, Silica Sand (714 μm)).

MATERIAL OF THE BED=S.S.715
SINGLE CYLINDER
VOLTS= 17.690 CURRENT(AMPS.)= 4.83
SUPERFICIAL VELOCITY OF AIR= 2.015 FT./SEC.
ST.HT.= 11.4 INCHES EX.HT.= 11.8 INCHES
PRESSURE DROP IN THE BED= .512 PSI

THETA	TEMP.	CRCOND	HLOCAL	NULOCAL
0.0	178.200	.046	32.409	167.075
15.0	178.076	-.416	31.986	164.907
30.0	177.000	-.887	31.850	164.351
45.0	174.320	-.290	33.315	172.282
60.0	171.000	.342	35.089	181.945
75.0	167.820	-.699	35.217	183.085
90.0	163.200	-1.843	35.921	187.459
105.0	156.400	1.548	42.410	222.579
120.0	152.400	5.353	48.290	254.279
135.0	155.505	1.671	42.980	225.733
150.0	161.600	-1.680	36.769	192.142
165.0	165.579	-1.371	35.418	184.470
180.0	166.800	-1.121	35.187	183.085

AVERAGE TEMPERATURE OF THE CYLINDER=166.283
TEMPERATURE IN THE CORE OF THE CYL.= 172.500
TEMPERATURE OF THE AIR STREAM= 74.40
AVERAGE HEAT TRANSFER COEFICIENT= 36.915
NUS.NO.(F.T.)=192.16 NUS.NO.(A.T.)=205.47
PR.NO.(F.T.)= .7109 PR.NO.(A.T.)= .7112
REY.NO.(F.T.)= 874.62 REY.NO.(A.T.)=1013.75

MATERIAL OF THE BED=S.S.715
SINGLE CYLINDER
VOLTS= 19.290 CURRENT(AMPS.)= 5.25
SUPERFICIAL VELOCITY OF AIR= 2.407 FT./SEC.
ST.HT.= 11.4 INCHES EX.HT.= 12.3 INCHES
PRESSURE DROP IN THE BED= .518 PSI

THETA	TEMP.	CRCOND	HLOCAL	NULOCAL
0.0	183.100	.719	37.153	190.830
15.0	183.562	-.234	36.042	185.055
30.0	183.500	-1.184	35.119	180.326
45.0	181.227	-.488	36.574	188.136
60.0	177.800	.240	38.512	198.644
75.0	174.472	-.200	39.325	203.386
90.0	170.700	-.673	40.377	209.469
105.0	166.073	.519	43.611	227.110
120.0	162.500	1.816	46.631	243.557
135.0	161.760	.920	46.109	240.977
150.0	162.800	.008	44.673	233.272
165.0	164.035	-.338	43.720	228.058
180.0	164.600	-.660	43.106	224.750

AVERAGE TEMPERATURE OF THE CYLINDER=171.858
TEMPERATURE IN THE CORE OF THE CYL.= 175.900
TEMPERATURE OF THE AIR STREAM= 74.10
AVERAGE HEAT TRANSFER COEFICIENT= 40.901
NUS.NO.(F.T.)=211.99 NUS.NO.(A.T.)=227.77
PR.NO.(F.T.)= .7103 PR.NO.(A.T.)= .7113
REY.NO.(F.T.)=1036.46 REY.NO.(A.T.)=1212.24

Table F-4. Cont'd. Local and Average Heat Transfer Results (Single Cylinder, Silica Sand (714 μm)).

MATERIAL OF THE BED=S.S.715
SINGLE CYLINDER
VOLTS= 13.280 CURRENT(AMPS.)= 5.25
SUPERFICIAL VELOCITY OF AIR= 2.766 FT./SEC.
ST.HT.= 11.4 INCHES EX.HT.= 13.5 INCHES
PRESSURE DROP IN THE BED= .518 PSI

THETA	TEMP.	CRCOND	HLCCAL	NULOCAL
0.0	180.500	-.445	36.798	189.425
15.0	180.051	-.257	37.142	191.263
30.0	179.000	-.068	37.700	194.303
45.0	177.658	-.226	38.024	196.183
60.0	175.800	-.390	38.549	199.188
75.0	173.178	-.254	39.701	205.579
90.0	170.000	-.111	41.150	213.636
105.0	166.729	.460	43.158	224.662
120.0	164.400	1.061	44.845	233.893
135.0	163.754	.349	44.445	231.936
150.0	163.800	-.370	43.704	228.059
165.0	163.479	.021	44.251	230.976
180.0	163.200	.415	44.782	233.798

AVERAGE TEMPERATURE OF THE CYLINDER=170.808
TEMPERATURE IN THE CORE OF THE CYL.= 174.900
TEMPERATURE OF THE AIR STREAM= 73.90
AVERAGE HEAT TRANSFER COEFICIENT= 41.121
NUS.NO.(F.T.)=213.35 NUS.NO.(A.T.)=229.07
PR.NO.(F.T.)= .7105 PR.NO.(A.T.)= .7113
REY.NO.(F.T.)=1193.16 REY.NO.(A,T.)=1393.79

MATERIAL OF THE BED=S.S.715
SINGLE CYLINDER
VOLTS= 19.290 CURRENT(AMPS.)= 5.25
SUPERFICIAL VELOCITY OF AIR= 3.259 FT./SEC.
ST.HT.= 11.4 INCHES EX.HT.= 13.5 INCHES
PRESSURE DROP IN THE BED= .518 PSI

THETA	TEMP.	CRCOND	HLCCAL	NULOCAL
0.0	177.500	.394	38.665	199.532
15.0	177.688	-.295	37.907	195.592
30.0	177.200	-.988	37.392	193.008
45.0	175.035	-.165	39.026	201.795
60.0	172.500	.696	40.882	211.829
75.0	170.873	-.115	40.736	211.352
90.0	169.000	-.957	40.689	211.432
105.0	165.884	.410	43.449	226.355
120.0	163.600	1.855	45.977	239.978
135.0	164.078	.524	44.415	231.736
150.0	165.600	-.783	42.388	220.881
165.0	166.142	-.287	42.634	222.062
180.0	166.100	.205	43.145	224.731

AVERAGE TEMPERATURE OF THE CYLINDER=169.950
TEMPERATURE IN THE CORE OF THE CYL.= 174.400
TEMPERATURE OF THE AIR STREAM= 73.80
AVERAGE HEAT TRANSFER COEFICIENT= 41.366
NUS.NO.(F.T.)=214.78 NUS.NO.(A.T.)=230.47
PR.NO.(F.T.)= .7106 PR.NO.(A.T.)= .7113
REY.NO.(F.T.)=1407.71 REY.NO.(A,T.)=1642.55

Table F-5. Local and Average Heat Transfer Results
(Single Cylinder, Glass Beads (230 μm)).

MATERIAL OF THE BED=G.B.230
SINGLE CYLINDER
VOLTS= 6.470 CURRENT(AMPS.)= 1.74
SUPERFICIAL VELOCITY OF AIR= .190 FT./SEC.
ST.HT.= 11.0 INCHES EX.HT.= 11.0 INCHES
PRESSURE DROP IN THE BED= .297 PSI

THETA	TEMP.	CRCOND	HLOCAL	NULOCAL
0.0	198.200	.300	3.722	18.950
15.0	198.599	.249	3.660	18.630
30.0	199.700	.197	3.580	18.205
45.0	201.331	.082	3.424	17.391
60.0	203.200	-.029	3.266	16.566
75.0	205.138	.177	3.425	17.351
90.0	207.600	.375	3.566	18.035
105.0	210.905	-.003	3.114	15.713
120.0	214.200	-.364	2.693	13.508
135.0	216.881	.290	3.282	16.498
150.0	220.500	.916	3.837	19.239
165.0	225.896	-.698	2.123	10.613
180.0	228.900	-2.237	.532	2.656

AVERAGE TEMPERATURE OF THE CYLINDER=209.792
TEMPERATURE IN THE CORE OF THE CYL.= 209.000
TEMPERATURE OF THE AIR STREAM= 70.50
AVERAGE HEAT TRANSFER COEFICIENT= 3.173
NUS.NO.(F.T.)= 16.02 NUS.NO.(A.T.)= 17.78
PR.NO.(F.T.)= .7072 PR.NO.(A.T.)= .7117
REY.NO.(F.T.)= 77.94 REY.NO.(A,T.)= 97.03

MATERIAL OF THE BED=G.B.230
SINGLE CYLINDER
VOLTS= 16.060 CURRENT(AMPS.)= 4.30
SUPERFICIAL VELOCITY OF AIR= .351 FT./SEC.
ST.HT.= 11.0 INCHES EX.HT.= 11.4 INCHES
PRESSURE DROP IN THE BED= .493 PSI

THETA	TEMP.	CRCOND	HLOCAL	NULOCAL
0.0	150.500	-5.374	28.092	148.540
15.0	146.962	-1.451	33.563	177.978
30.0	141.000	2.956	40.934	218.089
45.0	137.901	.951	40.678	217.246
60.0	136.200	-1.223	39.536	211.416
75.0	134.072	2.203	44.331	237.434
90.0	135.000	5.589	47.108	252.136
105.0	142.435	2.883	40.101	213.416
120.0	154.400	.651	32.562	171.631
135.0	167.774	-.398	27.138	141.463
150.0	180.300	-1.201	23.210	119.754
165.0	189.805	-2.183	20.297	103.945
180.0	193.600	-3.159	18.634	95.148

AVERAGE TEMPERATURE OF THE CYLINDER=153.158
TEMPERATURE IN THE CORE OF THE CYL.= 164.700
TEMPERATURE OF THE AIR STREAM= 71.20
AVERAGE HEAT TRANSFER COEFICIENT= 34.392
NUS.NO.(F.T.)=181.46 NUS.NO.(A.T.)=192.44
PR.NO.(F.T.)= .7124 PR.NO.(A.T.)= .7116
REY.NO.(F.T.)= 156.18 REY.NO.(A,T.)= 178.32

Table F-5. Cont'd. Local and Average Heat Transfer Results (Single Cylinder, Glass Beads (230 μm)).

MATERIAL OF THE BED=G.B.230
SINGLE CYLINDER
VOLTS= 21.390 CURRENT(AMPS.)= 5.80
SUPERFICIAL VELOCITY OF AIR= .461 FT./SEC.
ST.HT.= 11.0 INCHES EX.HT.= 11.8 INCHES
PRESSURE DROP IN THE BED= .455 PSI

THETA	TEMP.	CRCOND	HLOCAL	NULOCAL
0.0	164.400	-1.925	50.190	262.273
15.0	162.865	-.660	52.322	273.761
30.0	160.000	.657	55.338	290.232
45.0	157.826	.163	56.227	295.428
60.0	156.000	-.315	56.930	299.571
75.0	154.005	.544	59.160	311.823
90.0	153.000	1.429	60.762	320.527
105.0	154.427	1.831	60.152	316.940
120.0	159.200	2.136	57.310	300.776
135.0	167.199	-.236	50.370	262.605
150.0	174.700	-2.252	44.714	231.682
165.0	178.228	-1.214	44.217	228.452
180.0	178.900	-.249	44.901	231.861

AVERAGE TEMPERATURE OF THE CYLINDER=162.425
TEMPERATURE IN THE CORE OF THE CYL.= 171.300
TEMPERATURE OF THE AIR STREAM= 71.60
AVERAGE HEAT TRANSFER COEFICIENT= 53.751
NUS.NO.(F.T.)=281.34 NUS.NO.(A.T.)=300.56
PR.NO.(F.T.)= .7116 PR.NO.(A.T.)= .7115
REY.NO.(F.T.)= 202.15 REY.NO.(A,T.)= 234.05

MATERIAL OF THE BED=G.B.230
SINGLE CYLINDER
VOLTS= 21.090 CURRENT(AMPS.)= 5.74
SUPERFICIAL VELOCITY OF AIR= .661 FT./SEC.
ST.HT.= 11.0 INCHES EX.HT.= 12.2 INCHES
PRESSURE DROP IN THE BED= .466 PSI

THETA	TEMP.	CRCOND	HLOCAL	NULOCAL
0.0	152.600	-1.887	57.165	301.430
15.0	151.391	-.335	59.614	314.654
30.0	149.600	1.276	62.604	330.921
45.0	149.181	.082	61.742	326.476
60.0	148.900	-1.124	60.761	321.364
75.0	147.310	-.254	62.935	333.288
90.0	145.300	.657	65.574	347.830
105.0	144.130	.784	66.753	354.411
120.0	144.200	.900	66.805	354.669
135.0	145.481	.209	64.367	344.557
150.0	147.100	-.456	62.909	333.209
165.0	148.156	-.427	62.061	328.436
180.0	148.500	-.403	61.805	326.990

AVERAGE TEMPERATURE OF THE CYLINDER=147.608
TEMPERATURE IN THE CORE OF THE CYL.= 154.300
TEMPERATURE OF THE AIR STREAM= 72.50
AVERAGE HEAT TRANSFER COEFICIENT= 63.017
NUS.NO.(F.T.)=333.64 NUS.NO.(A.T.)=351.84
PR.NO.(F.T.)= .7127 PR.NO.(A.T.)= .7114
REY.NO.(F.T.)= 296.51 REY.NO.(A,T.)= 334.82

Table F-5. Cont'd. Local and Average Heat Transfer Results (Single Cylinder, Glass Beads (230 μm)).

MATERIAL OF THE BED=G.B.230
SINGLE CYLINDER
VOLTS= 21.200 CURRENT(AMPS.)= 5.77
SUPERFICIAL VELOCITY OF AIR= .902 FT./SEC.
ST.HT.= 11.0 INCHES EX.HT.= 13.2 INCHES
PRESSURE DROP IN THE BED= .449 PSI

THETA	TEMP.	CRCOND	HLOCAL	NULOCAL
0.0	145.600	-.714	65.158	345.369
15.0	145.177	-.160	66.095	350.457
30.0	144.500	.402	67.280	356.935
45.0	144.215	.045	67.188	356.529
60.0	144.000	-.316	67.030	355.749
75.0	143.451	-.066	67.301	360.000
90.0	142.800	.189	68.684	364.875
105.0	142.344	.073	69.015	366.770
120.0	142.000	-.044	69.240	368.064
135.0	141.698	.268	69.854	371.417
150.0	141.800	.578	70.062	372.492
165.0	142.515	-.151	68.623	364.633
180.0	143.000	-.868	67.433	358.173

AVERAGE TEMPERATURE OF THE CYLINDER=143.233
TEMPERATURE IN THE CORE OF THE CYL.= 149.400
TEMPERATURE OF THE AIR STREAM= 73.10
AVERAGE HEAT TRANSFER COEFICIENT= 68.097
NUS.NO.(F.T.)=361.63 NUS.NO.(A.T.)=379.83
PR.NO.(F.T.)= .7129 PR.NO.(A.T.)= .7114
REY.NO.(F.T.)= 406.78 REY.NO.(A,T.)= 455.67

MATERIAL OF THE BED=G.B.230
SINGLE CYLINDER
VOLTS= 21.140 CURRENT(AMPS.)= 5.77
SUPERFICIAL VELOCITY OF AIR= 1.032 FT./SEC.
ST.HT.= 11.0 INCHES EX.HT.= 13.5 INCHES
PRESSURE DROP IN THE BED= .455 PSI

THETA	TEMP.	CRCOND	HLOCAL	NULOCAL
0.0	145.000	-2.190	64.505	341.994
15.0	143.760	-.336	67.524	358.356
30.0	142.000	1.597	71.184	378.306
45.0	141.885	.483	70.185	373.033
60.0	142.500	-.628	68.459	363.681
75.0	142.511	-.342	68.735	365.143
90.0	142.000	-.056	69.531	369.521
105.0	141.409	.254	70.440	374.531
120.0	141.200	.567	70.968	377.399
135.0	141.615	-.019	69.357	371.901
150.0	142.000	-.599	68.988	366.635
165.0	141.770	-.026	69.793	370.985
180.0	141.500	.551	70.645	375.591

AVERAGE TEMPERATURE OF THE CYLINDER=142.158
TEMPERATURE IN THE CORE OF THE CYL.= 147.700
TEMPERATURE OF THE AIR STREAM= 73.40
AVERAGE HEAT TRANSFER COEFICIENT= 69.444
NUS.NO.(F.T.)=369.01 NUS.NO.(A.T.)=387.16
PR.NO.(F.T.)= .7129 PR.NO.(A.T.)= .7113
REY.NO.(F.T.)= 466.12 REY.NO.(A,T.)= 520.98

Table F-6. Local and Average Heat Transfer Results (5 Rows, P/D_t = 1.5, Ottawa Sand (514 μm)).

MATERIAL OF THE BED=O.S.514
P/D= 1.50 NUMBER OF ROWS= 5
VOLTS= 8.345 CURRENT(AMPS.)= 2.30
SUPERFICIAL VELOCITY OF AIR= .536 FT./SEC.
ST.HT.= 11.3 INCHES EX.HT.= 11.3 INCHES
PRESSURE DROP IN THE BED= .354 PSI

THETA	TEMP.	CRCOND	HLOCAL	NULOCAL
0.0	141.600	-2.302	10.981	57.854
15.0	140.538	-.465	13.068	68.911
30.0	138.900	1.458	15.396	81.295
45.0	138.450	.589	14.642	77.343
60.0	138.700	-.292	13.697	72.338
75.0	138.976	.706	14.624	77.217
90.0	140.100	1.667	15.306	80.743
105.0	143.197	2.168	15.092	79.410
120.0	149.100	2.504	14.256	74.643
135.0	157.838	-.047	10.315	53.622
150.0	166.500	-2.056	7.221	37.271
165.0	172.052	-1.918	6.776	34.821
180.0	173.900	-1.871	6.645	34.100

AVERAGE TEMPERATURE OF THE CYLINDER=148.508
TEMPERATURE IN THE CORE OF THE CYL.= 150.300
TEMPERATURE OF THE AIR STREAM= 84.50
AVERAGE HEAT TRANSFER COEFICIENT= 12.430
NUS.NO.(F.T.)= 65.12 NUS.NO.(A.T.)= 68.18
PR.NO.(F.T.)= .7117 PR.NO.(A.T.)= .7114
REY.NO.(F.T.)= 235.49 REY.NO.(A,T.)= 261.01

MATERIAL OF THE BED=O.S.514
P/D= 1.50 NUMBER OF ROWS= 5
VOLTS= 15.530 CURRENT(AMPS.)= 4.19
SUPERFICIAL VELOCITY OF AIR= .812 FT./SEC.
ST.HT.= 11.3 INCHES EX.HT.= 11.5 INCHES
PRESSURE DROP IN THE BED= .487 PSI

THETA	TEMP.	CRCOND	HLOCAL	NULOCAL
0.0	171.700	1.145	30.215	155.278
15.0	172.349	-.258	28.599	146.899
30.0	172.500	-1.649	27.158	139.482
45.0	170.181	-.830	28.752	147.937
60.0	166.300	.036	31.012	160.063
75.0	162.351	.525	33.062	171.192
90.0	159.300	1.053	34.911	181.215
105.0	159.469	3.459	37.687	195.753
120.0	163.300	5.495	37.643	194.760
135.0	175.269	-.370	27.565	141.266
150.0	186.500	-4.899	19.984	101.551
165.0	189.661	-1.609	22.532	114.240
180.0	189.100	1.541	25.811	130.914

AVERAGE TEMPERATURE OF THE CYLINDER=171.383
TEMPERATURE IN THE CORE OF THE CYL.= 170.200
TEMPERATURE OF THE AIR STREAM= 84.80
AVERAGE HEAT TRANSFER COEFICIENT= 29.734
NUS.NO.(F.T.)=152.85 NUS.NO.(A.T.)=163.03
PR.NO.(F.T.)= .7091 PR.NO.(A.T.)= .7114
REY.NO.(F.T.)= 344.17 REY.NO.(A,T.)= 394.80

Table F-6. Cont'd. Local and Average Heat Transfer Results (5 Rows, P/D_t = 1.5, Ottawa Sand (514 μm)).

MATERIAL OF THE BED=O.S.514
P/D= 1.50 NUMBER OF ROWS= 5
VOLTS= 17.620 CURRENT(AMPS.)= 4.82
SUPERFICIAL VELOCITY OF AIR= 1.037 FT./SEC.
ST.HT.= 11.3 INCHES EX.HT.= 12.0 INCHES
PRESSURE DROP IN THE BED= .506 PSI

THETA	TEMP.	CRCOND	HLOCAL	NULOCAL
0.0	167.800	-.138	40.810	210.145
15.0	167.700	-.056	40.942	210.840
30.0	167.500	.026	41.124	211.813
45.0	167.048	-.895	40.430	208.313
60.0	165.000	-1.864	40.525	209.145
75.0	160.269	-.941	44.130	228.626
90.0	154.000	.110	49.312	256.793
105.0	147.901	1.394	55.421	290.064
120.0	143.700	2.862	60.807	319.366
135.0	142.877	3.077	61.857	325.105
150.0	145.900	3.085	58.909	308.834
165.0	151.855	-1.733	49.064	255.954
180.0	155.300	-5.958	42.326	220.175

AVERAGE TEMPERATURE OF THE CYLINDER=156.275
TEMPERATURE IN THE CORE OF THE CYL.= 160.400
TEMPERATURE OF THE AIR STREAM= 86.20
AVERAGE HEAT TRANSFER COEFICIENT= 48.667
NUS.NO.(F.T.)=252.96 NUS.NO.(A.T.)=266.35
PR.NO.(F.T.)= .7107 PR.NO.(A.T.)= .7115
REY.NO.(F.T.)= 448.94 REY.NO.(A,T.)= 502.19

MATERIAL OF THE BED=O.S.514
P/D= 1.50 NUMBER OF ROWS= 5
VOLTS= 18.330 CURRENT(AMPS.)= 5.02
SUPERFICIAL VELOCITY OF AIR= 1.253 FT./SEC.
ST.HT.= 11.3 INCHES EX.HT.= 12.5 INCHES
PRESSURE DROP IN THE BED= .537 PSI

THETA	TEMP.	CRCOND	HLOCAL	NULOCAL
0.0	157.000	1.812	46.446	243.332
15.0	158.185	.347	44.343	232.089
30.0	160.000	-1.069	41.987	219.427
45.0	160.285	-1.005	41.908	218.961
60.0	158.700	-.962	42.764	223.729
75.0	155.449	-.626	44.869	235.376
90.0	151.100	-.265	47.836	251.845
105.0	146.406	.507	51.782	273.672
120.0	142.500	1.373	55.630	294.938
135.0	140.390	1.350	57.368	304.669
150.0	140.200	1.286	57.469	305.247
165.0	141.485	-.255	54.836	290.964
180.0	142.400	-1.746	52.592	278.853

AVERAGE TEMPERATURE OF THE CYLINDER=150.367
TEMPERATURE IN THE CORE OF THE CYL.= 152.900
TEMPERATURE OF THE AIR STREAM= 75.90
AVERAGE HEAT TRANSFER COEFICIENT= 49.191
NUS.NO.(F.T.)=259.13 NUS.NO.(A.T.)=273.15
PR.NO.(F.T.)= .7123 PR.NO.(A.T.)= .7111
REY.NO.(F.T.)= 556.08 REY.NO.(A,T.)= 627.10

Table F-6. Cont'd. Local and Average Heat Transfer Results (5 Rows, P/D_t = 1.5, Ottawa Sand (514 μm)).

MATERIAL OF THE BED=O.S.514
P/D= 1.50 NUMBER OF ROWS= 5
VOLTS= 19.420 CURRENT(AMPS.)= 5.30
SUPERFICIAL VELOCITY OF AIR= 1.679 FT./SEC.
ST.HT.= 11.3 INCHES EX.HT.= 13.3 INCHES
PRESSURE DROP IN THE BED= .537 PSI

THETA	TEMP.	QRCOND	HLOCAL	NULOCAL
0.0	165.300	1.380	46.658	242.732
15.0	166.342	.410	45.171	234.794
30.0	168.200	-.533	43.335	224.904
45.0	169.105	-1.077	42.368	219.726
60.0	167.800	-1.650	42.407	220.162
75.0	163.714	-.584	45.505	237.042
90.0	158.500	.594	49.569	259.331
105.0	153.963	.509	52.309	274.698
120.0	150.300	.407	54.742	288.345
135.0	147.408	.690	57.208	302.053
150.0	145.600	.980	58.956	311.742
165.0	145.068	.370	58.790	310.995
180.0	145.100	-.247	58.146	307.582

AVERAGE TEMPERATURE OF THE CYLINDER=157.600
TEMPERATURE IN THE CORE OF THE CYL.= 160.500
TEMPERATURE OF THE AIR STREAM= 76.10
AVERAGE HEAT TRANSFER COEFICIENT= 50.229
NUS.NO.(F.T.)=262.98 NUS.NO.(A.T.)=278.83
PR.NO.(F.T.)= .7116 PR.NO.(A.T.)= .7111
REY.NO.(F.T.)= 736.48 REY.NO.(A,T.)= 839.77

MATERIAL OF THE BED=O.S.514
P/D= 1.50 NUMBER OF ROWS= 5
VOLTS= 19.360 CURRENT(AMPS.)= 5.30
SUPERFICIAL VELOCITY OF AIR= 2.097 FT./SEC.
ST.HT.= 11.3 INCHES EX.HT.= 14.0 INCHES
PRESSURE DROP IN THE BED= .518 PSI

THETA	TEMP.	QRCOND	HLOCAL	NULOCAL
0.0	168.400	1.023	44.987	233.362
15.0	169.181	.263	43.861	227.378
30.0	170.500	-.480	42.512	220.148
45.0	170.946	-.860	41.931	217.062
60.0	169.600	-1.260	42.143	218.398
75.0	166.022	-.630	44.489	231.232
90.0	161.200	.054	47.714	248.984
105.0	156.240	.011	50.606	265.164
120.0	151.300	-.037	53.868	283.412
135.0	146.591	1.046	58.540	309.190
150.0	143.500	2.230	62.355	330.167
165.0	143.019	.587	61.143	323.876
180.0	143.400	-1.066	59.148	313.212

AVERAGE TEMPERATURE OF THE CYLINDER=158.667
TEMPERATURE IN THE CORE OF THE CYL.= 160.900
TEMPERATURE OF THE AIR STREAM= 76.50
AVERAGE HEAT TRANSFER COEFICIENT= 50.101
NUS.NO.(F.T.)=261.99 NUS.NO.(A.T.)=277.94
PR.NO.(F.T.)= .7115 PR.NO.(A.T.)= .7111
REY.NO.(F.T.)= 917.71 REY.NO.(A,T.)=1047.45

Table F-7. Local and Average Heat Transfer Results (5 Rows, P/D_t = 1.5, Silica Sand (715 μm)).

MATERIAL OF THE BED=S.S.715
P/D= 1.50 NUMBER OF ROWS= 5
VOLTS= 9.980 CURRENT(AMPS.)= 2.75
SUPERFICIAL VELOCITY OF AIR= .747 FT./SEC.
ST.HT.= 11.3 INCHES EX.HT.= 11.3 INCHES
PRESSURE DROP IN THE BED= .234 PSI

THETA	TEMP.	CRCOND	HLOCAL	NULOCAL
0.0	155.200	1.122	14.530	76.346
15.0	155.876	.026	13.324	69.971
30.0	156.600	-1.051	12.131	63.667
45.0	156.056	-.007	13.262	69.635
60.0	155.500	1.052	14.411	75.700
75.0	156.525	1.074	14.268	74.888
90.0	159.500	1.071	13.809	72.300
105.0	164.558	1.246	13.279	69.233
120.0	172.100	1.368	12.483	64.662
135.0	181.881	-.363	9.754	50.146
150.0	190.800	-1.819	7.534	38.466
165.0	195.854	-1.344	7.626	38.788
180.0	197.300	-.934	7.933	40.306

AVERAGE TEMPERATURE OF THE CYLINDER=168.458
TEMPERATURE IN THE CORE OF THE CYL.= 167.300
TEMPERATURE OF THE AIR STREAM= 74.20
AVERAGE HEAT TRANSFER COEFICIENT= 11.925
NUS.NO.(F.T.)= 61.97 NUS.NO.(A.T.)= 66.39
PR.NO.(F.T.)= .7107 PR.NO.(A.T.)= .7113
REY.NO.(F.T.)= 323.06 REY.NO.(A,T.)= 375.84

MATERIAL OF THE BED=S.S.715
P/D= 1.50 NUMBER OF ROWS= 5
VOLTS= 12.840 CURRENT(AMPS.)= 3.50
SUPERFICIAL VELOCITY OF AIR= 1.388 FT./SEC.
ST.HT.= 11.3 INCHES EX.HT.= 11.5 INCHES
PRESSURE DROP IN THE BED= .423 PSI

THETA	TEMP.	CRCOND	HLOCAL	NULOCAL
0.0	153.700	.241	22.449	118.072
15.0	153.918	.265	22.413	117.861
30.0	154.600	.288	22.249	116.930
45.0	155.636	-.208	21.475	112.768
60.0	156.300	-.695	20.814	109.239
75.0	156.037	-.097	21.481	112.761
90.0	155.600	.506	22.199	116.571
105.0	156.703	3.195	24.600	129.063
120.0	163.600	5.436	25.199	131.453
135.0	178.764	.466	17.386	89.580
150.0	195.000	-3.212	11.456	58.292
165.0	204.592	-2.364	11.238	56.792
180.0	207.400	-1.716	11.603	58.526

AVERAGE TEMPERATURE OF THE CYLINDER=167.608
TEMPERATURE IN THE CORE OF THE CYL.= 168.200
TEMPERATURE OF THE AIR STREAM= 74.50
AVERAGE HEAT TRANSFER COEFICIENT= 19.788
NUS.NO.(F.T.)=102.88 NUS.NO.(A.T.)=110.12
PR.NO.(F.T.)= .7107 PR.NO.(A.T.)= .7112
REY.NO.(F.T.)= 601.10 REY.NO.(A,T.)= 698.02

Table F-7. Cont'd. Local and Average Heat Transfer Results (5 Rows, P/D_t = 1.5, Silica Sand (715 μm)).

MATERIAL OF THE BED=S.S.715
P/D= 1.50 NUMBER OF ROWS= 5
VOLTS= 15.880 CURRENT(AMPS.)= 4.37
SUPERFICIAL VELOCITY OF AIR= 1.854 FT./SEC.
ST.HT.= 11.3 INCHES EX.HT.= 12.2 INCHES
PRESSURE DROP IN THE BED= .455 PSI

THETA	TEMP.	CRCOND	HLOCAL	NULOCAL
0.0	158.700	.478	33.024	172.988
15.0	159.047	.163	32.577	170.596
30.0	159.700	-.148	32.020	167.587
45.0	160.063	-.490	31.543	165.043
60.0	159.500	-.838	31.405	164.398
75.0	157.401	-1.093	31.957	167.579
90.0	153.300	-1.396	33.355	175.503
105.0	147.422	.656	38.178	201.853
120.0	142.600	3.020	43.172	229.144
135.0	141.412	1.743	42.601	226.328
150.0	142.800	.404	40.439	214.608
165.0	144.855	-.650	38.227	202.534
180.0	145.900	-1.667	36.647	193.996

AVERAGE TEMPERATURE OF THE CYLINDER=151.700
TEMPERATURE IN THE CORE OF THE CYL.= 153.800
TEMPERATURE OF THE AIR STREAM= 74.40
AVERAGE HEAT TRANSFER COEFICIENT= 35.857
NUS.NO.(F.T.)=188.92 NUS.NO.(A.T.)=199.58
PR.NO.(F.T.)= .7123 PR.NO.(A.T.)= .7112
REY.NO.(F.T.)= 823.22 REY.NO.(A,T.)= 932.67

MATERIAL OF THE BED=S.S.715
P/D= 1.50 NUMBER OF ROWS= 5
VOLTS= 17.900 CURRENT(AMPS.)= 4.92
SUPERFICIAL VELOCITY OF AIR= 2.312 FT./SEC.
ST.HT.= 11.3 INCHES EX.HT.= 13.0 INCHES
PRESSURE DROP IN THE BED= .474 PSI

THETA	TEMP.	CRCOND	HLOCAL	NULOCAL
0.0	169.500	1.824	38.478	199.750
15.0	170.943	.476	36.588	189.713
30.0	173.400	-.823	34.402	178.020
45.0	174.484	-.938	33.910	175.321
60.0	173.500	-1.071	34.118	176.539
75.0	170.334	-.789	35.550	184.422
90.0	165.500	-.496	37.752	196.623
105.0	159.881	.498	41.235	215.767
120.0	155.200	1.612	44.688	234.748
135.0	152.891	1.051	45.384	238.858
150.0	152.400	.446	45.055	237.224
165.0	152.717	-.019	44.411	233.772
180.0	153.000	-.481	43.791	230.452

AVERAGE TEMPERATURE OF THE CYLINDER=163.542
TEMPERATURE IN THE CORE OF THE CYL.= 166.000
TEMPERATURE OF THE AIR STREAM= 74.50
AVERAGE HEAT TRANSFER COEFICIENT= 39.518
NUS.NO.(F.T.)=206.16 NUS.NO.(A.T.)=219.92
PR.NO.(F.T.)= .7112 PR.NO.(A.T.)= .7112
REY.NO.(F.T.)=1007.41 REY.NO.(A,T.)=1162.55

Table F-7. Cont'd. Local and Average Heat Transfer Results
(5 Rows, P/D_t = 1.5, Silica Sand (715 μm)).

MATERIAL OF THE BED=S.S.715
P/D= 1.50 NUMBER OF ROWS= 5
VOLTS= 17.940 CURRENT(AMPS.)= 4.92
SUPERFICIAL VELOCITY OF AIR= 2.613 FT./SEC.
ST.HT.= 11.3 INCHES EX.HT.= 13.2 INCHES
PRESSURE DROP IN THE BED= .493 PSI

THETA	TEMP.	CRCOND	HLCCAL	NULOCAL
0.0	168.200	1.241	38.438	199.736
15.0	169.191	.392	37.204	193.166
30.0	171.000	-.435	35.693	185.048
45.0	172.109	-.613	35.109	181.856
60.0	171.900	-.797	35.001	181.325
75.0	169.998	-.948	35.555	184.484
90.0	166.100	-1.130	36.911	192.135
105.0	160.462	.357	40.868	213.728
120.0	155.500	2.035	45.006	236.338
135.0	153.366	1.018	45.142	237.472
150.0	153.000	-.055	44.274	232.974
165.0	152.874	.030	44.429	233.813
180.0	152.800	.114	44.555	234.493

AVERAGE TEMPERATURE OF THE CYLINDER=163.000
TEMPERATURE IN THE CORE OF THE CYL.= 165.800
TEMPERATURE OF THE AIR STREAM= 74.60
AVERAGE HEAT TRANSFER COEFICIENT= 39.723
NUS.NO.(F.T.)=207.30 NUS.NO.(A.T.)=221.03
PR.NO.(F.T.)= .7112 PR.NO.(A.T.)= .7112
REY.NO.(F.T.)=1139.50 REY.NO.(A.T.)=1313.65

MATERIAL OF THE BED=S.S.715
P/D= 1.50 NUMBER OF ROWS= 5
VOLTS= 17.930 CURRENT(AMPS.)= 4.92
SUPERFICIAL VELOCITY OF AIR= 3.407 FT./SEC.
ST.HT.= 11.3 INCHES EX.HT.= 13.5 INCHES
PRESSURE DROP IN THE BED= .474 PSI

THETA	TEMP.	CRCOND	HLCCAL	NULOCAL
0.0	169.100	1.211	38.057	197.613
15.0	170.094	.433	36.901	191.449
30.0	172.000	-.325	35.436	183.566
45.0	173.394	-.545	34.717	179.638
60.0	173.600	-.768	34.422	178.081
75.0	172.117	-1.038	34.681	179.635
90.0	168.400	-1.348	35.770	185.841
105.0	162.501	.154	39.736	207.455
120.0	156.900	1.866	44.113	231.382
135.0	153.956	1.193	44.992	236.569
150.0	153.100	.456	44.728	235.346
165.0	153.139	.071	44.321	233.198
180.0	153.300	-.314	43.847	230.673

AVERAGE TEMPERATURE OF THE CYLINDER=164.200
TEMPERATURE IN THE CORE OF THE CYL.= 167.300
TEMPERATURE OF THE AIR STREAM= 74.60
AVERAGE HEAT TRANSFER COEFICIENT= 39.230
NUS.NO.(F.T.)=204.52 NUS.NO.(A.T.)=218.28
PR.NO.(F.T.)= .7111 PR.NO.(A.T.)= .7112
REY.NO.(F.T.)=1482.98 REY.NO.(A.T.)=1712.79

Table F-8. Local and Average Heat Transfer Results
(5 Rows, P/D_t = 1.5, Glass Beads (230 μm)).

MATERIAL OF THE BED=G.B.230
P/D= 1.50 NUMBER OF ROWS= 5
VOLTS= 6.550 CURRENT(AMPS.)= 1.80
SUPERFICIAL VELOCITY OF AIR= .185 FT./SEC.
ST.HT.= 11.2 INCHES EX.HT.= 11.2 INCHES
PRESSURE DROP IN THE BED= .322 PSI

THETA	TEMP.	CRCOND	HLOCAL	NULOCAL
0.0	194.900	.735	5.071	25.578
15.0	195.649	.418	4.725	23.821
30.0	197.400	.105	4.345	21.878
45.0	199.466	-.054	4.109	20.663
60.0	201.400	-.207	3.886	19.518
75.0	203.098	.314	4.348	21.815
90.0	205.600	.815	4.765	23.868
105.0	209.742	.191	4.009	20.031
120.0	214.400	-.391	3.290	16.391
135.0	218.221	-.395	3.180	15.811
150.0	220.900	-.402	3.103	15.402
165.0	222.423	-.351	3.115	15.451
180.0	222.900	-.303	3.151	15.624

AVERAGE TEMPERATURE OF THE CYLINDER=208.100
TEMPERATURE IN THE CORE OF THE CYL.= 206.000
TEMPERATURE OF THE AIR STREAM= 87.10
AVERAGE HEAT TRANSFER COEFICIENT= 3.915
NUS.NO.(F.T.)= 19.58 NUS.NO.(A.T.)= 21.40
PR.NO.(F.T.)= .7072 PR.NO.(A.T.)= .7117
REY.NO.(F.T.)= 74.28 REY.NO.(A.T.)= 89.50

MATERIAL OF THE BED=G.B.230
P/D= 1.50 NUMBER OF ROWS= 5
VOLTS= 18.090 CURRENT(AMPS.)= 4.95
SUPERFICIAL VELOCITY OF AIR= .346 FT./SEC.
ST.HT.= 11.2 INCHES EX.HT.= 11.7 INCHES
PRESSURE DROP IN THE BED= .449 PSI

THETA	TEMP.	CRCOND	HLOCAL	NULOCAL
0.0	168.500	-1.505	36.391	188.915
15.0	167.353	-.349	38.015	197.530
30.0	165.500	.843	39.988	208.099
45.0	164.758	.347	39.814	207.322
60.0	164.700	-.155	39.337	204.847
75.0	164.851	.912	40.338	210.033
90.0	166.800	1.936	40.530	210.695
105.0	171.724	.213	36.854	190.812
120.0	177.100	-1.336	33.388	172.117
135.0	180.304	-.653	33.022	169.799
150.0	182.000	-.010	33.135	170.154
165.0	183.309	-.302	32.446	166.442
180.0	183.900	-.591	31.980	163.979

AVERAGE TEMPERATURE OF THE CYLINDER=172.050
TEMPERATURE IN THE CORE OF THE CYL.= 175.200
TEMPERATURE OF THE AIR STREAM= 75.50
AVERAGE HEAT TRANSFER COEFICIENT= 36.753
NUS.NO.(F.T.)=190.24 NUS.NO.(A.T.)=204.21
PR.NO.(F.T.)= .7101 PR.NO.(A.T.)= .7112
REY.NO.(F.T.)= 148.50 REY.NO.(A.T.)= 173.31

Table F-8. Cont'd. Local and Average Heat Transfer Results
(5 Rows, P/D_t = 1.5, Glass Beads (230 μm)).

MATERIAL OF THE BED=G.B.230
P/D= 1.50 NUMBER OF ROWS= 5
VOLTS= 18.090 CURRENT(AMPS.)= 4.95
SUPERFICIAL VELOCITY OF AIR= .486 FT./SEC.
ST.HT.= 11.2 INCHES EX.HT.= 12.5 INCHES
PRESSURE DROP IN THE BED= .455 PSI

THETA	TEMP.	CRCOND	HLOCAL	NULOCAL
0.0	150.900	.756	47.463	249.981
15.0	151.289	-.107	46.361	244.103
30.0	151.500	-.963	45.377	238.877
45.0	150.517	-.323	46.620	245.621
60.0	149.000	.337	48.241	254.481
75.0	147.844	.322	48.986	258.655
90.0	147.200	.304	49.402	260.987
105.0	147.071	.417	49.602	262.074
120.0	147.600	.525	49.353	260.643
135.0	148.896	.376	48.348	255.067
150.0	150.800	.231	46.999	247.558
165.0	152.883	-.626	44.892	236.058
180.0	153.900	-1.457	43.476	228.415

AVERAGE TEMPERATURE OF THE CYLINDER=149.750
TEMPERATURE IN THE CORE OF THE CYL.= 153.400
TEMPERATURE OF THE AIR STREAM= 75.60
AVERAGE HEAT TRANSFER COEFICIENT= 47.470
NUS.NO.(F.T.)=250.26 NUS.NO.(A.T.)=263.72
PR.NO.(F.T.)= .7123 PR.NO.(A.T.)= .7112
REY.NO.(F.T.)= 216.07 REY.NO.(A,T.)= 243.55

MATERIAL OF THE BED=G.B.230
P/D= 1.50 NUMBER OF ROWS= 5
VOLTS= 20.020 CURRENT(AMPS.)= 5.48
SUPERFICIAL VELOCITY OF AIR= .692 FT./SEC.
ST.HT.= 11.2 INCHES EX.HT.= 13.2 INCHES
PRESSURE DROP IN THE BED= .468 PSI

THETA	TEMP.	CRCOND	HLOCAL	NULOCAL
0.0	157.000	-1.145	51.523	270.115
15.0	156.283	-.093	53.037	278.213
30.0	155.400	.981	54.688	287.087
45.0	155.561	-.294	53.308	279.804
60.0	155.200	-1.573	52.268	274.425
75.0	152.837	-.218	55.243	290.614
90.0	150.100	1.227	58.694	309.466
105.0	148.840	.688	59.128	312.079
120.0	148.700	.129	58.679	309.744
135.0	149.064	.657	58.921	310.927
150.0	150.500	1.162	58.327	307.430
165.0	153.215	-.655	54.541	286.830
180.0	154.800	-2.384	51.724	271.661

AVERAGE TEMPERATURE OF THE CYLINDER=152.633
TEMPERATURE IN THE CORE OF THE CYL.= 157.000
TEMPERATURE OF THE AIR STREAM= 75.10
AVERAGE HEAT TRANSFER COEFICIENT= 55.703
NUS.NO.(F.T.)=293.09 NUS.NO.(A.T.)=309.70
PR.NO.(F.T.)= .7122 PR.NO.(A.T.)= .7112
REY.NO.(F.T.)= 306.25 REY.NO.(A,T.)= 347.07

Table F-8. Cont'd. Local and Average Heat Transfer Results
(5 Rows, P/D_t = 1.5, Glass Beads (230 μm)).

MATERIAL OF THE BED=G.B.230
P/D= 1.50 NUMBER OF ROWS= 5
VOLTS= 19.920 CURRENT(AMPS.)= 5.47
SUPERFICIAL VELOCITY OF AIR= .827 FT./SEC.
ST.HT.= 11.2 INCHES EX.HT.= 13.9 INCHES
PRESSURE DROP IN THE BED= .449 PSI

THETA	TEMP.	CRCOND	HLOCAL	NULOCAL
0.0	149.900	.507	58.773	309.653
15.0	150.231	.207	58.215	306.628
30.0	150.900	-.090	57.403	302.186
45.0	151.332	-.703	56.462	297.126
60.0	150.600	-1.329	56.393	296.944
75.0	148.264	.171	59.748	315.213
90.0	146.200	1.765	63.083	333.374
105.0	146.123	.488	61.874	327.002
120.0	146.800	-.782	60.020	317.027
135.0	146.805	.058	60.855	321.440
150.0	146.900	.896	61.613	325.417
165.0	147.894	-.182	59.700	315.056
180.0	148.600	-1.236	58.067	306.261

AVERAGE TEMPERATURE OF THE CYLINDER=148.442
TEMPERATURE IN THE CORE OF THE CYL.= 152.400
TEMPERATURE OF THE AIR STREAM= 76.20
AVERAGE HEAT TRANSFER COEFICIENT= 59.481
NUS.NO.(F.T.)=313.76 NUS.NO.(A.T.)=330.13
PR.NO.(F.T.)= .7124 PR.NO.(A.T.)= .7111
REY.NO.(F.T.)= 367.96 REY.NO.(A,T.)= 413.48

MATERIAL OF THE BED=G.B.230
P/D= 1.50 NUMBER OF ROWS= 5
VOLTS= 19.940 CURRENT(AMPS.)= 5.46
SUPERFICIAL VELOCITY OF AIR= 1.629 FT./SEC.
ST.HT.= 11.2 INCHES EX.HT.= 15.5 INCHES
PRESSURE DROP IN THE BED= .455 PSI

THETA	TEMP.	CRCOND	HLOCAL	NULOCAL
0.0	150.200	-.657	57.319	301.870
15.0	149.970	.468	58.624	308.802
30.0	150.500	1.585	59.328	312.374
45.0	152.663	-.788	55.333	290.819
60.0	153.500	-3.081	52.436	275.399
75.0	150.468	-.572	57.197	301.158
90.0	146.500	2.179	63.189	333.796
105.0	144.818	.772	63.269	334.679
120.0	144.300	-.694	62.276	329.560
135.0	143.488	.828	64.554	341.843
150.0	143.900	2.344	65.684	347.710
165.0	146.695	-.574	60.268	318.314
180.0	148.600	-3.309	55.941	295.000

AVERAGE TEMPERATURE OF THE CYLINDER=148.017
TEMPERATURE IN THE CORE OF THE CYL.= 151.700
TEMPERATURE OF THE AIR STREAM= 76.40
AVERAGE HEAT TRANSFER COEFICIENT= 59.895
NUS.NO.(F.T.)=316.00 NUS.NO.(A.T.)=332.33
PR.NO.(F.T.)= .7124 PR.NO.(A.T.)= .7111
REY.NO.(F.T.)= 725.03 REY.NO.(A,T.)= 813.91

Table F-9. Local and Average Heat Transfer Results
(5 Rows, P/D_t = 1.3, Ottawa Sand (514 μm)).

MATERIAL OF THE BED=O.S.514
P/D= 1.30 NUMBER OF ROWS= 5
VOLTS= 12.000 CURRENT(AMPS.)= 3.50
SUPERFICIAL VELOCITY OF AIR= .511 FT./SEC.
ST.HT.= 11.4 INCHES EX.HT.= 11.4 INCHES
PRESSURE DROP IN THE BED= .316 PSI

THETA	TEMP.	CRCOND	HLOCAL	NULOCAL
0.0	216.700	-.255	11.808	59.381
15.0	216.531	.197	12.274	61.728
30.0	217.000	.647	12.686	63.782
45.0	218.794	-.331	11.565	58.080
60.0	219.500	-1.296	10.545	52.936
75.0	217.991	1.504	13.464	67.652
90.0	221.400	4.221	15.916	79.801
105.0	236.029	1.620	12.305	61.159
120.0	256.600	-.541	8.990	44.172
135.0	275.881	-1.047	7.611	36.996
150.0	290.400	-1.498	6.604	31.808
165.0	298.324	-1.120	6.709	32.133
180.0	300.600	-.787	6.967	33.317

AVERAGE TEMPERATURE OF THE CYLINDER=243.925
TEMPERATURE IN THE CORE OF THE CYL.= 243.600
TEMPERATURE OF THE AIR STREAM= 69.80
AVERAGE HEAT TRANSFER COEFICIENT= 10.668
NUS.NO.(F.T.)= 52.79 NUS.NO.(A.T.)= 59.83
PR.NO.(F.T.)= .7079 PR.NO.(A.T.)= .7118
REY.NO.(F.T.)= 199.48 REY.NO.(A,T.)= 261.05

MATERIAL OF THE BED=O.S.514
P/D= 1.30 NUMBER OF ROWS= 5
VOLTS= 12.000 CURRENT(AMPS.)= 3.50
SUPERFICIAL VELOCITY OF AIR= .732 FT./SEC.
ST.HT.= 11.4 INCHES EX.HT.= 11.5 INCHES
PRESSURE DROP IN THE BED= .436 PSI

THETA	TEMP.	CRCOND	HLOCAL	NULOCAL
0.0	167.200	1.263	19.808	103.227
15.0	168.160	.179	18.521	96.441
30.0	169.500	-.900	17.192	89.425
45.0	169.285	-.919	17.213	89.548
60.0	167.100	-.958	17.587	91.657
75.0	163.659	1.337	20.562	107.467
90.0	163.000	3.695	23.067	120.627
105.0	168.581	2.508	20.771	108.121
120.0	179.500	1.379	17.806	91.866
135.0	193.127	-.807	13.794	70.412
150.0	204.600	-2.592	10.763	54.482
165.0	209.947	-1.412	11.433	57.662
180.0	211.000	-.330	12.419	62.591

AVERAGE TEMPERATURE OF THE CYLINDER=178.800
TEMPERATURE IN THE CORE OF THE CYL.= 174.000
TEMPERATURE OF THE AIR STREAM= 72.10
AVERAGE HEAT TRANSFER COEFICIENT= 17.064
NUS.NO.(F.T.)= 88.09 NUS.NO.(A.T.)= 95.34
PR.NO.(F.T.)= .7097 PR.NO.(A.T.)= .7115
REY.NO.(F.T.)= 312.63 REY.NO.(A,T.)= 370.82

Table F-9. Cont'd. Local and Average Heat Transfer Results (5 Rows, P/D_t = 1.3, Ottawa Sand (514 μm)).

MATERIAL OF THE BED=O.S.514
P/D= 1.30 NUMBER OF ROWS= 5
VOLTS= 12.000 CURRENT(AMPS.)= 3.50
SUPERFICIAL VELOCITY OF AIR= .902 FT./SEC.
ST.HT.= 11.4 INCHES EX.HT.= 11.8 INCHES
PRESSURE DROP IN THE BED= .490 PSI

THETA	TEMP.	CRCOND	HLOCAL	NULOCAL
0.0	148.100	.758	24.352	128.763
15.0	148.399	-.423	23.077	121.995
30.0	148.000	-1.610	22.015	116.420
45.0	145.595	-.637	23.784	126.021
60.0	142.100	.411	26.052	138.423
75.0	139.005	.478	27.324	145.532
90.0	136.600	.547	28.409	151.594
105.0	135.188	1.638	30.134	160.972
120.0	136.000	2.680	30.809	164.474
135.0	139.532	-.457	26.176	139.359
150.0	142.400	-3.307	22.224	118.055
165.0	141.721	-.361	25.423	135.117
180.0	140.500	2.666	28.916	153.832

AVERAGE TEMPERATURE OF THE CYLINDER=141.567
TEMPERATURE IN THE CORE OF THE CYL.= 139.900
TEMPERATURE OF THE AIR STREAM= 73.60
AVERAGE HEAT TRANSFER COEFICIENT= 26.002
NUS.NO.(F.T.)=138.21 NUS.NO.(A.T.)=144.91
PR.NO.(F.T.)= .7130 PR.NO.(A.T.)= .7113
REY.NO.(F.T.)= 407.55 REY.NO.(A.T.)= 454.92

MATERIAL OF THE BED=O.S.514
P/D= 1.30 NUMBER OF ROWS= 5
VOLTS= 12.000 CURRENT(AMPS.)= 3.50
SUPERFICIAL VELOCITY OF AIR= 1.097 FT./SEC.
ST.HT.= 11.4 INCHES EX.HT.= 12.0 INCHES
PRESSURE DROP IN THE BED= .461 PSI

THETA	TEMP.	CRCOND	HLOCAL	NULOCAL
0.0	130.000	-.129	30.750	164.948
15.0	129.872	-.355	30.593	164.119
30.0	129.300	-.586	30.674	164.622
45.0	128.039	-.643	31.332	168.307
60.0	126.000	-.712	32.491	174.778
75.0	123.246	-.174	34.844	187.793
90.0	120.300	.428	37.624	203.173
105.0	117.751	.811	40.123	217.028
120.0	116.000	1.217	42.129	228.137
135.0	115.261	.731	42.358	229.486
150.0	115.200	.224	41.911	227.071
165.0	115.360	-.065	41.444	224.519
180.0	115.500	-.352	41.040	222.314

AVERAGE TEMPERATURE OF THE CYLINDER=121.592
TEMPERATURE IN THE CORE OF THE CYL.= 122.900
TEMPERATURE OF THE AIR STREAM= 73.20
AVERAGE HEAT TRANSFER COEFICIENT= 36.784
NUS.NO.(F.T.)=198.47 NUS.NO.(A.T.)=205.14
PR.NO.(F.T.)= .7130 PR.NO.(A.T.)= .7114
REY.NO.(F.T.)= 512.43 REY.NO.(A.T.)= 554.22

Table F-9. Cont'd. Local and Average Heat Transfer Results (5 Rows, P/D_t = 1.3, Ottawa Sand (514 μm)).

MATERIAL OF THE BED=O.S.514
P/D= 1.30 NUMBER OF ROWS= 5
VOLTS= 12.000 CURRENT(AMPS.)= 3.50
SUPERFICIAL VELOCITY OF AIR= 1.488 FT./SEC.
ST.HT.= 11.4 INCHES EX.HT.= 12.8 INCHES
PRESSURE DROP IN THE BED= .480 PSI

THETA	TEMP.	CRCOND	HLOCAL	NULOCAL
0.0	120.200	-.113	36.925	199.443
15.0	120.108	-.303	36.806	198.823
30.0	119.700	-.497	36.934	199.566
45.0	118.798	-.568	37.575	203.147
60.0	117.300	-.692	38.751	209.711
75.0	115.201	-.323	41.067	222.545
90.0	112.800	.085	43.954	238.548
105.0	110.462	.454	47.040	255.677
120.0	108.500	.863	50.005	272.124
135.0	107.165	.887	51.936	282.869
150.0	106.500	.895	52.950	288.510
165.0	106.417	.224	52.407	285.568
180.0	106.500	-.448	51.607	281.193

AVERAGE TEMPERATURE OF THE CYLINDER=113.025
TEMPERATURE IN THE CORE OF THE CYL.= 113.500
TEMPERATURE OF THE AIR STREAM= 72.80
AVERAGE HEAT TRANSFER COEFICIENT= 44.474
NUS.NO.(F.T.)=241.34 NUS.NO.(A.T.)=248.15
PR.NO.(F.T.)= .7125 PR.NO.(A.T.)= .7114
REY.NO.(F.T.)= 704.96 REY.NO.(A,T.)= 752.35

MATERIAL OF THE BED=O.S.514
P/D= 1.30 NUMBER OF ROWS= 5
VOLTS= 12.000 CURRENT(AMPS.)= 3.50
SUPERFICIAL VELOCITY OF AIR= 2.288 FT./SEC.
ST.HT.= 11.4 INCHES EX.HT.= 13.5 INCHES
PRESSURE DROP IN THE BED= .474 PSI

THETA	TEMP.	CRCOND	HLOCAL	NULOCAL
0.0	120.500	.536	36.959	199.664
15.0	120.680	-.056	36.232	195.713
30.0	120.800	-.644	35.554	192.035
45.0	120.314	-.783	35.781	193.322
60.0	119.000	-.940	36.648	198.178
75.0	116.778	-.772	38.688	209.509
90.0	113.800	-.597	41.687	226.176
105.0	110.425	.657	46.676	253.780
120.0	107.600	2.121	51.816	282.225
135.0	106.111	1.180	53.060	289.273
150.0	105.500	.148	52.983	288.960
165.0	105.143	.297	53.706	292.970
180.0	105.000	.446	54.088	295.062

AVERAGE TEMPERATURE OF THE CYLINDER=113.242
TEMPERATURE IN THE CORE OF THE CYL.= 112.800
TEMPERATURE OF THE AIR STREAM= 72.40
AVERAGE HEAT TRANSFER COEFICIENT= 44.028
NUS.NO.(F.T.)=238.96 NUS.NO.(A.T.)=245.87
PR.NO.(F.T.)= .7124 PR.NO.(A.T.)= .7114
REY.NO.(F.T.)=1084.22 REY.NO.(A,T.)=1158.48

Table F-10. Local and Average Heat Transfer Results
(5 Rows, P/D_t = 1.3, Silica Sand (714 μm)).

MATERIAL OF THE BED=S.S.715
P/D= 1.30 NUMBER OF ROWS= 5
VOLTS= 12.080 CURRENT(AMPS.)= 3.30
SUPERFICIAL VELOCITY OF AIR= 1.057 FT./SEC.
ST.HT.= 11.5 INCHES EX.HT.= 11.5 INCHES
PRESSURE DROP IN THE BED= .348 PSI

THETA	TEMP.	CRCOND	HLOCAL	NULOCAL
0.0	154.500	1.908	24.343	126.862
15.0	155.571	.358	22.457	116.926
30.0	157.200	-1.137	20.469	106.432
45.0	157.559	-.572	20.929	108.792
60.0	157.000	-.012	21.654	112.612
75.0	156.357	.308	22.166	115.338
90.0	156.200	.629	22.534	117.270
105.0	157.538	2.820	24.326	126.454
120.0	163.400	4.648	24.564	127.081
135.0	175.591	.608	17.875	91.582
150.0	189.000	-2.447	12.622	64.025
165.0	197.884	-2.353	11.547	58.213
180.0	200.900	-2.387	11.156	56.132

AVERAGE TEMPERATURE OF THE CYLINDER=166.750
TEMPERATURE IN THE CORE OF THE CYL.= 165.800
TEMPERATURE OF THE AIR STREAM= 84.80
AVERAGE HEAT TRANSFER COEFICIENT= 19.902
NUS.NO.(F.T.)=102.68 NUS.NO.(A.T.)=109.12
PR.NO.(F.T.)= .7097 PR.NO.(A.T.)= .7114
REY.NO.(F.T.)= 451.38 REY.NO.(A.T.)= 514.21

MATERIAL OF THE BED=S.S.715
P/D= 1.30 NUMBER OF ROWS= 5
VOLTS= 14.760 CURRENT(AMPS.)= 4.05
SUPERFICIAL VELOCITY OF AIR= 1.438 FT./SEC.
ST.HT.= 11.5 INCHES EX.HT.= 11.5 INCHES
PRESSURE DROP IN THE BED= .392 PSI

THETA	TEMP.	CRCOND	HLOCAL	NULOCAL
0.0	180.000	6.679	31.060	158.805
15.0	185.119	.960	24.132	122.906
30.0	192.400	-4.129	17.518	88.749
45.0	192.541	-2.146	19.472	98.644
60.0	187.500	-.178	22.472	114.251
75.0	181.742	1.156	25.111	128.219
90.0	178.500	2.585	27.345	139.970
105.0	180.378	3.003	27.290	139.491
120.0	188.700	3.198	25.593	130.005
135.0	203.259	.446	20.161	101.395
150.0	219.000	-1.696	15.768	78.538
165.0	230.361	-2.192	13.946	69.017
180.0	234.600	-2.740	12.955	63.959

AVERAGE TEMPERATURE OF THE CYLINDER=195.567
TEMPERATURE IN THE CORE OF THE CYL.= 198.600
TEMPERATURE OF THE AIR STREAM= 83.10
AVERAGE HEAT TRANSFER COEFICIENT= 21.724
NUS.NO.(F.T.)=109.82 NUS.NO.(A.T.)=119.38
PR.NO.(F.T.)= .7073 PR.NO.(A.T.)= .7112
REY.NO.(F.T.)= 590.03 REY.NO.(A.T.)= 703.28

Table F-10. Cont'd. Local and Average Heat Transfer Results
(5 Rows, P/D_t = 1.3, Silica Sand (714 μm)).

MATERIAL OF THE BED=S.S.715
P/D= 1.30 NUMBER OF ROWS= 5
VOLTS= 18.080 CURRENT(AMPS.)= 5.00
SUPERFICIAL VELOCITY OF AIR= 1.909 FT./SEC.
ST.HT.= 11.5 INCHES EX.HT.= 12.3 INCHES
PRESSURE DROP IN THE BED= .461 PSI

THETA	TEMP.	CRCOND	HLOCAL	NULOCAL
0.0	192.700	2.547	35.969	181.973
15.0	194.778	.142	32.940	166.412
30.0	197.200	-2.168	29.933	150.973
45.0	195.772	-.794	31.714	160.108
60.0	192.400	.626	34.139	172.754
75.0	189.495	-.515	33.916	171.978
90.0	185.400	-1.742	34.074	173.292
105.0	178.822	.846	39.138	200.027
120.0	174.000	3.748	44.087	226.162
135.0	174.728	1.031	41.047	210.446
150.0	177.500	-1.607	37.225	190.443
165.0	178.254	-.489	38.032	194.461
180.0	178.000	.617	39.243	200.688

AVERAGE TEMPERATURE OF THE CYLINDER=185.308
TEMPERATURE IN THE CORE OF THE CYL.= 193.000
TEMPERATURE OF THE AIR STREAM= 84.80
AVERAGE HEAT TRANSFER COEFICIENT= 36.151
NUS.NO.(F.T.)=183.86 NUS.NO.(A.T.)=198.21
PR.NO.(F.T.)= .7076 PR.NO.(A.T.)= .7114
REY.NO.(F.T.)= 793.07 REY.NO.(A,T.)= 928.51

MATERIAL OF THE BED=S.S.715
P/D= 1.30 NUMBER OF ROWS= 5
VOLTS= 18.200 CURRENT(AMPS.)= 5.04
SUPERFICIAL VELOCITY OF AIR= 2.484 FT./SEC.
ST.HT.= 11.5 INCHES EX.HT.= 13.0 INCHES
PRESSURE DROP IN THE BED= .466 PSI

THETA	TEMP.	CRCOND	HLOCAL	NULOCAL
0.0	171.500	4.131	45.950	236.311
15.0	174.366	.637	41.141	211.105
30.0	178.500	-2.607	36.143	184.862
45.0	178.907	-.915	37.670	192.617
60.0	177.400	.779	39.980	204.664
75.0	176.407	-.694	38.924	199.412
90.0	174.000	-2.234	38.434	197.269
105.0	168.241	-.529	42.893	221.165
120.0	161.500	1.445	48.611	252.019
135.0	156.468	.854	51.269	266.900
150.0	152.800	.171	53.255	278.061
165.0	149.811	1.157	56.635	296.469
180.0	148.500	2.179	58.778	308.020

AVERAGE TEMPERATURE OF THE CYLINDER=167.367
TEMPERATURE IN THE CORE OF THE CYL.= 171.700
TEMPERATURE OF THE AIR STREAM= 84.10
AVERAGE HEAT TRANSFER COEFICIENT= 44.773
NUS.NO.(F.T.)=231.02 NUS.NO.(A.T.)=245.71
PR.NO.(F.T.)= .7097 PR.NO.(A.T.)= .7113
REY.NO.(F.T.)=1060.57 REY.NO.(A,T.)=1210.79

Table F-10. Cont'd. Local and Average Heat Transfer Results
(5 Rows, P/D_t = 1.3, Silica Sand (714 μm)).

MATERIAL OF THE BED=S.S.715
P/D= 1.30 NUMBER OF ROWS= 5
VOLTS= 18.190 CURRENT(AMPS.)= 5.04
SUPERFICIAL VELOCITY OF AIR= 3.244 FT./SEC.
ST.HT.= 11.5 INCHES EX.HT.= 15.1 INCHES
PRESSURE DROP IN THE BED= .466 PSI

THETA	TEMP.	CRCOND	HLOCAL	NULOCAL
0.0	170.500	3.359	45.125	232.459
15.0	172.871	.635	41.310	212.404
30.0	176.500	-1.924	37.189	190.673
45.0	177.395	-.859	37.887	194.118
60.0	176.500	.189	39.302	201.507
75.0	175.175	-1.156	38.514	197.667
90.0	171.500	-2.607	38.692	199.157
105.0	164.192	.511	45.488	235.522
120.0	157.800	4.194	52.978	275.744
135.0	156.543	1.365	50.975	265.596
150.0	157.500	-1.516	47.462	247.097
165.0	157.124	-.152	49.073	255.562
180.0	156.500	1.231	50.870	265.056

AVERAGE TEMPERATURE OF THE CYLINDER=167.217
TEMPERATURE IN THE CORE OF THE CYL.= 170.400
TEMPERATURE OF THE AIR STREAM= 83.00
AVERAGE HEAT TRANSFER COEFICIENT= 43.901
NUS.NO.(F.T.)=226.75 NUS.NO.(A.T.)=241.27
PR.NO.(F.T.)= .7098 PR.NO.(A.T.)= .7112
REY.NO.(F.T.)=1387.87 REY.NO.(A,T.)=1587.12

MATERIAL OF THE BED=S.S.715
P/D= 1.30 NUMBER OF ROWS= 5
VOLTS= 17.930 CURRENT(AMPS.)= 4.98
SUPERFICIAL VELOCITY OF AIR= 3.823 FT./SEC.
ST.HT.= 11.5 INCHES EX.HT.= 15.3 INCHES
PRESSURE DROP IN THE BED= .461 PSI

THETA	TEMP.	CRCOND	HLOCAL	NULOCAL
0.0	168.700	5.149	46.199	238.565
15.0	172.305	.947	40.378	207.905
30.0	177.800	-2.876	34.323	175.962
45.0	179.037	-1.433	35.298	180.790
60.0	177.200	-.027	37.404	191.847
75.0	174.448	-1.074	37.455	192.528
90.0	169.500	-2.241	38.439	198.363
105.0	161.535	.813	45.514	236.403
120.0	155.000	4.457	53.110	277.351
135.0	154.063	2.116	51.395	268.604
150.0	156.500	-.272	47.413	247.290
165.0	158.962	-.837	45.340	235.998
180.0	160.000	-1.392	44.178	229.754

AVERAGE TEMPERATURE OF THE CYLINDER=166.725
TEMPERATURE IN THE CORE OF THE CYL.= 169.000
TEMPERATURE OF THE AIR STREAM= 81.80
AVERAGE HEAT TRANSFER COEFICIENT= 42.598
NUS.NO.(F.T.)=220.32 NUS.NO.(A.T.)=234.49
PR.NO.(F.T.)= .7100 PR.NO.(A.T.)= .7111
REY.NO.(F.T.)=1639.61 REY.NO.(A,T.)=1877.51

Table F-11. Local and Average Heat Transfer Results (5 Rows, P/D_t = 1.3, Glass Beads (230 μm)).

MATERIAL OF THE BED=G.B.230
P/D= 1.30 NUMBER OF ROWS= 5
VOLTS= 6.540 CURRENT(AMPS.)= 1.80
SUPERFICIAL VELOCITY OF AIR= .150 FT./SEC.
ST.HT.= 11.5 INCHES EX.HT.= 11.5 INCHES
PRESSURE DROP IN THE BED= .205 PSI

THETA	TEMP.	CRCOND	HLOCAL	NULOCAL
0.0	252.500	.447	3.199	15.653
15.0	253.196	.213	2.955	14.453
30.0	254.700	-.018	2.700	13.196
45.0	256.332	.061	2.755	13.449
60.0	258.200	.139	2.804	13.678
75.0	260.526	.088	2.720	13.247
90.0	263.200	.039	2.632	12.802
105.0	266.001	-.050	2.505	12.163
120.0	268.600	-.136	2.384	11.559
135.0	270.693	-.140	2.353	11.390
150.0	272.200	-.145	2.329	11.263
165.0	273.101	-.143	2.320	11.214
180.0	273.400	-.140	2.318	11.204

AVERAGE TEMPERATURE OF THE CYLINDER=263.308
TEMPERATURE IN THE CORE OF THE CYL.= 262.000
TEMPERATURE OF THE AIR STREAM= 81.50
AVERAGE HEAT TRANSFER COEFICIENT= 2.601
NUS.NO.(F.T.)= 12.65 NUS.NO.(A.T.)= 14.33
PR.NO.(F.T.)= .7085 PR.NO.(A.T.)= .7111
REY.NO.(F.T.)= 56.26 REY.NO.(A,T.)= 73.90

MATERIAL OF THE BED=G.B.230
P/D= 1.30 NUMBER OF ROWS= 5
VOLTS= 10.880 CURRENT(AMPS.)= 2.98
SUPERFICIAL VELOCITY OF AIR= .256 FT./SEC.
ST.HT.= 11.5 INCHES EX.HT.= 11.5 INCHES
PRESSURE DROP IN THE BED= .360 PSI

THETA	TEMP.	CRCOND	HLOCAL	NULOCAL
0.0	208.800	1.099	11.188	56.125
15.0	210.146	.673	10.659	53.423
30.0	213.400	.253	9.995	49.998
45.0	217.446	-.031	9.426	47.036
60.0	221.400	-.298	8.896	44.286
75.0	224.894	.320	9.294	46.175
90.0	229.400	.903	9.608	47.613
105.0	236.204	.291	8.619	42.552
120.0	244.000	-.268	7.668	37.693
135.0	250.904	-.671	6.947	34.021
150.0	255.300	-1.058	6.371	31.125
165.0	256.357	-.341	7.044	34.393
180.0	256.100	.371	7.767	37.925

AVERAGE TEMPERATURE OF THE CYLINDER=232.658
TEMPERATURE IN THE CORE OF THE CYL.= 227.500
TEMPERATURE OF THE AIR STREAM= 81.60
AVERAGE HEAT TRANSFER COEFICIENT= 8.667
NUS.NO.(F.T.)= 42.87 NUS.NO.(A.T.)= 47.72
PR.NO.(F.T.)= .7079 PR.NO.(A.T.)= .7111
REY.NO.(F.T.)= 99.67 REY.NO.(A,T.)= 125.58

Table F-11. Cont'd. Local and Average Heat Transfer Results
(5 Rows, P/D_t = 1.3, Glass Beads (230 μm)).

MATERIAL OF THE BED=G.B.230
P/D= 1.30 NUMBER OF ROWS= 5
VOLTS= 21.140 CURRENT(AMPS.)= 5.80
SUPERFICIAL VELOCITY OF AIR= .411 FT./SEC.
ST.HT.= 11.5 INCHES EX.HT.= 12.0 INCHES
PRESSURE DROP IN THE BED= .430 PSI

THETA	TEMP.	CRCOND	HLOCAL	NULOCAL
0.0	200.500	-1.612	39.168	197.566
15.0	198.666	-.979	40.431	204.186
30.0	194.300	-.333	42.656	216.079
45.0	189.020	.152	45.221	229.945
60.0	184.100	.683	47.885	244.381
75.0	180.867	1.626	50.342	257.559
90.0	181.200	2.537	51.093	261.332
105.0	185.926	.194	46.581	237.403
120.0	191.100	-1.937	42.289	214.707
135.0	192.930	-.715	42.794	216.989
150.0	193.000	.474	43.957	222.875
165.0	193.541	-.034	43.242	219.164
180.0	194.000	-.537	42.565	215.661

AVERAGE TEMPERATURE OF THE CYLINDER=190.158
TEMPERATURE IN THE CORE OF THE CYL.= 195.900
TEMPERATURE OF THE AIR STREAM= 81.40
AVERAGE HEAT TRANSFER COEFICIENT= 44.778
NUS.NO.(F.T.)=227.50 NUS.NO.(A.T.)=246.63
PR.NO.(F.T.)= .7077 PR.NO.(A.T.)= .7111
REY.NO.(F.T.)= 170.33 REY.NO.(A,T.)= 202.05

MATERIAL OF THE BED=G.B.230
P/D= 1.30 NUMBER OF ROWS= 5
VOLTS= 19.700 CURRENT(AMPS.)= 5.43
SUPERFICIAL VELOCITY OF AIR= .516 FT./SEC.
ST.HT.= 11.5 INCHES EX.HT.= 12.7 INCHES
PRESSURE DROP IN THE BED= .430 PSI

THETA	TEMP.	CRCOND	HLOCAL	NULOCAL
0.0	172.200	-3.385	42.883	221.051
15.0	169.488	-1.312	46.351	239.447
30.0	164.200	.918	51.561	267.510
45.0	159.797	.632	54.059	281.490
60.0	156.500	.309	56.032	292.557
75.0	153.924	.711	58.371	305.422
90.0	152.500	1.124	59.915	313.871
105.0	152.593	.512	59.227	310.246
120.0	153.500	-.098	57.894	303.036
135.0	154.491	.195	57.418	300.295
150.0	155.800	.479	56.715	296.296
165.0	157.557	-.479	54.487	284.242
180.0	158.500	-1.408	52.899	275.744

AVERAGE TEMPERATURE OF THE CYLINDER=157.975
TEMPERATURE IN THE CORE OF THE CYL.= 164.000
TEMPERATURE OF THE AIR STREAM= 80.50
AVERAGE HEAT TRANSFER COEFICIENT= 54.992
NUS.NO.(F.T.)=286.78 NUS.NO.(A.T.)=303.27
PR.NO.(F.T.)= .7111 PR.NO.(A.T.)= .7111
REY.NO.(F.T.)= 224.76 REY.NO.(A,T.)= 254.53

Table F-11. Cont'd. Local and Average Heat Transfer Results (5 Rows, P/D_t = 1.3, Glass Beads (230 μm)).

MATERIAL OF THE BED=G.B.230
P/D= 1.30 NUMBER OF ROWS= 5
VOLTS= 21.200 CURRENT(AMPS.)= 5.80
SUPERFICIAL VELOCITY OF AIR= .797 FT./SEC.
ST.HT.= 11.5 INCHES EX.HT.= 13.5 INCHES
PRESSURE DROP IN THE BED= .436 PSI

THETA	TEMP.	CRCOND	HLOCAL	NULOCAL
0.0	200.000	-4.076	36.668	185.093
15.0	195.758	-1.584	40.642	205.753
30.0	187.500	1.140	46.590	237.277
45.0	180.521	.436	49.026	251.008
60.0	174.500	-.371	51.305	263.915
75.0	168.558	1.335	56.471	291.876
90.0	165.200	3.168	60.495	313.529
105.0	166.447	.691	57.172	296.008
120.0	169.000	-1.708	53.155	274.639
135.0	169.479	-.234	54.335	280.628
150.0	169.500	1.230	55.787	288.120
165.0	170.987	-.168	53.479	275.872
180.0	172.100	-1.566	51.454	265.187

AVERAGE TEMPERATURE OF THE CYLINDER=175.292
TEMPERATURE IN THE CORE OF THE CYL.= 179.900
TEMPERATURE OF THE AIR STREAM= 80.30
AVERAGE HEAT TRANSFER COEFICIENT= 51.873
NUS.NO.(F.T.)=266.67 NUS.NO.(A.T.)=285.95
PR.NO.(F.T.)= .7092 PR.NO.(A.T.)= .7111
REY.NO.(F.T.)= 337.85 REY.NO.(A,T.)= 392.54

MATERIAL OF THE BED=G.B.230
P/D= 1.30 NUMBER OF ROWS= 5
VOLTS= 21.380 CURRENT(AMPS.)= 5.77
SUPERFICIAL VELOCITY OF AIR= 1.153 FT./SEC.
ST.HT.= 11.5 INCHES EX.HT.= 15.0 INCHES
PRESSURE DROP IN THE BED= .455 PSI

THETA	TEMP.	CRCOND	HLOCAL	NULOCAL
0.0	179.000	-.766	46.379	238.363
15.0	178.070	-.963	46.612	239.759
30.0	175.000	-1.189	47.863	246.797
45.0	169.898	.100	51.824	268.325
60.0	165.000	1.536	56.117	291.721
75.0	162.363	.785	57.040	297.166
90.0	161.200	-.014	57.013	297.313
105.0	160.362	.315	57.911	302.205
120.0	160.100	.645	58.422	304.936
135.0	160.677	-.138	57.243	298.638
150.0	161.000	-.913	56.248	293.372
165.0	160.180	.077	57.799	301.665
180.0	159.500	1.086	59.280	309.569

AVERAGE TEMPERATURE OF THE CYLINDER=165.258
TEMPERATURE IN THE CORE OF THE CYL.= 168.100
TEMPERATURE OF THE AIR STREAM= 77.30
AVERAGE HEAT TRANSFER COEFICIENT= 54.742
NUS.NO.(F.T.)=284.52 NUS.NO.(A.T.)=303.32
PR.NO.(F.T.)= .7107 PR.NO.(A.T.)= .7111
REY.NO.(F.T.)= 498.76 REY.NO.(A,T.)= 574.31

Table F-12. Local and Average Heat Transfer Results
(5 Rows, P/D_t = 1.1, Glass Beads (230 μm)).

MATERIAL OF THE BED=G.B.230
P/D= 1.10 NUMBER OF ROWS= 5
VOLTS= 8.940 CURRENT(AMPS.)= 2.44
SUPERFICIAL VELOCITY OF AIR= .151 FT./SEC.
ST.HT.= 11.5 INCHES EX.HT.= 11.5 INCHES
PRESSURE DROP IN THE BED= .303 PSI

THETA	TEMP.	CRCOND	HLCCAL	NULOCAL
0.0	177.300	3.119	11.006	57.044
15.0	180.195	.979	8.663	44.798
30.0	185.500	-1.031	6.309	32.484
45.0	189.150	-.639	6.481	33.277
60.0	191.100	-.274	6.735	34.525
75.0	192.492	.482	7.413	37.963
90.0	195.200	1.209	7.994	40.851
105.0	200.446	.140	6.660	33.899
120.0	206.100	-.844	5.412	27.435
135.0	209.650	-.900	5.201	26.299
150.0	210.400	-.972	5.097	25.760
165.0	208.718	.118	6.259	31.668
180.0	207.400	1.231	7.429	37.626

AVERAGE TEMPERATURE OF THE CYLINDER=196.775
TEMPERATURE IN THE CORE OF THE CYL.= 190.500
TEMPERATURE OF THE AIR STREAM= 68.60
AVERAGE HEAT TRANSFER COEFICIENT= 6.785
NUS.NO.(F.T.)= 34.63 NUS.NO.(A.T.)= 38.14
PR.NO.(F.T.)= .7082 PR.NO.(A.T.)= .7120
REY.NO.(F.T.)= 63.09 REY.NO.(A.T.)= 77.34

MATERIAL OF THE BED=G.B.230
P/D= 1.10 NUMBER OF ROWS= 5
VOLTS= 11.070 CURRENT(AMPS.)= 3.04
SUPERFICIAL VELOCITY OF AIR= .202 FT./SEC.
ST.HT.= 11.5 INCHES EX.HT.= 11.5 INCHES
PRESSURE DROP IN THE BED= .417 PSI

THETA	TEMP.	CRCOND	HLCCAL	NULOCAL
0.0	186.000	.161	11.604	59.678
15.0	186.053	-.197	11.241	57.810
30.0	185.600	-.557	10.926	56.207
45.0	184.085	-.067	11.565	59.569
60.0	182.400	.437	12.240	63.130
75.0	181.671	.630	12.510	64.558
90.0	182.500	.815	12.609	65.024
105.0	185.182	.564	12.087	62.202
120.0	189.300	.320	11.452	58.743
135.0	194.178	-.093	10.610	54.217
150.0	198.800	-.476	9.850	50.160
165.0	202.132	-.706	9.364	47.569
180.0	203.400	-.939	9.037	45.864

AVERAGE TEMPERATURE OF THE CYLINDER=188.883
TEMPERATURE IN THE CORE OF THE CYL.= 188.200
TEMPERATURE OF THE AIR STREAM= 69.60
AVERAGE HEAT TRANSFER COEFICIENT= 11.231
NUS.NO.(F.T.)= 57.63 NUS.NO.(A.T.)= 63.01
PR.NO.(F.T.)= .7089 PR.NO.(A.T.)= .7118
REY.NO.(F.T.)= 85.33 REY.NO.(A.T.)= 103.21

Table F-12. Cont'd. Local and Average Heat Transfer Results (5 Rows, P/D_t = 1.1, Glass Beads (230 μm)).

MATERIAL OF THE BED=G.B.230
P/D= 1.10 NUMBER OF ROWS= 5
VOLTS= 16.040 CURRENT(AMPS.)= 4.39
SUPERFICIAL VELOCITY OF AIR= .251 FT./SEC.
ST.HT.= 11.5 INCHES EX.HT.= 11.5 INCHES
PRESSURE DROP IN THE BED= .379 PSI

THETA	TEMP.	CRCOND	HLOCAL	NULOCAL
0.0	246.900	-5.700	10.054	49.678
15.0	237.905	-2.503	14.073	69.889
30.0	219.600	1.118	19.673	98.781
45.0	202.699	.986	21.850	110.979
60.0	188.700	.796	24.068	123.543
75.0	177.325	1.868	27.556	142.740
90.0	170.400	3.051	30.476	158.769
105.0	169.678	2.504	30.123	157.026
120.0	174.500	1.846	28.214	146.491
135.0	183.114	.029	24.427	125.942
150.0	191.800	-1.531	21.160	108.354
165.0	197.130	-1.298	20.461	104.350
180.0	198.800	-1.114	20.369	103.751

AVERAGE TEMPERATURE OF THE CYLINDER=194.642
TEMPERATURE IN THE CORE OF THE CYL.= 196.400
TEMPERATURE OF THE AIR STREAM= 69.30
AVERAGE HEAT TRANSFER COEFICIENT= 23.101
NUS.NO.(F.T.)=118.04 NUS.NO.(A.T.)=129.68
PR.NO.(F.T.)= .7083 PR.NO.(A.T.)= .7119
REY.NO.(F.T.)= 105.23 REY.NO.(A,T.)= 128.43

MATERIAL OF THE BED=G.B.230
P/D= 1.10 NUMBER OF ROWS= 5
VOLTS= 16.590 CURRENT(AMPS.)= 4.55
SUPERFICIAL VELOCITY OF AIR= .303 FT./SEC.
ST.HT.= 11.5 INCHES EX.HT.= 12.0 INCHES
PRESSURE DROP IN THE BED= .392 PSI

THETA	TEMP.	CRCOND	HLOCAL	NULOCAL
0.0	207.700	-3.724	17.783	90.043
15.0	203.493	-.802	21.364	108.502
30.0	196.900	2.351	25.638	130.844
45.0	194.495	.328	24.053	122.980
60.0	193.000	-1.761	22.245	113.868
75.0	188.463	.066	24.967	128.254
90.0	184.100	2.033	27.862	143.621
105.0	183.614	.935	26.871	138.568
120.0	185.500	-.169	25.355	130.549
135.0	187.730	.548	25.601	131.585
150.0	191.400	1.225	25.539	130.892
165.0	197.104	-.885	22.366	114.129
180.0	200.300	-2.869	19.827	100.929

AVERAGE TEMPERATURE OF THE CYLINDER=192.483
TEMPERATURE IN THE CORE OF THE CYL.= 188.700
TEMPERATURE OF THE AIR STREAM= 68.60
AVERAGE HEAT TRANSFER COEFICIENT= 24.219
NUS.NO.(F.T.)=124.02 NUS.NO.(A.T.)=136.12
PR.NO.(F.T.)= .7086 PR.NO.(A.T.)= .7120
REY.NO.(F.T.)= 127.61 REY.NO.(A,T.)= 155.46

Table F-13. Local and Average Heat Transfer Results
(3 Rows, P/D_t = 1.5, Ottawa Sand (514 μm)).

MATERIAL OF THE BED=O.S.514
P/D= 1.50 NUMBER OF ROWS= 3
VOLTS= 8.570 CURRENT(AMPS.)= 2.34
SUPERFICIAL VELOCITY OF AIR= .506 FT./SEC.
ST.HT.= 11.3 INCHES EX.HT.= 11.3 INCHES
PRESSURE DROP IN THE BED= .322 PSI

THETA	TEMP.	CRCOND	HLOCAL	NULOCAL
0.0	146.300	-2.355	10.480	54.974
15.0	145.143	-.442	12.639	66.362
30.0	143.400	1.562	15.031	79.036
45.0	143.037	.647	14.199	74.686
60.0	143.500	-.276	13.170	69.244
75.0	143.973	.504	13.843	72.754
90.0	145.100	1.258	14.348	75.339
105.0	147.935	2.114	14.618	76.576
120.0	153.700	2.773	14.234	74.207
135.0	162.726	-.088	10.051	52.012
150.0	171.600	-2.358	6.751	34.687
165.0	176.837	-1.816	6.778	34.685
180.0	178.400	-1.385	7.066	36.118

AVERAGE TEMPERATURE OF THE CYLINDER=153.275
TEMPERATURE IN THE CORE OF THE CYL.= 154.500
TEMPERATURE OF THE AIR STREAM= 85.10
AVERAGE HEAT TRANSFER COEFICIENT= 12.033
NUS.NO.(F.T.)= 62.75 NUS.NO.(A.T.)= 65.95
PR.NO.(F.T.)= .7112 PR.NO.(A.T.)= .7114
REY.NO.(F.T.)= 220.43 REY.NO.(A,T.)= 245.90

MATERIAL OF THE BED=O.S.514
P/D= 1.50 NUMBER OF ROWS= 3
VOLTS= 10.480 CURRENT(AMPS.)= 2.85
SUPERFICIAL VELOCITY OF AIR= .817 FT./SEC.
ST.HT.= 11.3 INCHES EX.HT.= 11.3 INCHES
PRESSURE DROP IN THE BED= .562 PSI

THETA	TEMP.	CRCOND	HLOCAL	NULOCAL
0.0	141.400	-.747	19.938	105.009
15.0	141.018	-.354	20.472	107.856
30.0	140.200	.046	21.178	111.653
45.0	139.235	-.561	20.946	110.515
60.0	137.600	-1.205	20.967	110.777
75.0	135.080	.853	24.135	127.777
90.0	133.500	3.067	27.106	143.686
105.0	134.920	3.603	26.961	142.753
120.0	140.300	3.815	24.909	131.313
135.0	149.465	.120	18.230	95.375
150.0	158.800	-2.649	13.185	68.454
165.0	164.632	-2.259	12.424	64.193
180.0	166.500	-2.017	12.332	63.624

AVERAGE TEMPERATURE OF THE CYLINDER=144.058
TEMPERATURE IN THE CORE OF THE CYL.= 145.100
TEMPERATURE OF THE AIR STREAM= 85.10
AVERAGE HEAT TRANSFER COEFICIENT= 20.547
NUS.NO.(F.T.)=107.98 NUS.NO.(A.T.)=112.61
PR.NO.(F.T.)= .7120 PR.NO.(A.T.)= .7114
REY.NO.(F.T.)= 360.91 REY.NO.(A,T.)= 396.85

Table F-13. Cont'd. Local and Average Heat Transfer Results (3 Rows, P/D_t = 1.5, Ottawa Sand (514 μm)).

MATERIAL OF THE BED=O.S.514
P/D= 1.50 NUMBER OF ROWS= 3
VOLTS= 17.570 CURRENT(AMPS.)= 4.82
SUPERFICIAL VELOCITY OF AIR= .977 FT./SEC.
ST.HT.= 11.3 INCHES EX.HT.= 11.5 INCHES
PRESSURE DROP IN THE BED= .524 PSI

THETA	TEMP.	CRCOND	HLCCAL	NULOCAL
0.0	169.700	-.198	39.684	204.087
15.0	169.583	.018	39.955	205.500
30.0	169.500	.235	40.211	206.831
45.0	169.470	-.782	39.209	201.681
60.0	168.000	-1.830	38.870	200.169
75.0	163.835	-.855	41.999	217.008
90.0	158.200	.235	46.398	240.841
105.0	152.965	1.602	51.337	267.630
120.0	150.100	3.082	55.019	287.507
135.0	150.955	1.736	52.996	276.739
150.0	154.300	.409	49.181	256.110
165.0	158.142	-1.244	44.955	233.364
180.0	160.000	-2.804	42.247	218.970

AVERAGE TEMPERATURE OF THE CYLINDER=160.825
TEMPERATURE IN THE CORE OF THE CYL.= 165.500
TEMPERATURE OF THE AIR STREAM= 85.90
AVERAGE HEAT TRANSFER COEFICIENT= 45.088
NUS.NO.(F.T.)=233.54 NUS.NO.(A.T.)=246.86
PR.NO.(F.T.)= .7102 PR.NO.(A.T.)= .7115
REY.NO.(F.T.)= 420.19 REY.NO.(A,T.)= 473.53

MATERIAL OF THE BED=O.S.514
P/D= 1.50 NUMBER OF ROWS= 3
VOLTS= 18.580 CURRENT(AMPS.)= 5.10
SUPERFICIAL VELOCITY OF AIR= 1.233 FT./SEC.
ST.HT.= 11.3 INCHES EX.HT.= 12.5 INCHES
PRESSURE DROP IN THE BED= .562 PSI

THETA	TEMP.	CRCOND	HLCCAL	NULOCAL
0.0	168.100	1.860	46.823	241.303
15.0	169.366	.412	44.709	230.173
30.0	171.400	-.983	42.282	217.327
45.0	171.846	-1.456	41.590	213.696
60.0	169.500	-1.966	42.240	217.442
75.0	163.988	-.789	46.490	240.377
90.0	157.100	.600	52.346	272.187
105.0	150.889	1.114	57.688	301.511
120.0	146.300	1.689	62.459	327.691
135.0	143.829	1.494	64.794	340.636
150.0	143.300	1.239	65.109	342.442
165.0	144.132	-.125	62.854	330.355
180.0	144.800	-1.456	60.826	319.517

AVERAGE TEMPERATURE OF THE CYLINDER=157.342
TEMPERATURE IN THE CORE OF THE CYL.= 161.500
TEMPERATURE OF THE AIR STREAM= 84.90
AVERAGE HEAT TRANSFER COEFICIENT= 53.030
NUS.NO.(F.T.)=275.69 NUS.NO.(A.T.)=290.71
PR.NO.(F.T.)= .7107 PR.NO.(A.T.)= .7114
REY.NO.(F.T.)= 533.72 REY.NO.(A,T.)= 599.31

Table F-13. Cont'd. Local and Average Heat Transfer Results (3 Rows, P/D_t = 1.5, Ottawa Sand (514 μm)).

MATERIAL OF THE BED=O.S.514
P/D= 1.50 NUMBER OF ROWS= 3
VOLTS= 20.190 CURRENT(AMPS.)= 5.50
SUPERFICIAL VELOCITY OF AIR= 1.478 FT./SEC.
ST.HT.= 11.3 INCHES EX.HT.= 13.0 INCHES
PRESSURE DROP IN THE BED= .562 PSI

THETA	TEMP.	CRCOND	HLCCAL	NULOCAL
0.0	176.800	1.671	49.218	251.855
15.0	178.144	.640	47.507	242.851
30.0	180.800	-.356	45.223	230.709
45.0	182.643	-1.482	43.245	220.314
60.0	181.300	-2.651	42.694	217.725
75.0	175.347	-1.003	47.302	242.322
90.0	167.400	.899	53.824	277.470
105.0	160.518	1.122	58.837	305.004
120.0	155.500	1.354	63.151	328.720
135.0	152.682	1.972	66.328	346.063
150.0	152.800	2.529	66.774	348.355
165.0	155.766	-.599	60.967	317.283
180.0	157.800	-3.519	56.336	292.693

AVERAGE TEMPERATURE OF THE CYLINDER=167.517
TEMPERATURE IN THE CORE OF THE CYL.= 171.800
TEMPERATURE OF THE AIR STREAM= 85.20
AVERAGE HEAT TRANSFER COEFICIENT= 54.048
NUS.NO.(F.T.)=278.60 NUS.NO.(A.T.)=296.18
PR.NO.(F.T.)= .7095 PR.NO.(A.T.)= .7114
REY.NO.(F.T.)= 629.98 REY.NO.(A,T.)= 717.99

MATERIAL OF THE BED=O.S.514
P/D= 1.50 NUMBER OF ROWS= 3
VOLTS= 20.190 CURRENT(AMPS.)= 5.50
SUPERFICIAL VELOCITY OF AIR= 1.844 FT./SEC.
ST.HT.= 11.3 INCHES EX.HT.= 13.5 INCHES
PRESSURE DROP IN THE BED= .537 PSI

THETA	TEMP.	CRCOND	HLCCAL	NULOCAL
0.0	176.000	1.039	48.790	249.893
15.0	176.823	.372	47.701	244.163
30.0	178.400	-.261	46.259	236.495
45.0	179.375	-.982	45.083	230.316
60.0	178.300	-1.705	44.884	229.484
75.0	174.129	-1.248	47.492	243.606
90.0	167.500	-.767	51.838	267.297
105.0	159.871	1.243	59.143	306.854
120.0	154.300	3.599	66.098	344.517
135.0	153.213	1.838	65.322	340.760
150.0	154.900	.020	61.989	322.937
165.0	156.690	-.679	59.593	309.949
180.0	157.800	-1.360	58.167	302.305

AVERAGE TEMPERATURE OF THE CYLINDER=166.717
TEMPERATURE IN THE CORE OF THE CYL.= 170.800
TEMPERATURE OF THE AIR STREAM= 84.80
AVERAGE HEAT TRANSFER COEFICIENT= 54.070
NUS.NO.(F.T.)=278.98 NUS.NO.(A.T.)=296.46
PR.NO.(F.T.)= .7097 PR.NO.(A.T.)= .7114
REY.NO.(F.T.)= 787.28 REY.NO.(A,T.)= 896.82

Pressure Fluctuation Measurements

Table F-14 is a guide to review the pressure signals obtained during the tests and the resulting plots using Fast Fourier transform techniques. Included in these tables are Figure 20 through 27 contained in the main body of the thesis. Here they have been regrouped in the order in which they were obtained. The pressure signals presented in Figure 20, 21, F-3, F-8, F-12, and F-17 are traces obtained in a chart recorder. These signals have also been recorded on an FM recorder for processing in the Fast Fourier transform analyzer. In each case the outputs are probability density functions, auto correlation functions, and normalized power spectral density functions. Figure 20 through 26 contained in the main body of the thesis and Figure F-1 through F-8 contained here are for Ottawa sand $P/D_t = 1.3$ and five rows tube bundles with the cylinder containing pressure transducer located centrally in the arrangement. Similarly, Figure 27 in the main body of the thesis and Figure F-8 through F-21 contained here are for glass beads under the identical arrangement.

The local pressure signals obtained for Ottawa sand at a superficial velocity of 0.7 ft/sec ($\frac{U}{U_{mf}} = 0.95$) were too weak to obtain meaningful results from Fast Fourier transform analyzer. Hence, they have not been reported here. More complete analysis of the pressure fluctuations for U = 0.89 ft/sec ($\frac{U}{U_{mf}} = 1.20$) are contained in Figure 21 through 24 and Figure F-1 and F-2. For each of the six angular locations shown in

Table F-14. Arrangement of Figures Related to Local Pressure Fluctuations.

	Superficial Velocity ft/sec	Figure Number	Angular Positions	Functional Plot*
Ottawa Sand (514 μm) (P/D_t = 1.3, 5 Rows)	0.70	20	0,30,60,90,120,180	Pressure Signals
	0.89	21	0,30,60,90,120,150,180	Pressure Signals
	0.89	24	0,90,180	PDF
	0.89	23	90	ACF
	0.89	22	0,90,180	NPSDF
	0.89	F-1	30,60,120,150	PDF
	0.89	F-2	30,60,120,150	NPSDF
	1.14 and 1.56	F-3	0,90,180	Pressure Signals
	1.14	F-4	0,90,180	PDF
	1.14	26	90	ACF
	1.14	25	0,90,180	NPSDF
	1.56	F-5	0,90,180	PDF
	1.56	F-6	0	ACF
	1.56	F-7	0,90,180	NPSDF
Glass Beads (230 μm) (P/D_t = 1.3, 5 Rows)	0.29	F-8	0,30,60,90,120,150,180	Pressure Signals
	0.29	F-9	0,90,180	PDF
	0.29	27	0,90,180	NPSDF
	0.29	F-10	40,60,120,150	PDF
	0.29	F-11	30,60,120,150	NPSDF
	0.35	F-12	0,45,90,120,180,	Pressure Signals
	0.35	F-13	0,90,180	PDF
	0.35	F-14	0,90,180	NPSDF
	0.35	F-15	45,120	PDF
	0.35	F-16	45,120	NPSDF
	0.50	F-17	0,45,90,135,180	Pressure Signals
	0.50	F-18	0,90,180	PDF
	0.50	F-19	0,90,180	NPSDF
	0.50	F-20	45,135	PDF
	0.50	F-21	45,135	NPSDF

*PDF - Probability Density Function
ACF - Auto-Correlation Function
NPSDF - Normalized Power Spectral Density Function

Figure 21, probability density functions (Figure 24 and F-1) and normalized power spectral density functions (Figure 22 and F-2) are reported. Figure 23 is auto correlation function for angular position of degrees. Figure 25, 26, and Figure F-3 through F-7 are also for Ottawa sand at U = 1.14 and 1.56 ft/sec ($\frac{U}{U_{mf}}$ = 1.55 and 2.1, respectively) for angular locations 0, 90, and 180 degrees. There the auto correlation function for only the 90 degree position and U = 1.14 ft/sec is shown.

Figure 27 and Figure F-8 through F-21 are for glass beads. They are in three groups. Figure 27 and Figure F-8 through F-11 are for U = 0.29 ft/sec (U/U_{mf} = 1.80) and 30 degree interval angular positions between 0 and 180 degrees. Figure F-12 through F-16 are for U = 0.35 ft/sec (U/U_{mf} = 2.2) and for angular positions 0, 45, 90, 120, and 180 degrees orientation. Similarily, Figure F-17 through F-21 are for U = 0.50 ft/sec (U/U_{mf} = 3.13) and angular positions 0, 45, 90, 135, and 180 degrees orientation. No auto correlation functions are reported for the case of glass beads.

Table F-15 summarizes the results of the Figure 21 through 27 and Figure F-1 through F-21. For the case of Ottawa sand and glass beads and for the three superficial velocities selected the r.m.s. values of pressure fluctuations at each of the angular locations are listed. At higher values of U/U_{mf} for each of the two materials it has been possible to determine the frequency of dominant peak and they are contained in the table. These frequencies are related to bubble

passage around the cylinder as influenced by the neighboring tubes. Even though heat transfer tests were carried out using silica sand, no effort was made to record local pressure fluctuations and, hence, the absence of dominant frequencies and r.m.s. values of pressure fluctuations for this material in this investigation.

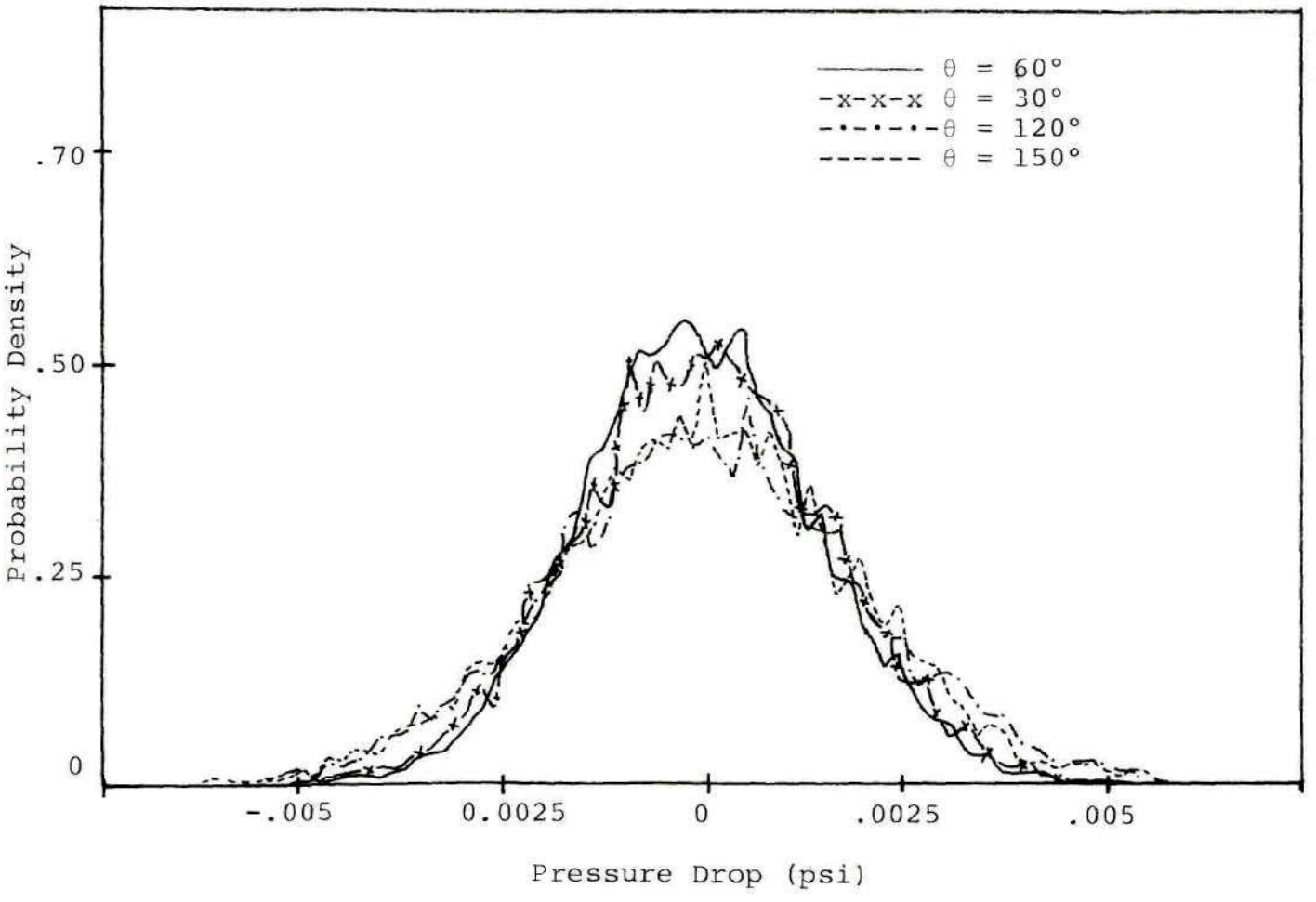

Figure F-1. Probability Density Function
(Ottawa Sand (514 μm), P/D_t = 1.3, and U = .89 ft/sec)

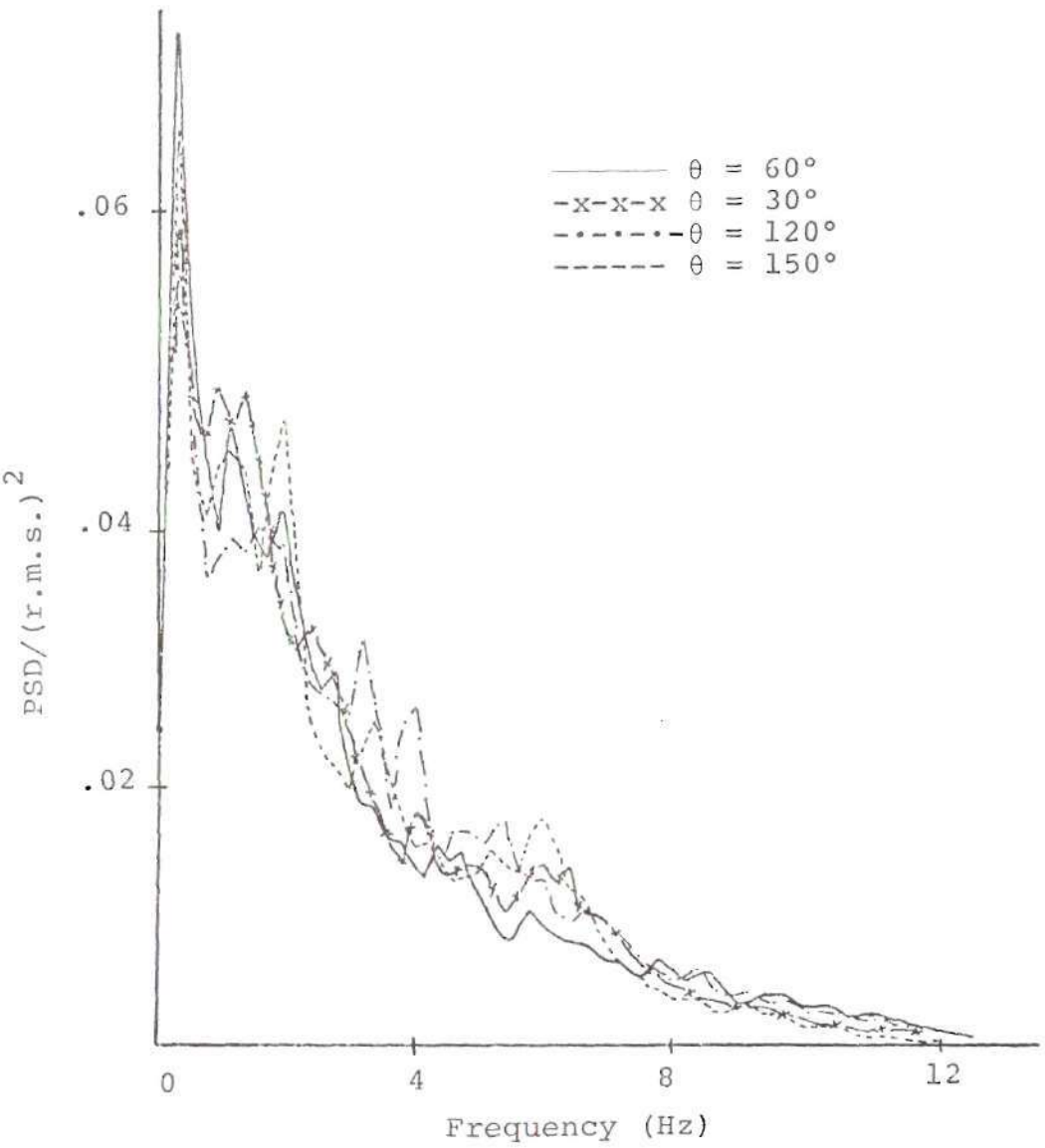

Figure F-2. Normalized Power Spectral Density Function. (Ottawa Sand (514 μm), P/D_t = 1.3, and U = .89 ft/sec)

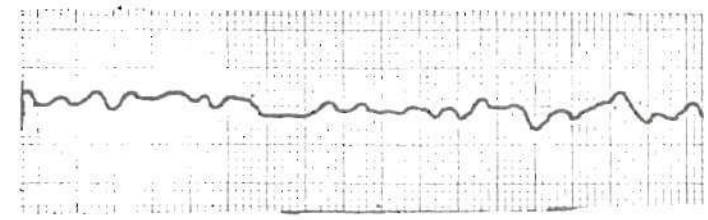

θ = 180°

θ = 90°

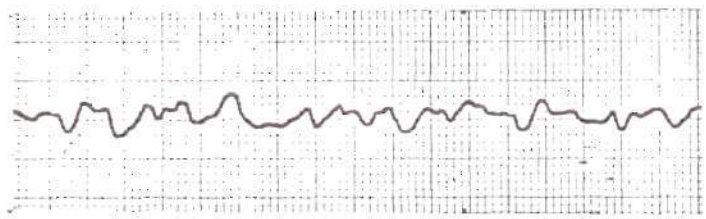

θ = 0°

(a)

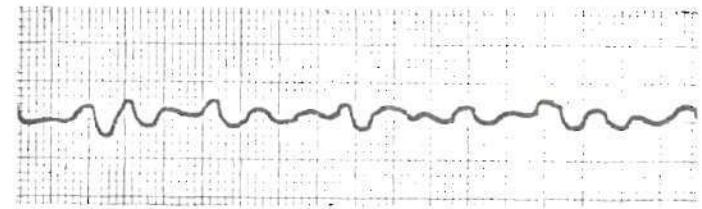

θ = 180°

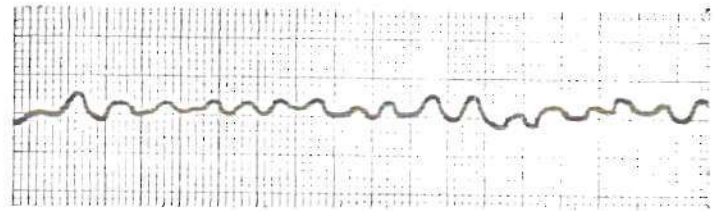

θ = 90°

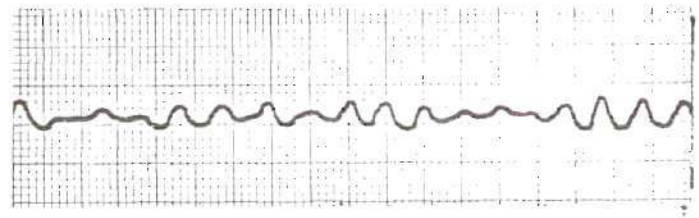

θ = 0°

(b)

Figure F-3. Representative Pressure Signal at Different Locations
(a) Ottawa Sand (514 μm), P/D_t = 1.3 and U = 1.14 ft/sec
(b) Ottawa Sand (514 μm), P/D_t = 1.3 and U = 1.56 ft/sec

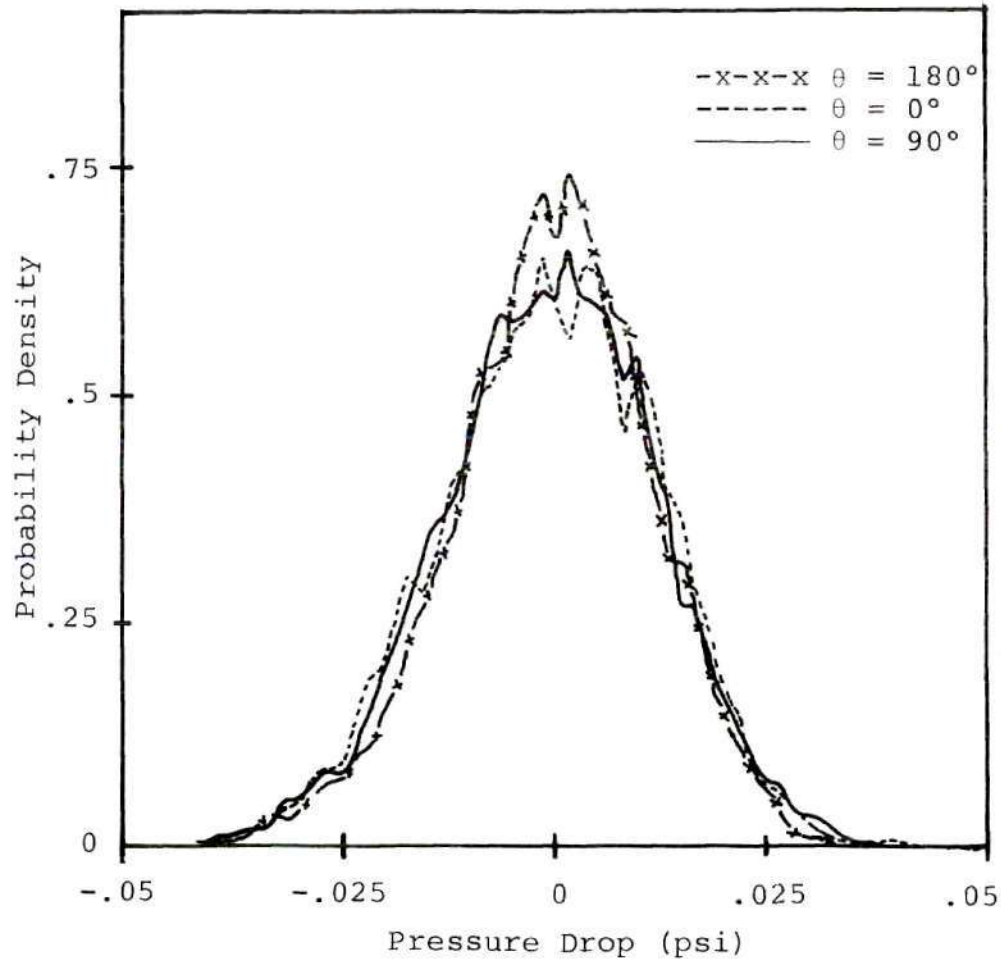

Figure F-4. Probability Density Function.
(Ottawa Sand (514 μm), P/D_t = 1.3, and U = 1.14 ft/sec)

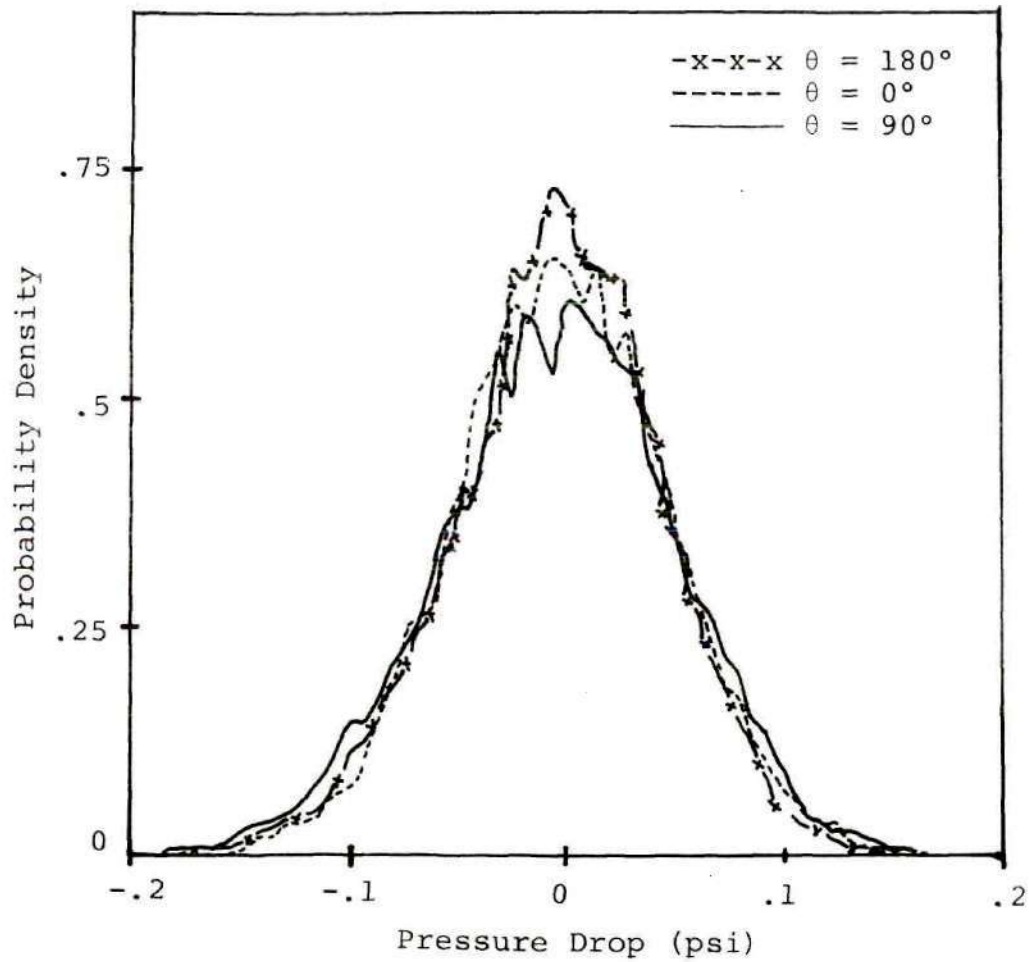

Figure F-5. Probability Density Function
(Ottawa Sand (514 μm), P/D_t = 1.3 and U = 1.56 ft/sec)

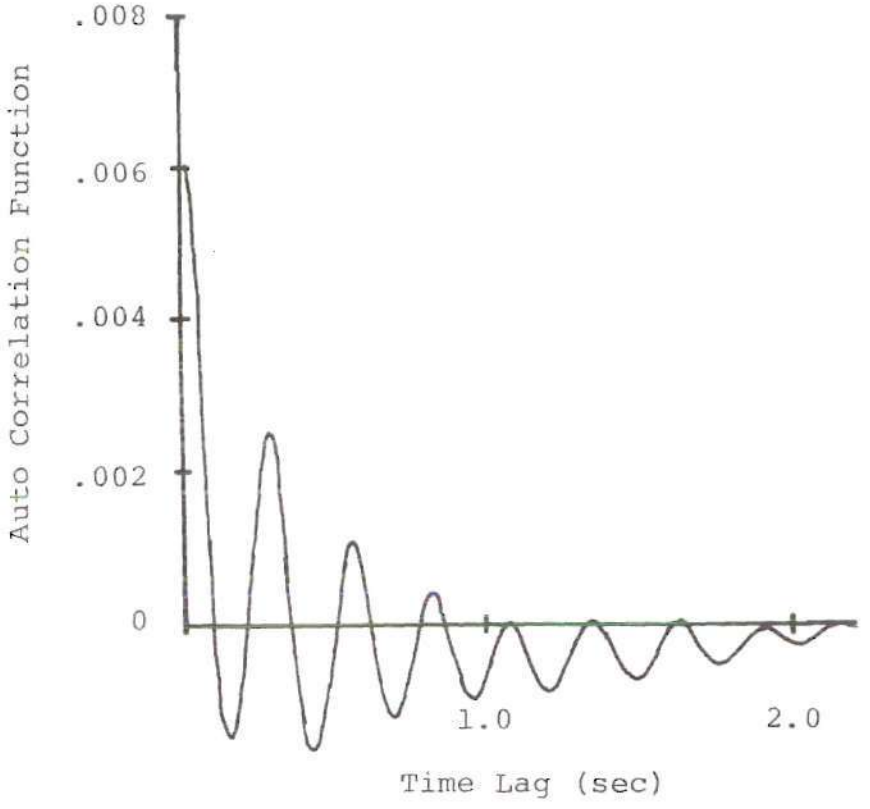

Figure F-6. Auto-Correlation Function (Ottawa Sand (514 μm), P/D_t = 1.3, and U = 1.56 ft/sec, θ = 0)

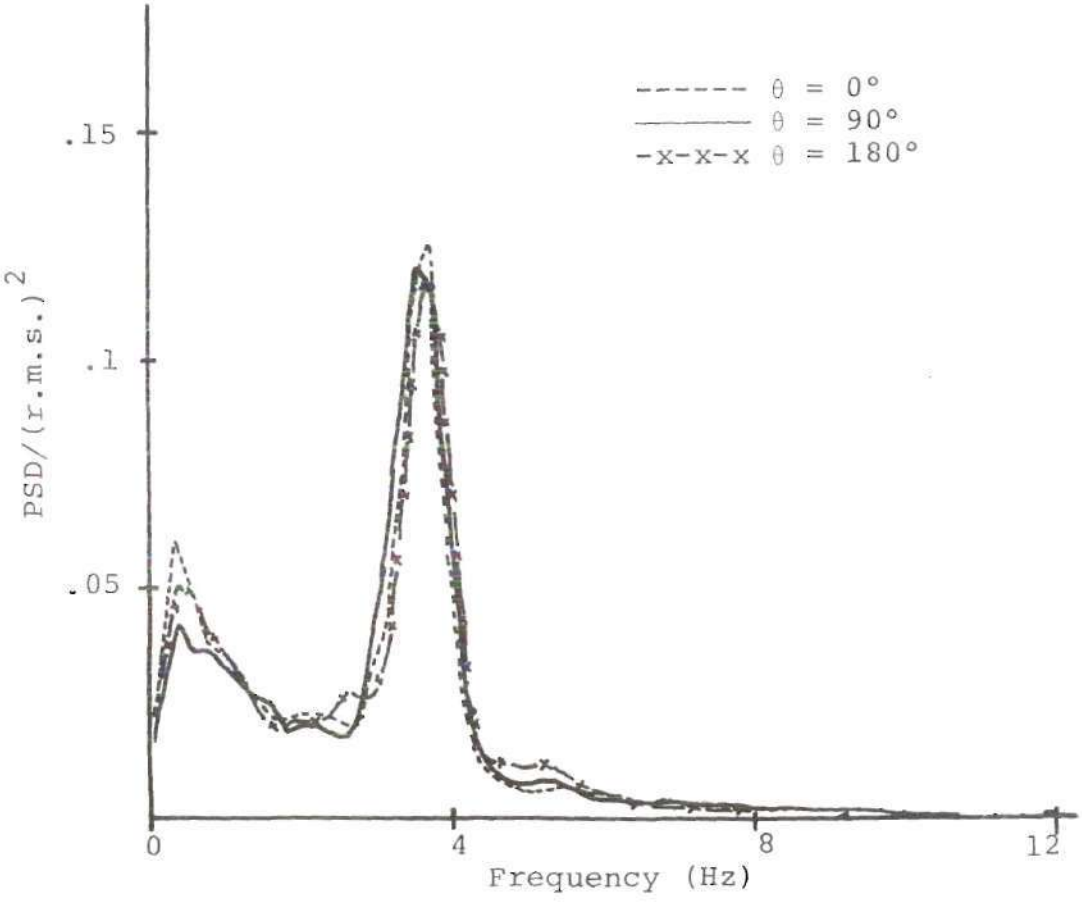

Figure F-7. Normalized Power Spectral Density Function.
(Ottawa Sand (514 μm), P/D_t = 1.3, and U = 1.56 ft/sec)

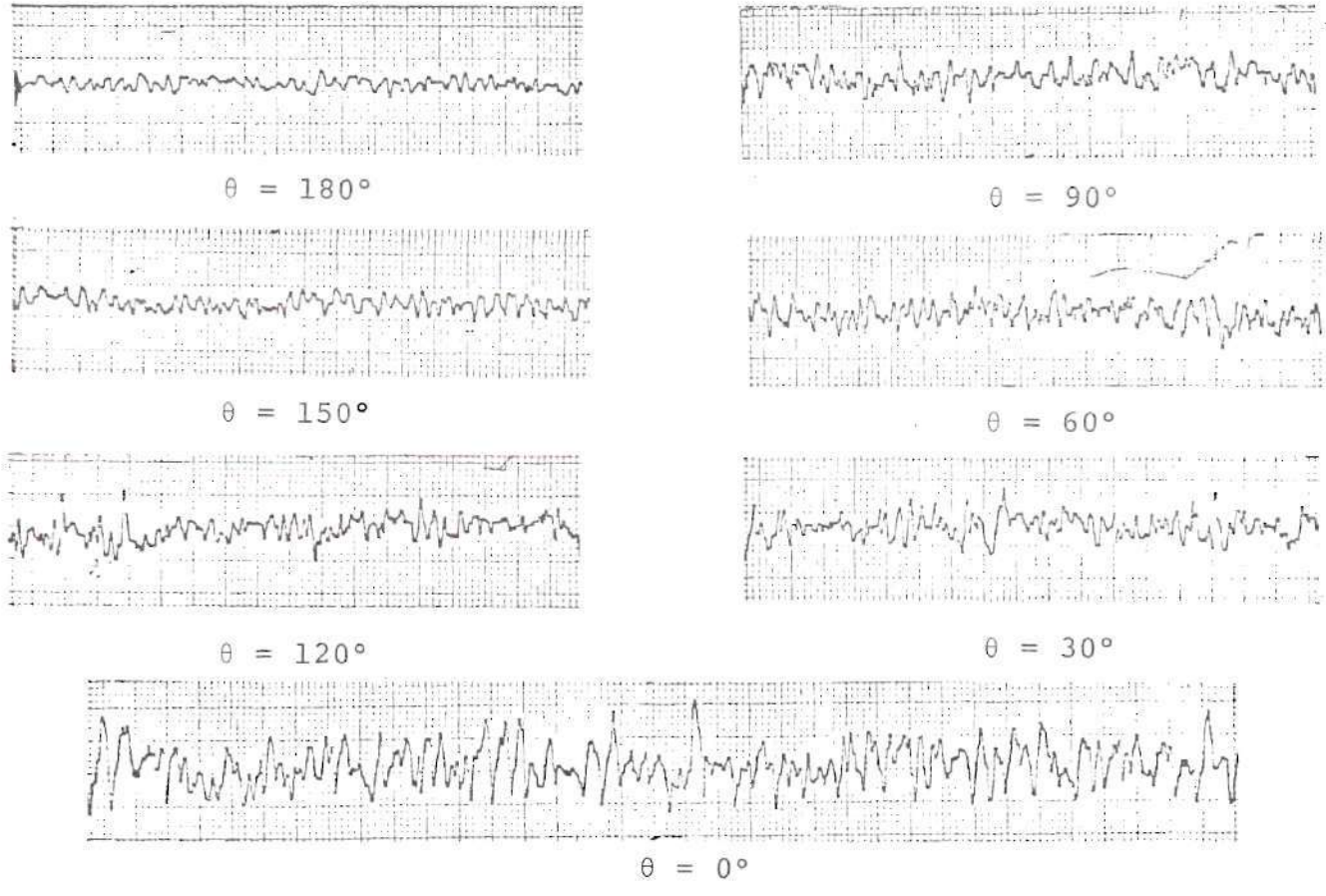

Figure F-8. Representative Pressure Signal at Different Locations. (Glass Beads (230 μm), P/D_t = 1.3 and U = .29 ft/sec)

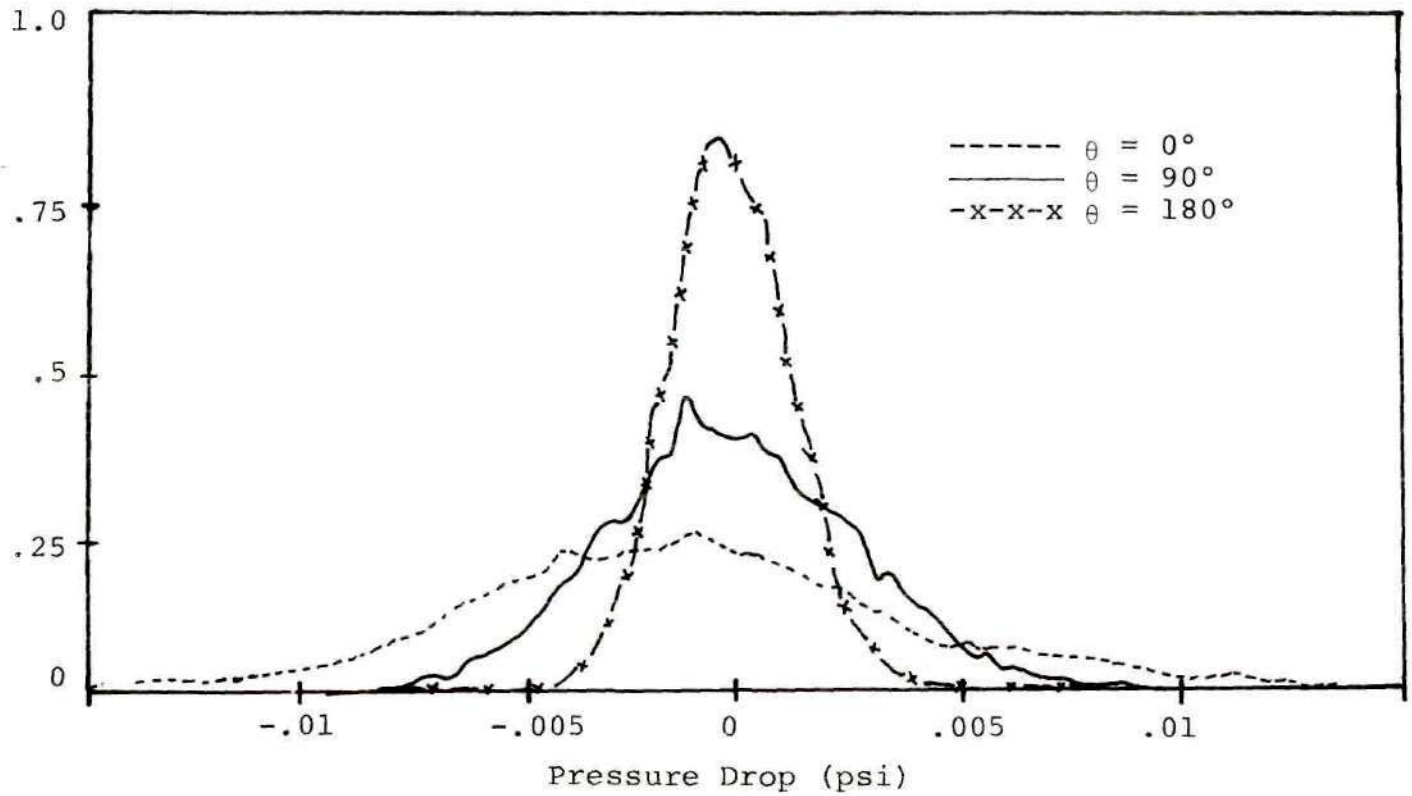

Figure F-9. Probability Density Function.
(Glass Beads (230 μm), P/D_t = 1.3, and U = .29 ft/sec)

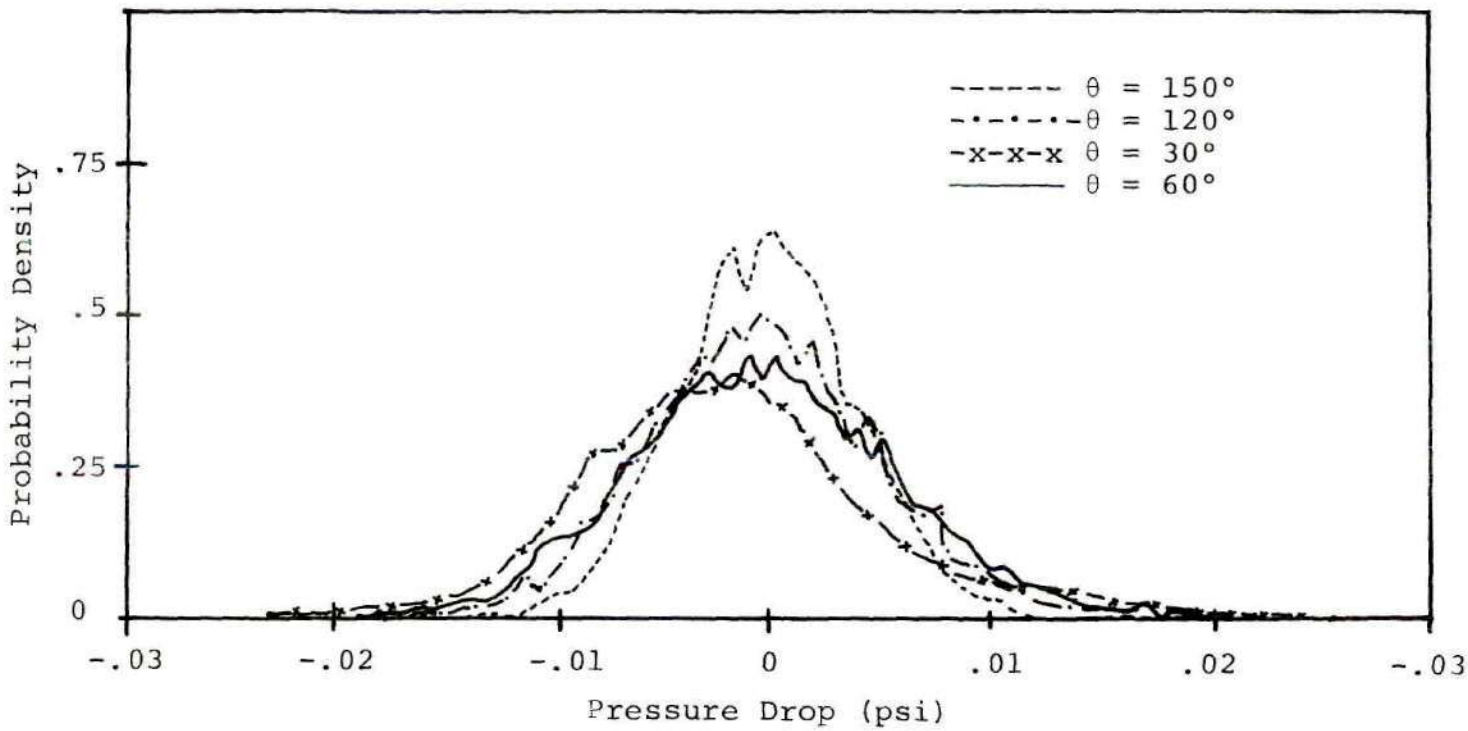

Figure F-10. Probability Density Function.
(Glass Beads (230 μm), P/D_t = 1.3 and U = .29 ft/sec)

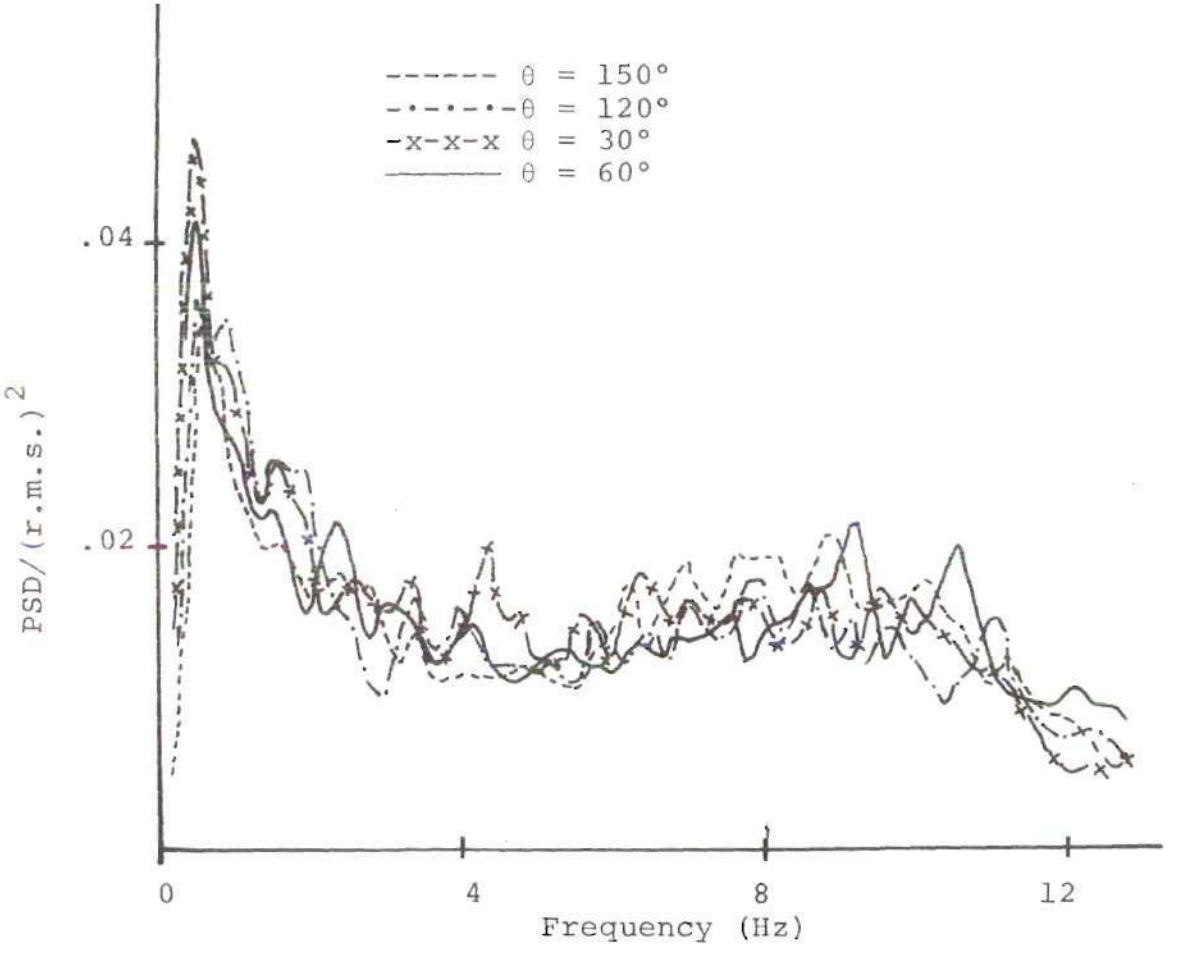

Figure F-11. Normalized Power Spectral Density Function. (Glass Beads (230 μm), P/D_t = 1.3 and U = .29 ft/sec)

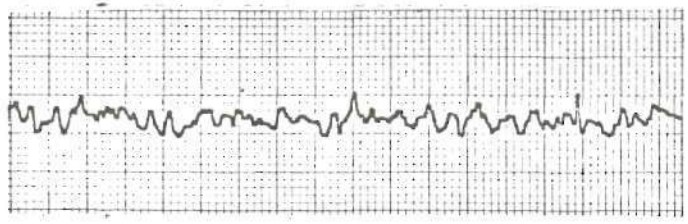

θ = 180°

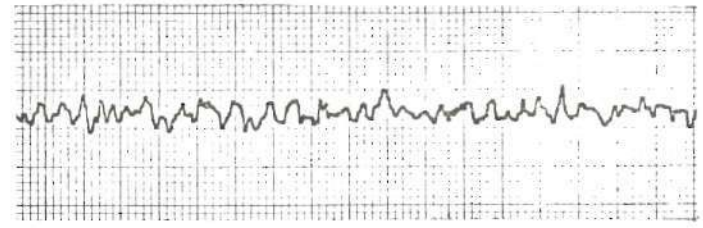

θ = 90°

θ = 120°

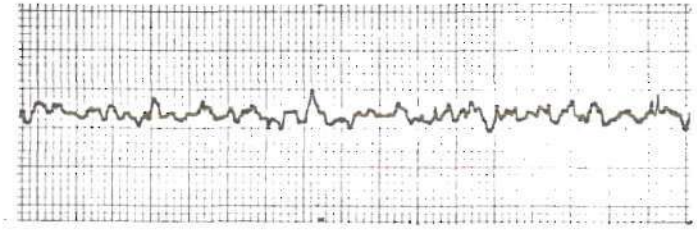

θ = 45°

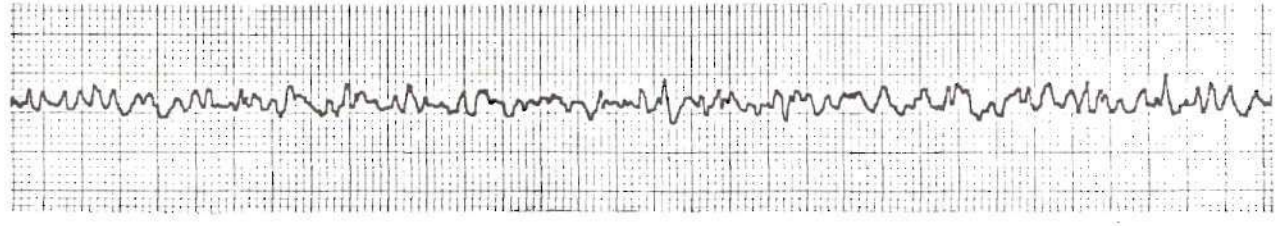

θ = 0°

Figure F-12. Representative Pressure Signal at Different Locations. (Glass Beads (230 μm), P/D_t = 1.3 and U = .35 ft/sec)

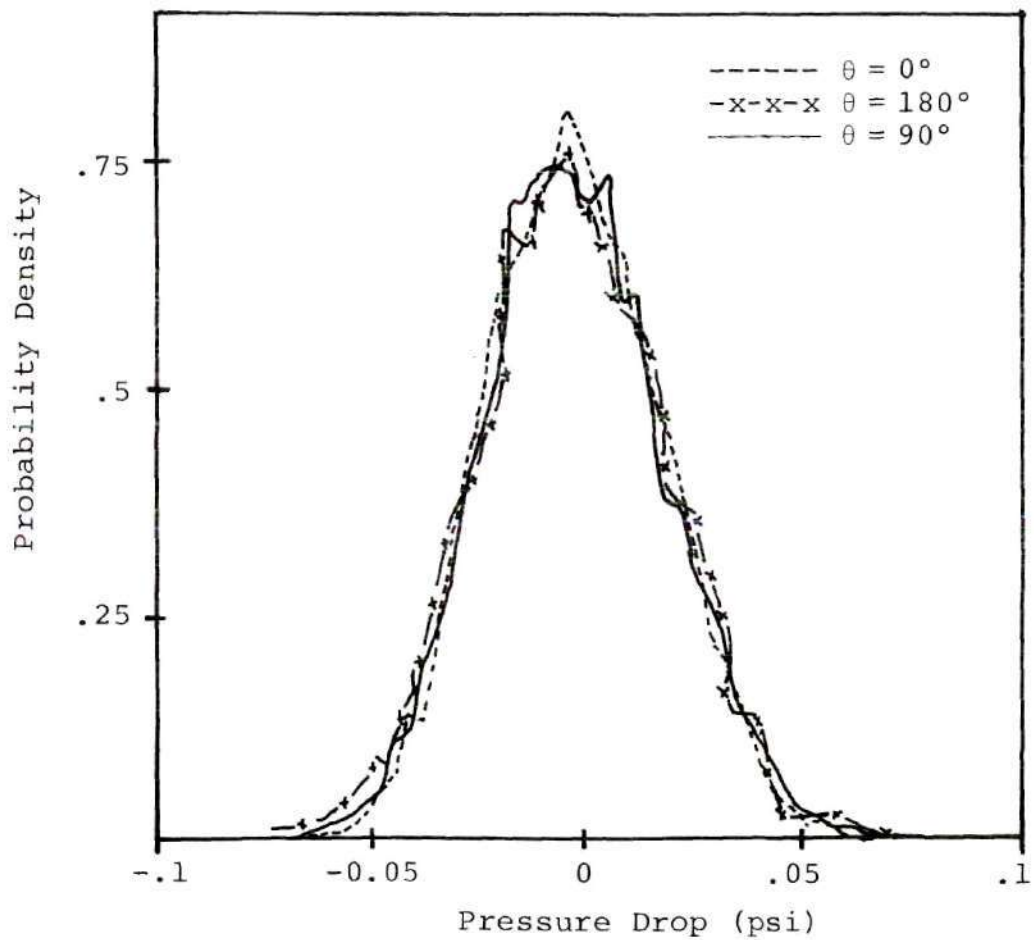

Figure F-13. Probability Density Function.
(Glass Beads (230 μm), P/D_t = 1.3 and U = .35 ft/sec)

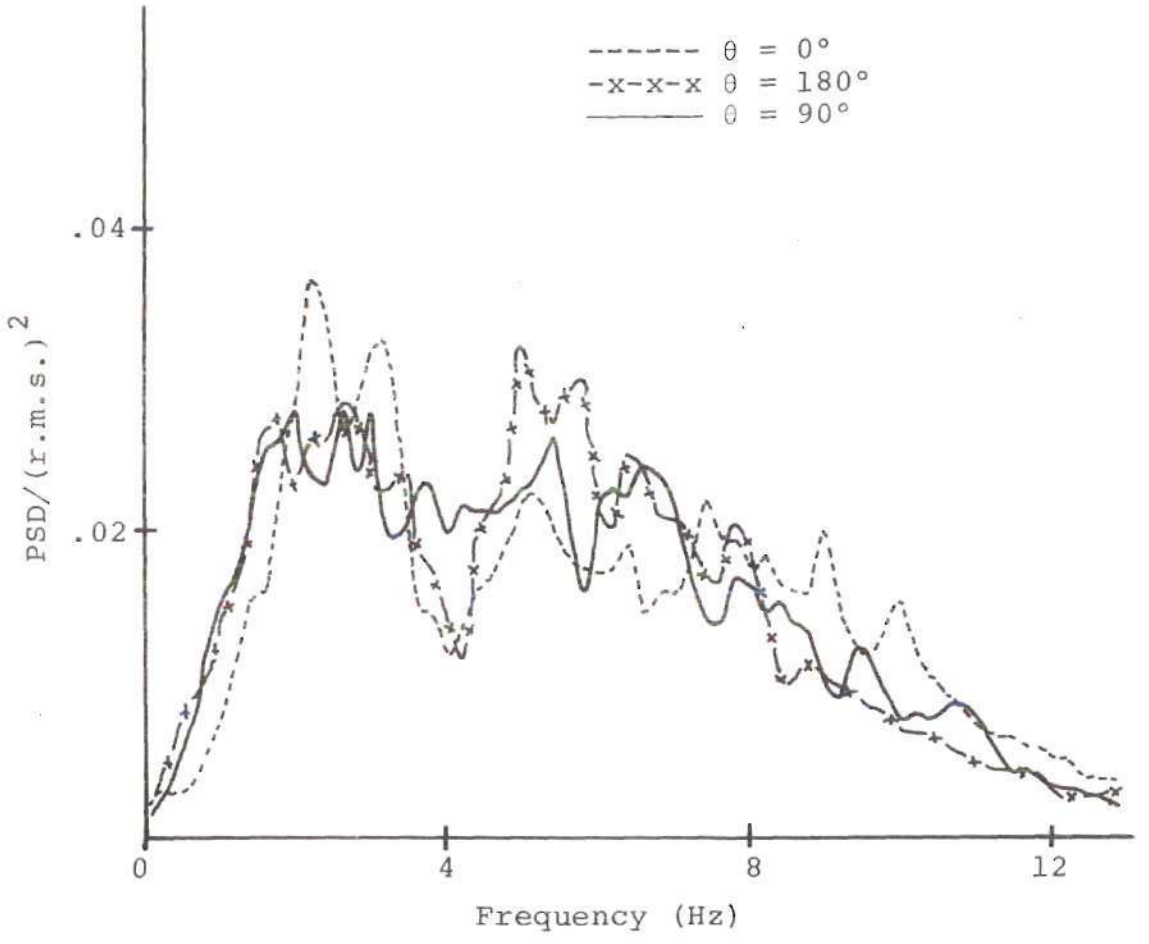

Figure F-14. Normalized Power Spectral Density Function. (Glass Beads (230 μm), P/D_t = 1.3 and U = .35 ft/sec)

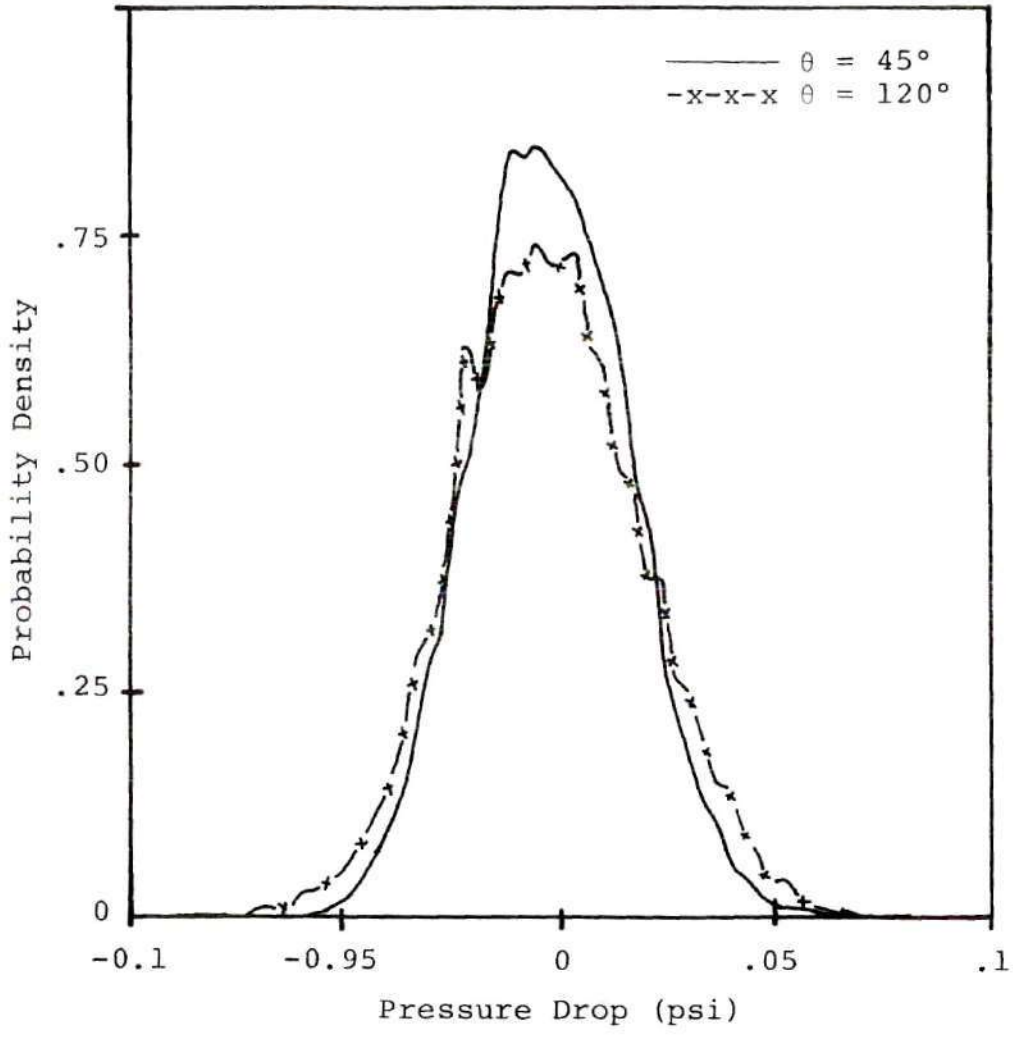

Figure F-15. Probability Density Function.
(Glass Beads (230 μm), P/D_t = 1.3 and U = .35 ft/sec)

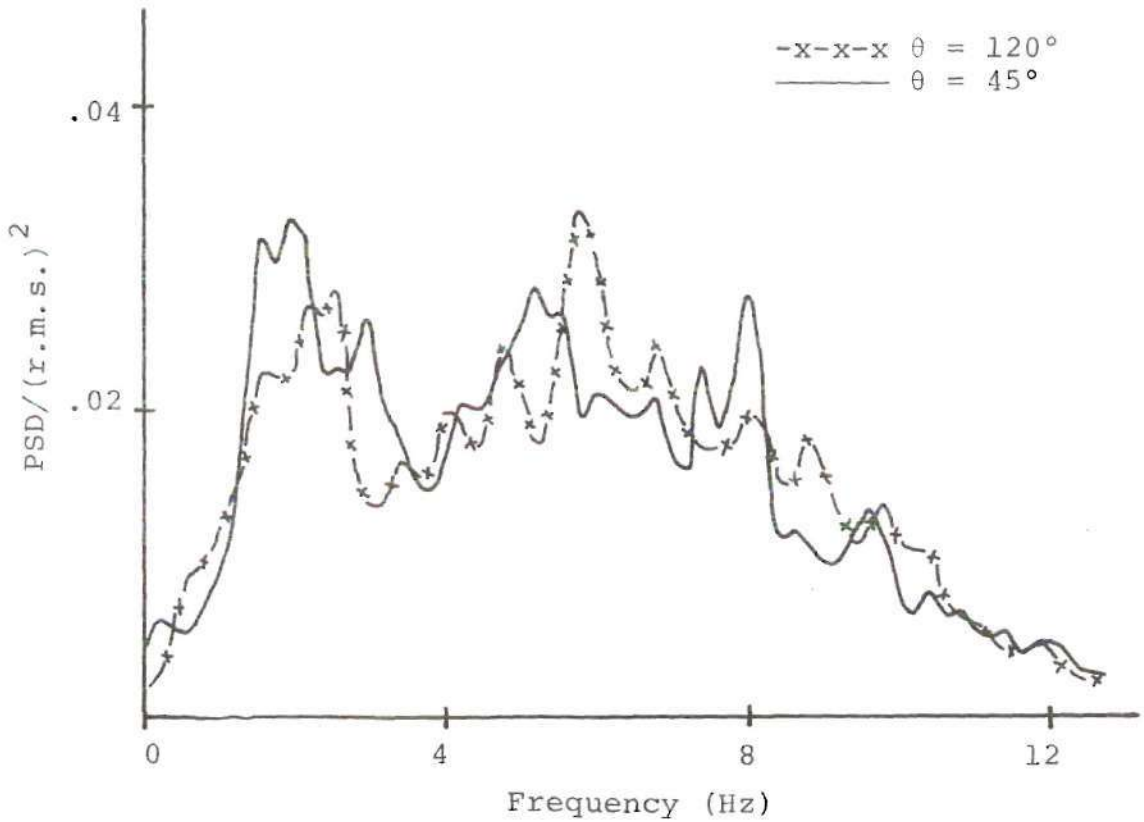

Figure F-16. Normalized Power Spectral Density Function. (Glass Beads (230 μm), P/D_t = 1.3 and U = .35 ft/sec)

θ = 180°

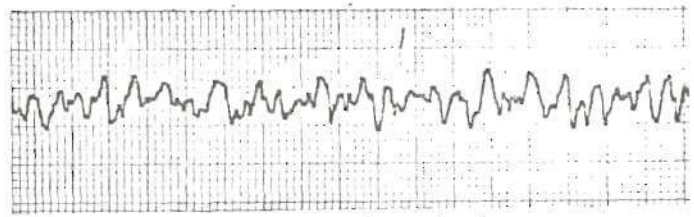

θ = 90°

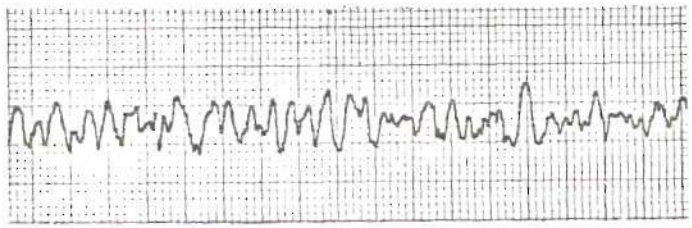

θ = 135°

θ = 45°

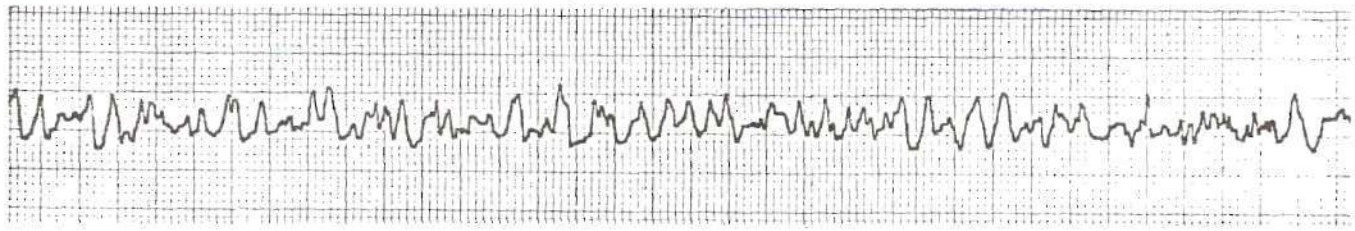

θ = 0°

Figure F-17. Representative Pressure Signal at Different Locations. (Glass Beads (230 μm), P/D_t = 1.3 and U = .50 ft/sec)

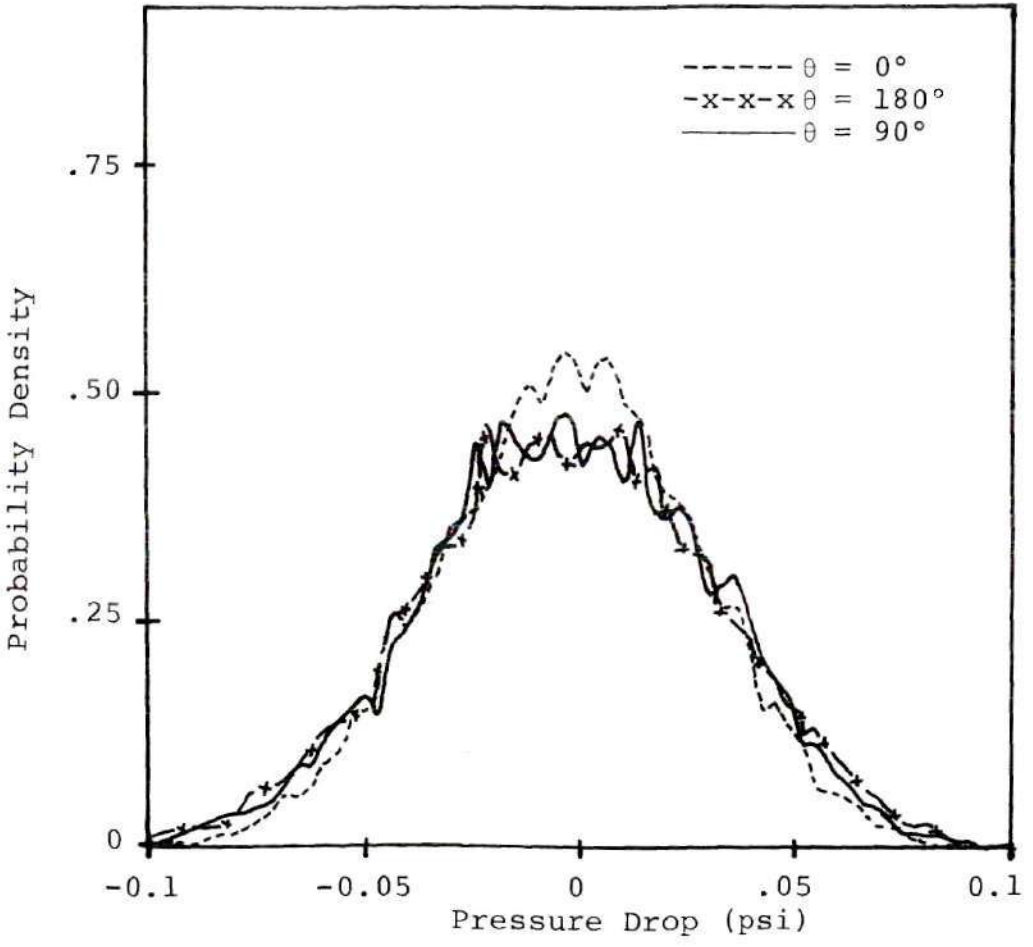

Figure F-18. Probability Density Function.
(Glass Beads (230 μm), P/D_t = 1.3 and U = .50 ft/sec)

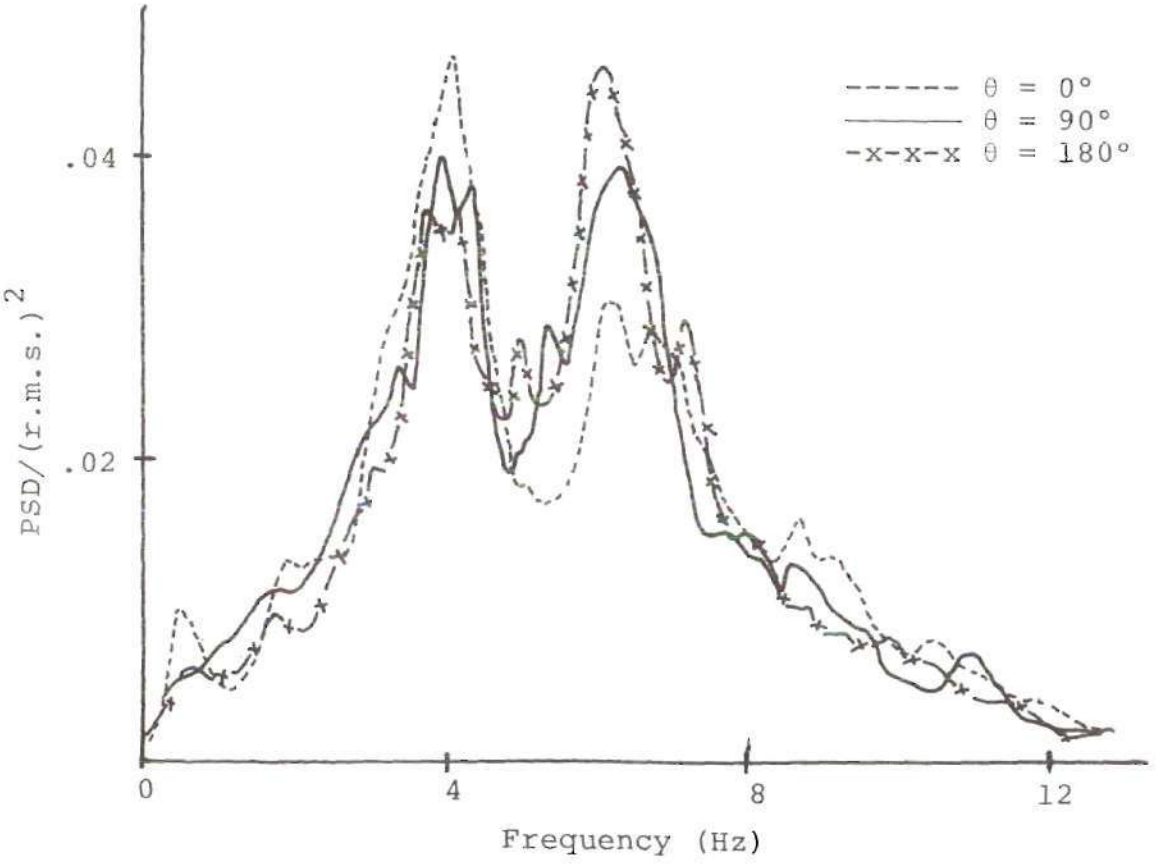

Figure F-19. Normalized Power Spectral Density Function. (Glass Beads (230 μm), P/D_t = 1.3 and U = .50 ft/sec)

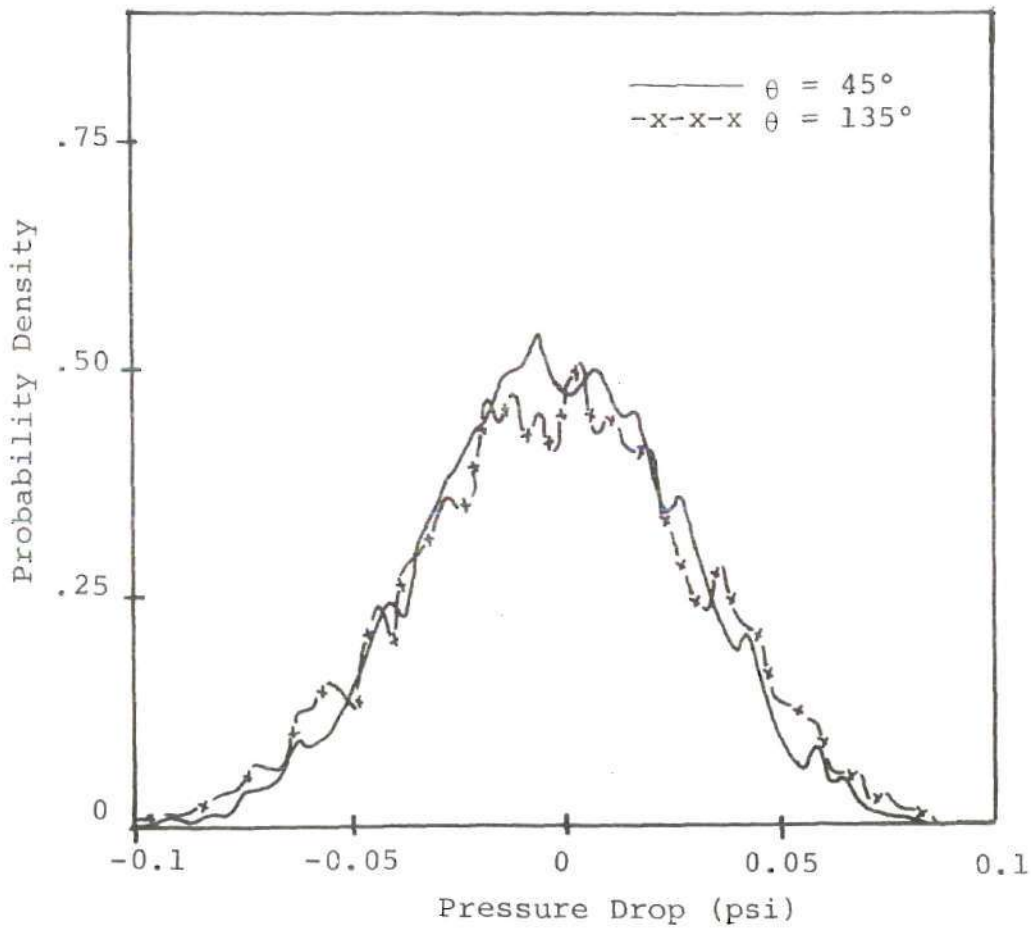

Figure F-20. Probability Density Function.
(Glass Beads (230 μm), P/D_t = 1.3 and U = .50 ft/sec)

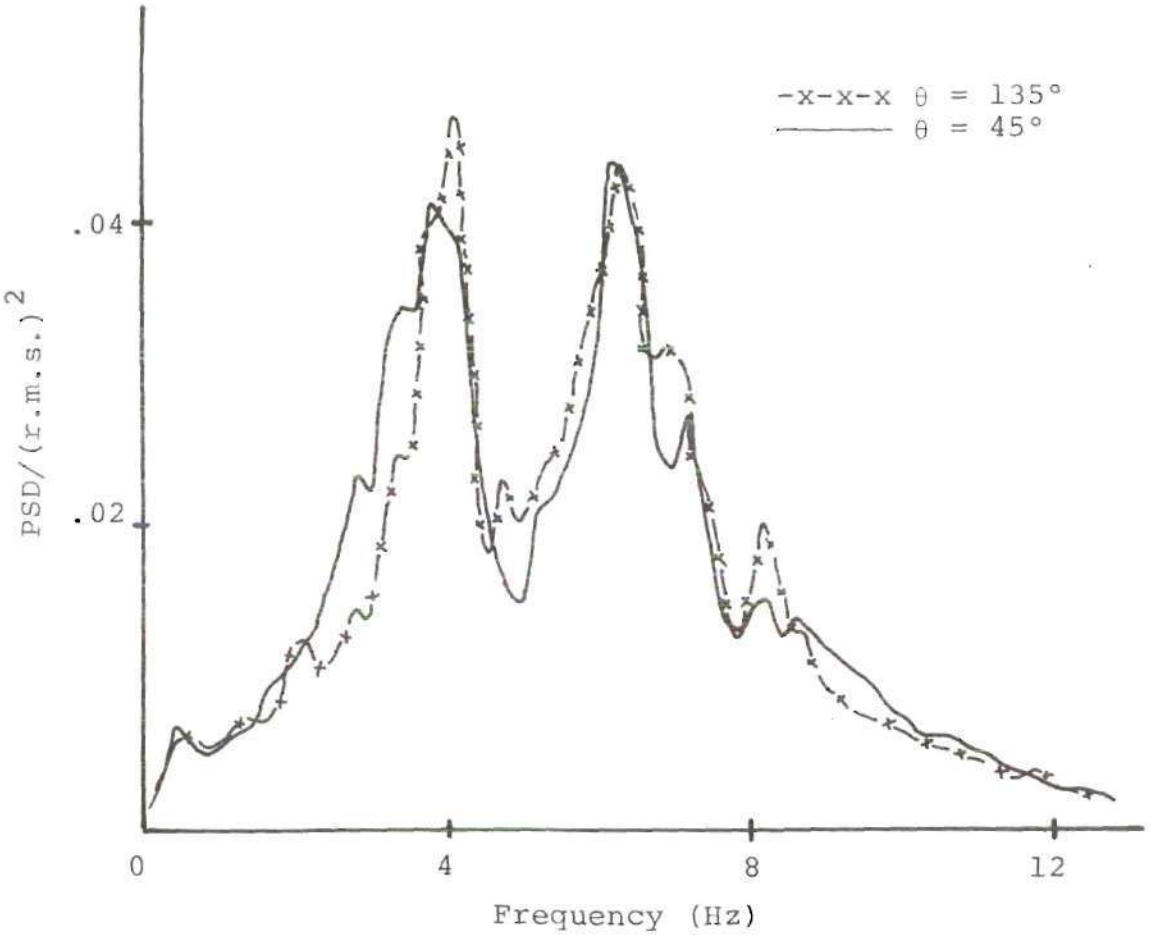

Figure F-21. Normalized Power Spectral Density Function. (Glass Beads (230 μm), P/D_t = 1.3 and U = .50 ft/sec)

Table F-15. Dominant Frequency and r.m.s. Values of Pressure Fluctuations (P/D_t = 1.3, 5 Rows).

Bed Material	Fluidizing Velocity (ft/sec)	U/U_{mf}	Angular Location θ	Frequency of Dominant Peak	r.m.s. Values of Pressure Fluctuations (psi)
Ottawa sand (514 μm)	0.89	1.20	0°	-	.0049
			30°	-	.0034
			60°	-	.0033
			90°	-	.0038
			120°	-	.0044
			150°	-	.0042
			180°	-	.0041
	1.14	1.55	0°	3.1	.0274
			90°	3.3	.0269
			180°	3.4	.0258
	1.56	2.1	0°	3.6	.055
			90°	3.5	.061
			180°	3.7	.054
Glass beads (230 μm)	0.29	1.80	0°	-	.014
			30°	-	.009
			60°	-	.007
			90°	-	.007
			120°	-	.006
			150°	-	.004
			180°	-	.003
	0.35	2.2	0°	-	.044
			45°	-	.042
			90°	-	.046
			120°	-	.050
			180°	-	.047
	0.5	3.13	0°	6.3	.069
			45°	6.2	.069
			90°	6.4	.077
			135°	6.3	.077
			180°	6.2	.081

BIBLIOGRAPHY

1. Ainshtein, V. G. and Gel'perin, N. I., "Heat Transfer Between a Fluidized Bed and a Surface," International Chemical Engineering, Vol. 6, No. 1, (1966), p. 67.

2. Andeen, B. R. and L. R. Glicksman, "Heat Transfer to Horizontal Tubes in Shallow Fluidized Beds," ASME paper no. 76-HT-67, (1976).

3. Andeen, B. R., L. R. Glicksman and W. N. Rohsenow, Heat Transfer Lab. Report No. 80047-85, Department of Mechanical Engineering, MIT, (1974).

4. Baerg, A., J. Klassen and P. E. Gishler, "Heat Transfer in a Fluidized Solids Bed," Can. Journ. Research., (1950), F28, 287-307.

5. Bartel, W. J. and W. E. Genetti, "Heat Transfer from a Horizontal Bundle of Bare and Finned Tubes in an Air Fluidized Bed," AICHE Symp. Series, 128, (1973), 85-93.

6. Bartel, W. J., W. E. Genetti and E. S. Grimmett, "Heat Transfer From a Horizontal Discontinuous Finned Tube in a Fluidized Bed," AICHE Symp. Series, 116, 67, (1971), 85-89.

7. Baskakov, A. P., "The Mechanism of Heat Transfer Between a Fluidized Bed and a Surface," Intern. Chem. Eng., 4, (1964), 320-324.

8. Bendat, J. S. and A. G. Piersol, "Random Data: Analysis and Measurement Procedures," Wiley-Interscience, (1971).

9. Berg, B. V. and A. P. Baskakov, "Investigation of Local Heat Transfer Between a Fixed Horizontal Cylinder and a Fluidized Bed," Int. Chem. Eng., Vol. 14, No. 3, (1974), p. 440.

10. Botterill, J. S. M., "Fluid-Bed Heat Transfer," Academic Press, London, New York, San Fransisco, (1975).

11. Botterill, J. S. M. and M. H. D. Butt, "Achieving High Heat Transfer Rates in Fluidized Beds," Brit. Chem. Eng., Vol. 13, No. 7, (1968), 1000-1004.

12. Botterill, J. S. M., K. A. Redish, D. K. Ross, and J. R. Williams, "The Mechanism of Heat Transfer to Fluidized Beds," Proceedings of the Symposium on the Interaction Between Fluids and Particles, Inst. Chem. Eng., (1962), 183-189.

13. Botterill, J. S. M. and J. R. Williams, "Mechanism of Heat Transfer to Gas-Fluidized Beds," Instn. Chem. Engrs., Trans. V. 41, N5, (1963), 217-30.

14. Brusenback, R. A., Ph. D. Thesis, Northwestern University, Evanston, Ill. (1963).

15. Chen, J. C., "Heat Transfer to Tubes in Fluidized Beds," ASME paper no. 76-H7-75, (1976).

16. Couderc, J. P., H. Angelino, M. Enjalbert, and C. Guiglion, "Excahnge Thermiques en Fluidisation Gazeuse," Chem. Eng. Sic., 22, (1967), 99-107.

17. Davidson, J. F. and D. Harrison, "Fluidization," Academic Press, London and New York, (1971).

18. Dow, W. M. and M. Jakob, "Heat Transfer Between a Vertical Tube and a Fluidized Air-Sold Mixture," Chem. Engng. Prog. Vol. 47, (1951), 537-648.

19. Fakhimi, S., Ph. D. Dissertation, University of Cambridge, (1969).

20. Fiacco, R. J., Sc. D. Thesis, Stevens Institute of Technology, Hobuken, N. J., (1964).

21. Gabor, J. D., "Heat Transfer to Particle Beds with Gas Flows Less Than or Equal to that Required for Incipient Fluidization," Chem. Eng. Sco., Vol. 25, (1970), 979-984.

22. Gamson, B. W., "Heat and Mass Transfer in a Fluid-Solid System," Chem. Eng. Progr., (1951), 47, No. 1, 19-28.

23. Gel'perin, N. I., V. G. Ainshtein, N. A. Romanova, "Gidravlika i teploobmen v psevdoozhizhennon sloe s vertikal'nym puchkom trub," Kimicheskaya Promyshlennost, N11, (Nov. 1962), 1-8.

24. Gel'perin, N. I., V. Ya. Kruglikov and V. G. Ainshtein, "Heat Transfer Between a Fluidized Bed and the Surface of a Single Tube in Longitudinal and Transverse Gas Flow (In Russian)," Kmim. Prom., (1958), No. 6, 358-363.

25. Gel'perin, N. I., V. G. Ainshtein, and A. V. Zaikovskii, "Variation of Heat Transfer Intensity Around the Perimeter of a Horizontal Tube in a Fluidized Bed," Inzhenerno-Fizicheskii Zhurnal, Vol. 10, No. 6, (1966), 799-802.

26. Genetti, W. E. and J. G. Knudsen, In Pirie "Fluidization," Tripartite Chemical Engineering Conf., Montreal, (1968), 147.

27. Genetti, W. E., R. A. Schmall, and E. S. Grimmett, "The Effect of Tube Orientation on Heat Transfer with Bare and Finned Tubes in Fluidized Bed," AICHE Symp. Series, 116, (1971), 90-96.

28. Glass, D. H., Ph. D. Dissertation, University of Cambridge, (1967).

29. Glass, D. H. and D. Harrison, "Flow Patterns Near a Solid Obstacle in a Fluidized Bed," Chem. Eng. Sci., 19, (1964), 1001-1002.

30. Harakas, N. K. and K. O. Beatty, Jr., "Moving Bed Heat Transfer:I Effect of Interstitial Gas with Fin Particles," Chem. Eng. Progr. Symp. Series No. 41, Vol. 59, (1963), 122-128.

31. Hilby, J. W., "Periodic Phenomena Connected with Gas-Solid Fluidization," Proceedings of the International Symposium on Fmuidization, Findhoven, Netherlands Univ. Press, Amersterdam, (1967), 90.

32. Hilpert, R., Forsch. Gebiete Ingenieruw, 4, 215 (1933).

33. Holman, J. P., "Experimental Methods for Engineers," McGraw-Hill Book Company, (1971).

34. Jones, B. R. E. and D. I. Pyle, "On Stability, Dynamics, and Bubbling in Fluidized Beds," AICHE Symp. Series 116, (1971), 1-10.

35. Kang, W. K., J. P. Sutherland and G. L. Osberg, "Pressure Fluctuations in a Fluidized Bed With and Without Screen Cylindrical Packings," I & EC Fundamentals, Vol. 6, No. 4, (1967), 499-504.

36. Keairns, D. L., "Heat Transfer from Horizontal Tubes in a Rectangular Fluidized Bed," Research Report 68-9D3-273-R3, Westinghouse Research Laboratories, Pittsburgh, Pa. (1968).

37. Kline, S. J. and McClintock, F. A., "Describing Uncertainties in Single Sample Experiments," Mechanical Engineering, (1953), Vol. 75, pp. 3-8.

38. Kunii, D. and O. Levenspiel, "Fluidization Engineering," John Wiley and Sons, Inc., New York, (1969).

39. Lese, H. K. and R. I. Kermode, "Heat Transfer From a Horizontal Tube to a Fluidized Bed in the Presence of Unheated Tubes," The Canadian Journal of Chemical Engineering, Vol. 50, (1972), 44-48.

40. Leva, M., "Fluidization," McGraw-Hill, New York, (1959).

41. Levenspiel, O. and J. S. Walton, "Bed Wall Heat Transfer in Fluidized Systems," Chem. Eng. Progr. Symp. Ser., (1954), 50, No. 9, 1-13.

42. Lirag, R. C. and H. Littman, "Statistical Study of the Pressure Fluctuations in a Fluidized Bed," AICHE Symp. Series 116, (1971), 11-22.

43. Mickley, H. S. and D. F. Fairbanks, "Mechanism of Heat Transfer to Fluidized Beds," A. I. Ch. E. Journ., (1955), I, 374-384.

44. Mickley, H. S. and C. A. Trilling, "Heat Transfer Characteristics of Fluidized Beds," Ind. Eng. Chem., 41, (1949), 1135-1147.

45. Morgan, C., Ph. D., Dissertation, University of Cambridge, (167).

46. Natush, M. J. and H. Blenke, Paper C4.4, IV International Congress CHISA, Prague, 11-15 Setp., (1972).

47. Noack, R., "Lokaler Warmeubergang an Horizontalen Rohren in Wirbelschichten," Chem. Ing. Tech. 42, (1970), 371-376.

48. Ozkaynak, T. F. and J. C. Chen, "Average Residence Times of Emulsion and Void Phases at the Surface of Heat Transfer Tubes in Fluidized Beds," 15 National Heat Transfer Conference, San Fransisco, (1975).

49. Patel, R. D., Ph. D. Thesis, Purdue University, Lafayette, Indiana, (1967).

50. Petrie, J. C., W. A. Freeby, and J. A. Buckham, "In-Bed Heat Exchangers," Chemical Engineering Progress, Vol. 64, No. 7, (1968), 45-57.

51. Petrie, J. C., W. A. Freeby, and J. A. Buckham, "Heat Transfer From Horizontal Tube Bundles to Air Fluidized Beds," A paper presented at the 60th Annual Meeting of the AICHE, N. Y., (Nov. 1967).

52. Prasanna, K. V., "Heat Transfer From Transversely Vibrating Cylinders in Low Turbulence Air Streams," Ph.D. Thesis. School of Mechanical and Aerospace Engineering, Illinois Institute of Technology, Chicago, (1964).

53. Priebe, S. J., Ph. D. Thesis, Montana State University, (1975).

54. Rowe, P. N. and B. A. Partridge, "An X-Ray Study of Bubbles in Fluidized Beds," Trans. Instn. Chem. Engrs., Vol. 43, (1965), 157-175.

55. Shuster, W. W. and P. Kisliak, "The Measurement of Fluidization Quality," Chem. Eng. Progr. 48, (1952), 455-58.

56. Sutherland, K. S., "Rept. ANL-6907," Argonne National Laboratory, (1964).

57. Toomey, R. and H. Johnstone, "Heat Transfer Between Beds of Fluidized Solids and the Walls of the Container," Chem. Eng. Progr. Symp. Ser., (1953), 49, No. 5, 51-63.

58. Vakhrushev, I. A., Ya. A. Botnikov, and N. G. Zenchenkov, "Heat Transfer from a Fluidized Bed of Hot Coke to the Surface of Horizontal Tubes," International Chemical Engineering, Vol. 3, No. 2, (1963), 207-210.

59. Van Heerden, C., A. P. Nobel and D. Van Krevelen, "Mechanism of Heat Transfer in Fluidized Beds," Ind. Eng. Chem., (1953), 45, No. 6, 1237-1242.

60. Vreedenberg, H. A., "Heat Transfer Between Fluidized Beds and Vertically Inserted Tubes," Journ. Appl. Chem., (1952), 2, Suppl. Issue, 26-33.

61. Vreedenberg, H., "Heat Transfer Between a Fluidized Bed and a Horizontal Tube," Chem. Eng. Sci., (1958), 9, No. 1, 52-60.

62. Vreedenberg, H. A., "Heat Transfer Between a Fluidized Bed and a Vertical Tube," Chem. Eng. Sci., (1960), 11, 274-285.

63. Wasan, D. T. and M. S. Ahluwalia, "Consecutive Film and Surface Renewal Mechanism for Heat or Mass Transfer from a Wall," Chem. Eng. Sci., Vol. 24, (1969), 1535-1541.

64. Wender, L. and G. T. Cooper, "Heat Transfer Between Fluidized-Solids Beds and Boundary Surfaces - Correlation of Data," A. I. Ch. E. Journ., (1958), 4, No. 1, 15-23.

65. Winter, O., "Density and Pressure Fluctuations in Gas Fluidized Beds," AICHE J. Vol. 14, No. 3, (1968), 426-34.

66. Yoshida, K., D. Kunii, and O. Levenspiel, "Heat Transfer Mechanisms Between Wall Surface and Fluidized Bed," Intern. J. Heat Mass Transfer, Vol. 12, (1969), 529-536.

67. Zabrodsky, S. S., "Hydrodynamics and Heat Transfer in Fluidized Beds," The M.I.T. Press, (1966).

68. Zenz, F. A. and D. F. Othmer, "Fluidization and Fluid-Particle Systems," Reinhold Publish. Corp., N. Y., (1960).

69. Ziegler, E. N. and W. T. Brazelton, "Mechanism of Heat Transfer to Fixed Surfaces in Fluidized Bed," Indus. and Eng. Chem. - Fundamentals, Vol. 3, No. 2, (1964), 94-98.

VITA

Ravinder Kumar Bansal was born in Ambala Cantt, India on February 26, 1949, the son of Dr. and Mrs. C. M. Bansal. He got his primary education in the public schools of Kasauli and Ambala Cantt, India. In 1967, he joined M.N.R. Engineering College, Allahabad, and graduated with a Bachelor of Mechanical Engineering degree in September 1971.

In January of 1972 he came to the United States and entered the graduate program in the School of Mechanical Engineering at Arizona State University, and graduated with a Master of Science degree in 1974. During the period of December 1972 to September 1974, he worked as a Graduate Research Assistant in the School of Mechanical Engineering and also as Assistant Radiation Safety Officer at Arizona State University.

In September, 1974 he was awarded graduate research assistantship in the School of Mechanical Engineering at Georgia Institute of Technology. Since January, 1977 he has been employed as Staff Engineer by Union Carbide Corp., Linde Division at their Tonawanda (N. Y.) facility.